

**A HIGH RESOLUTION SEISMIC REFLECTION STUDY OF
THE CARBONIFEROUS BAY ST. GEORGE SUBBASIN,
WESTERN NEWFOUNDLAND**

CENTRE FOR NEWFOUNDLAND STUDIES

**TOTAL OF 10 PAGES ONLY
MAY BE XEROXED**

(Without Author's Permission)

TERESIA KANYIVA NGUURI



National Library
of Canada

Acquisitions and
Bibliographic Services Branch

395 Wellington Street
Ottawa, Ontario
K1A 0N4

Bibliothèque nationale
du Canada

Direction des acquisitions et
des services bibliographiques

395, rue Wellington
Ottawa (Ontario)
K1A 0N4

Your file: *Votre référence*

Our file: *Notre référence*

NOTICE

The quality of this microform is heavily dependent upon the quality of the original thesis submitted for microfilming. Every effort has been made to ensure the highest quality of reproduction possible.

If pages are missing, contact the university which granted the degree.

Some pages may have indistinct print especially if the original pages were typed with a poor typewriter ribbon or if the university sent us an inferior photocopy.

Reproduction in full or in part of this microform is governed by the Canadian Copyright Act, R.S.C. 1970, c. C-30, and subsequent amendments.

AVIS

La qualité de cette microforme dépend grandement de la qualité de la thèse soumise au microfilmage. Nous avons tout fait pour assurer une qualité supérieure de reproduction.

S'il manque des pages, veuillez communiquer avec l'université qui a conféré le grade.

La qualité d'impression de certaines pages peut laisser à désirer, surtout si les pages originales ont été dactylographiées à l'aide d'un ruban usé ou si l'université nous a fait parvenir une photocopie de qualité inférieure.

La reproduction, même partielle, de cette microforme est soumise à la Loi canadienne sur le droit d'auteur, SRC 1970, c. C-30, et ses amendements subséquents.

Canada

**A HIGH RESOLUTION SEISMIC REFLECTION STUDY OF THE
CARBONIFEROUS BAY ST. GEORGE SUBBASIN,
WESTERN NEWFOUNDLAND.**

BY

© TERESIA KANYIVA NGUURI, B.ED (SCIENCE) (HONS)

**A thesis submitted to the School of Graduate
Studies in partial fulfilment of the
requirements for the degree of
Master of Science.**

**Department of Earth Sciences
Memorial University of Newfoundland**

November 1992

St. John's Newfoundland



National Library
of Canada

Acquisitions and
Bibliographic Services Branch

395 Wellington Street
Ottawa, Ontario
K1A 0N4

Bibliothèque nationale
du Canada

Direction des acquisitions et
des services bibliographiques

395, rue Wellington
Ottawa (Ontario)
K1A 0N4

Your file Votre référence

Our file Notre référence

The author has granted an irrevocable non-exclusive licence allowing the National Library of Canada to reproduce, loan, distribute or sell copies of his/her thesis by any means and in any form or format, making this thesis available to interested persons.

L'auteur a accordé une licence irrévocable et non exclusive permettant à la Bibliothèque nationale du Canada de reproduire, prêter, distribuer ou vendre des copies de sa thèse de quelque manière et sous quelque forme que ce soit pour mettre des exemplaires de cette thèse à la disposition des personnes intéressées.

The author retains ownership of the copyright in his/her thesis. Neither the thesis nor substantial extracts from it may be printed or otherwise reproduced without his/her permission.

L'auteur conserve la propriété du droit d'auteur qui protège sa thèse. Ni la thèse ni des extraits substantiels de celle-ci ne doivent être imprimés ou autrement reproduits sans son autorisation.

ISBN 0-315-82671-1

Canada

ABSTRACT

A seismic reflection profile from onshore Bay St. George Subbasin in western Newfoundland was reprocessed and reinterpreted to determine the structure and extent of the Carboniferous rocks. The main emphasis of reprocessing was placed on velocity analyses and dip move-out (DMO). The quality of the data was improved significantly by the reprocessing. A few features which had not been discovered before became evident. An example of this is an unconformity at a depth of 3.0 km to 5.0 km.

The basin has the configuration of a half graben dipping to the east. The maximum thickness of the Carboniferous sediments is about 5 km in individual depocentres. The basin appears to be bounded downwards by unconformity "U", which separates the Carboniferous rocks from either Lower Palaeozoic rocks or Precambrian rocks.

The fault system is very complex. A few faults correspond to the surface geology. The pattern of faults suggest that the basin was opened by strike slip movements and later deformed by compressional forces.

ACKNOWLEDGEMENT

I would wish to express my gratitude to the following for the support and resources they gave me during my study in Memorial University of Newfoundland:

My thesis supervisor, Dr. Jeremy Hall for his guidance, advice, stimulation, encouragement and freedom of thought necessary for producing this piece of work;

Dr. Hugh Miller for allowing me to use his computer for potential fields data processing. I also appreciate his ideas on the interpretation of gravity and magnetic data;

Drs. James Wright, Garry Quinlan, Cedric Wright, Joe Hodych, E.R. Deutsch, Mike Rochester, Henry Williams and G.S. Murthy for teaching me and for any advice they gave me during my stay in Memorial University;

George Langdon for his guidance on the geology and the tectonics of the Bay St. George Subbasin;

Tony Kocurko for attending to all the technical problems of the CONVEX C1 XL mini-supercomputer in the geophysics unit;

Brian Roberts for his assistance on the processing, especially for making some of the original processing jobs available to me;

The entire technical and supporting staff of department of Earth Sciences for their support and any help they gave me;

Texaco Limited for giving me permission to cite material directly from STARPAK processing and reference manuals;

Canadian International Development Agency (CIDA) for awarding me a scholarship to study in Canada;

The Kenya High Commission at Ottawa for managing efficiently my finances and the programme on behalf of CIDA;

My fellow graduate colleagues, Bill Nickerson, Khalid, Satria Bijakana, Peng, Ron Wiseman, Seyed Mohamoud, Sue Webb, Estelle Blais, for their daily help in one way or another especially with the computers;

Last but not least my entire family back in Kenya for their daily support, prayers and encouragement in one way or another.

DEDICATION

This piece of work is dedicated to my mother, Helenia Mũthoni Njagĩ and my beautiful daughter, Christine Mũmbi, without whom this would not have been possible.

In loving memory of my father, Njagĩ Ngũũri.

TABLE OF CONTENTS

ABSTRACT	ii
ACKNOWLEDGEMENT	iii
DEDICATION	v
LIST OF TABLES	ix
LIST OF FIGURES	x
Chapter 1: Introduction	
Chapter 2: Regional geology of the Bay St. George Carboniferous Subbasin	
2.1 Introduction	3
2.2 Pre-Late Devonian/Carboniferous geology	3
2.3 Late Devonian to Carboniferous Rocks	6
2.3.1 Introduction	6
2.3.2 The Anguille Group	10
2.3.3 The Codroy Group	11
2.3.4 The Barachois Group	12
2.4 Structural History	13
2.5 Previous Geophysical Studies	16
2.5.1 Introduction	16
2.5.2 Physical Parameters	17
2.5.2.1 Density	17
2.5.2.2 Magnetic Susceptibilities	19
2.5.3 Potential fields data	20
2.5.3.1 Qualitative Study	20
.....	25
2.5.4 Seismic data	29
Chapter 3: Seismic Reflection Profile	
3.1 Introduction	33
3.2 Acquisition	34
3.3 Processing	35
3.3.1 Introduction	35
3.3.2 Pre-stack processing	37
3.3.2.1 Geometry and Binning	37
3.3.2.2 Field static corrections	40

3.3.2.3 CMP gather	44
3.3.2.4 Velocity analysis	44
3.3.2.4.1 Constant-Velocity Stacks (CVS)	44
3.3.2.4.2 Constant velocity normal moveout (CVNMO)	45
3.3.2.4.3 Velocity spectra	46
3.3.2.4.4 Velocity field definition	54
3.3.2.5 Mute	54
3.3.2.6 Dip Moveout correction (DMO)	57
3.3.2.6.1 DMO Theory	57
3.3.2.6.2 Application of DMO	59
3.3.2.7 Automatic Gain Control (AGC)	60
3.3.2.8 Stack	61
3.3.3 Post Stack Processing	66
3.3.3.1 Residual static correction	66
3.3.3.2 Finite-difference migration	73
3.3.3.3 Filtering	75
3.3.3.3.1 Bandpass filter	75
3.3.3.3.2 Coherency filtering	75
3.3.3.4 Final display	79
3.3.4 Other processing	81
Chapter 4: Interpretation	
4.1 Introduction	82
4.2 Description of the seismic line	82
4.2.1 Reflections	82
4.2.2 Faults	87
4.3 Interpretation of the seismic line	89
4.3.1 Introduction	89
4.3.2 Reflector "R"	89
4.3.3 Packages "A" to "G"	92
4.3.4 Unconformity "U"	93
4.4 Geological Models	93
4.4.1 Introduction	93
4.4.2 Model A - "R" as the Anguille/Codroy contact with or without décollement	95
4.4.3 Model B - "R" as the Codroy - Barachois upon Pre-Late Devonian-Carboniferous basement with or without décollement	97
4.4.4 Model C - A non-marine downlap within a half graben	99

Chapter 5: Conclusions

References	106
Appendix A	112
Appendix B	123

LIST OF TABLES

Table 2.1. Summary of the geology of Bay St. George Subbasin.

Table 2.2. Rock Densities.

Table 3.1. Velocity definition before dip moveout (DMO) correction.

Table 3.2. Velocity definition after dip moveout (DMO) correction.

Table 3.3. Mute specifications.

Table 3.4. Horizon and window length used to define reference trace.

Table A.1. Field statics specifications.

LIST OF FIGURES

- Figure 2.1. General geology of the Maritimes basin, showing its relative position to the Appalachian mobile belt and the location of the Bay St. George subbasin.
- Figure 2.2. The Bay St. George subbasin: outcrop geology in the vicinity of the seismic line.
- Figure 2.3. Stratigraphy of the bay St George's subbasin, showing correlations with other rock units in the Maritimes basin.
- Figure 2.4. Bouguer anomaly map of the Bay St. George subbasin.
- Figure 2.5. Residual anomaly map of the Bay St. George subbasin after fitting a third order trend.
- Figure 2.6. Polynomial surface fitted to the Bouguer anomaly map.
- Figure 2.7. Magnetic data reduced to the pole after fitting a third order trend to the original data.
- Figure 2.8. Cross-section near Robinson's river showing geology, 2.5-D and 3-D gravity models.
- Figure 2.9. Modelled interpretation for profile B-B' oriented NW-SE (see fig. 2.2).
- Figure 2.10. An example of a seismic line from the Cabot Strait area; the central portion is similar to Robinson's river data.
- Figure 3.1. Data processing sequence.
- Figure 3.2. Binning strategy chart (in folder).
- Figure 3.3. Shot record 250 from TWT 0.0 to 0.2 s showing example of section used to estimate refraction picks.
- Figure 3.4. Shot record 1 from TWT 0.0 to 0.2 showing portion used to estimate velocity of the weathered layer.
- Figure 3.5. Shot record 250 from TWT 0.0 to 2 s. (a) Before applying field statics.

(b) After field statics corrections.

Figure 3.6. CMP 1000. (a) Before notching 60 Hz. (b) After applying a notch filter to reject 60 Hz, 120 Hz, 180 Hz etc i.e multiples of 60 Hz noise.

Figure 3.7. Constant velocity stacks (CVS) of all velocities analyzed (in folder, labelled a to t).

Figure 3.8. Constant velocity normal moveout (CVNMO) of CMP 630 before DMO correction (in folder).

Figure 3.9. Velocity Spectrum of CMP 950, TWT 0.0 to 2.0 s. (a) Velocity spectrum before DMO correction, (b) after DMO correction.

Figure 3.10. Constant velocity normal moveout (CVNMO) of CMP 950 after DMO correction (in folder). (a) Before DMO correction (in folder). (b) After DMO correction (in folder).

Figure 3.11. Velocity field contours before DMO correction (in folder).

Figure 3.12. Velocity field contours after DMO correction (in folder).

Figure 3.13. CMP 630 (a) Before front muting. (b) After muting. (c) With NMO stretch. (d) NMO stretch muted.

Figure 3.14. CMP 630. (a) Before DMO correction. (b) After DMO correction.

Figure 3.15. Stacked section before DMO correction, with no post stack processing.

Figure 3.16. Stacked section after DMO correction, with no post stack processing (also in folder).

Figure 3.17. Stacked section after residual statics corrections.

Figure 3.18. Migrated section after DMO and residual statics corrections.

Figure 3.19. Bandpass filter test panels (in folder).

Figure 3.20. Flow chart of calculation steps in the coherency filter.

Figure 3.21. The migrated section after applying bandpass and coherency filters.

Figure 3.22. Final display of the processed profile (in folder). This is a 1:1 section if an average velocity of 4 km/s is assumed for the whole section.

Figure 3.23. Deconvolution of CMP 630.

Figure 4.1. The seismic profile as processed previously.

Figure 4.2. Main reflection packages, faults and unconformity of the seismic profile.

Figure 4.3. The St. George coalfield basin. (a) Knight' cross-section projected onto the seismic line. (b) Line drawing of the seismic line taken from the reflectors picked on Figure 4.2.

Figure 4.4. Model A - "R" as the Anguille/Codroy contact \pm décollement.

Figure 4.5. Model B - "R" as the Codroy-Barachois upon Pre-Carboniferous basement \pm décollement.

Figure 4.6. Model C - Non-Marine downlap within a half graben.

Figure B.1. Plot of equation B.4 P_0 was set to zero for this plot.

Figure B.2. Plot of equation B.4 for different values of P_0 's and t_0 's.

Chapter 1: Introduction

The main objective of this project was to reprocess and interpret a seismic profile across Robinson's river, Bay St. George subbasin of western Newfoundland. This study was undertaken to try and define the structure and the extent of the Carboniferous rocks. The processed data had indicated that the basin could be as deep as 4 km (Hall et al., 1992). However, this was not clear due to the complex structure of the profile. It was felt that reprocessing the profile especially with special emphasis on pre-stack migration i.e. dip moveout correction (DMO) would improve the data quality and hopefully the interpretation.

The basin, which forms the eastern portion of the Magdalen basin (figure 2.1), has been a target of many geophysical and geological studies dating as early as the 1950's. Vernall (1954) compiled a gravity report of the St. George's Bay lowlands onshore. Spector (1969) reported and interpreted an aeromagnetic survey conducted in 1969 by Lockwood Geophysical. Knight (1983) mapped the geology of the Carboniferous rocks onshore. Peavy (1985) compiled a potential fields study on the area. This study suggested that the basin could attain a depth of up to 4 km. The study was not well constrained by other geophysical data. Kilfoil (1988) attempted an integrated geophysical study on the basin onshore using all available geophysical data at that time. The conclusion was that the basin could be a half graben about 2 to 4 km depth. Miller et al. (1990) combined both the studies of Peavy (1985) and Kilfoil (1988) and found that the basin could be as deep as 3 km.

The data for the current project were acquired in October 1989 for Memorial University of Newfoundland and the Government of Newfoundland and Labrador through a contract with Capilano Geophysical Limited of Calgary Alberta. The aim of conducting this seismic survey was to try and image the structure of the basin onshore using seismic reflection. The offshore section of basin had been covered by a seismic reflection survey of Mobil Oil in 1971 and 1973. These seismic sections are generally poor in quality, though the structures they reveal are similar to those of the current seismic profile. The Cabot Strait area, 75 km southeast of the study area, had been covered by a reflection survey of Petro-Canada, between 1981 and 1983. Very little seismic data covered the onshore section of the basin. Therefore, the seismic survey was deemed necessary. These data were of very high quality, but needed careful processing because of the complexity of the structure.

Data were processed using the STARPAK software centred around a CONVEX C1 XL mini-supercomputer. Apart from DMO, careful front muting, field statics based on refraction picks and more velocity analyses, most of the other processors are as mentioned by Hall et al. (1992). DMO is considered a powerful tool in cleaning up the data and helping image complex structures.

The interpreted seismic profile favours the hypothesis that the basin is a half graben of depths up to 5 km. Most of the structural features and stratigraphy of the basin are discussed in the text and 3 models are produced.

Chapter 2: Regional geology of the Bay St. George Carboniferous Subbasin

2.1 Introduction

The Bay St. George Subbasin forms part of the Maritimes Carboniferous basin of Atlantic Canada (see Fig. 2.1). The basin formed as a pull-apart basin within a post-Acadian dextral strike-slip system (Wilson, 1962). In this project most of the geological discussion is derived from the work of Knight (1983), unless otherwise stated. The geology here will only be outlined; for a detailed geology the reader is referred to Knight (1983). Figure 2.2 is a general geology map of the study area.

2.2 Pre-Late Devonian/Carboniferous geology

The pre-Carboniferous basement, where not exposed, is likely composed of Precambrian age rocks (Williams, 1978), similar to those of the Indian Head Complex. Knight's (1983) interpretation indicates that the basement to the immediate northwest of the onshore Anguille outcrop was reduced to a peneplain of Grenville rocks during the Tournaisian, prior to deposition of the uppermost Anguille Group.

At the hinge of the Flat Bay anticline, conglomerates assigned to the Anguille Group rest unconformably on Grenvillian basement, probably similar to that of the Indian Head complex (Knight 1982). This means that the lower Palaeozoic carbonate sequence may be limited in its southward extent from the Port au Port peninsula (Knight 1983; Williams, 1985) toward the Bay St. George Subbasin, and may not underlie the Carboniferous, as is interpreted by Watts (1972) in the East Magdalen

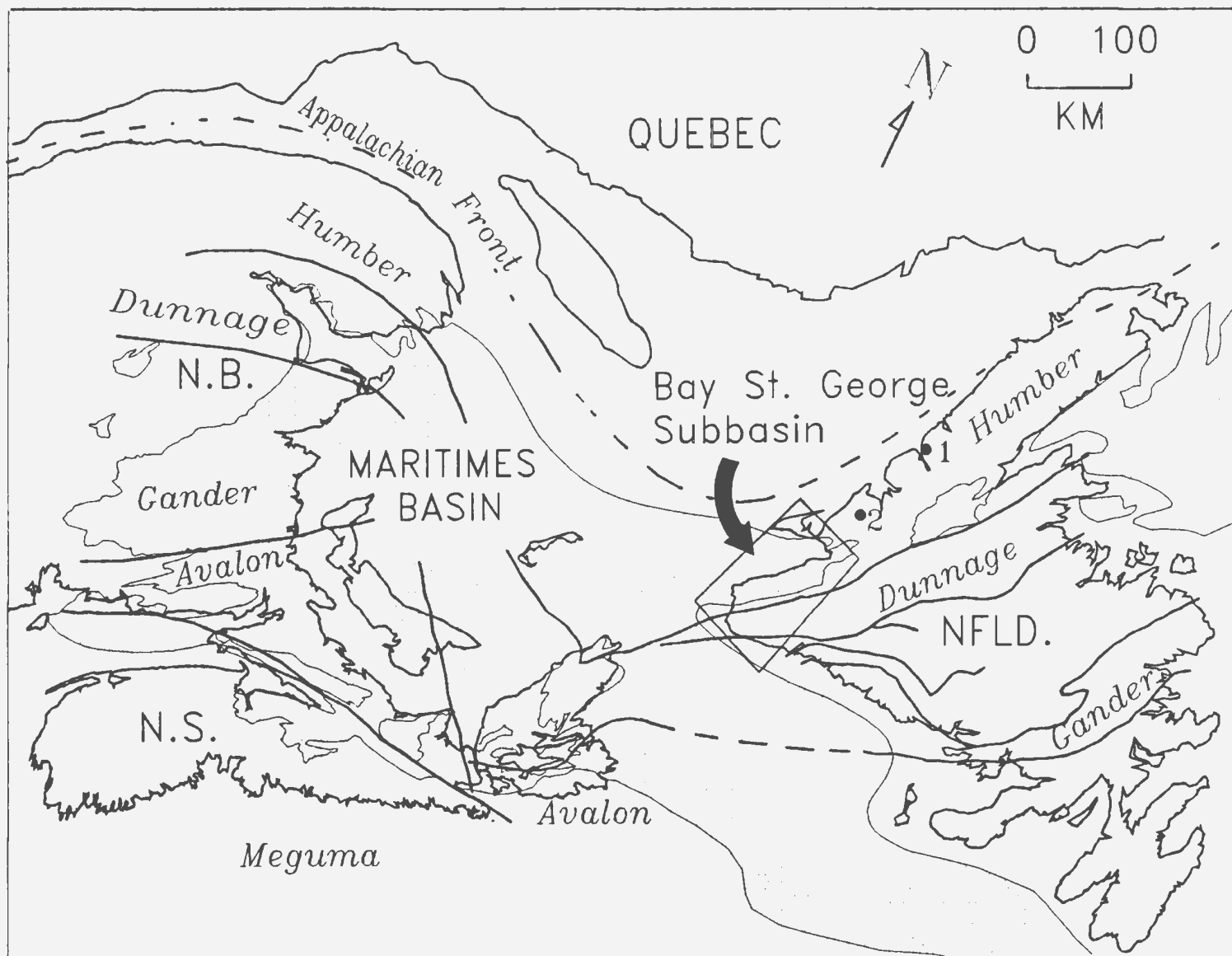


Figure 2.1. General geology of the Maritimes basin, showing its position relative to the Appalachian mobile belt and the location of the Bay St. George subbasin (modified from Hall et al., 1992).

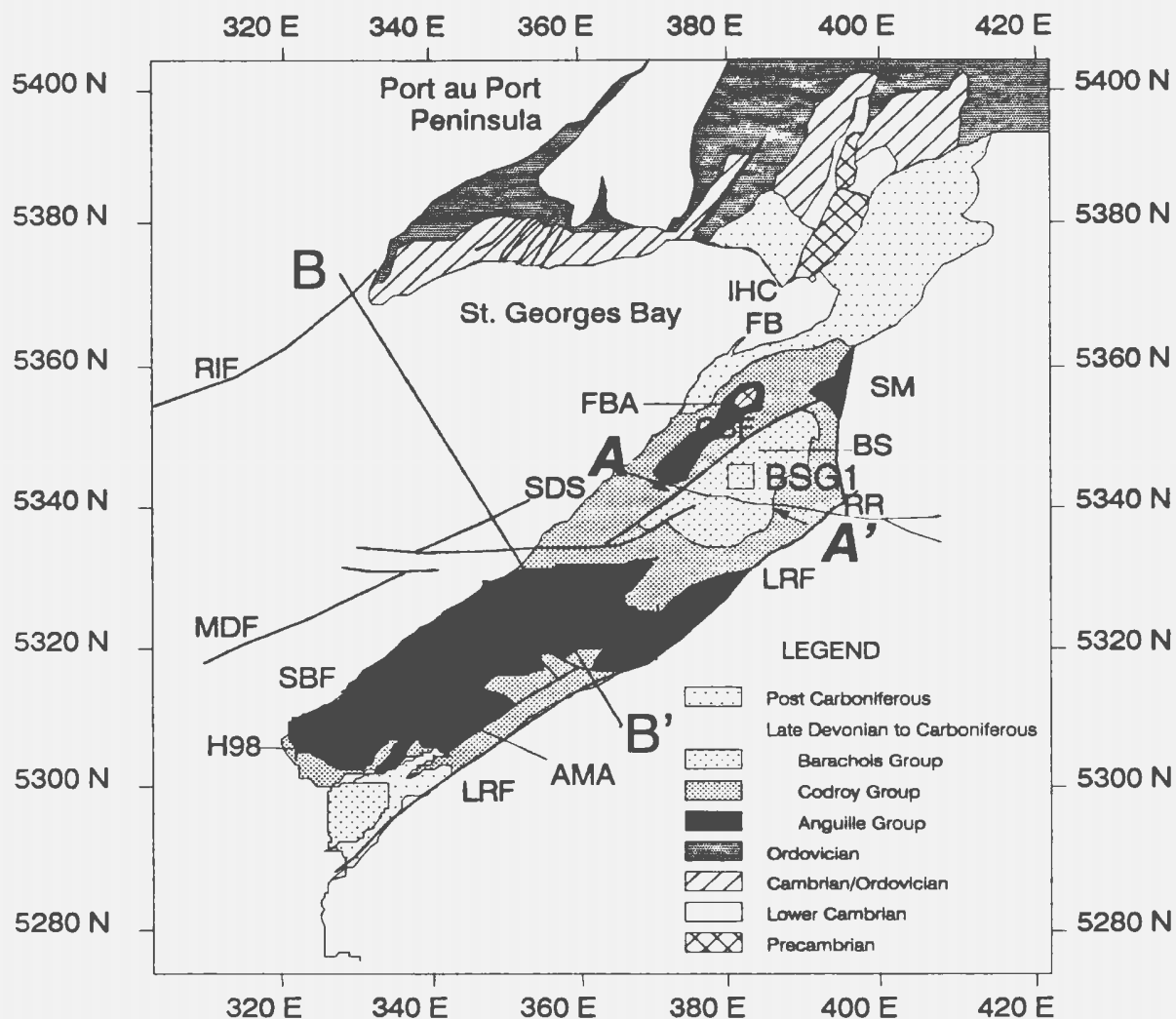


Fig.2.2. The Bay St. George subbasin: outcrop geology in the vicinity of the seismic line (modified from Schillereff and Williams (1979), Knight (1983) and Williams (1985)).

Abbreviations: AMA = Anguille Mountains Anticline, BS = Barachois Synclinorium, FB = Flat Bay, FBA = Flat Bay Anticline, IHC = Indian Head Complex, LRF = Long Range Fault, SBF = Snakes Bight Fault, SDS = St. David's Synclinorium, SM = Steel Mountain Complex, BSG1 = Memorial University drillhole, H98 = Union Brinex H-98 well CBF = Crabbes Brook Fault, MDF = Mid-Bay Fault, RIF = Red Island Fault, RR = Robison's River.

Heavy lines are the major faults mapped by Knight (1983) and Schilleriff and Williams (1979).

Arrows A and A' indicate the two ends of the seismic profile presented in this study. The potential field profile shown in Figure 2.7 is close to and parallel to the seismic line.

B-B' is one of the gravity profiles interpreted by Kilfoil (1988) and quoted in this paper.

basin. Onshore, exposures of the Indian Head Complex consist of foliated dioritic to granodioritic gneisses which become more massive toward the south, with outcrops of anorthosites and layered gabbroic rocks cut by foliated rocks of granitic composition (Williams, 1985). Lenses and bands of magnetite occur within the foliated gabbros, and are the probable cause of the magnetic anomalies observed over the complex (Peavy, 1985).

2.3 Late Devonian to Carboniferous Rocks

2.3.1 Introduction

A succession of late Devonian to Carboniferous age strata overlies Precambrian basement in the Bay St. George subbasin. These sediments have been subdivided into three groups, each distinguishable by its character and mode of deposition.

1. The Anguille Group (late Devonian to Early Mississippian), consists of nonmarine sequences of mostly red to grey fluviodeltaic shale to coarse sandstones, with local conglomerates.
2. The Codroy Group (Upper Mississippian) consists of both marine and nonmarine sequences of siliciclastics, evaporites and calcareous sediments.
3. The Barchois Group (lower Pennsylvanian) is made up of red to grey siltstone-sandstone sequences of fluvial origin with minor mudstones and coals.

The stratigraphy and sedimentology is further summarised in table 2.1 and figure 2.3.

Table 2.1. List of abbreviations

cg - conglomerate	peb - pebbly(es)
ss - sandstone	mic- micaceous
slst - siltstone	ark - arkosic
sh - shale	arg - argillaceous
mdst - mudstone	fluv - fluvial
lut - lutite	x-b - cross-bedded
carb - carbonate	plan - planer
ls - limestone	lam - laminated
dol - dolomite	c - coarse
evap - evaporites	rd - red
gyp - gypsum	gn - green
anh - anhydrite	gy - grey
hal - halite	brn - brown
pot - potash salts	bk - black
clch - caliche	seq(s) - sequence(s)

Table 2.1. Summary of the geology of Bay St. George Subbasin (modified from Knight, 1983)

Group	Formation/ Member	Lithology	Dipositional enviroment	Thickn- ess(m)	Age	Corre- lation
Barachois	Undivided Barachois	gy peb ss; gy-bk mdst, sh, coal	Meandering river channels; floodplain.	1500- 1600	Latest Westp- halian	Pictouan
	Searston Formation	rd slst; gn-rd peb ss; minor bk sh mdst; minor brn cg		2500	Namur- ian	Canso Fm. of Nova Scotia
Codroy	Woody Cape Fm.	gy-gn-bk slst with mic ss, gy-bk carb, rd beds.	Deltaic	690	Visean	Windsor
	Overfall Brook Mbr.	rd-brn massive to x-b ark to arg ss; minor cg, slst, mdst.	Northwest progradation of alluvium; salt formation in depressions;	>345		C
	Mollichignick Member	rd slst, mic ss, ark to arg peb ss near margins; coarse up seqs marine carb near middle.	inland sea with small deltas; Arid but large perenial river from distant source; wide rivers and associated meanderbelts;	2275		D
	Highlands Member	rd-gy ss to slst; cg to N and E; fining up seqs x-b and pian ss; minor cich, lam ls.	semiarid in Mollichignick Mbr. to humid in Overfall Brook Member.	884		E
	Jefferies Village Member	rd-gy sh, mdst, slst, ss, minor cg interbed with carb and eva: gyp, anh, hal, pot; coarsens up near top.		1400-2000		
	Codroy Road Fm.	Rd slst to ss, lam ss; near top gy sh, evap; gyp anh; minor carb and gy-bk slst.	Central lagoonal area; Progradation of alluvium from Long Range	120-300		Windsor B
Anguille	Ship Cove Fm.	lam ls; minor gyp nodules, rd-gy sh mdst.	Tidal and subtidal conditions; north to south transgression.	18-20	Tournaisian	Windsor A
	Spout Falls Fm.	rd-gy fluv. ss, slst, calc-ark-mic ss; well-bedded; minor cg near margins.	Gravelly, fluvial; semi-arid conditions.	780-2250		Upper Horton
	Friars Cove Fm.	Cg to ss; gy ss-cg-sh; x-b c ss at top; minor thick bk sh seqs; ss peb of Cam-Ord Origin.	Fluvio-deltaic; shallow lacustrine setting.	500-1300		NB Albert Fm.
	Snake's Bight Fm.	bk lut, gy ss, sh; thin slst to thick ark ss (flysch); minor dol, mdst, concretions.	Turbidites; deep narrow perenial lake.	785-1000		NB Albert Fm.
	Kennels Brook Fm.	Gn-gy peb ss to cg; rd ss to rd-gn slate; fining up seqs; minor brn mdst, ls.	Fluviatile, fanglomerate and shallow lacustrine.	>3200	Famen- nian	Pre- Horton

2.3.2 The Anguille Group

The Anguille Group, which is the oldest and thickest of the sedimentary groups, is exposed in anticlinal structures. It shows rapid changes of facies. Knight (1983) interpreted that the Anguille records the creation and infill of a deep lake measuring about 30 km by 100 km. The detritus for the infill was mainly derived from the southeast of the Long Range Fault. A northwest trending marginal fault, parallel to the Snakes Bight Fault onshore, is assumed to lie concealed beneath Codroy strata just offshore at the present day coastline. The early subbasin may be viewed as a graben type feature, though its evolution is complicated by lateral strike-slip movements along the faults defining its margins to the southeast and northwest.

The Kennels Brook Formation, the lowest in the Group, consists of a thick molassic sequence, comprising fluvial redbeds with minor lacustrine sediments that may have extended beyond the margins of the early subbasin. The strata are correlated with lower Horton or pre-Horton in other parts of the Maritimes Basin. The thickness of this formation is not known because the basal contact is nowhere exposed in the Anguille region; a drill hole (H98, see Figure 2.2) which penetrated 2200 m may not have drilled the true stratigraphic thickness. The conformably overlying Snakes Bight Formation, which is correlated with the Albert formation of New Brunswick, is composed of deep water clastic sediments typically deposited in alluvial fan-delta and submarine fan (turbidite) environments. The Friars Cove Formation consists of grey sandstones to black shales, and represents the transition

from a lacustrine through fluvio-deltaic to fluvial plain setting. This formation is equivalent to the well-known, petroliferous Albert Formation of the Horton Group in New Brunswick. The overlying Spout Falls Formation is correlated with the uppermost Horton in the Maritimes and consists of fluvatile rock sequences localized in three areas: (1) red and grey sandstones, minor siltstones and conglomerate, with abundant scouring and well-bedded sheet geometry, are found mainly in the south; (2) grey and minor red conglomerates and sandstones overly the Grenvillian basement in the Flat Bay anticline (Fischell's Brook Mbr.); (3) a thick sequence of fault-bound, red arkosic rocks (Brow Pond Lentic) may also be partly equivalent to upper Codroy rocks. This unit is approximately 780-2250 metres thick and is thought to represent an exhumed fault scarp (Knight 1983).

2.3.3 The Codroy Group

This Group is similar to the Windsor Group of the Maritimes. It represents a regional transgression and shift to marine and marginal marine conditions in early Viscean time.

The lowest Ship Cove Formation, which on average has a thickness of 18-20 metres, is mostly composed of well-laminated, grey limestones, becoming shalier and containing gypsum and marls upward. This formation is correlated with the Macumber Formation of the early Viscean of Nova Scotia and New Brunswick (Windsor Subzone A, in part).

The overlying Codroy Road Formation is made up of fine grained, red and grey siliciclastics, evaporites and minor carbonate. Redbeds in the south give way to evaporites in the north. The thickness varies from 120 metres at Ship Cove to about 300 metres in the Codroy Valley. This formation is roughly equivalent to Windsor subzone B (early Viséan).

The Robinson's River Formation is composed of four more or less equivalent members: the Jeffrey's Village Member of about 1400-2100 metres thickness, the Highlands Member (884+ m) in the St George's lowlands, and the Mollichignick (2275+ m) and Overfall Brook (345+ m) in the Codroy lowlands. The formation is a complex succession of terrigenous clastic rocks with lesser amounts of carbonates and evaporites and is correlated with the upper half of the Viséan; that is, it is roughly equivalent to subzones C, D, and E of the Windsor in the other parts of the Maritimes.

The Woody Cape Formation, consisting of predominantly grey, green and black fine grained siliciclastics, intercalated with micaceous sandstones, grey and black carbonates, and minor redbeds, has a thickness of about 690 metres. The Formation is placed in Windsor subzones D and E, which makes it partly equivalent to Overfall Brook and Mollichignick members earlier described.

3.3.4 The Barachois Group

Rocks of this Group occur in two outcrop areas and represent two different periods

of deposition. In the south, the early Namurian Searston Formation represents the Canso strata of the Maritimes Basin, while deposits in the St. George's Bay lowlands in the north are probably Westphalian in age, although neither the top nor the base is well defined in age. Lithologies include buff-weathering, grey sandstone intercalated with grey siltstone and/or grey to black mudstones, shales and occasional coal beds. Conglomerates and sandstones lying unconformably on the basement in the southeast are included but may belong to the Codroy Group. The thickness is not known exactly, but may be about 2500 metres for the Searston beds in the Codroy lowlands and about 1600 metres in the St. George's Coalfield.

The Searston Formation is equivalent to the Canso Formation of Nova Scotia, but the uppermost Barachois beds near Stephenville may be Pictouan (latest Westphalian) in age. The coal-bearing beds are Westphalian A to C in age but it is not clear whether the Namurian B and C are represented.

2.4 Structural History

The strata are principally deformed by north easterly trending folds and faults produced during the Hercynian Orogeny in post or late Pennsylvanian times (Knight, 1983). Major structures trend parallel or subparallel to the Long Range Fault and associated faults within the subbasin (see Figure 2.2). Folds vary from open and upright to tight and overturned. Fault types include high angle faults (dips of 60-90 degrees), thrust faults and decollement zones (Knight, 1983). The structural style is

generally simple in the north where Precambrian basement gneisses underlie Carboniferous strata at shallow depth (Riley, 1962, Belt, 1969). In the south, particularly beneath the southern Anguille Mountains, the structure is complex and reflects the great thickness of the succession and the relative degrees of competence of the different lithologies.

Major folds that show a northeasterly trend include the Anguille Anticline, Flat Bay Anticline and the Barachois Synclinorium. The Anguille Anticline is a large anticlinorium which exposes the Anguille Group strata in the Anguille Mountains, and is modified by numerous subsidiary folds. It is also cut by the Snake's Bight Fault close to its axial plane. At its northern limits it varies from moderately dipping to overturned. In the south, folds are arranged en echelon to the faults which strike generally in a northeasterly direction; in the north the Anguille Anticline swings to 068 degrees. The Flat Bay Anticline, which is a harmonic folding of both Anguille and Codroy strata around a core of Grenville basement, trends 037 degrees. The Barachois Synclinorium is a broad open feature and trends 027 degrees.

There are few structures of northwesterly trend. The St David's Syncline, which is situated between the Anguille and the Flat Bay anticlines, is peculiar because it trends at right angles to other regional structures.

Knight (1983) mapped various thrust faults and decollement zones. Many of these developed locally within relatively incompetent evaporites and shales of the Snake's Bight and Codroy Road Formation respectively. Thrust faults of local extent occur

where there is competency contrast, for example where the thick black sandstone units overlie thick black shale units in the Snake's Bight Formation (Knight, 1983). A decollement zone is developed at the base of the Codroy Road Formation in the central and northern areas where fine siliciclastics and evaporites of the Formation overlie the Ship Cove Formation.

High angle faults of northeasterly, northwesterly and easterly orientation are mapped by Knight (1983). The major ones of these are the northeasterly faults which include the Long Range Fault (Cabot Fault), the Snake's Bight and the Crabbes Brook Faults. En echelon fold trends are associated with several of these faults which show right-lateral strike slip motion. Some faults show slickensides. The Long Range Fault, the most prominent of these faults, extends as a general straight feature along the full extent of the southern margin of the subbasin. This fault, though rarely exposed, is confirmed by aeromagnetic data (Miller et al., 1990). In the Codroy area, the fault is exposed twice on the Branch river and poorly on Stephen Brook. In the north the fault is not exposed at all. Field observations indicate two periods of movement, firstly strike-slip and secondly oblique-slip which have occurred most recently. South of the basin the fault dips generally southward at high angles, but locally is vertical or dips at high angles into the basin. Sediments within the basin adjacent to the fault generally dip steeply away from it, or are deformed in overturned synclines.

The Snake's Bight Fault which transects the Anguille Anticline is represented by a prominent northwestward facing fault scarp. This fault trends parallel to the Long

Range Fault in the southwest but further northeast it swings eastward. The angle of intersection between the Snake's Bight and the Long Range Faults is approximately 25 degrees. In a manner similar to that of the Snake's Bight Fault, the Crabbes Brook and the Ryan's Hill Faults trend subparallel to the Long Range Fault. These two show a downthrow to the southeast of several thousand metres and evidence of significant right-lateral movement, and show compression in an associated array of en echelon faults.

2.5 Previous Geophysical Studies

2.5.1 Introduction

The Bay St. George's basin has been studied using most of the common geophysical methods, including potential field surveys with concomitant measurement of rock density and magnetic susceptibilities, and reflection seismic.

In 1984 an underwater gravity survey was conducted from the CSS Dawson. In the summers of 1983 and 1984 gravity surveys were carried out in the areas onshore by personnel from Memorial University of Newfoundland. The Bouguer anomaly map (Fig. 2.4) in the current project combines data from all surveys that have been carried out to date.

The magnetic data (Fig. 2.7) is digitized from the existing aeromagnetic maps of the government of Canada (Kilfoil and Bruce, 1991). The data area covers onshore

part of the basin only.

Mobil Oil obtained seismic data in 1971 and 1973 covering the central offshore region. The Lithoprobe East seismic reflection line 86-4 traverses the outer limits of the basin. Between 1981 and 1983, Petro Canada conducted a major seismic reflection survey in the Cabot Strait which is 75 km southeast of the study area.

2.5.2 Physical Parameters

Densities and magnetic susceptibilities for the samples of pre-Carboniferous basement and Carboniferous sediment rocks collected or obtained from drill cores were studied by Peavy (1985) and Kilfoil (1988). The results of their study are summarised in Table 2.2.

2.5.2.1 Density

Each sample was identified with respect to group, formation and or member and general lithology. The overall density of each member or formation was calculated by weighting the average density obtained for each rock type within the unit by its percent composition. To get an estimate of the density for a particular group, the thickness contribution of the members of the group were used as weighting factors.

Halite, gypsum and anhydrite from drill cores were sampled to obtain representative densities for the evaporite sequences. Average density of the evaporites is close to that of the Codroy Group, in which most of the evaporites are found. It

should be noted, however, that the known evaporite deposits contain significantly more gypsum and salt than anhydrite, thus the average density of an evaporite deposit is significantly lower than that of the Codroy rocks (Miller et al., 1990).

Table 2.2. Rock Densities (Miller et al., 1990).

Group	Geological Unit (Fm/Mbr)	Density \pm SD (g/cm ³)
Anguille	Kennels Brook	2.58 \pm 0.11
	snakes Bight	2.67 \pm 0.10
	Friars Cove	2.67 \pm 0.04
	Spout Falls	2.59 \pm 0.04
	Fischell's Cong.	2.32 \pm 0.03
	Average	2.63\pm0.06
Codroy	Ship Cove	2.72 \pm 0.03
	Codroy Road	2.48 \pm 0.14
	Robinson's River/	
	Jeffrey's Village	2.40 \pm 0.09
	Highlands	2.53 \pm 0.13
	Brow Pond Lentil	2.58 \pm 0.03
	Robinson's River/	
	Overfall Brook	2.44 \pm 0.08
	Mollichignick	2.55 \pm 0.12
	Average	2.47\pm0.09
Barachois	Searston	2.51 \pm 0.08
	Upper Series	2.56 \pm 0.08
	Average	2.54\pm0.08
Evaporites	Anhydrite	2.97 \pm 0.03
		2.28 \pm 0.03
		2.18 \pm 0.03

Representative densities of 2.63, 2.47 and 2.54 g/cm³ were obtained by Peavy and

Kilfoil (1988) from thickness-averaged samples from the Anguille, Codroy and Barachois groups respectively. Anguille units show higher densities and hence density contrasts (relative to 2.67 g/cm^3) lower in magnitude than the overlying Codroy and Barachois Groups. This is consistent with Knight's (1983) observation that competent, well cemented, Anguille clastics contrast sharply with the more friable, younger Carboniferous clastics. Consistent results were obtained for samples from the Indian Head basement. These samples of anorthositic to granitic compositions are locally gneissic (Williams, 1985) and have densities averaging $2.68 \pm 0.07 \text{ g/cm}^3$. This is in contrast to the measured densities of rock samples from the more anorthositic Steel Mountain Complex which averaged $2.83 \pm 0.034 \text{ g/cm}^3$ with 10 samples giving values above 2.70 g/cm^3 (Peavy, 1985).

The greater variability in density of Steel Mountain samples is caused by a few samples of high density, two of which are greater than 3.20 g/cm^3 .

There were no samples available for measurement from offshore. Knight (1983) considers that the offshore Carboniferous sediments most likely belong to the Codroy Group. Thus, these sediments are considered to have densities similar to those of the Codroy Group (Table 2.2).

2.5.2.2 Magnetic Susceptibilities

The sediments have such low susceptibility that they can be considered transparent to an external inducing field (Peavy, 1985). In comparison, samples of basement

rocks show susceptibilities that vary from near zero to 6000×10^{-6} cgs units (Peavy, 1985). Samples from the Indian Head Complex show consistently low susceptibilities, i.e., $< 100 \times 10^{-6}$ cgs units, but gabbroic lenses or layers rich in titaniferous magnetite within the complex (Williams, 1985) would be expected to have higher values. Samples from the Steel Mountain anorthosite were responsible for most of the variability in magnetic content of the basement samples measured, because they contained magnetite rich lenses or zones (Murthy and Rao, 1976).

2.5.3 Potential fields data

2.5.3.1 Qualitative Study

In order to separate the effects of the basement from those of the underlying sediments the gravity and magnetic data were subjected to a regional-residual separation procedure consisting of fitting third-order polynomial surfaces to the data sets. These maps are especially useful in discerning basement trends since removal of a low-order regional field eliminates the long wavelength portion of the field arising from general basement geometry (Miller et al., 1990). Figure 2.5 is the residual anomaly map after a residual-regional separation by fitting a third-order polynomial (Figure 2.6) to the Bouguer anomaly data (Figure 2.4). The polynomial surface was capable of discerning the main features in the region. This kind of polynomial fitting is similar to strike sensitive filtering as can be observed in Figure 2.6. The lows and highs can be seen clearer after the polynomial fitting (c.f. Figure 2.4 with Figure 2.5).

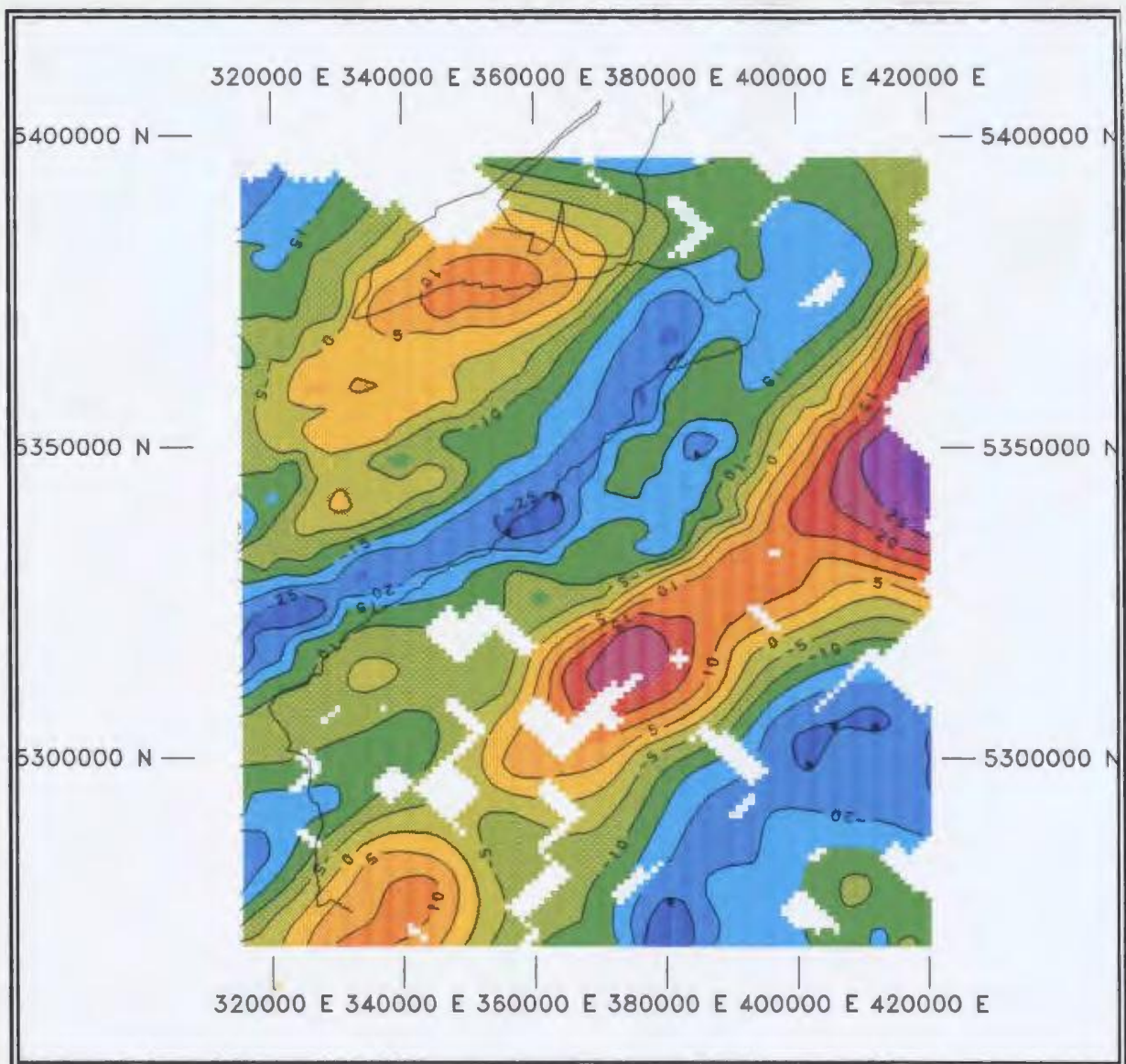


Figure 2.4. Bouguer anomaly map of the St. George subbasin. Contour intervals at 5 mgals. Empty spaces are areas with no data.

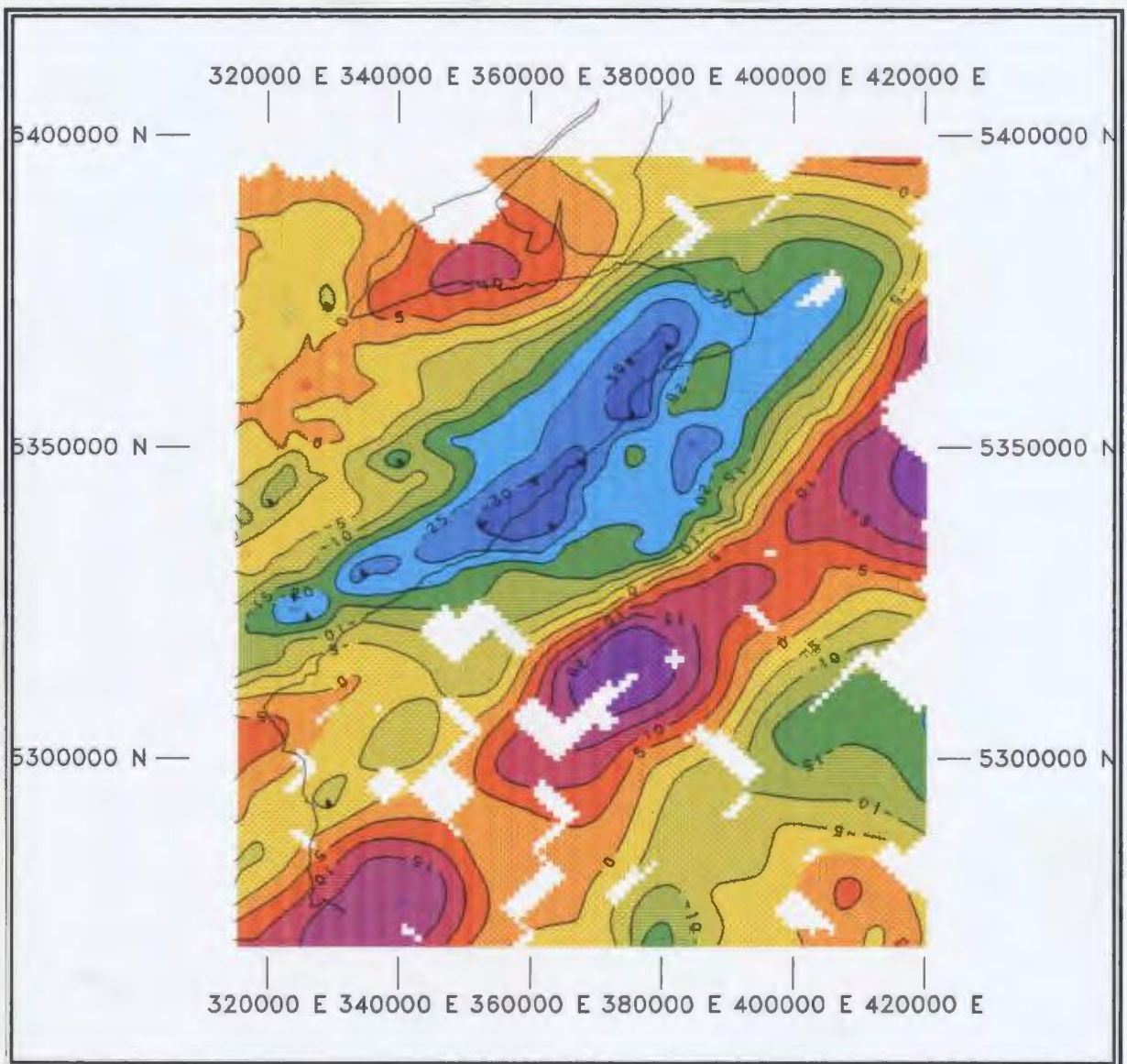


Figure 2.5. Residual anomaly map of the St. George subbasin after fitting a third order polynomial surface to the Bouguer anomaly map of figure 2.4.

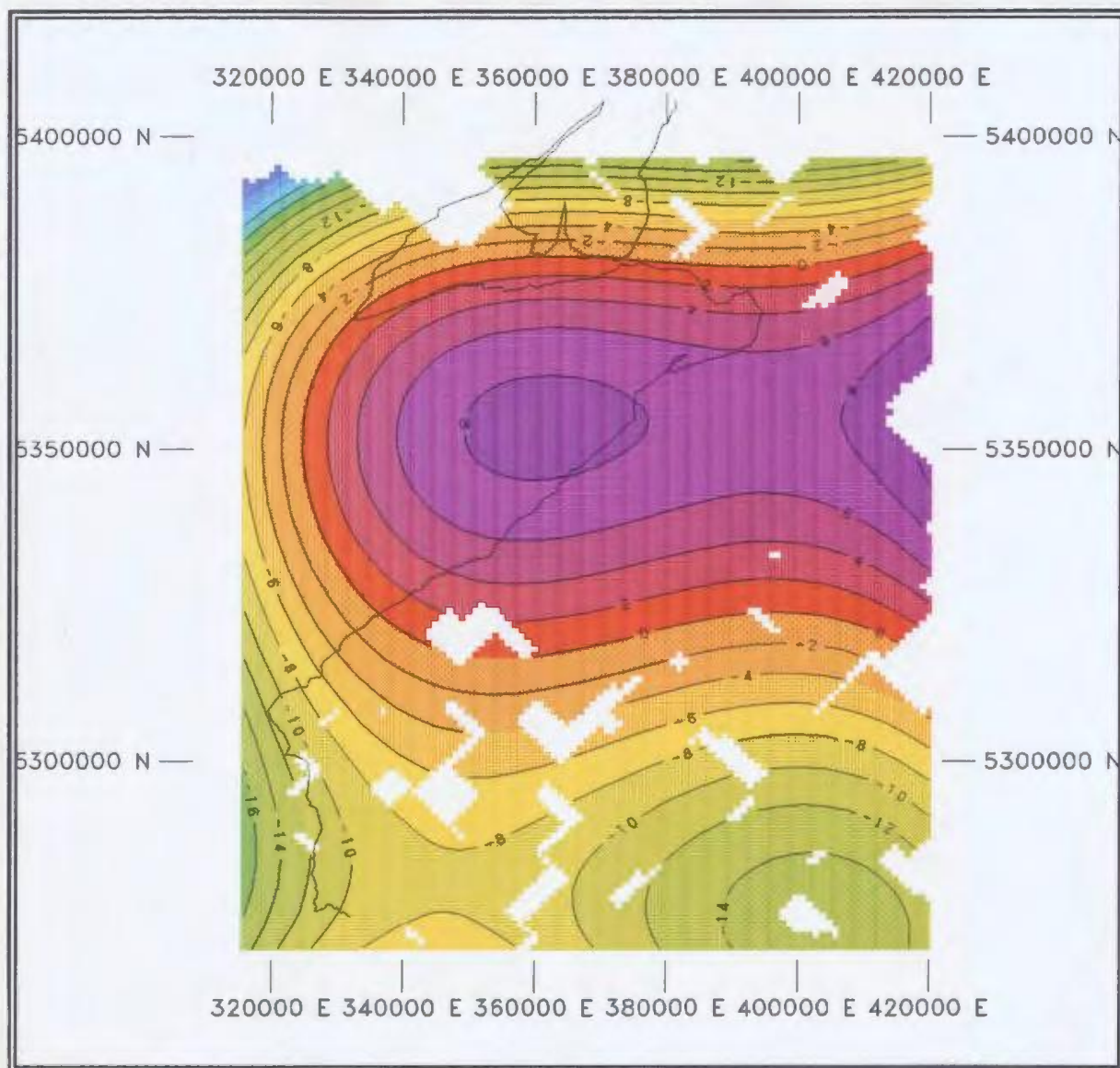


Figure 2.6. Plot of polynomial surface fitted to the Bouguer anomaly map.

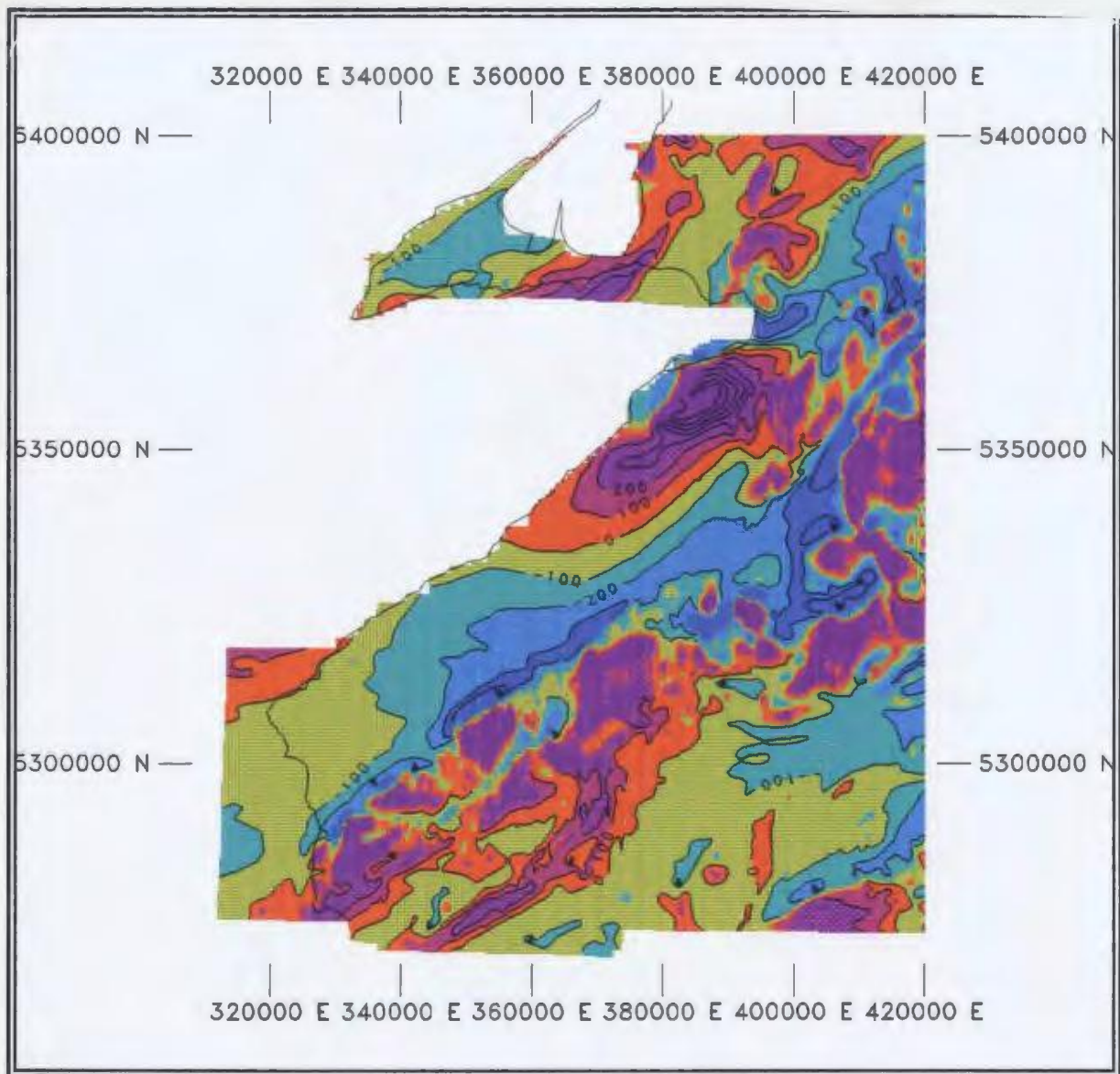


Figure 2.7. Magnetic data after fitting a third order polynomial surface to the original data. Contour intervals 100 nanoT.

Positive residual gravity anomalies correspond to small dimension basement topographic highs, and negative residuals indicate local thicker sedimentary accumulations, or even the presence of evaporites (Miller et al., 1990). The residual maps indicate that the sediments occur on both gravity and magnetic low (see Figures 2.5 and 2.7). There are some areas within the sedimentary basin with magnetic highs, especially the Flat Bay anticline. This is assumed to be floored by the Indian Head Complex. Other magnetic highs could be related to the basement which is assumed to have lenses of magnetite (Peavy, 1985). More negative gravity anomalies in the offshore correlate with the thickening of the Carboniferous sediments there. The strong northeast trending gradient with a positive step to the southeast corresponds to the Long Range Fault that defines the boundary of the basin (Miller et al., 1990). The Anguille and Flat Bay anticlines are expressed as relative gravity highs paralleling the general trend of the Long Range Fault. The general pattern of closely spaced gravity contours associated with these features suggests that both are fault-bounded to the west, with westward downthrow and thickening of the sedimentary wedge.

In addition to the strong northeasterly trends, secondary east-west trends are also significant. East-west lineations formed by the truncation and apparent dextral offset of residual gravity features indicate the presence of the east-west trends. Strike sensitive filtering also discerns these features.

Legend of figure 2.7

1	Pre-Carboniferous Basement
5	Spout Falls Formation
5A	Fischell's Conglomerate
6	Ship Cove Formation
7	Codroy Road Formation
8	Robinson's River Formation (undivided)
8A	Jeffrey's Village Member
8B	Highlands Member
11	Undivided Barachois Group

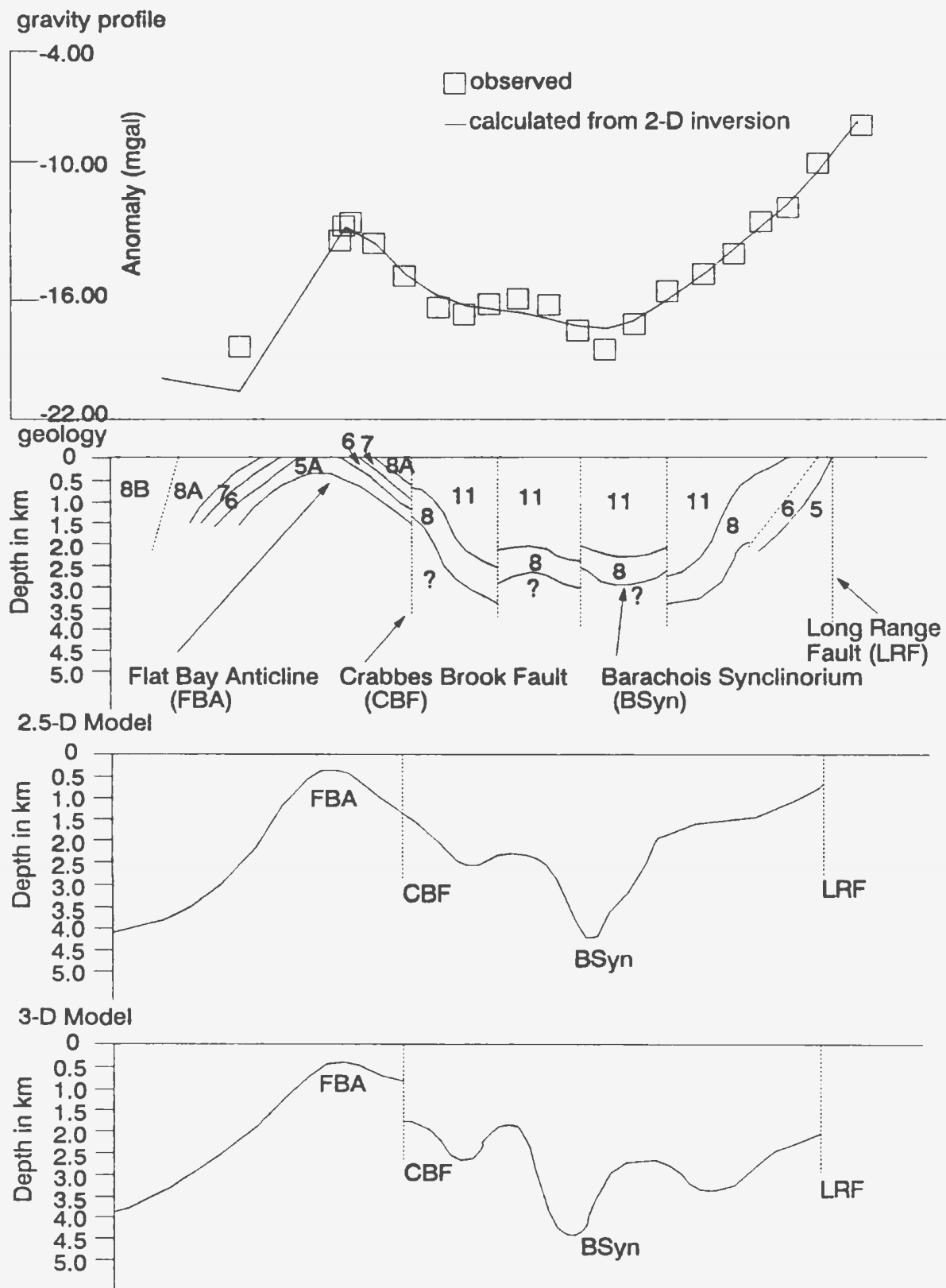


Figure 2.8. Cross-section near Robinson's River showing gravity profile, geology, 2-D and 3-D gravity models (after Peavy, 1985).

2.5.3.2 Quantitative Analysis

Peavy (1985) used a 2.5-D gravity inversion and 3-D forward modelling on profiles across the subbasin in order to determine the basement topography and the thickness of the sediments. Before undertaking the inversion qualitative interpretation of the gravity and magnetic data was made similar to that discussed above. In all the profiles a density contrast of -0.18 g/cm^3 between the average sediments and basement was used. All stations with positive anomalies were removed from the profiles because the density contrast is negative. A strike length of 60 km, determined from a geology map, was used in all of the 16 profiles.

From the 2.5-D inversion model, the Crabbes Brook Fault was interpreted to have an apparent downthrow to the west of 1.5-2.0 km at the northern end, reduced to 0.5 km near the Anguille Anticline. The average depth of the Barachois Synclitorium determined from this study was ~ 4 km. The average thickness of the sediments in the Brow Pond area was about 1.5 km. The thickness of the Anguille strata in the southern part of the area was not well defined owing to the limited number of data points in this area.

The results of the 3-D modelling were in good agreement with the 2.5-D inversion. Figure 2.8 is a cross-section close to and parallel with the Robinson's River seismic line showing the geology and 2.5-D and 3-D models. The only difference between the two models was a 2 mgal discrepancy in the Barachois area.

Potential fields solutions are non-unique. All the above results need to be

constrained with other geophysical data. Kilfoil (1988) tried to use some of the available offshore seismic data in the area to constrain his models. Four profiles were modelled. One of the models (Figure 2.9) is shown here alongside the interpretation of a seismic line across the same section. The modelling process was one of interactive forward modelling after inversion techniques had been developed and used to determine the configuration of the evaporite deposits (Kilfoil, 1988). The model shown here demonstrates that the Carboniferous sediments fill a half-graben structure with the thickest sediments just offshore. In contrast the sediments are thinner onshore. Offshore sediments are up to 6 km thick, while onshore sediments attain thicknesses up to 3 km (Miller et al., 1990).

2.5.4 Seismic data

Kilfoil (1988) used the offshore data acquired by Mobil Oil in the early 1970's to do an integrated gravity, magnetic and seismic interpretation of Bay St. George.

The most prominent reflector, identified on most of the seismic sections and denoted by the thick line in Figure 2.8, is interpreted as the pre-Carboniferous basement. From this section it is obvious that the basin thickens, in general monoclinaly, to the southeast. The southeastward dip of the strong reflector is interrupted locally by at least one basement fault downthrown to the northwest. Basement reflector picks on the seismic lines trending east-northeast have very little dip, indicating that these lines are oriented nearly parallel to basin strike, as is

expected from trends observed on the gravity maps (Miller et al., 1990).

The seismic data support the interpretation that the basin is an asymmetrical half-graben with the basement dipping toward the Bay St. George southeastern coastline and striking subparallel to the Long Range Fault, which defines the basin margin.

The Mid-Bay and Red Island strike-slip faults have also been mapped in Bay St. George (Langdon, pers. comm., 1992). These two faults trend parallel or subparallel to the Long Range Fault and take up some of the dextral offset associated with the regional strike-slip system.

Salt structures that have been mapped offshore trend parallel to the regional fault system and probably are oriented according to stress conditions at the time of faulting. These salt structures are offset by subsidiary east-west faults discussed earlier.

The Cabot Strait seismic data displays features similar to the Robinson's River data; this particularly applies to the structural style of the detachment within the salt at the base of the Codroy (see Figure 2.10). The basin in this area, bounded by the Long Range Fault and the southward extension of the St. George's Bay "Coastal Fault", is similar in shape and dimension to that observed in the Robinson's River area (Langdon, pers. comm., 1992).

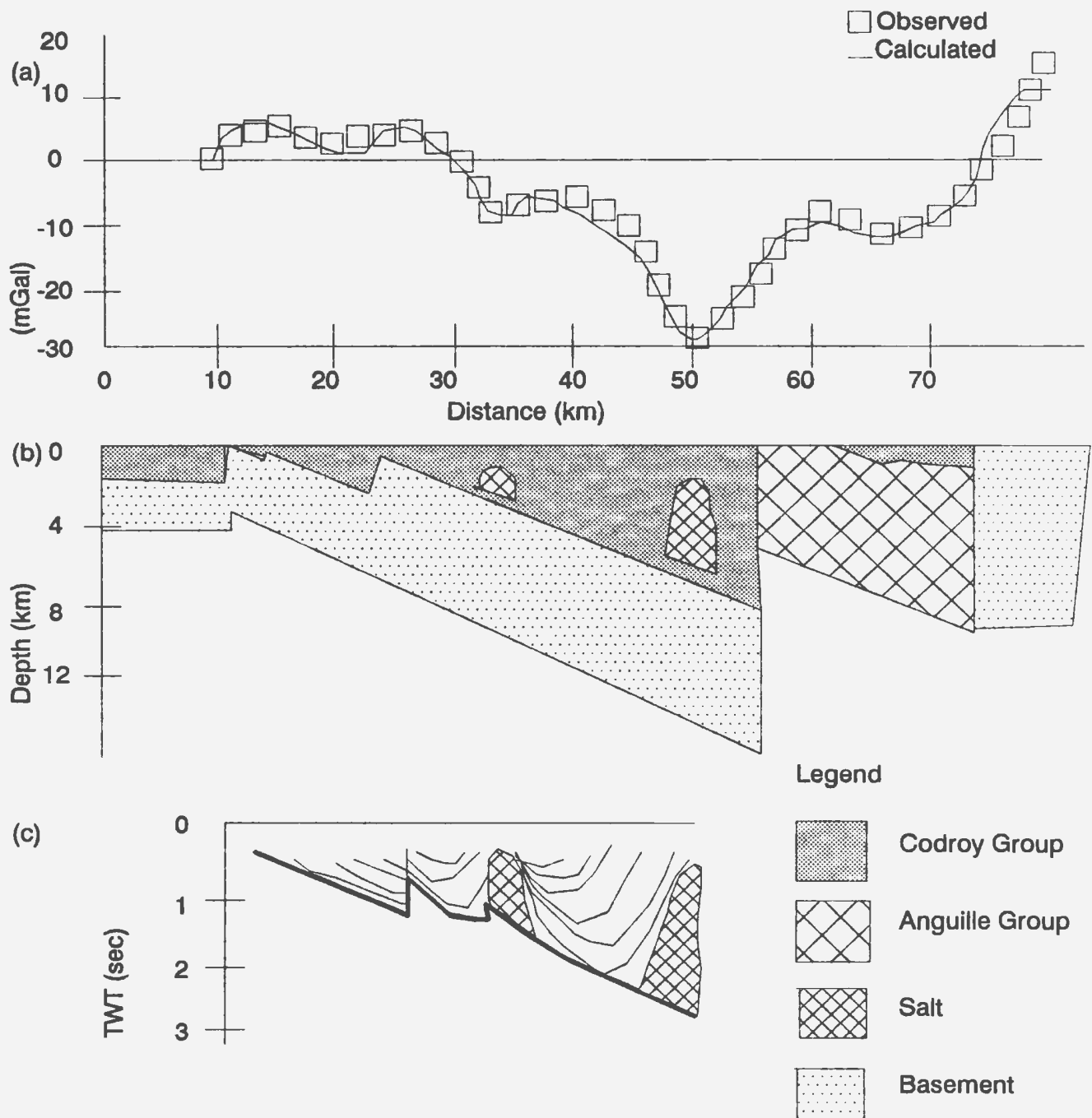


Figure 2.9. Modelled interpretation for profile B-B' oriented NW-SE (fig. 2.2) from Kilfoil (1988). a. Distance along profile in km indicated below gravity profile. b. Geological model inferred from gravity and seismic data along B-B'. c. Two-way travel time line drawing of significant reflectors along the seismic line (E-20). Thick, dark line represents basement, thin lines are intra-carboniferous reflectors. Salt indicated by hatched pattern. Line is shown in correct lateral position relative to the longer gravity profile in (b). Vertical scale is two-way travel time in seconds. Horizontal scale is the same as in (a).

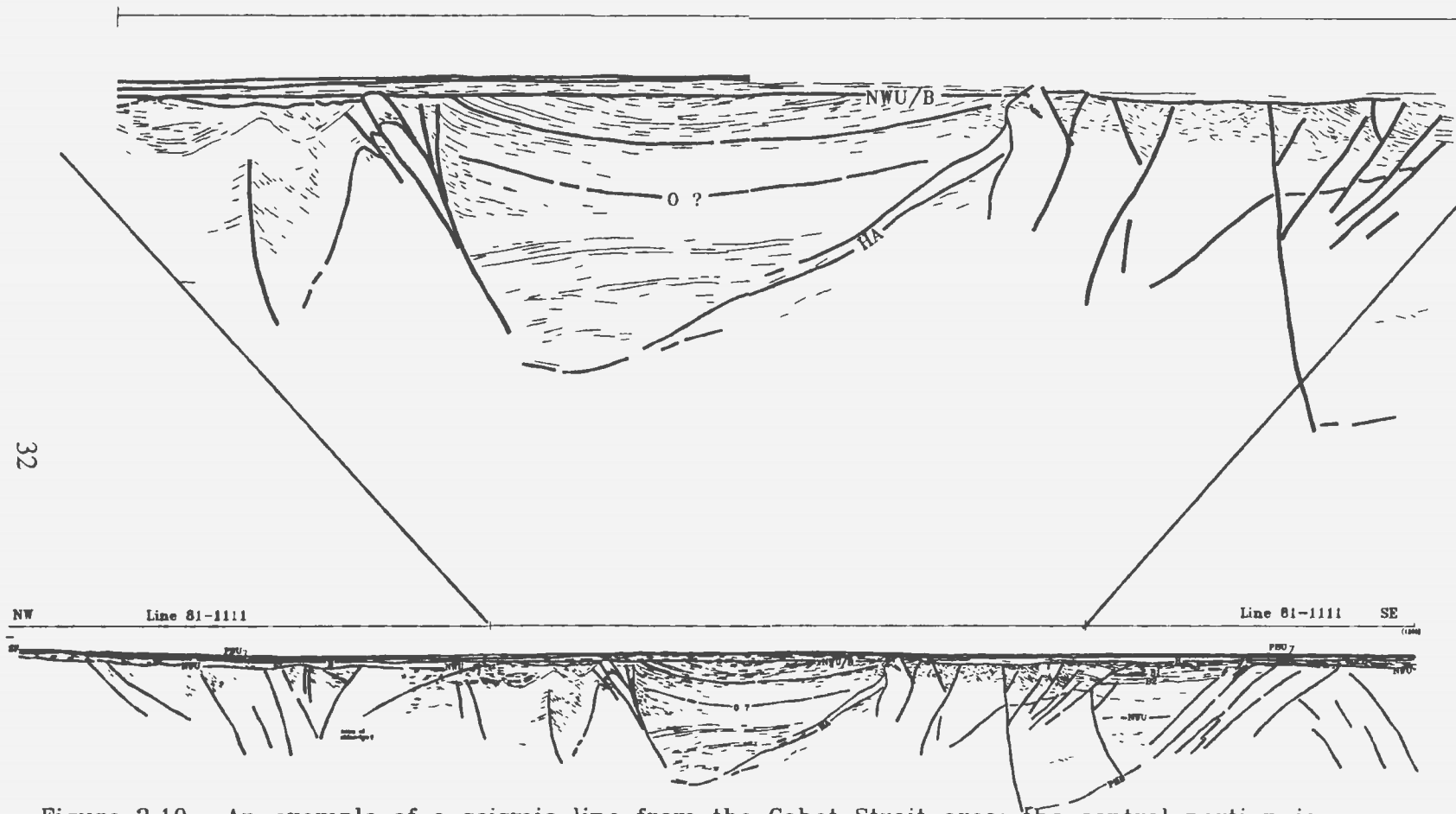


Figure 2.10. An example of a seismic line from the Cabot Strait area; the central portion is similar to the graben shown on the Robinson's data (modified from Langdon and Hall, in prep.).

Chapter 3: Seismic Reflection Profile

3.1 Introduction

The aim of the seismic survey was to image, by the seismic reflection method, the subsurface structure of the Carboniferous and older age rocks occupying an area of land in the vicinity of Robinson's River in the Bay St. George sub-basin of western Newfoundland (see Figure 2.2). Surface mapping and shallow borings had indicated a complex structure in the Carboniferous rocks in the area, but the overall structure appeared to be basinal (i.e. synclinal) with a possible thickness of 4 km of Carboniferous rocks in the area east of the Trans-Canada Highway (Knight, 1983). Thus, the seismic line was designed to test this structure.

12.68 km of seismic data were acquired and processed. The processed data show several sets of reflecting geological boundaries, some as deep as the base of the recorded section. A strong reflector at shallow depth, i.e. less than 2 km, appears to limit the downward extension of the complex structure mapped at the surface. Below the strong reflector are bands of reflectivity with apparently simpler structure.

After inspecting the processed data, it was felt that reprocessing of this line would possibly improve the events and hopefully the interpretation.

Therefore, the processing in this project was carried out more carefully than previously done. A few procedures were included that had not been carried out originally. Examples of these include field statics based on refraction picks, prestack migration i.e. dip moveout correction (DMO) and more velocity analyses.

3.2 Acquisition

The seismic profile was acquired for Memorial University of Newfoundland and the Government of Newfoundland and Labrador through a contract with Capilano Geophysical Limited of Calgary, Alberta. The field parameters and their tolerance for discretionary choice at the start of the survey, were agreed upon before the survey with staff of the Provincial Department of Mines and Energy. The parameters were as follows :

Recording instruments:	240 channel DFS V with Calder FS, recorded on digital magnetic tape in SEG Y format;
geophone group interval	20 m;
spread	symmetrical split, 26 station gap at v.p.;
geophones	12 per group, spaced at 1.5 m, 14 Hz;
source type	Vibroseis: 4 mertz vibrators (max. peak force 44000 lbs each) over 30 m;
vibration point (v.p) interval	40 m;
common depth point coverage	6000 percent (60 fold stack);
vibrator sweeps	4 per v.p. with 8 m move-up, each 8 s, non-linear 20-90 Hz;
record length	4 s (correlated data); data also recorded uncorrelated (12 s length);
sample rate	2 ms;
noise rejection	diversity stack plus alternating sweep anti-phase for 60 Hz rejection.

A gap of 13 stations (260 m) each side of the v.p. was chosen as a compromise of retaining data at short offset and avoiding high amplitude vibrator-generated noise

based on tests conducted at the beginning of the acquisition.

A 20-90 Hz non-linear (2 db/octave pre-emphasis) sweep ensured that ground-roll was avoided and the recording of high frequencies retained.

Because the spread length including the gap at the v.p. exceeded 5 km, and the total length was only 12-13 km, it was decided to roll in to the spread from the first geophone station using the same v.p. interval, and to roll off the end of the final spread. There was no gap employed during the roll-on and roll-off. The roll-on and -off was to ensure that the reflection point coverage extended the full length of the line and that the fold of the coverage near the line ends built up rapidly to the standard 60-fold.

Data were recorded using DFS instruments and a Calder Field System, with paper monitors of all shots produced on a Seistronix camera, and data recorded on digital magnetic tape in both correlated and uncorrelated form in SEG Y demultiplexed format at 6250 dpi.

3.3 Processing

3.3.1 Introduction

These field data were processed using the STARPAK software running on a CONVEX C1 XL mini-supercomputer.

The processing included crooked line binning, field statics based on refraction picks, dip moveout correction, CMP gather, notching of 60 Hz, NMO correction

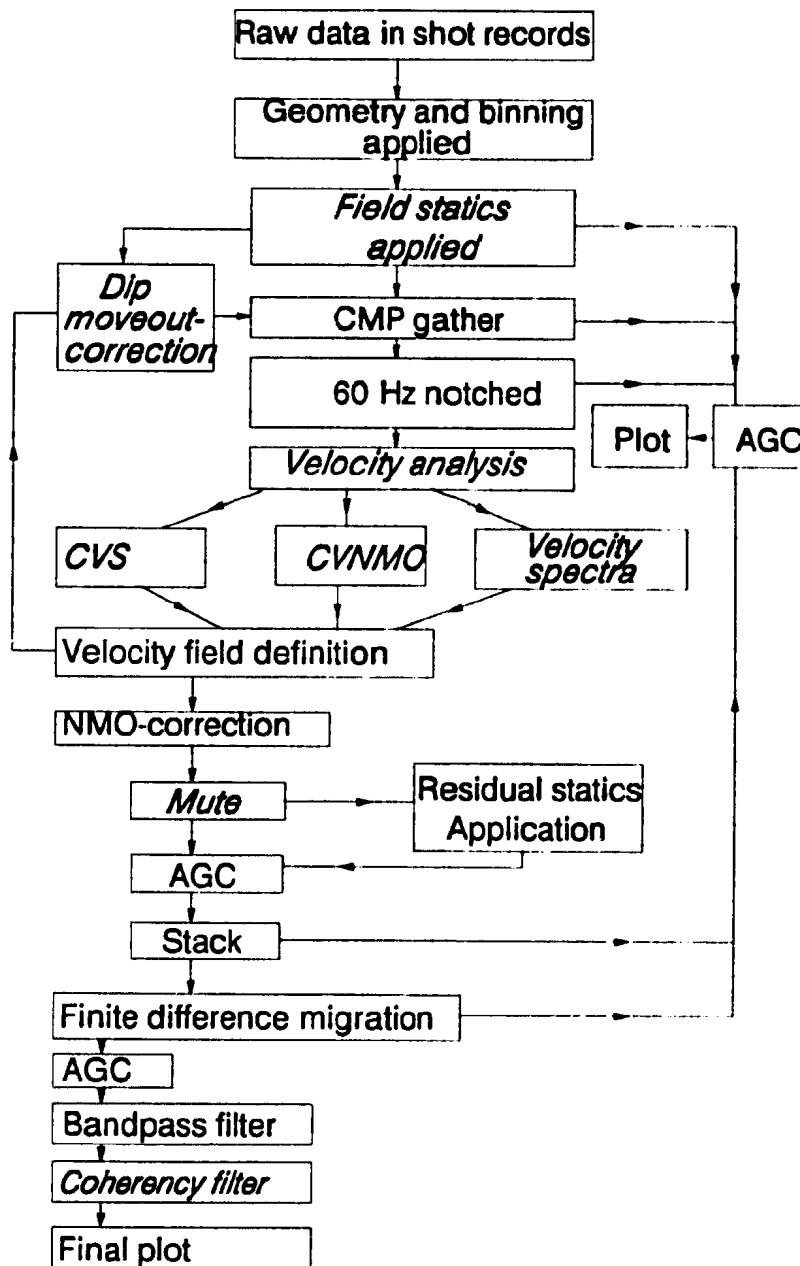


Figure 3.1. Data processing sequence. The processes in italics are either new or those done thoroughly in this project compared to previous processing of Hall et al. (1992).

based on velocity analyses and constant velocity stacks, front mute, gain equalization, CMP stack, residual statics, time-varying bandpass filter, trace sum, finite difference time migration, coherency filtering and display. The order of the processing procedure is summarized in Figure 3.1.

3.3.2 Pre-stack processing

3.3.2.1 Geometry and Binning

The binning strategy in this project was as determined previously in the original processing.

The binning that was applied was a crooked line that was based on a processing line that gave a best fit to the midpoint distribution along the line. Owing to the surface gradients and line bends, the distribution of 635 stations at a surface-taped interval of 20 m corresponds to a total horizontal crooked line length of 12.05 km as opposed to 12.68, the taped surface distance. Thus, on the final sections, every 10th station number was annotated for every 19th CMP rather than every 20th, so as to compensate for the difference in surface and crooked line geometries. The geometry of the job was set in the original data processing. The binning procedure included setting up of the bins of width and length of 10 and 20 m respectively and applying them to the shot records.

After binning only 72316 traces out of a total of 76320 (240 traces for each of the 318 shot records) traces fell into 1251 bins because 4875 traces did not fall into any

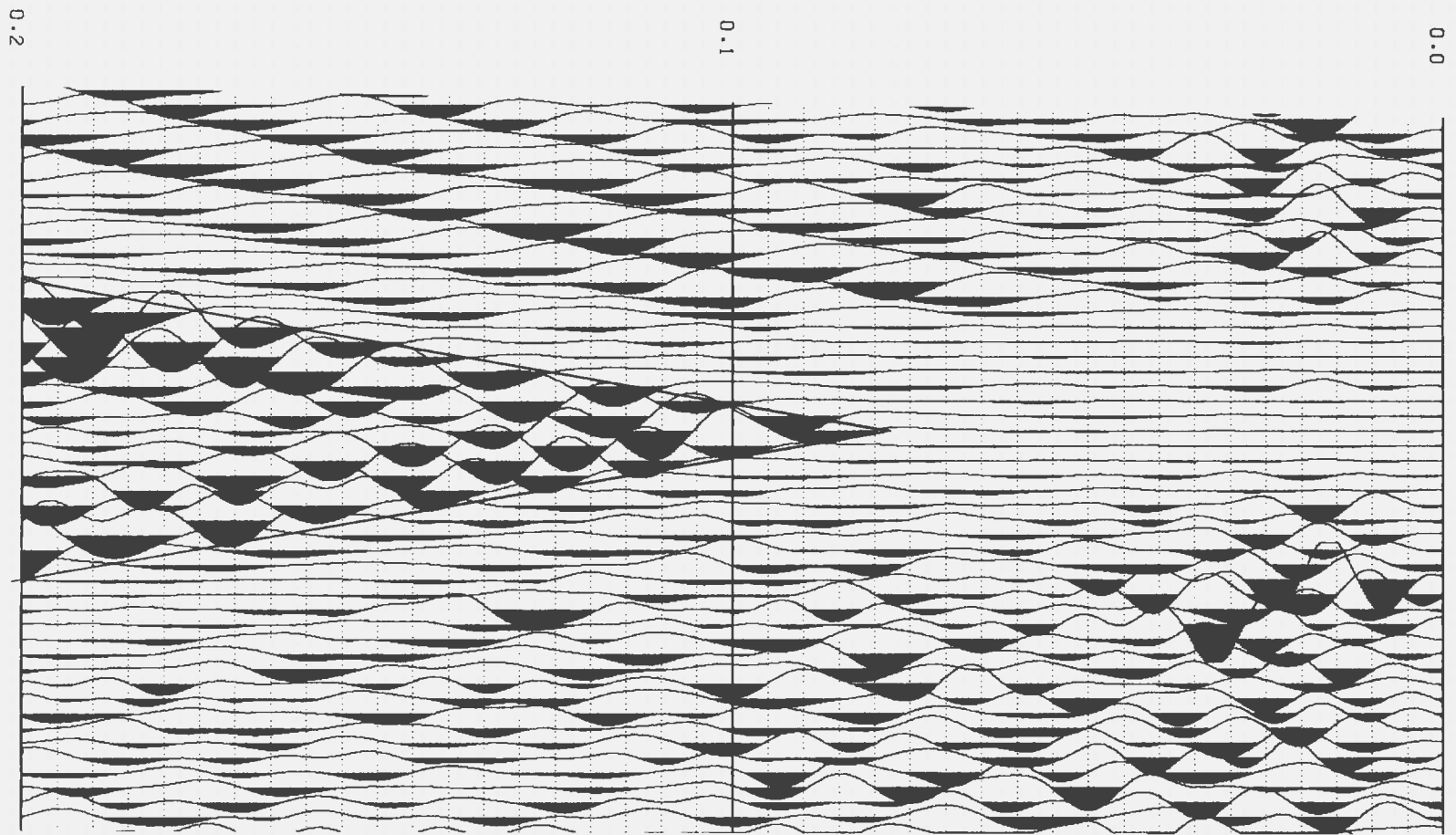


Figure 3.3. Shot record 250 from TWT 0.0 to 0.2 s showing example of section used to estimate refraction picks.

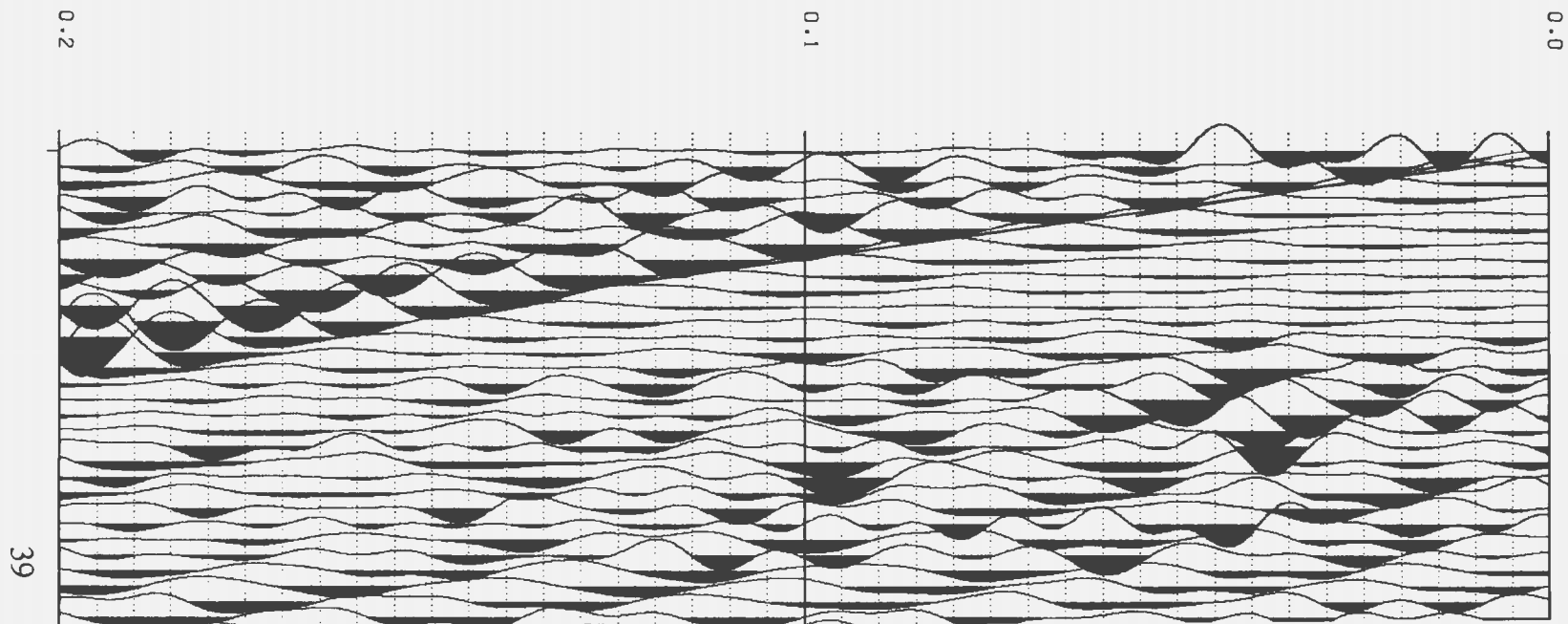


Figure 3.4. Shot record 1 from TWT 0.0 to 0.2 showing portion used to estimate velocity of the weathered layer.

bin. There were 70574 traces in at most one bin, 871 traces in at most 2 bins and no traces falling in at most 3 bins. The maximum fold of any bin was 104 traces. The binning chart, Figure 3.2, is in folder. The binning width and length was 10 m and 20 m respectively.

3.3.2.2 Field static corrections

The aim of field statics corrections is to correct for the irregularities in the topography and in the thickness of the weathered layer in the subsurface.

The field statics corrections were based on velocities estimated from the first breaks of the shot records. All the shots were plotted using vertical and horizontal scales of 100 cm/s and 5 traces/cm respectively (see Figure 3.3). Only the first 0.2 seconds of the shot records were analyzed because this was the only region of the data with reasonably good refractions. The vertical scale ensured time picking a resolution of 1 ms, thus quite accurate velocities and time intercepts could be picked. From each shot record, time intercept (t_i) and velocity of the bedrock (v_b) could be determined. The velocity of the weathered layer (v_w) was determined from the direct arrivals of the non-gapped records (see Figure 3.4). The assumption made at this point was that the direct seismic wave travelled at the top of the weathered layer. Thus, the slope of the direct wave is the reciprocal of the velocity of this layer. The following two equations were used to get the thickness of the weathered layer (z_w) and the static correction (Yilmaz, 1987) (t_D) respectively;

$$Z_w = \frac{v_b v_w t_1}{2 (v_b^2 - v_w^2)^{\frac{1}{2}}} \quad (3.1)$$

$$t_D = \frac{-Z_w}{v_w} + \frac{(E_D - E_s + Z_w)}{v_b} \quad (3.2)$$

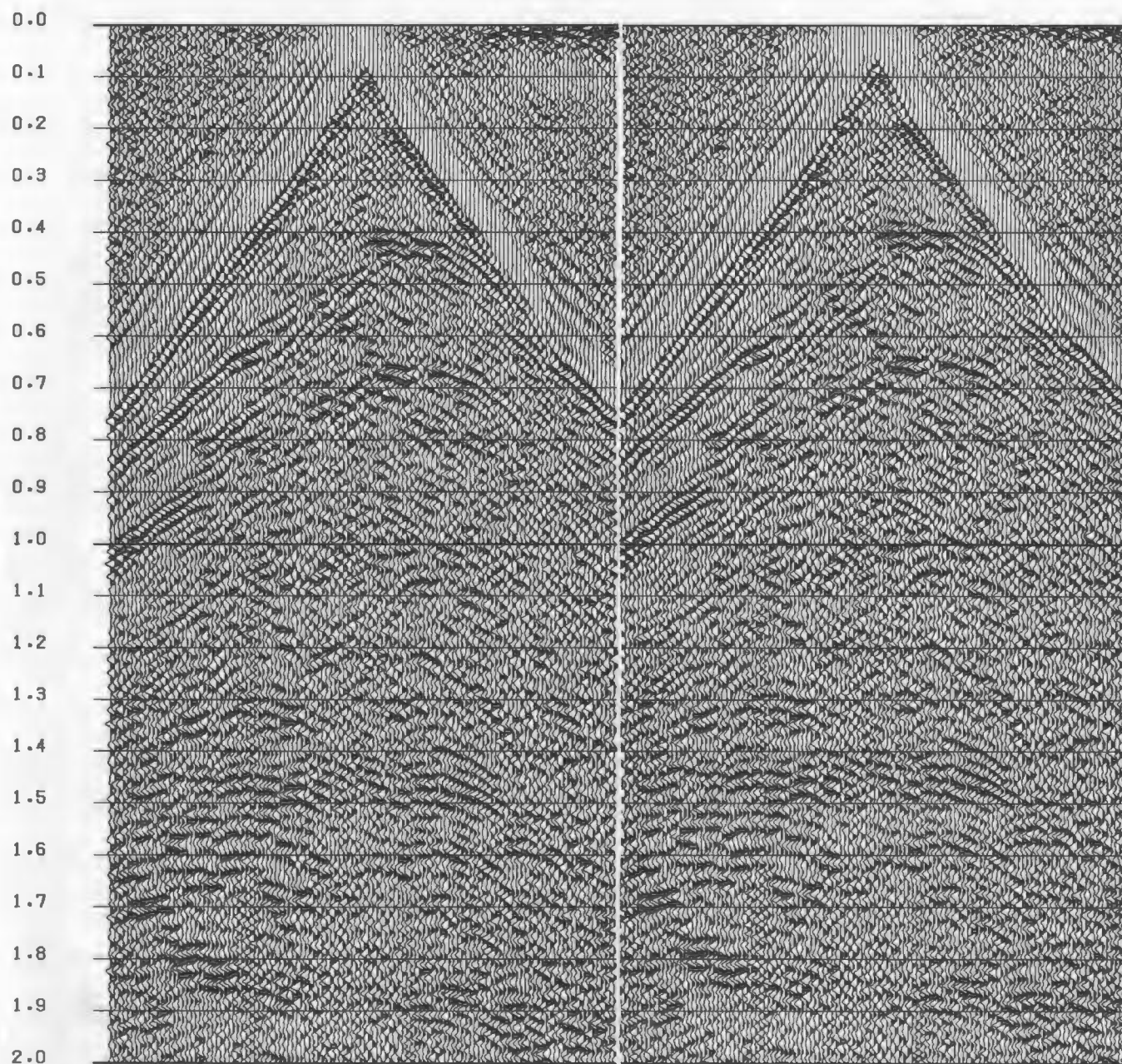
where E_D and E_s are the datum plane and the elevation in metres respectively. The datum plane was chosen as 150 m, to keep the statics as close to zero as possible. This was to ensure that the data were not shifted too much for further processing ; this is especially important for velocity analyses.

From the results obtained it was observed that v_b varied from 2.8 km/s to approximately 5.0 km/s and the lowest value of t_D was -39 ms while the highest value was +6 ms (see Appendix A). The velocity of the weathered layer (v_w) was estimated to be about 2.0 km/s. This value is high but is the best estimate from the non-gapped shot records (see Figure 3.4).

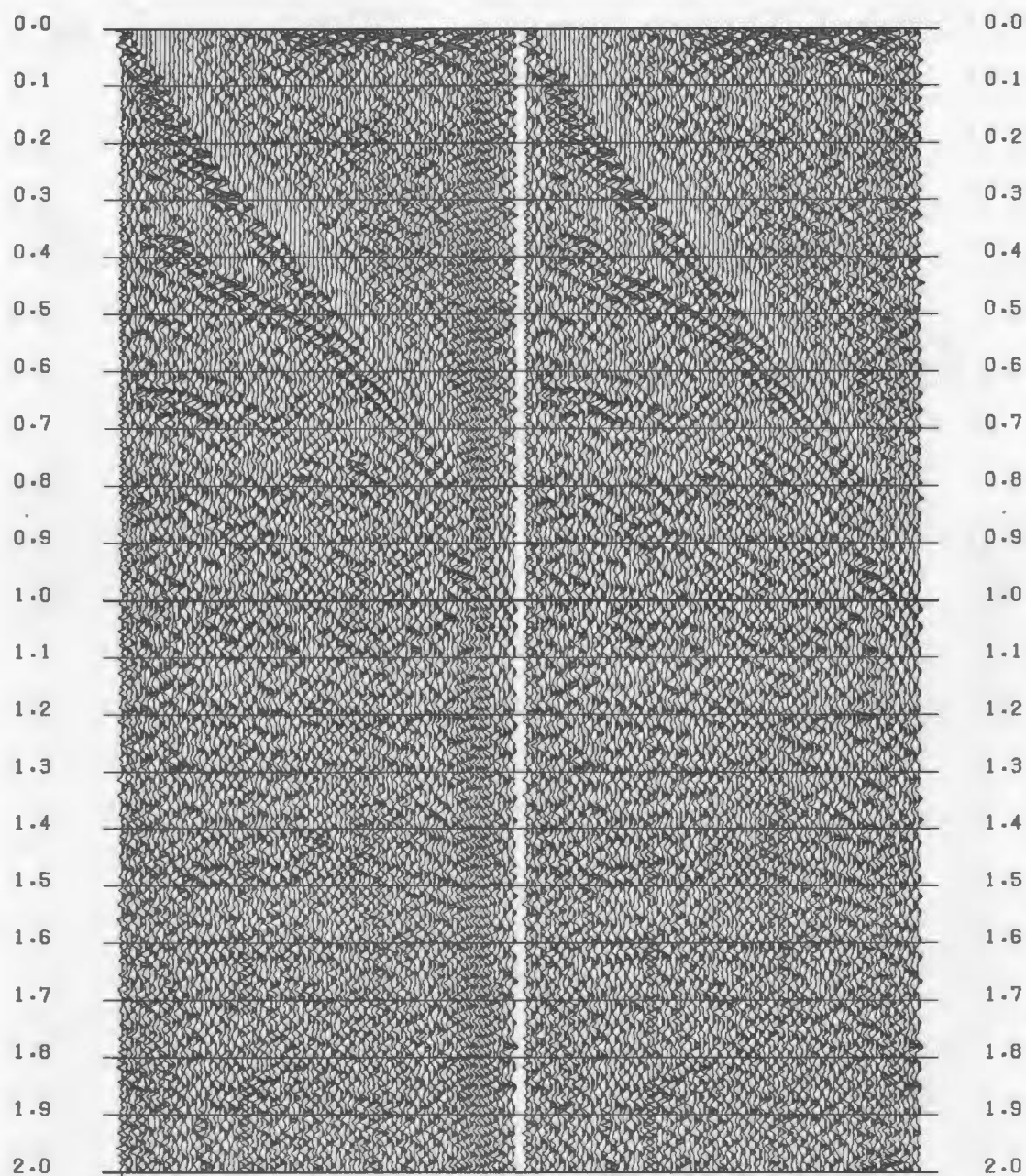
The values for the elevation were measured during the data collection.

The values of statics calculated were applied to the shot records after binning and geometry had been applied. The time, t_D , was simply added to each shot and the appropriate receiver traces respectively.

Figure 3.5 displays the results of field static corrections. From Figure 3.5b it can



(a) (b)
 Figure 3.5. Shot record 250 from twt 0.0 to 2.0 sec. (a) Before applying field statics.
 (b) After field statics corrections. There is not much difference between the two
 records, except that the events are shifted in (b) slightly upwards.



(a) (b)
 Figure 3.6. CMP 1000. (a) Before notching 60 Hz. (b) After applying a notch filter to reject 60 Hz, 120 Hz, 180 Hz etc i.e. multiples of 60 Hz noise.

be observed that there is not much difference between the two shot records. This was expected because of the modest values of t_0 .

3.3.2.3 CMP gather

After binning and geometry were established, the data which had been either corrected for field statics or corrected for both field statics and dip moveout was sorted into CMP records. All the CMPs were saved on tape ready for further processing. Every 20 th CMP was plotted to check for any kind of noise inherent in the data. Though 60 Hz noise was minimized during data acquisition, this noise was still present in the CMP gathers. To eliminate this noise, a notch filter, which rejected 60 Hz, 120 Hz, 180 Hz, i.e. multiples of 60 Hz, was used (see Figure 3.6). This filter was applied in the time domain.

3.3.2.4 Velocity analysis

3.3.2.4.1 Constant-Velocity Stacks (CVS)

The whole set of data was NMO-corrected at constant velocities and stacked. The velocities ranged from 2500 m/s to 5500 m/s. The choice of these velocities was based on refraction picks (Table A1) and previous processing by Hall et al. (1992). At low velocities (2500 m/s to 3300 m/s) an increment of 100 m/s was used, otherwise at high velocities (3500 m/s to 5500 m/s) the increment was 200 m/s. At lower velocities the normal moveout, defined by the following equation (Robinson,

1983):

$$\Delta t_{NMO} = \frac{x^2}{2 t_0 V_{NMO}^3} \quad (3.3)$$

is large, thus it was felt that small increments of velocity would retain more information, i.e. events would not come into, and fall out of, focus between velocities. At larger velocities the increment was increased, since the likelihood of losing data between velocities is less.

The CVS were done for only the first 2 seconds of the data and all stacks (see Figures 3.7a to 3.7t, in folder) were plotted on paper for visual analysis. This is because most of the reflectors for which velocity estimation is critical are in this section. Figures 3.7a to 3.7t display all the velocities which were analyzed. The velocity picks on figures 3.7a to 3.7t were made after a comparison between these figures and the velocity spectra, and at the same time trying to discriminate against possible multiples. The data in this project image a complex structure, so CVS were particularly useful in choosing the stack with the best possible event continuity (Yilmaz, 1987).

The CVS were used to compare velocity picks from CVNMO and velocity spectra.

3.3.2.4.2 Constant velocity normal moveout (CVNMO)

Every 50 th CMP was NMO-corrected at constant velocities that ranged from 2500

to 5500 m/s at increments of 200 m/s. The results were displayed on paper for velocity picks (see Figure 3.8, in folder). This type of velocity analysis was important in determining velocities at $T(TWT)=0$. Otherwise, it was difficult to pick velocities from this analysis owing to the complex structure of this seismic line. Nonetheless, CVNMO gave a good velocity check to the velocity spectra and CVS.

3.3.2.4.3 Velocity spectra

Velocity analysis using contours (semblance plots) were performed on every 50 th CMP. The contours plotted were normalised semblance, which implies that the highest possible value is unity. For clarity, only values 0.3-1.0 at intervals of 0.1 were contoured. This ensured that the effects of noise were minimized. Velocity spectra display stacking velocity analyses from CMP gathered records.

Let us say we have traces a_1, a_2, \dots, a_N and we want to find semblance at a certain time 'T'. This is found for a set of velocities (V_1, V_2, \dots, V_m). The move-out time using a hyperbolic normal move-out velocity v_j for a trace with range ' r_i ' is (STARPAK Reference Manual, 1989):

$$T_i(V_j) = \sqrt{T^2 + \frac{r_i^2}{V_j^2}} \quad (3.4)$$

The move-out times are rounded to the nearest sample point:

$$w_{ij} = (T_i(V_j) + \frac{SR}{2}) \quad (3.5)$$

where T_i is the time at velocity v_j and r_i is the range while SR is the sample rate.

For a window length 'u' and a single velocity V_j , we have a grid of move-out data;

$a_1(w_{1j}), a_1(w_{1j} + SR), \dots, a_1(w_{1j} + u),$

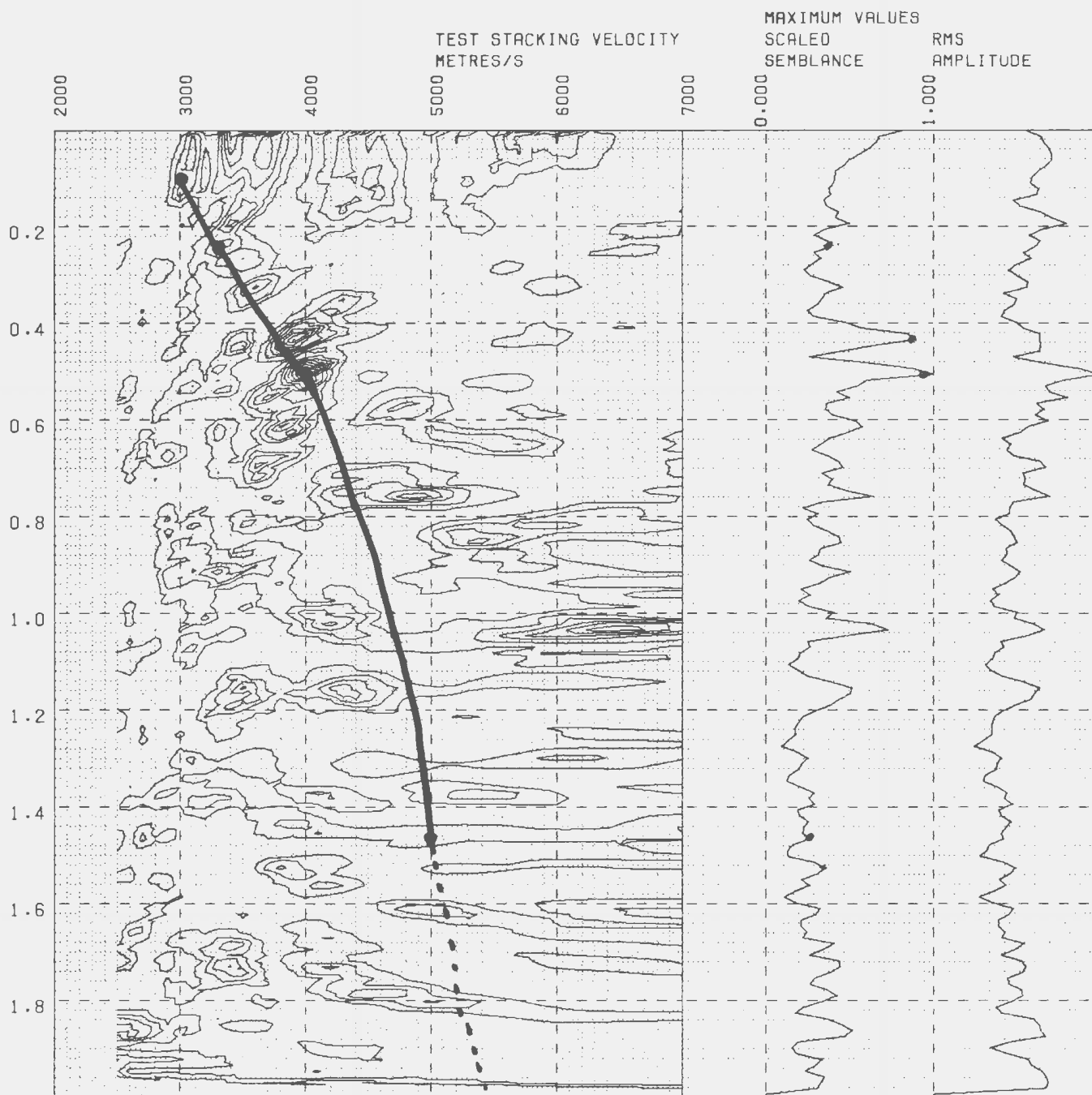
$a_2(w_{2j}), a_2(w_{2j} + SR), \dots, a_2(w_{2j} + u),$

$a_N(w_{Nj}), a_N(w_{Nj} + SR), \dots, a_N(w_{Nj} + u).$ One of the ways of measuring the goodness of the move-out velocity is by finding the semblance, defined as:

$$Semblance = \frac{(\sum x_i)^2}{\sum x_i^2} \quad (3.6)$$

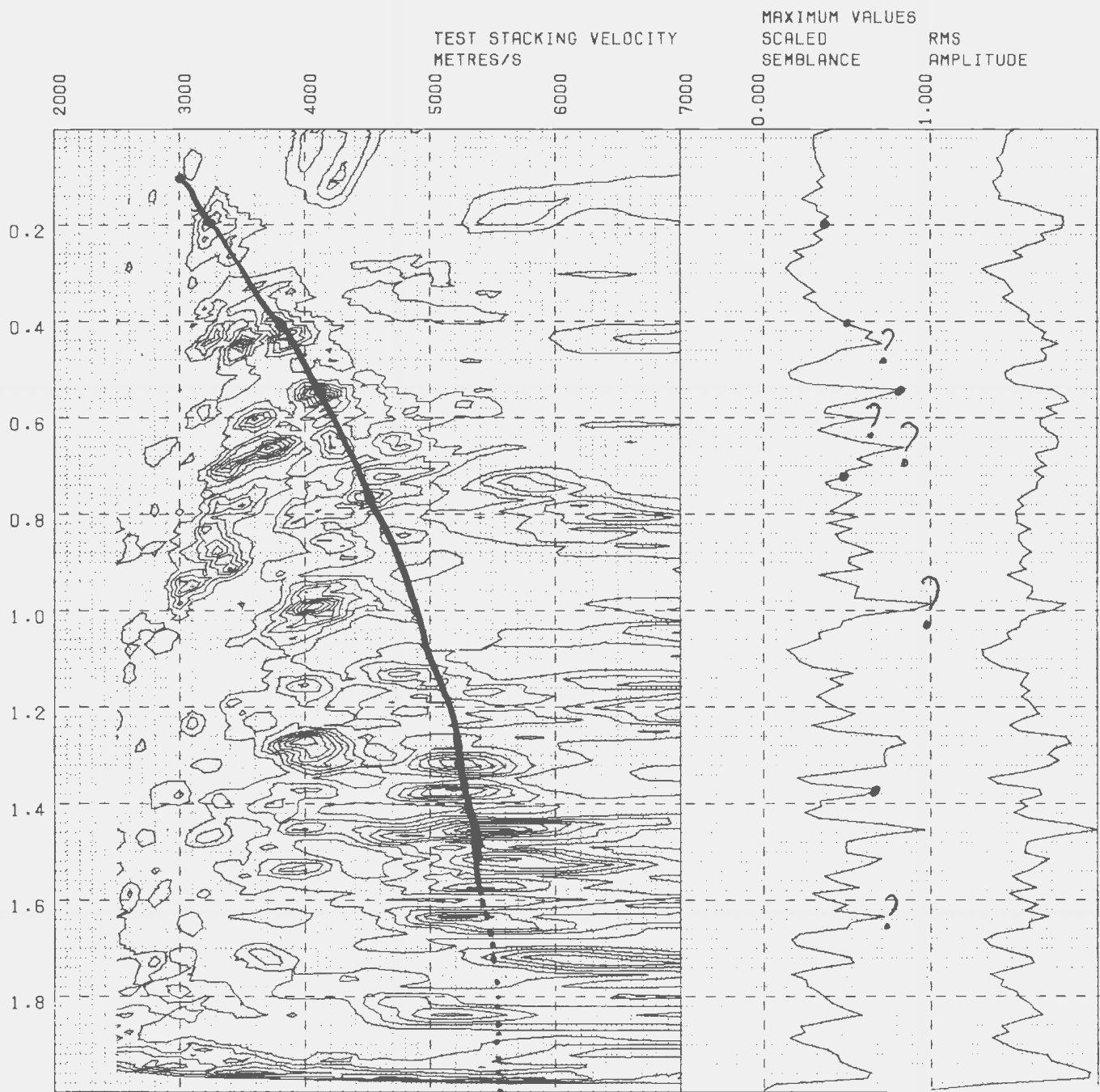
for a set of numbers. Semblance is unity when all the numbers are equal and as low as zero when the summed value is zero. In the case of multiple time samples in the window, the multichannel semblance is defined to be (Neidell and Taner, 1971):

$$SEM_j = \frac{\sum_{u=0}^u (\sum_{i=1}^N a_i(w_{ij} + u))^2}{N \times \sum_{u=0}^u \sum_{i=1}^N a_i(w_{ij} + u)^2} \quad (3.7)$$



(a)

Figure 3.9. Velocity spectrum of CMP 950. (a) Velocity spectrum before DMO correction. (b) velocity spectrum after DMO correction. Notice the increase in magnitude of both semblance and amplitude after DMO correction. Black dots are possible velocity picks. The question marks indicate probable multiples.



(b)
Figure 3.9 (cont.)

It should be noted that semblance includes cross-terms between traces and also terms of the overall energy of the traces.

To calculate the semblance, interpolation was done between the highest and the lowest velocities, which were 2500 and 5500 m/s, using a velocity increment of 100 m/s.

Let an input trace be divided in fixed time gates t_1, \dots, t_n . Then the amplitude is defined as ;

$$A = \sqrt{\text{Re}X(f)^2 + \text{Im}X(f)^2}$$

where $x(f)$ is the Fourier transform of the input trace in time series. The RMS amplitude plotted in Figure 3.9 is defined as (Yilmaz, 1987) ;

$$A_{RMS} = \sqrt{A_{t1}^2 + A_{t2}^2 + \dots + A_{tn}^2}$$

In most instances only a single CMP was analyzed at a time, though in some cases the average semblance of about 10 to 12 CMPs were contoured. This was to check for continuity of real events and to discriminate against false events. Only the first 2 seconds of the data were analyzed because most of the reflectors are in this region. Velocity spectra were measured on CMPs both before and after DMO correction (see Figure 3.9). From a comparison of Figures 3.9a and 3.9b, it can be observed that the

Table 3.1. Velocity definition before DMO-correction.

CMP	T	V	T	V	T	V	T	V	T	V	T	V
50	100	3050	220	3200	3500	5500						
100	100	3000	260	3300	3500	5500						
150	140	3500	220	3700	3500	5500						
160	0	3300	200	3700	520	4000	3500	5500				
270	0	3300	200	3700	520	4000	3500	5500				
300	0	2700	300	2800	560	4000	3500	5500				
350	0	2700	300	2800	580	4100	3500	5500				
400			200	2800	300	3100	1300	4500	3500	5500		
450			200	3100	360	3300	440	3800	1300	4500	3500	5500
500					400	3450	840	4200	3500	5500		
550	80	2900	240	3300	460	3700	1020	4700	1640	5000	3550	5500
600	0	2700	140	3400	480	3900	1440	5000	3500	5500		
650	0	2900	240	3200	460	4100	1280	4500	1500	5000	3500	5500
700	0	3300	200	3600	520	4400	1500	5000	3500	5500		
750	140	3400	560	4400	1400	5000	3500	5500				
800	120	2900	600	4100	1220	4400	1600	5000	3500	5500		
850	140	3000	260	3400	600	4000	1380	4600	1800	5000	3500	5500
900	200	2900	300	3500	520	3750	600	4100	1800	5000	3500	5500
950	100	3000	220	3400	500	4000	1460	5000	3500	5500		
1000	200	3200	380	3900	640	4300	1460	5000	3500	5500		
1050	200	3200	300	3400	600	4200	1500	4900	3500	5500		
1100	0	3300	220	3600	600	4000	1440	5100	3500	5500		

T is two way time in ms and V is velocity in m/s.

Table 3.2. Velocity definition after DMO-correction.

CMP	T	V	T	V	T	V	T	V	T	V	T	V	T	V
50	120	3000	220	3200									3500	5500
100	40	3000	100	3100	260	3300	380	3700	440	4000	500	4400	3500	5500
150	0	3300	210	3500	440	4200	3500	5500						
200	80	3600	500	4000	3500	5500								
250	0	3300	80	3700	600	4100	1100	4600	3500	5500				
300	210	2600	500	3600	940	4400	3500	5500						
350	0	2800	560	3400	820	3900	940	4300	1740	4800	3500	5500		
400	0	2700	300	3100	660	3300	860	3800	1600	4700	3500	5500		
450	0	2700	380	3400	440	3700	660	4000	1300	4600	3500	5500		
500	0	2800	220	3100	400	3400	600	3800	1080	4700	3500	5500		
550	80	2900	460	3900	840	4600	1080	4700	1640	5000	3500	5500		
600	100	2900	220	3200	460	4000	1180	4600	1440	5000	3500	5500		
650	0	3300	340	3600	460	4100	800	4500	1300	4800	1500	5000	3500	5500
700	0	3300	300	3700	500	4000	960	4600	1080	4800	1540	5000	3500	5500
750	100	3400	600	4400	1000	4800	1560	5000	3500	5500				
800	60	3000	580	4200	1260	4600	1380	5000	3500	5500				
850	160	3000	600	4000	1300	4600	1580	5000	3500	5500				
900	100	2900	520	3700	600	4100	1440	5000	3500	5500				
950	100	3000	200	3200	400	3800	540	4100	760	4500	1380	5200	3500	5500
1000	0	3000	160	3100	380	3700	600	3900	740	4400	1380	5200	3500	5500
1050	0	3000	280	3400	600	4100	1360	5200	3500	5500				
1100	0	3300	320	3500	400	4200	600	4500	1720	5000	3500	5500		
1150	140	2800	300	3500	440	4200	980	4800	1600	5000	3500	5500		
1200	100	2700	400	4000	3500	5500								

T is two way time in ms and V is velocity in m/s.

Table 3.3. Mute specifications.

CMP	W	T	W	T	W	T	W	T	W	T
50	20	100	500	230	861	420	1558	600	1989	700
145	180	100	510	300	2385	760				
165	23	100	529	200	1500	530	2300	700	4336	950
265	19	100	500	300	4424	1060				
305	352	100	509	360	1538	800	3588	1100		
425	252	100	500	350	1700	700	2474	1060		
505	352	100	509	290	2486	900				
525	257	100	500	260	2200	780	2400	860		
565	232	100	540	220	2538	850				
625	280	100	590	290	2000	680	2500	770		
705	233	100	550	270	1770	600	2459	730		
745	654	100	809	350	2000	620				
765	635	100	960	340	2100	630				
785	630	100	950	360	2400	710				
805	342	100	513	260	1540	520	2350	720		
845	280	100	485	220	1540	640	2450	780		
885	336	100	500	240	1500	600	2100	650		
1005	60	100	500	210	1500	550	3400	950		
1085	38	100	500	200	1300	600	2500	860		
1125	75	100	500	190	1200	450	1900	580		
1145	19	100	500	230	1600	500				

T is two way time in ms and w is range in metres.

DMO corrected CMP has more picks than the CMP not DMO corrected. The magnitudes of the velocities did not vary much after DMO, (see Tables 3.1 and 3.2) but the amplitudes and the semblance of the events increased, as can be observed from Figure 3.9. The velocity picks on Figure 3.9 were based on high semblance and increase in velocity with increase in time. This was aimed at discriminating against possible multiples.

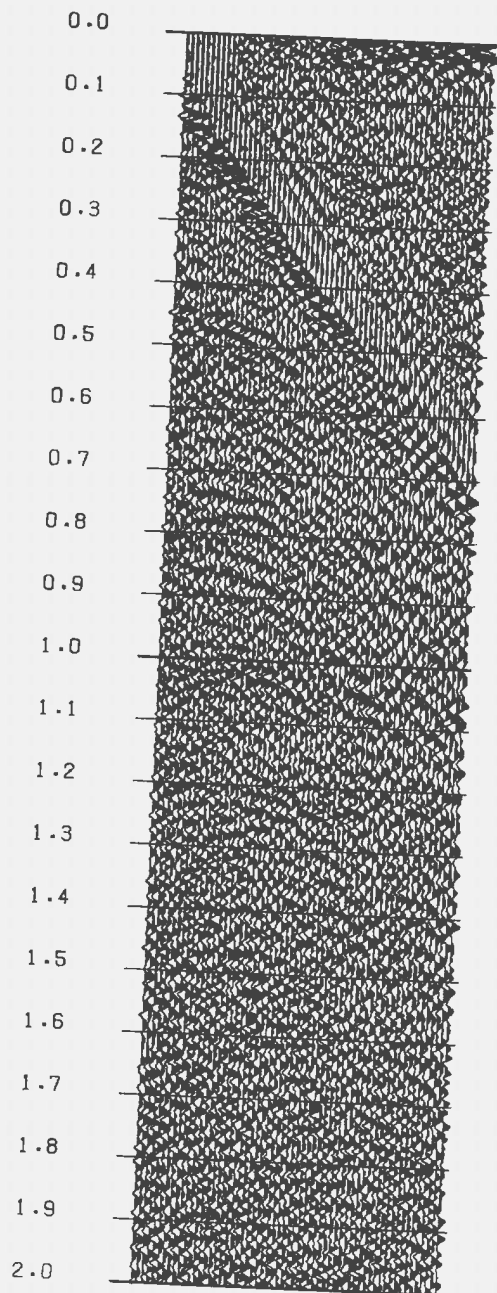
The velocity field specification was based primarily on velocity spectra with checks with CVS and CVNMO (cf. Figure 3.9 with Figure 3.10 in folder).

3.3.2.4.4 Velocity field definition

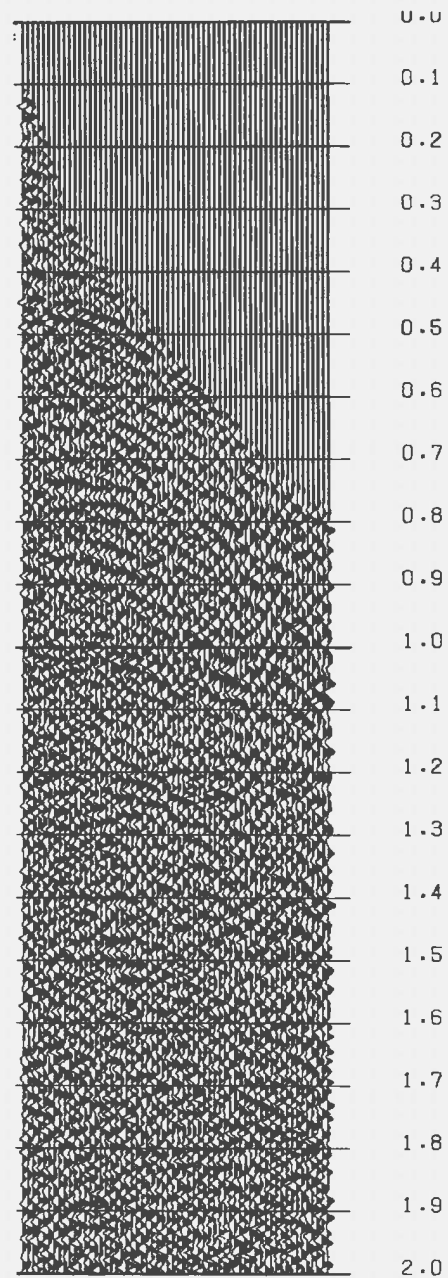
After all the velocity picks, the velocities were plotted as a function of CMPs. This was important in checking for typing errors and final adjustment of the velocities. The final results of velocity picks are displayed in tables 3.1, 3.2, Figures 3.11 and 3.12 (both Figures in folder).

3.3.2.5 Mute

Muting is used to alter portions of a trace to zero (mute). The aim of muting in this project was to remove refractions and wavelets distorted by normal moveout i.e. "stretch". A front mute, which sets amplitudes of all samples between the start of the trace and the given mute value to zero, was used as defined in table 3.3. A front taper of 40 ms was used to prevent sharp data edges (STARPAK Processing manual, 1989).

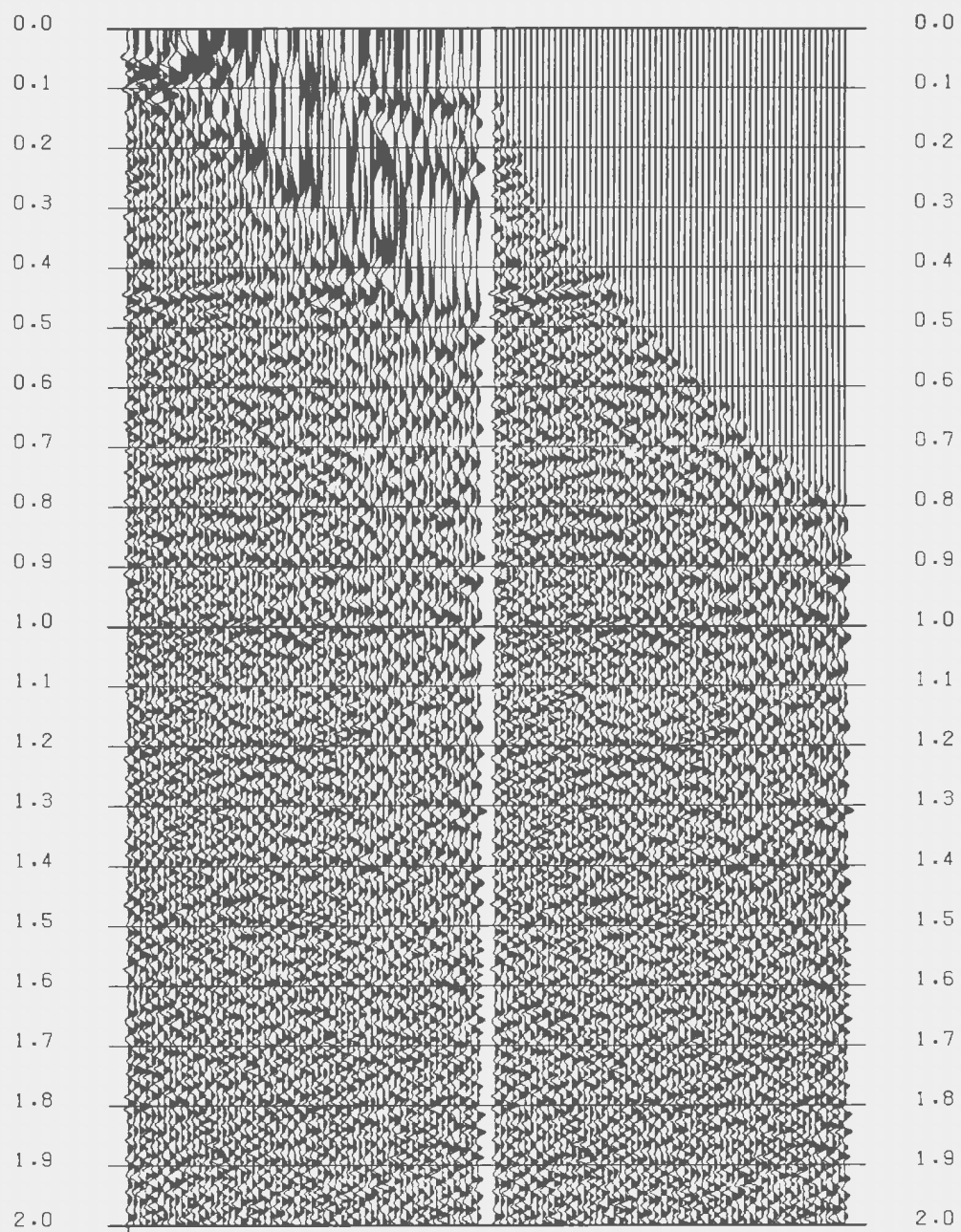


(a)



(b)

Figure 3.13. CMP 630. (a) Before front muting. (b) After muting. (c) With NMO stretch. (d) With NMO stretch muted.



(c)

(d)

Figure 3.13 (Cont.)

The mute values (Table 3.3) were determined by inspecting every 20 th CMP. A transparency was passed along the CMPs, such that every time the alignment of first arrivals on the CMP changed, the mute specifications were changed. Figure 3.13 illustrates the effects of front muting CMP 630 to remove refractions and NMO stretch.

3.3.2.6 Dip Moveout correction (DMO)

The aim of dip moveout-correction (DMO) is to remove the effects of a dipping layer on the moveout velocity in a CMP gather. A dipping reflector increases the moveout velocity, compared to a non-dipping reflector, by a factor of $1/\cos\theta$, where θ is angle of dip relative to horizontal. The assumption made in NMO-correction is that the ground is horizontally layered, which is not always the case. DMO is the process which corrects the effect of dip in the data after normal moveout (NMO) and transforms it to zero-offset data (Biondi and Ronen, 1987).

3.3.2.6.1 DMO Theory

The impulse response in time-space coordinates of the DMO operator derived by Biondi and Ronen (1987) is an ellipse:

$$\left(\frac{t}{t_1}\right)^2 + \left(\frac{x - x_1}{x_1}\right)^2 = 1 \quad (3.8)$$

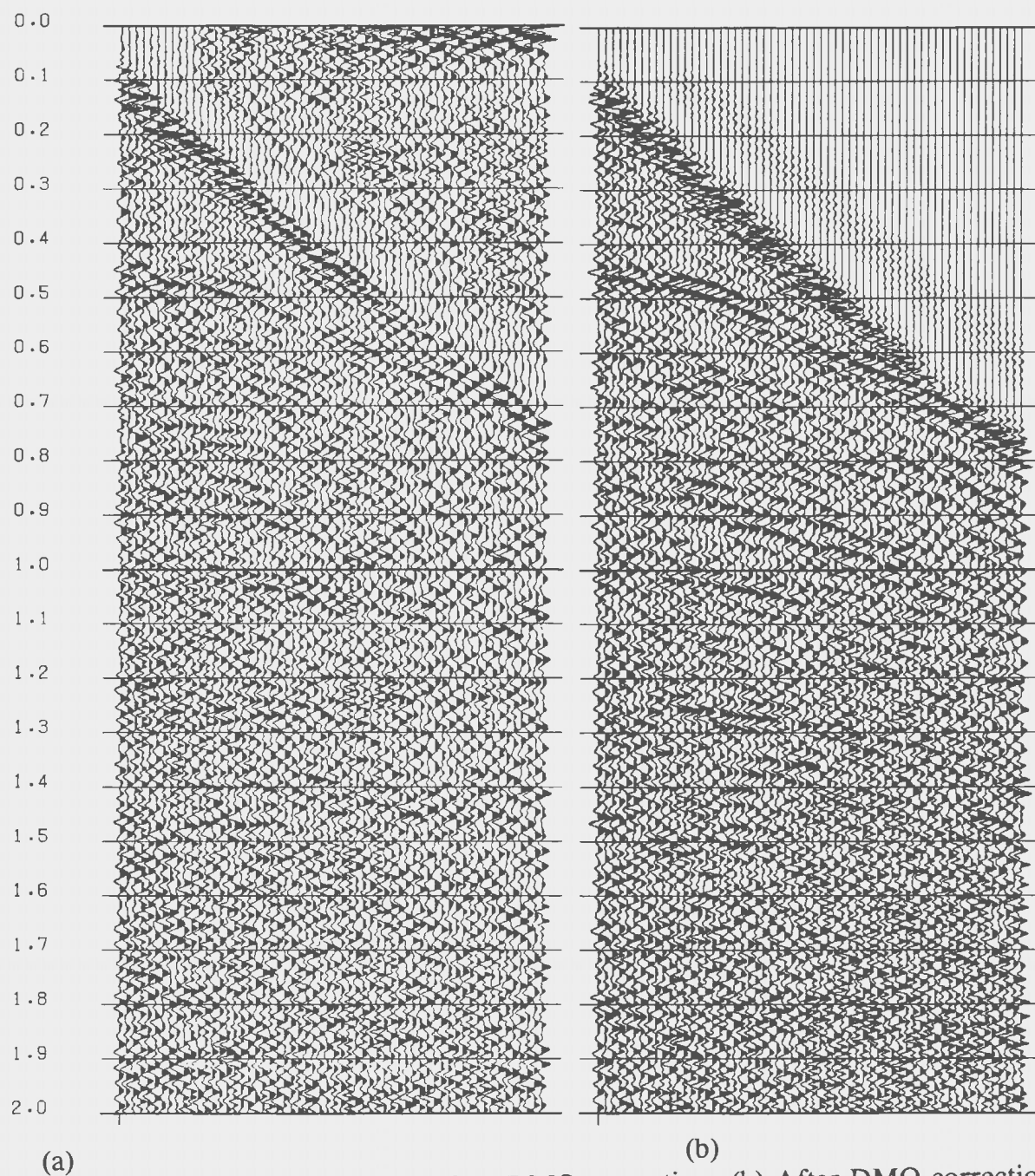


Figure 3.14. CMP 630. 9 (a) Before DMO correction. (b) After DMO correction. Note the improvement in the focus of events in (b). The muting in (b) was automatic in the process of DMO correction, but was reasonable.

where t_1 is the location of the impulse and x represents full offset. The above equation is only part of the operator, no amplitude information is included in it. Amplitude information is ignored at this point due to its uncertainty. The final result after all the analytical computations is:

$$\begin{aligned}
 g(m\Delta t, k) = & \sum_{n=-\infty}^{\infty} f(n\Delta t, k) [e^{jkl\Delta n[1 - \sqrt{1 - (\frac{m}{n} + 1)^2}]} \\
 & - e^{jkl\Delta n[1 - \sqrt{1 - (\frac{m}{n})^2}]} - e^{jkl\Delta n[1 + \sqrt{1 - (\frac{m}{n+1})^2}]} \\
 & + e^{jkl\Delta n[1 + \sqrt{1 - \frac{m^2}{n^2}}]}] \quad (3.9)
 \end{aligned}$$

where $t = m * \Delta t$ and $s = n * \Delta t$. The complete derivation of equation 3.9 is contained in Appendix B. The above expression is the DMO operator used in this project. It is implemented by stretching the space axis of an NMO-corrected shot gather, Fourier transforming the space axis, multiplying and integrating according to equation B.9, inverse transforming the space axis and then finally unstretching the space axis.

3.3.2.6.2 Application of DMO

DMO has to be applied in shot records whose geometry and binning have been established. Since this information is stored in the trace headers, velocity specification

can be defined in terms of CMP numbers. Therefore, velocities defined in section 3.3.2.4 were used to NMO correct the shot records, because DMO is only applied in STARPAK to data which have been NMO corrected. After DMO correction, NMO correction was removed from the shot gathers. The shot records were subsequently sorted to CMP records for further processing. DMO improves the events and removes a lot of noise from the data, as can be observed in Figure 3.14.

3.3.2.7 Automatic Gain Control (AGC)

This is a trace-wise amplitude balancing process and so does not preserve spatial relative amplitudes. The equalization of amplitudes by AGC for structural mapping and conventional plotting defeats attempts to discern amplitude variations associated with changes in gas/water saturation or lithology (Dobrin and Savit, 1988).

A fixed or variable length window slides down the trace one sample at a time. Within this window of the original unbalanced trace, the average of the absolute amplitudes is calculated (STARPAK processing manual, 1989);

$$A = \sum_{i=1}^N \frac{|a_i|}{N} \quad (3.10)$$

The ratio of the desired output average amplitude (AVGAMP) to the average amplitude calculated within the window is the gain scalar applied to the central sample point in the window:

$$S = \frac{AVGAMP}{A} \quad (3.11)$$

where AVGAMP is the average amplitude normalization level.

AGC was applied mainly before plotting (see Figure 3.1), except before stack, to suppress anomalous amplitudes.

The final plot was gained using a window of 500 ms, otherwise a window of 1000 ms was used always.

3.3.2.8 Stack

The aim of stacking is to sum together all NMO corrected traces in a CMP record and output one stacked trace for each record. It is a very powerful tool for improving the signal-to-noise ratio of the data (Rietsch, 1980). The data were not weighted, only a direct summation being applied to the traces. Before stacking the data, all CMPs were NMO-corrected using the velocities defined in section 3.3.2.4. Subsequently the data were muted to remove refraction arrivals and NMO stretch. The mutes are as specified in table 3.3.

Let a trace be represented as (Rietsch, 1980):

$$a_{ij} = s_j + n_{ij} \quad (3.12)$$

where a_{ij} is the j th sample of the first trace in the record, s_j is the j th sample of the signal, the same on all traces. n_{ij} is the noise at the j th sample of the i th trace. The stacked trace A_j is simply the sum of the 'L' traces in the record:

$$\begin{aligned} A_j &= \sum_i a_{ij} \quad (3.22) \\ &= \sum_i (s_j + n_{ij}) \\ &= L \times s_j + \sum_i n_{ij} \end{aligned} \quad (3.13)$$

The signal-to-noise ratio on a single trace is the ratio of the signal energy to the noise energy:

$$\left(\frac{s}{n_i} \right)^2 = \frac{\sum_j s_j^2}{\sum_j n_{ij}^2} = \frac{s^2}{n_i^2} \quad (3.14)$$

The signal-to-noise ratio of the stacked trace is:

$$\left(\frac{s}{N} \right)^2 = \frac{\sum_j (L \times s_j)^2}{\sum_j ((\sum_i n_{ij})^2)}$$

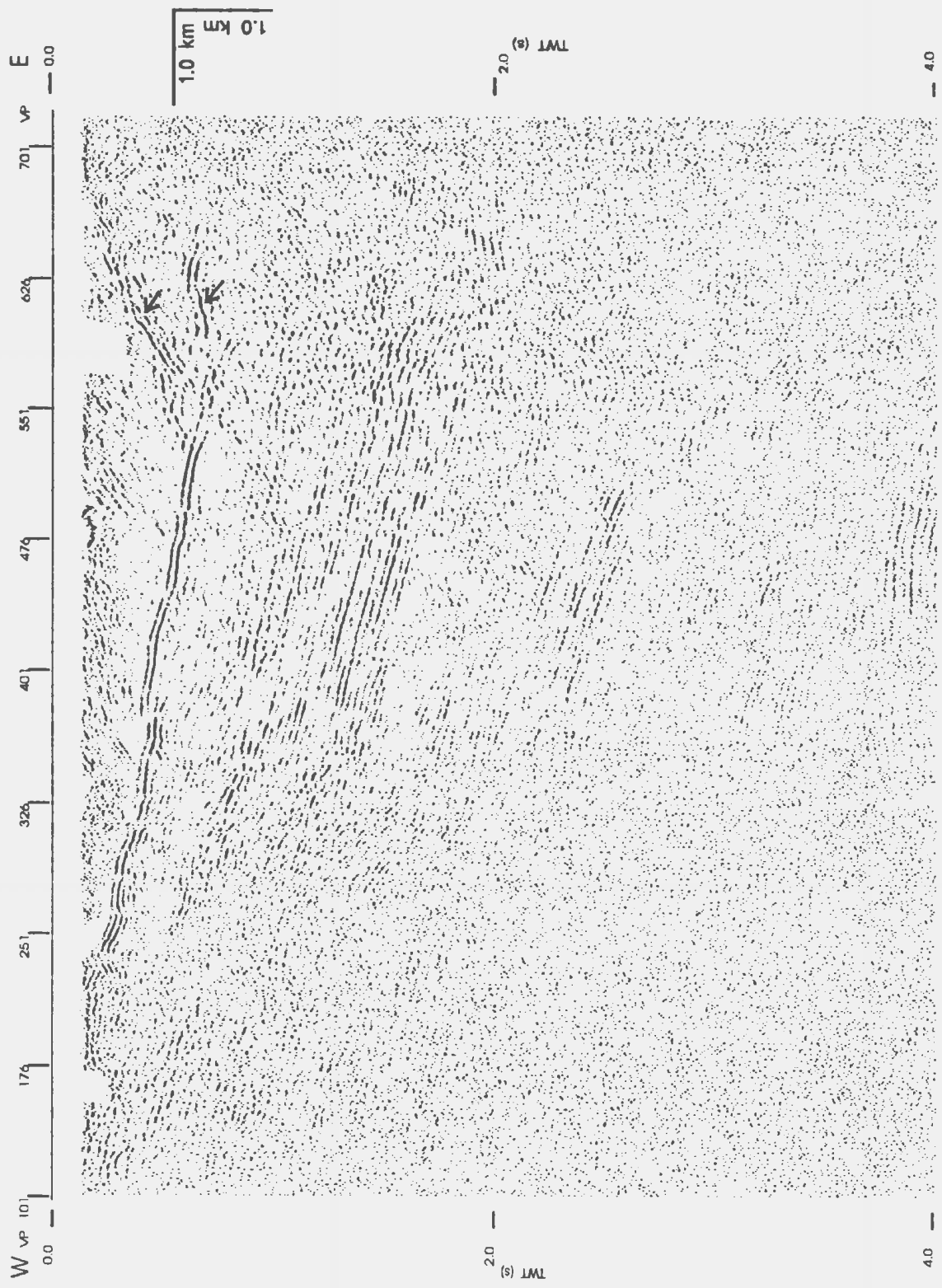


Figure 3.15. Stacked section without DMO and no post stack processing. This was a direct summation, no weighting was employed.

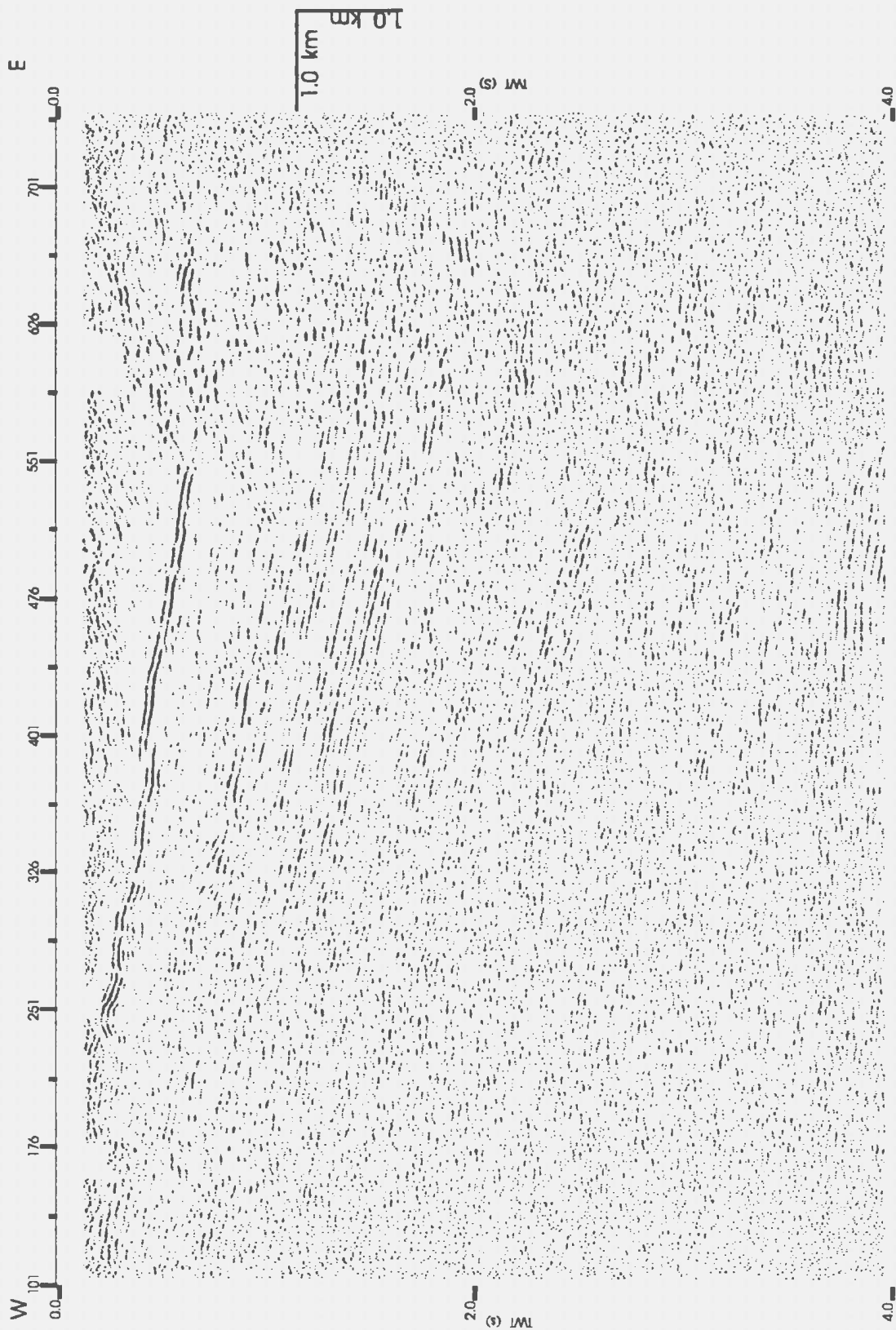


Figure 3.16. Stacked section with DMO and no post stack processing. Note the difference between this figure and Figure 3.15, especially the focusing of events and removal of artifacts (marked by arrows in Figure 3.15) in the vicinity of VP 551 to 626, TWT 0.3 to 0.6 seconds.

$$\begin{aligned}
&= \frac{L^2 \times S^2}{\sum_i \sum_k n_i n_k} \\
&= \frac{L^2 \times S^2}{\sum_i \sum_k (n_i \times n_k)} \quad (3.15)
\end{aligned}$$

It can be assumed that the noise is uncorrelated from trace to trace. This is reasonable for very long traces, so that $n_i \times n_k = 0$, for all cases where $i \neq k$. Furthermore, it can be assumed that the noise energy is about the same on all traces:

$$\begin{aligned}
\left(\frac{S}{N}\right)^2 &= \frac{L^2 \times S^2}{\sum_i (n_i \times n_i)} \\
&= \frac{L^2 \times S^2}{L \times n_i^2} \\
&= L \times \left(\frac{S}{n_i}\right)^2
\end{aligned}$$

$$\frac{S}{N} = \frac{S}{n_i} \times \sqrt{L}$$

$$\frac{S}{N} = \frac{s}{n_1} \times \sqrt{L} \quad (3.16)$$

From the above expression, it can be concluded that the stacking process increases the signal-to-noise ratio by a factor equal to the square root of the number of traces in a record. Therefore, the higher the fold of the data, the better the signal-to-noise ratio after stack. This seismic profile has an average fold of 60 traces per record, therefore stacking would theoretically be expected to improve the signal-to-noise ratio by approximately 7.7. Figure 3.15 displays the stacked data with no post stack processing.

After DMO correction, the CMPs were stacked after NMO correction using the velocity defined in table 3.2. This section, as seen in Figure 3.16 (also in folder) has better events than the section of Fig. 3.15, which was not DMO-corrected. For example the artifact at 0.2 to 0.6 s TWT in the vicinity of VP 570 to 611 has been removed by DMO-correction.

3.3.3 Post Stack Processing

Post stack processing consisted of residual static correction, finite-difference migration, time varying bandpass filter, coherency filtering, and final display.

3.3.3.1 Residual static correction

Residual statics corrects for deviations from proper hyperbolic trends. Field statics

corrections remove a significant part of these travel time distortions from the data. Nonetheless, these corrections usually do not account for rapid changes in elevation, the base weathering and weathering velocity (Yilmaz, 1987). From Figure 3.5, it can

Table 3.4. Horizon and window length used to define reference trace.

CMP	TWT	Window length
50	220	200
100	260	"
200	500	600
250	600	"
300	210	300
400	300	400
500	400	600
550	450	"
600	420	"
650	450	"
700	500	"
800	600	"
850	620	"
900	520	"
950	450	"
1000	600	"
1050	600	"
1100	600	"

be seen that the events do not define a good hyperbola even after field static corrections. Therefore, it was necessary to apply residual statics.

Building of a reference trace and determination of midpoint consistent statics is the

first step in residual static correction procedure. This reference trace is picked from the stacked data, where signal-to-noise ratio is high. Therefore, the DMO-corrected stack was used to pick the reference trace. Table 3.4 shows the horizon and the length of the window used, to define the reference trace.

The detailed composite static equation which is used to resolve the midpoint consistent statics into surface consistent statics for a trace is given by (STARPAK reference manual, 1989):

$$T_{ij} = S_i + R_j + C_k + N_k x_{ij}^2 + D_{k,y_{ij}} \quad (3.17)$$

where

T = total static applied

S = shot consistent shift

R = receiver consistent shift

C = cdp consistent shift

N = residual NMO coefficient (CMP consistent)

x = trace offset

D = cross dip coefficient (CMP consistent)

y = cross dip distance

and subscripts

i = shot index

j = receiver index

k = cdp index

The residual NMO term in eq. 3.17 arises in case of incorrect (but not too incorrect) moveout velocity has been applied to a hyperbolic event. The term N is constant for the gather k . The crossdip term in eq. 3.17 may be important if the dip of the subsurface geology is not in the direction of the processing line (Larner et. al., 1979). The angle between the dominant dip direction and the processing line direction leads to a time delay which is proportional to the crossdip distance. This distance is the distance of the trace midpoint perpendicular to the line of dominant dip direction which passes through the trace centroid. If g is defined as the subsurface dip, the time error is found to be:

$$dt = \frac{2 \sin g}{v} y = D y \quad (3.18)$$

where D is constant for CMP k .

Equation 3.17 can be expressed in matrix form as:

$$A x = b \quad (3.19)$$

where A is a matrix whose ij th component gives the contribution of j -th component

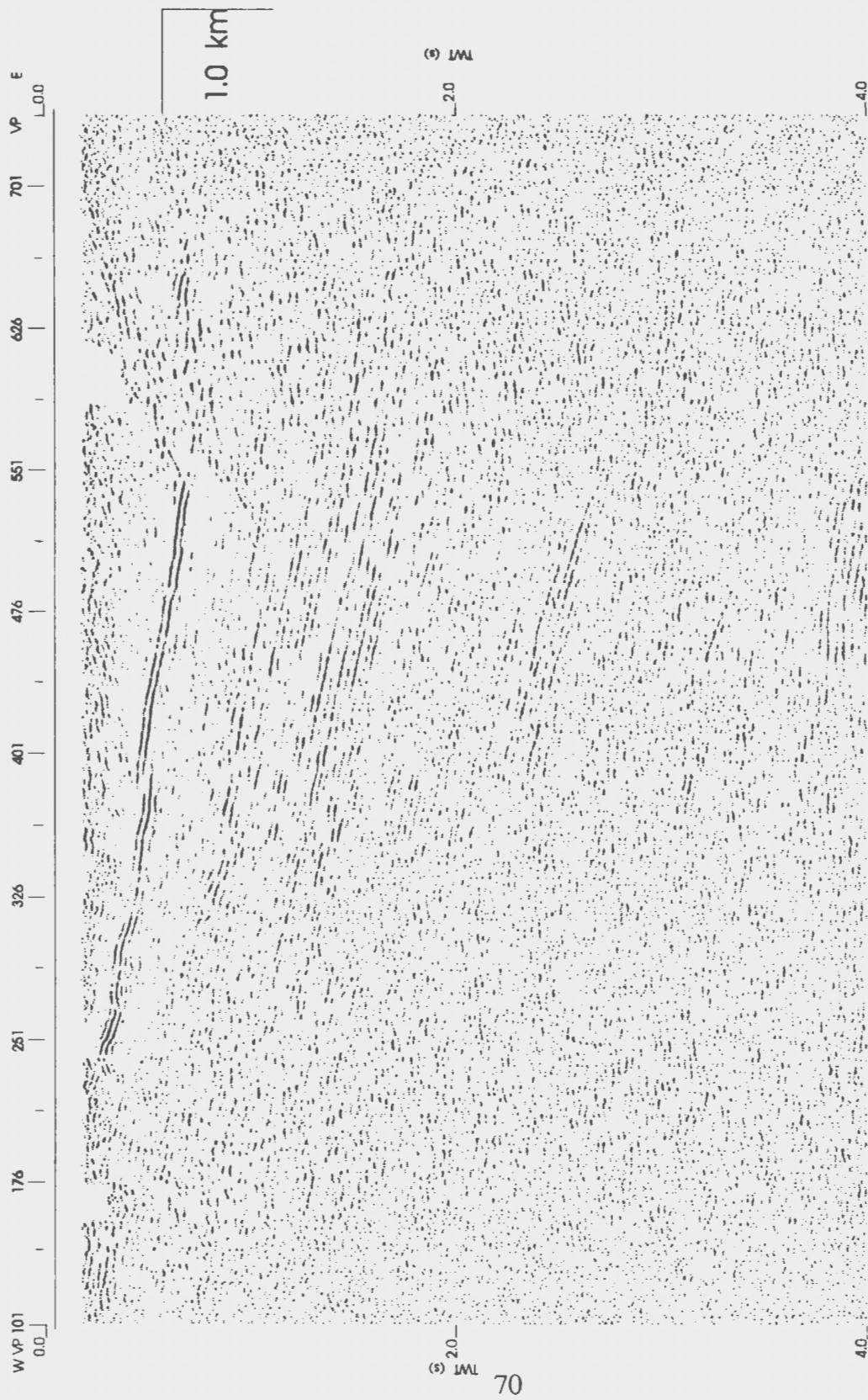


Figure 3.17. Stack section after residual statics corrections. Note that there is not much difference between this section and the section in Figure 3.16 i.e. before statics correction.

of x to the i -th equation, and is based on the geometry of experiment; x is the vector of the consistent shifts to be determined; and b is the vector measured shifts (T_i). If n_e is the number of equations and n_x is the number of unknown components, then the matrix A has the size n_e by n_x , the solution vector x is n_x by 1 and the measured vector b is n_e by 1.

The matrix A has very few non-zero components, i.e. it is sparse. The above equations are either underdetermined or over determined, therefore, they are solved by iterations, specifically the Gauss-Seidel method. In this approach the values of x recently found are used instead of values from previous iteration. For details of this method, the reader should refer to Wiggins et al. (1976). There are several additional steps which are used to make the Gauss-Seidel solution robust;

- (a) The residual NMO and cross-dip terms are not allowed to exceed a user specified threshold value.
- (b) The equations are weighted with a power of the normalised cross correlation.
- (c) Picks which are too large are down weighted.
- (d) Equations which produce large errors in the averaging technique are eliminated.

Before applying the statics calculated, the surface consistent statics were plotted. This was a checking procedure to get a feel of how the statics varied from one CMP to the other. From this plot, the maximum and minimum values of statics as a function of CMP values was +12 and -12 ms respectively. These values are significantly small and not much change is expected to the data after applying them.

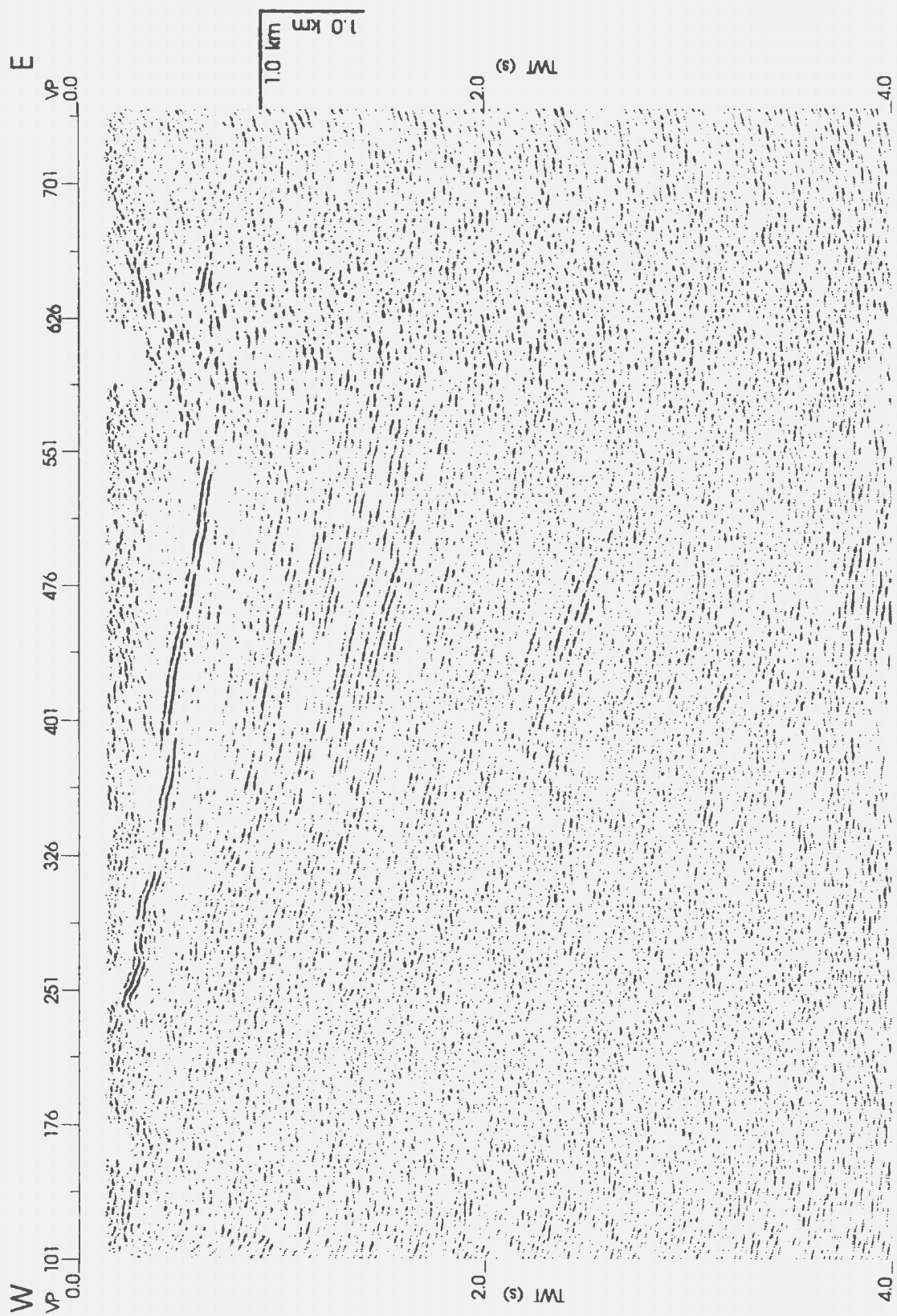


Figure 3.18 Migrated section. Notice the edge effects in this section as compared to Figure 3.17. To see clearly the results of migration look in Figure 3.22 in folder.

The surface consistent statics were finally applied to the CMPs which had been DMO corrected. The surface consistent static is the sum of receiver and shot static. This application finds the surface consistent static shift and applies it to the input trace.

After residual statics correction, the NMO corrected CMPs were stacked. From this stacked section (Figure 3.17) there is not much change as compared to figure 3.16, the section with no residual statics applied.

3.3.3.2 Finite-Difference migration

The aim of migration is to move dipping reflectors to their true subsurface positions and collapse diffractions, thereby delineating detailed subsurface features such as fault planes (Yilmaz, 1987). A 45-degree finite-difference migration was applied to the stacked section after residual statics corrections. To minimize edge effects the data were padded at the edges with 100 dead traces. The traces were also weighted at the edges to reduce their amplitudes because the traces at the edges had such high amplitudes that they were causing a lot of edge effects. Only 40 traces on either side of data were weighted as follows: CMP 23 which was the first trace in the data was given a weight of 0.00001 whereas CMP 62, the 40 th, was given a weight of 1.0. In between the weighting factors were interpolated using the CMPs. Similarly the last 40 traces (CMPs) were weighted in the reverse order so as to give the last CMP (1220) a weight of 0.00001 and CMP 1181 a weight of 1.0. After migration,

the CMPs were weighted back to normal.

The mathematics for finite-difference migration are very complex, therefore, in this project only the final equation will be quoted. The basis for the 15-degree finite-difference migration is (Yilmaz, 1987):

$$\frac{\partial^2 Q}{\partial \tau \partial t} = \frac{v^2 \partial^2 Q}{8 \partial y^2} \quad (3.20)$$

where Q is the retarded wave field, t is the input time, τ is the output time, and y is the midpoint coordinate. The above equation is derived from the dispersion relation, assuming that velocity varies vertically. Nonetheless, in practice, the velocity function in the equation can be varied laterally, provided it is smooth.

For 45-degree finite-difference, the above equation is modified to (Yilmaz, 1987):

$$\frac{i\beta_1}{\alpha_1 m} \frac{\partial^2 Q}{\partial z \partial y} - \frac{\partial^2 Q}{\partial y^2} + i \frac{m}{\alpha_1} \frac{\partial Q}{\partial z} = 0 \quad (3.21)$$

where m is equal to $2\omega/v$, β_1 and α_1 are coefficients such that for the 15-degree algorithm $\alpha_1 = 0.5$ and $\beta_1 = 0$ whereas for the 45-degree $\alpha_1 = 0.5$ and $\beta_1 = 0.25$.

After residual statics application, the section was migrated using the velocities of Table 3.2. Figure 3.18 displays the results of migration. From this figure it can be observed that diffractions are collapsed and fault planes are revealed (cf. Figure 3.16 with Figure 3.22, both figures also in folder).

3.3.3.3 Filtering

The data were filtered after migration using a bandpass filter and a coherency filter.

3.3.3.3.1 Bandpass filter

A bandpass filter, which varies with time, based on test panels (see Figure 3.19), was applied to the data after migration. In the region 0 to 2000 msec, a bandpass of 20 to 90 Hz was applied, while in the section 2500 to 4000 ms a bandpass of 20 to 60 Hz was used. The merge zone was 500 ms. Data between the two windows were merged from the end of the top window (2000 ms) to the beginning of the next lower window (2500 ms). All data were filtered. Filtering was done in time domain as shown below (STARPAK processing manual, 1989):

$$F(t) = \sum_u T(t - u) * O(u) \quad (3.22)$$

where T is the input trace, o is the filter operator, F is the filtered trace and * indicates convolution.

3.3.3.3.2 Coherency filtering

The aim of coherency filtering is to enhance reflectors for interpretation purposes. The filter that was used for this kind of processing is one that attenuates incoherent energy within a specified slope. For each input trace and time sample, the processor

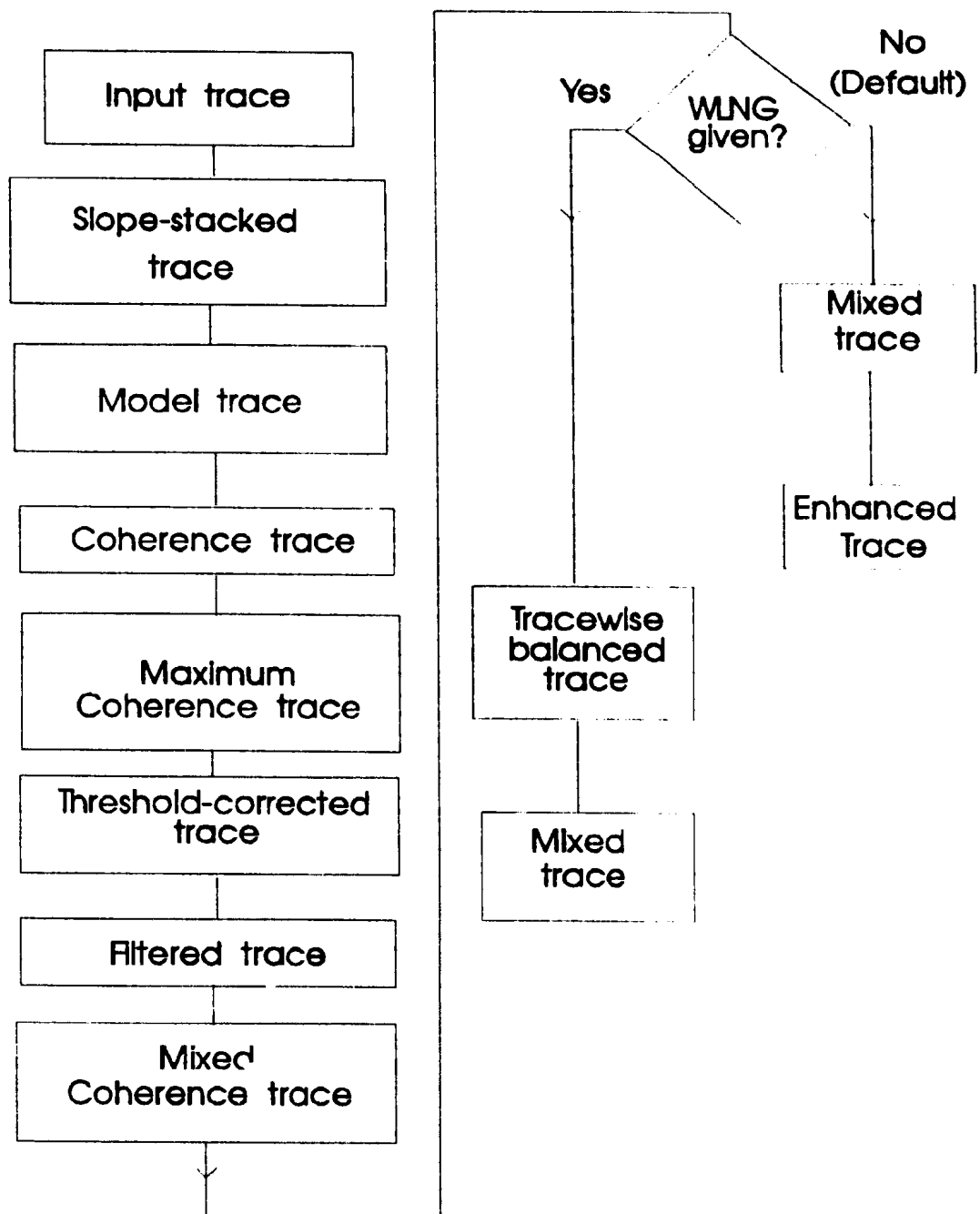


Figure 3.20. Calculation steps in the coherency filter (STARPAK reference manual, 1989).

checks the neighbouring traces for waveform alignment along several different time slopes (STARPAK Processing Manual, 1989). The degree of alignment is a measure of coherency. After finding coherences, data with low coherency are attenuated. Therefore, seismic events aligning with at least one of the slopes, generate large coherences and are preserved. The slope (FAN) used for the data was -6 to +6 ms/trace. The value of the slope determines the number of slopes to be generated for finding alignment. For example for a slope (FAN) of -6 to +6 ms/trace, 7 traces were generated at -6, -4, -2, 0, 2, 4, 6 ms/trace for sample rate of 2 ms. These generated slopes are used to find alignment for the input trace. A slope-stacked trace is formed by stacking the number of traces (i.e. 9, the number used in filtering this profile) along each slope thus generated. To the input trace a certain percentage of the slope-stacked trace is added to generate a model trace (see Figure 3.20). A coherence trace is formed by determining degree of alignment between the slope-stacked trace and the model trace at each slope within the user defined slope (FAN), using a user defined window. The maximum coherence trace is determined by finding the maximum coherence at each sample of the set of coherence traces. A threshold-coherence trace is formed by attenuating the model trace using $(\text{coherence}^{\text{POWER}})$ times (amplitude) for values of coherence below a certain value say THRESH (the values of POWER and THRESH for this project were 1 and 65 % respectively). A filtered trace is achieved by taking the amplitude of the threshold-coherence trace corresponding to the maximum coherence trace. For every input trace a corresponding

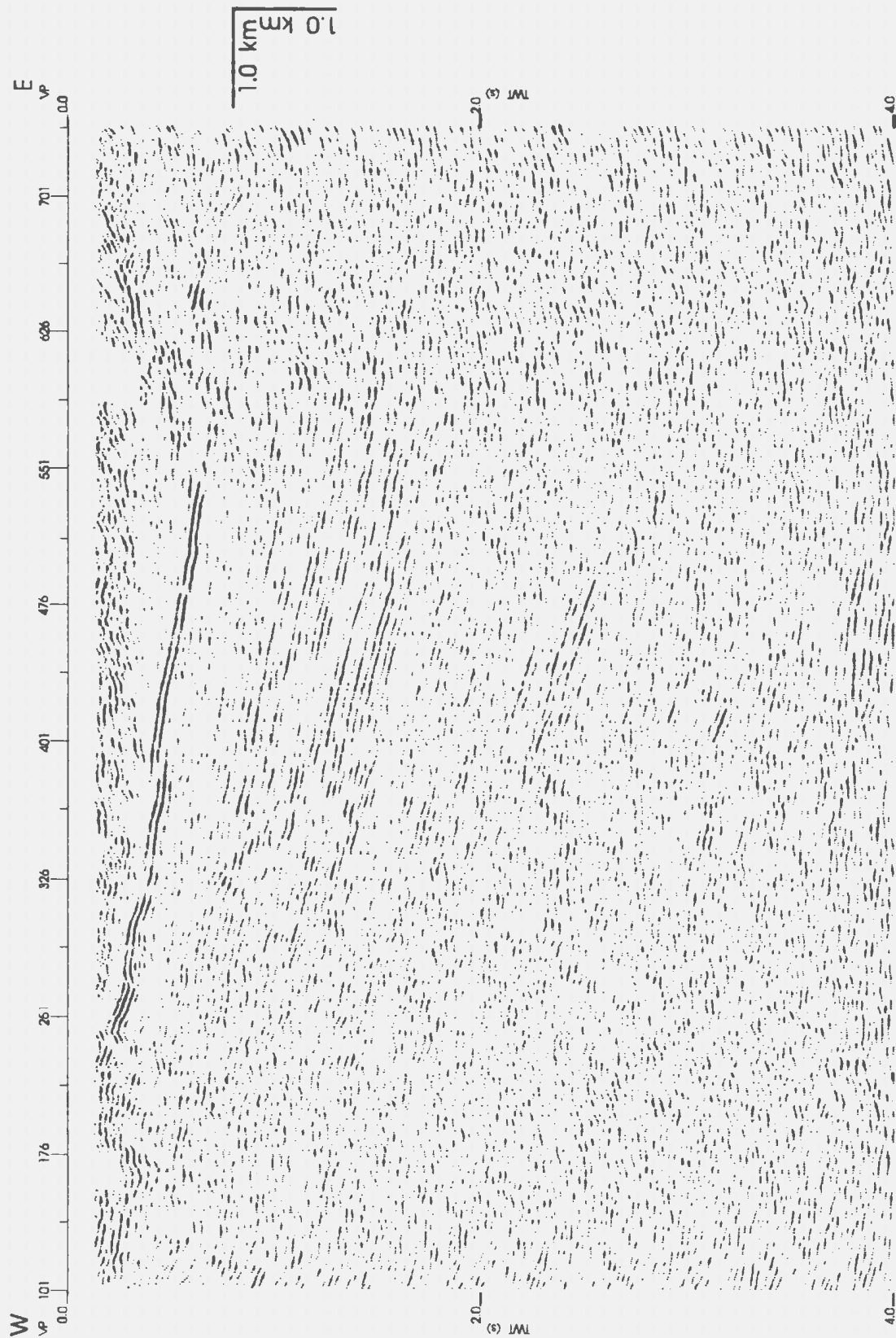


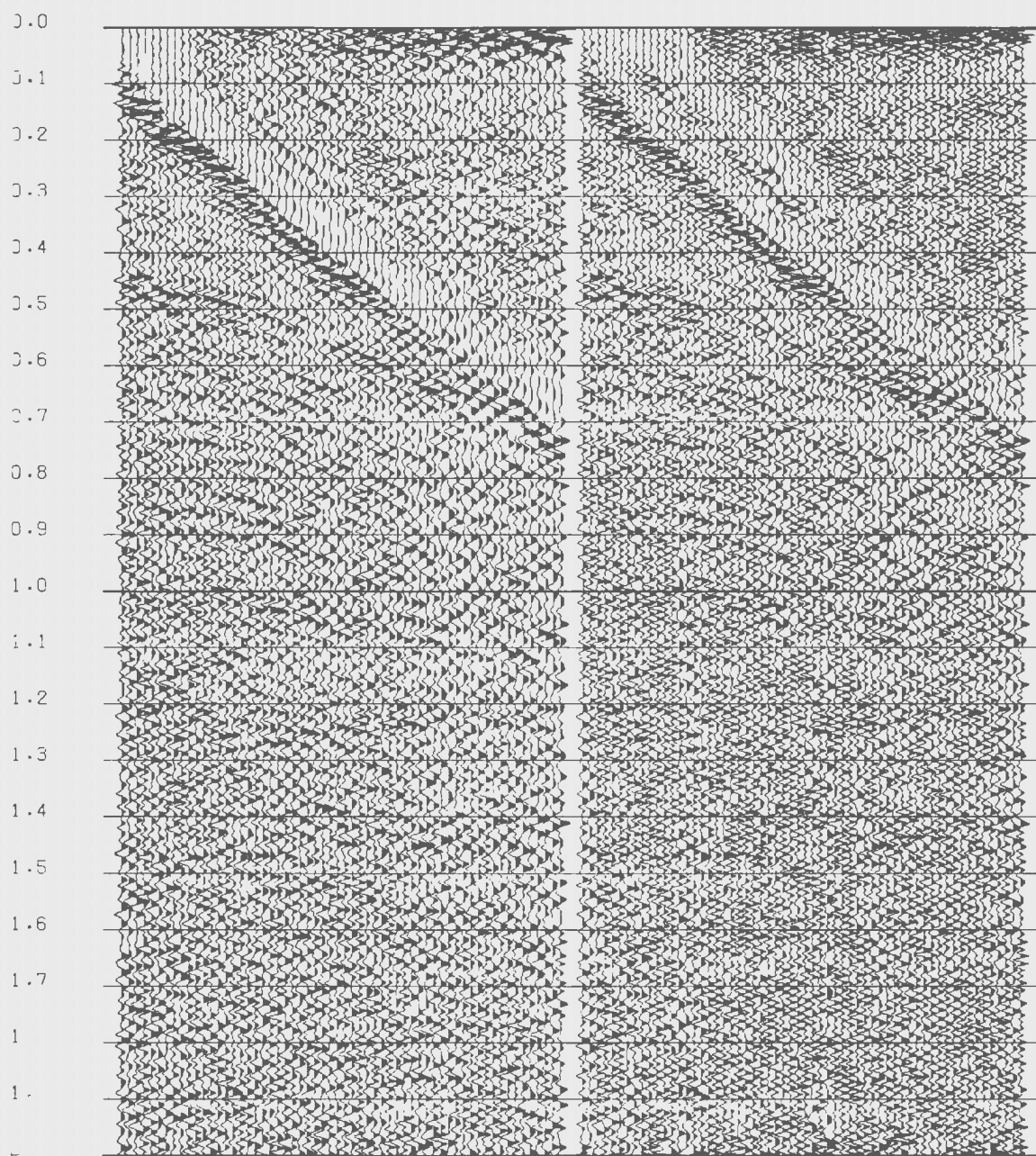
Figure 3.21. Migrated section after applying both bandpass and coherency filters. In this section the events are more focused than in Figure 3.18. The edge effects have been reduced.

output filtered trace is made. A mixed coherence trace is formed by adding (filtered trace) times (max. coh.^{COHMAX}) to (input trace) times (1 - max.coh.^{COHMAX}). The value of COHMAX is user defined, and for filtering these data its value was set to 0. If window (WLNG) is not given a certain percentage (PERCMIX) (100 % was used to filter these data) of the input trace is added to the filtered trace to get a mixed trace. A suite normalization is applied to the amplitudes of all mixed traces, such that the average absolute amplitudes of the output is equal to that of input. Otherwise, if window (WLNG) is given, the amplitudes of the filtered trace is balanced using the window WLNG to get tracewise balanced trace. To get the mixed trace, percentage (PERCMIX) of the tracewise balanced trace is added to (100 - PERCMIX) % of the input trace. In filtering these data, WLNG was not used, therefore, an enhanced trace was achieved by the former method. The choice of the parameters was based on the recommended values in STAPARK manual (1989).

Figure 3.21 displays the results of bandpass and coherency filtering. The events are better focused in Figure 3.21 than in Figure 3.18.

3.3.3.4 Final display

The final section (in folder, Figure 3.22) was plotted using a horizontal and a vertical scale of 14 traces/cm and 8 cm/s respectively. Two traces were summed to produce one trace. This is a 1:1 section if an average velocity of 4 km/s is assumed for the whole section.



(a) (b)
 Figure 3.23. Deconvolution of CMP 630. (a) Before spiking deconvolution. (b) After spiking deconvolution. The lag and operator length were 2 ms and 250 ms respectively. Notice the noise in (b).

3.3.4. Other processing

An attempt was made to apply spiking deconvolution to the data (see Figure 3.23).

From this figure, it can be observed that deconvolution introduces a lot of ringing noise to the data. Therefore, deconvolution was not applied to the data.

The data was quite clean, thus there was no need for such processing as F-K filtering, inner trace muting etc.

Chapter 4: Interpretation

4.1. Introduction

There are no deep boreholes in this part of the subbasin, therefore, the geologic interpretation will be based on seismic character and surface geology as mapped by Knight (1982). The nearest borehole (BSG1, see Figures 2.2 and 4.3) is located about 500 m north of the centre of the seismic line; it was drilled to a depth of 300 m and encountered only Barachois Group (Solomon, 1986).

Data quality varies throughout the profile. Though reprocessing has improved all the data significantly, (compare Figure 3.22 with Figure 4.1, both figures in folder) the best data occurs towards the centre of the line where several reflection packages occur.

Most of the reflection packages are as identified by Hall et al. (1992), except that they are more focused and distinct in the current profile. Uncorformity "U" and package "G" were not identified by Hall et al. (1992). The two non-reflective section below (part of "D") and above reflector "R" (part of "B") were not previously identified (Figure 4.1).

4.2. Description of the seismic line

4.2.1 Reflections

Reflector "R"

As illustrated on Figure 4.2 (in folder) and interpreted on Figures 4.3 - 4.6, the seismic character of the section changes across a strong reflector at 0.2 to 0.6 s

Legend of Figure 4.3.

a	Anguille
c	Codroy
b	Barachois
BSG1	Memorial University drill hole

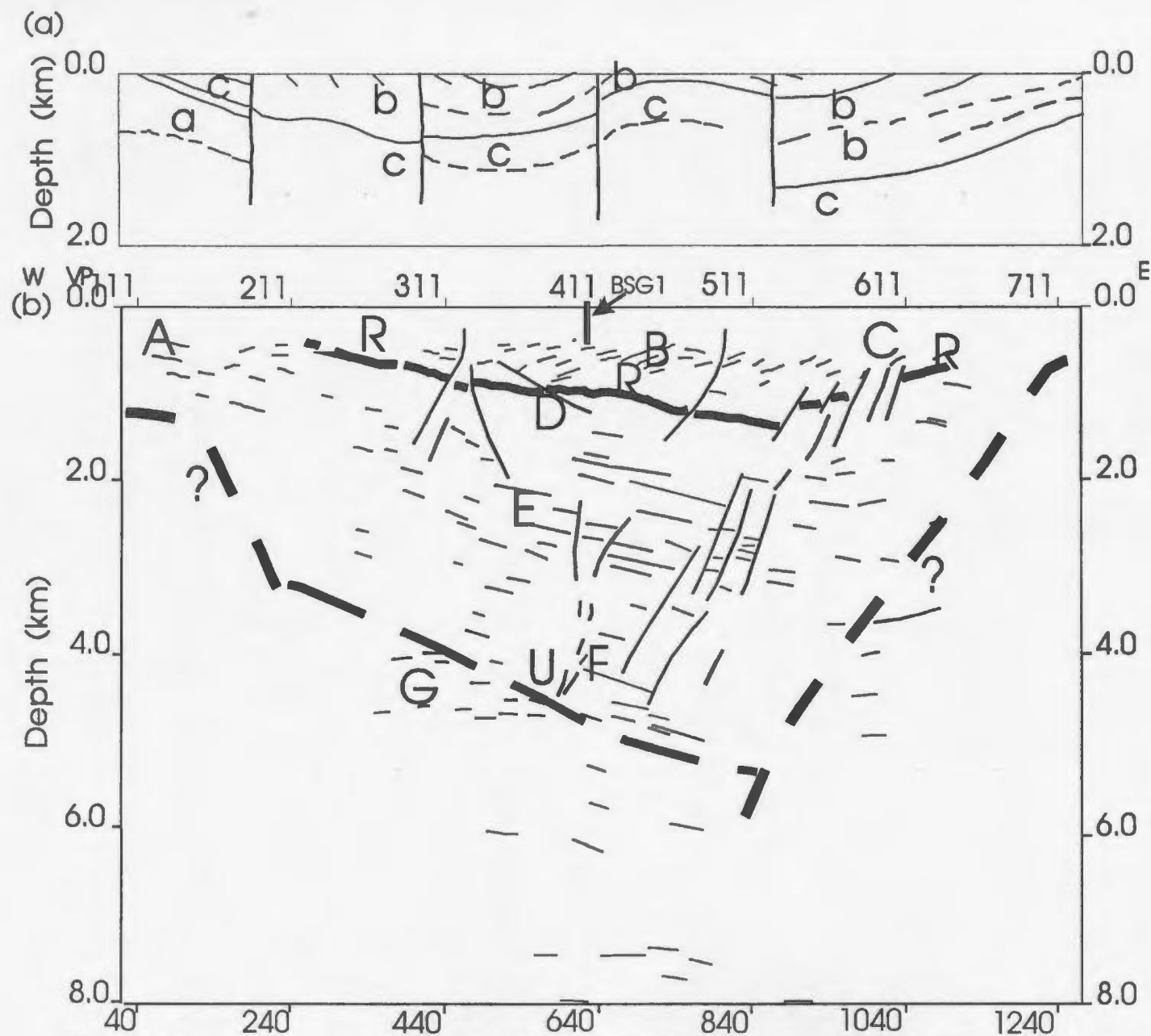


Figure 4.3. The St. George coalfield basin. (a) Knight's (1983) cross section projected onto the seismic profile. (b) Line drawing of the seismic profile taken from the reflectors picked on figure 4.2.

TWT. On the east, this reflector marked "R" can only be traced as small fragments which are separated from each other by faults. Reflector "R" divides the section into two groups of strata, i.e. westward-dipping reflectors (package "B" and "C") above the "R" and eastward pre-dominantly dipping packages "D" to "F" below (Hall et al., 1992).

Package "A"

This package consists of high amplitude discontinuous events at the west end of the seismic line. The dominant frequency of this package is about 30 Hz. The depth extent is about 0.6 s at dips of about 15°. There is a dip reversal at about VP 170, probably indicating the presence of a fault.

The high amplitude events give way downwards to a low amplitude zone with horizontal discontinuous events, similar to those observed in the deeper parts of the sections.

Package "B"

"B" is a relatively high amplitude package with most of the events dipping west at an angle of 20°, though some events are gently east dipping at angles $\leq 10^\circ$. A few folds which correlate well with the surface geology can be recognised.

This package loses its coherent reflectors above "R" to the west near VP 250 where it appears to be offset by a steep fault. Eastward at TWT larger than 0.3-0.45

seconds the package gives way to a much less reflective package overlying reflector "R" from VP 411 to 570.

Package "C" is probably part of "B".

Package "D"

Beneath reflector "R", this package is about 0.8 km to 1 km thick, if an average velocity of 4 km/s is assumed for the seismic section. It is present from VP 230 to 550 and appears to be fault-bounded at its eastern and western limits. This package which is both low reflective and of low amplitude, dips towards the east. It is cut by minor and major faults and it appears irregularly bedded.

Package "E"

Package "E" is present from VP 160 to 630 and is about 1.4 km thick. This package exhibits strong parallel reflectors that dip to the east but become nearly horizontal towards at their eastern extent. Dip reversals occur at about VP 590.

The package is faulted in a very complex manner towards the east end of the seismic profile (VP 550 to 671).

Package "F"

This package consists of brief series of strong but discontinuous reflectors at a depth of approximately 5 km. The section between "E" and "F" is weakly reflective,

though the events, where focused, dip towards the east. Below "F" there are discontinuous straight reflectors which are bounded at their top by unconformity "U".

Package "G"

This package comprises discontinuous straight reflectors and is separated from "F" by unconformity "U". It has generally low reflectivity except below "F", where events are clear. Package "G" appears to be interrupted occasionally by a few eastward dipping events. These may result from shear zones in the crystalline basement. Alternatively this would also imply that package "G" could represent two rocks of different ages, i.e. Lower Palaeozoic and Precambrian.

Unconformity "U"

Unconformity "U" separates "F" from "G". The seismic character and the eastward dips of "F" compared to those of "G" makes it possible to identify this event. It is clear in the centre of the section between 1.8 to 2.5 s TWT, but is not visible in the eastern and western faulted parts of the section.

4.2.2. Faults

The whole seismic section is cut by several steep normal faults. Many of these are minor without any pattern, though a few of them that are marked in Figure 4.2 adhere to an extensional pattern with minor compressional features present.

At the east end in the vicinity of VP 540 to 611, a complex fault system is interpreted. Again, no clear pattern of extension or compression can be established, and it is likely that a cross-section through a shear zone is being imaged. This is consistent with the regional geology, as the Cabot (Long Range Fault), a regional strike-slip feature, occurs only 5 km to the east of the seismic profile. Near the top of the section, reflector "R" is displaced by movements on faults in this shear zone (see figure 4.2).

At VP 380, 2-way time 0.4 s, reflector "R" appears to have been cut by a low angle reverse fault. To check the validity of this feature, the Fresnel width of this part of the seismic line was analyzed. The Fresnel width (w) is given by (Kleyn, 1984)

$$w = (2 z \lambda)^{\frac{1}{2}} \quad (4.1)$$

where z is depth and λ is the wavelength. If the dominant period is taken to be 20 ms, and velocity to be 3300 m/s, then w is ≈ 300 m. This means that the horizontal resolution at such a depth (0.4 s) is about 300 m. Therefore, the fault which is about 200 m wide may not be resolved exactly, therefore, the thrust fault may not be a true event based on this argument of Fresnel width. Nevertheless, this event could be real because after migration, which enhances lateral resolution, this fault is still evident.

The two faults, marked with question marks, on either side of the seismic section tend to limit either eastward or westward extension of packages "D" to "F". The fault

from 0.5 to 6 m (Figure 4.3) maybe a growth fault controlling sedimentation in a half-graben. This is a very common situation in the Horton subbasins in the Magdalene Basin (Durling and Mariller, 1993). It possible that packages "D" to "F" extend further than mapped here, but deformation along these growth faults prevents the detection of these packages.

4.3. Interpretation of the seismic line

4.3.1 Introduction

There are number of possible geological interpretations of reflector "R", packages "A" to "G" and unconformity "U". The interpretation made here will utilize all the geological and geophysical information available, especially surface geology, local drill hole data, nearby published and unpublished seismic lines, regional seismic character in the Maritimes Basin and the Bay St. George Subbasin, and regional geological setting.

4.3.2 Reflector "R"

There are four possible geological interpretations for reflector "R", as interpreted by Hall et al. (1992):

- 1) Anguille/Codroy contact;
- 2) Codroy/Pre-Carboniferous basement contact;
- 3) a décollement within the basin;

4) marine Codroy/non-marine Codroy-Barachois contact.

It should be noted however, that the third interpretation is not mutually exclusive of any of the other three.

The first interpretation of "R" as Anguille/Codroy is alluring. From the character of "R", it looks similar to a regional reflector that has been identified in offshore and onshore seismic in the Maritimes Basin as the Horton/Windsor contact (Nickerson, pers.comm.), which is chrono-and litho-stratigraphically equivalent to the Anguille/Codroy Group contact (Hall et al., 1992). A second, similar observation arises from these observations. Seismic profiles described and illustrated in St. George's Bay (see Figures 2.8 and 2.9) by Kilfoil (1988), Miller et al. (1990) and Langdon (1991) show a very similar reflector that is interpreted as near base Codroy upon Pre-Carboniferous rocks. This reflector defines a deep half graben beneath the bay.

In either of the above two situations, the strong reflection character near the base of the Codroy is probably related to the presence of evaporites in the Codroy Road Formation (see figure 2.3). In either case, regarding the seismic profile at hand, if "R" is interpreted to represent the near-base-Codroy, then the unconformity "U" would represent the contact between Pre-Codroy rocks (Anguille and/or Lower Palaeozoic) and the Precambrian.

The third interpretation calls for a décollement within the Carboniferous succession. This is favoured by the angular discordance reflectors in overlying

packages "B" on "R" and the contrast in deformation between strata above and below "R" as has been noted by Hall et al. (1992). Knight (1983) indicated that such a décollement could explain anomalous structural relationships that occur around the northern end of the Anguille Anticline, especially the marked contrast between the degree of deformation within the evaporitic and fine grained strata of the Codroy Group (Codroy Road Formation) and within the Anguille Group and the conformably overlying Ship Cove Formation limestones. The décollement is most likely to occur at the base of the evaporitic sediments of the Codroy Road Formation which could be the low amplitude non-reflective package above reflector "R" from VP 411 to VP 581. If this interpretation is correct, then "R" would combine elements of interpretation 1 and 3 or 2 and 3 (Hall et al., 1992).

As a fourth possible interpretation, reflector "R" could be a prominent limestone bed known as the Crabbes limestone (Bell, 1948; Knight 1983). This unit attains a thickness of up to 15 m in coastal sections of St. George's Bay and separates beds of the lower Codroy Group from non-marine strata belonging to the upper Codroy Group and the Barachois Group. It is most probable that the limestone is not the cause of the reflector, because it may be too thin to be responsible for the strong and continuous character of "R". Nonetheless, its position between contrasted lithologies may cause it to be coincident with the reflector.

4.3.3. Packages "A" to "G"

From Knight's (1982) geological mapping, package "A" contains sedimentary strata of the lower Codroy Group and the underlying Fischell's Brook Member of the Anguille Group. These rest unconformably upon Precambrian crystalline rocks that are known to be the core of the Flat Bay Anticline and are imaged by the horizontal low amplitude discontinuous reflectors below 0.4 to 0.6 s TWT. However, the demarcation between the sediments and the Precambrian cannot be determined from the seismic profile. The boundary marked in figures 4.3 to 4.6 at either end of the basin is structural rather than stratigraphic.

The interpretation of packages "B" to "E" is difficult to make on the basis of seismic character alone. Their interpretation depends on the most reasonable interpretation of reflector "R". If "R" is the Codroy/Anguille or the Carboniferous/basement boundary accentuated or modified by basal evaporitic décollement, then "B" must include either Codroy and Barachois strata, or both.

If "R" is indeed the Codroy/Anguille contact, packages "D" and probably "E" belong to the Anguille Group, which would be approximately 2.0 to 2.2 km thick.

In this scenario "D" consists of the uniform red sandstone of the Spout Falls Formation plus conglomerates of the Fischell's Brook Member. The low reflective nature of "D" is characteristic of sandstones and conglomerates as has been identified in the Gulf of Mexico (Stuart and Caughey, 1977). The reflective nature of "E" is typical of lacustrine and deltaic rocks of the Snake's Bight and Friars Cove

Formations. "E" has same seismic character as Horton (Anguille) Group sediments in the Magdalen Basin (Durling pers. comm., 1993). Package "E" appears to be continuous in the west and may be the same as package "A".

4.3.4 Unconformity "U"

The interpretation of "U" will depend on the interpretation of reflector "R" and packages "A" to "G". If "R" is Anguille/Codroy contact with "F" as the Lower Palaeozoic, then "U" is the Lower Palaeozoic/Precambrian contact. If lower Palaeozoic is absent, then "U" is the Carboniferous/Precambrian boundary. Alternatively "U" could be the Carboniferous/Lower Palaeozoic contact, if "F" is interpreted to belong to the Anguille Group and part of "G" to be Lower Palaeozoic.

4.4. Geological Models

4.4.1 Introduction

Some combinations of the alternative interpretations are feasible. In Figures 4.4 to 4.6, three of the most probable alternatives are shown. All the models are based solely on the alternative interpretations of reflector "R" and unconformity "U". Each of models A to C implies a different likely range for the Carboniferous underlying "R" (Hall et al., 1992) and different types of basement underlying "U".

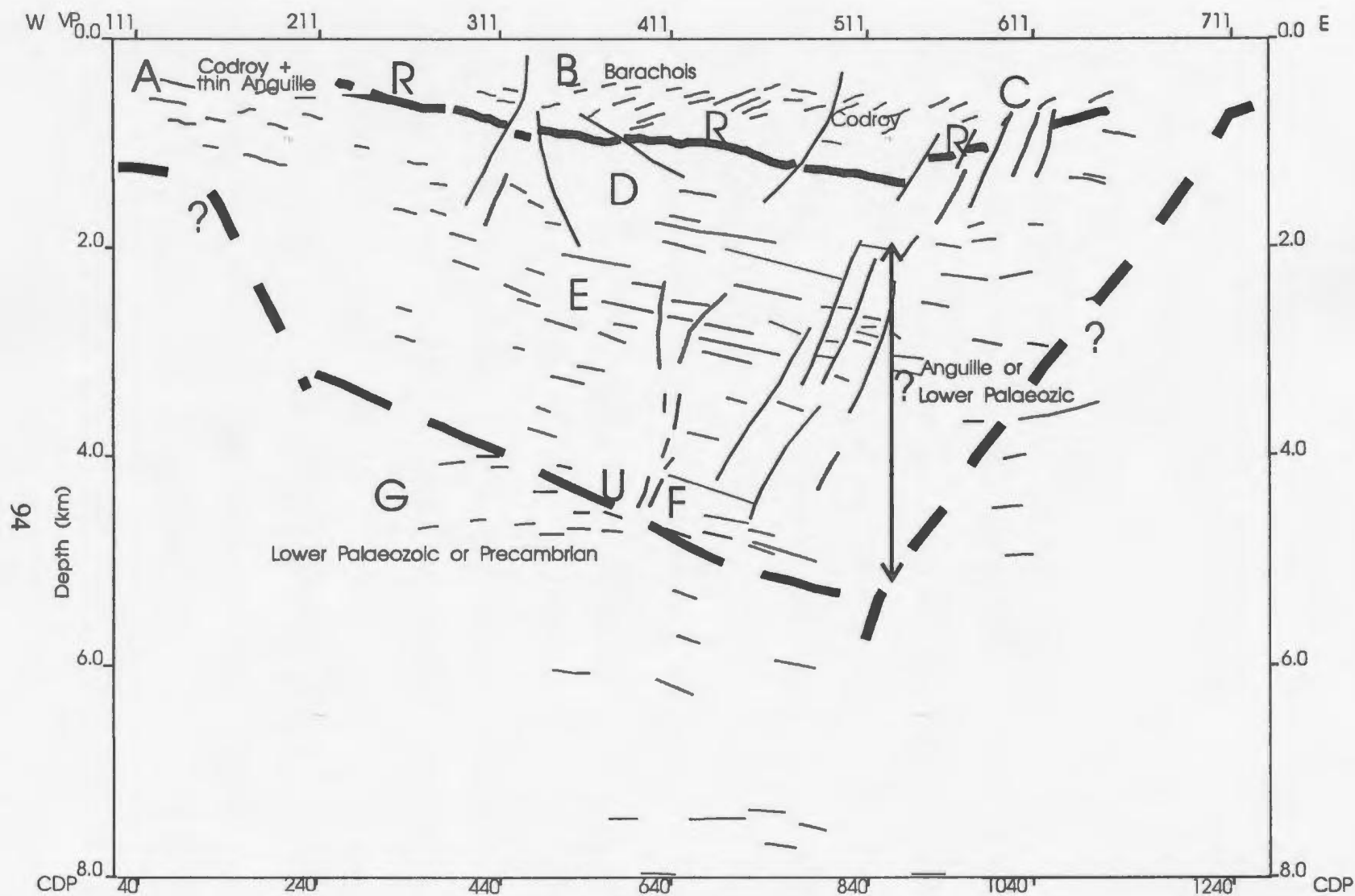


Figure 4.4. Model A - "R" as the Anguille/Codroy contact with or without decollement .
The rock units are as indicated in the figure.

4.4.2 Model A - "R" as the Anguille/Codroy contact with or without décollement

Figure 4.4 illustrates model A, which interprets "R" as the Anguille/Codroy contact with or without décollement. This model as discussed by Hall et al. (1992), is a compelling model because "R" can be correlated with Horton/Windsor contact as in offshore and onshore seismic interpretations of the Maritimes Basin (Nickerson, pers. comm., Durling and Mariller, 1990). This would imply that Codroy and Barachois Groups occur above "R", overlying the Anguille Group. The low reflective package overlying "R" could represent Codroy Group especially the Codroy Road Formation. Packages "D" and "E" may include Lower Palaeozoic Carbonates and flysch, but this is unlikely in this model because the erosional truncation of the Lower Palaeozoic is missing. The magnetic field data suggest that the Grenville basement is at depth below the Barachois syncline, because of the rapid loss of amplitude, short wavelength anomalies which characterise the field over exposed basement under the adjacent Flat Bay anticline, and immediately east of the Long Range fault (Fig 2.7). The gravity field across the Barachois syncline shows a low with an amplitude of 10-15 mGal (depending on the choice of regional field). The Barachois/Codroy sequence has a density contrast of 0.22 Mg/m³ (see Table 2.2) with basement and a thickening of this sequence from 0 to 1 km at the axis of the syncline would thus explain an anomaly of 9.2 mGal. This is barely enough to explain the observed low. It is thus likely that Anguille also underlies the syncline. From model A, 2.3 km of Anguille (to include reflector package E), given a density contrast of 0.09 Mg/m³ with basement, would

contribute no more than 8.7 mGal to the gravity low. Given that these estimates are directly from the 2-D slab formula (Telford et al., 1990), they overestimate the gravity effect, especially for 'tight' structures. It is concluded that model A provides match to the gravity data. "U" would probably be the contact between the Late Devonian to Carboniferous rocks and the Precambrian basement if the Lower Palaeozoic is missing in this model. Otherwise, "U" could be the Lower Palaeozoic/Precambrian contact if "F" is Lower Palaeozoic. Alternatively "U" could be Carboniferous/Lower Palaeozoic boundary (see Figure 4.4)

Anguille Group would correspond to Package "D" and probably "E" also (i.e Spout Falls, Friars Cove and Snake's Bight Formations). From the seismic profile at hand it is obvious that packages "D" and "E" are conformable to each other. This would mean that "E" is confined to a down-faulted block that lay east of the upthrust Grenvillian basement that now occupies the core of the Flat Bay Anticline (Hall et al., 1992). Anguille Group is likely to be about 2.0 to 2.2 km thick or more if all the way down to "U", contrasting greatly with the approximate 200 m mapped around the Flat Bay Anticline and forming part of package "A" in the seismic profile. If package "F" is included, the total thickness is about 4 km, which is usual for Horton (Anguille Group equivalent) subbasins in the Magdalene Basin (Durling and Marillier, 1993).

From this seismic profile, it can be observed that Anguille Group is not deformed much. The strata are generally flat lying, though interrupted by faults here and there. This can be explained, possibly, by the nature of Precambrian basement which is

crystalline and magnetic compared to the non-crystalline and non-magnetic basement beneath the Anguille Mountains where the Anguille Group is quite deformed.

The Lower Palaeozoic may be either confined to package "F" or absent in this model. Deformation at the east end of the seismic profile (VP 511 to 640) probably indicates salt movements and basal detachment. There is a possibility that a shear zone is being imaged here i.e. from VP 511 to 640, TWT 0.2 s to 0.6 s. Surface geology, nearby drill holes and the apparent conflict of overlying west dipping reflectors with "R" at the west end of the line, suggest that Barachois Group may rest directly upon "R" from VP 250 to VP 390. This would mean that if Codroy Group is present in the west end of the line, it must be very thin (< 200 m). Otherwise, it is evident that the Codroy Group may be present from VP 390 to 590.

4.4.3 Model B - "R" as the Codroy - Barachois upon Pre-Late Devonian-Carboniferous basement with or without décollement

Figure 4.5 shows model B, where "R" is interpreted as the Codroy-Barachois upon Pre-Carboniferous basement plus or minus décollement. This model, proposed by Hall et al. (1992) incorporates the interpretation of packages "B" and "C" as in model A. However, "R" would mark the Codroy-Barachois/Pre-Carboniferous contact. The Pre Carboniferous basement rocks would likely include Lower Palaeozoic orogenic flysch ("D") and carbonates ("E") of the Anticosti Platform which overlay the Precambrian crystalline basement. In this model, unconformity "U" would separate Lower

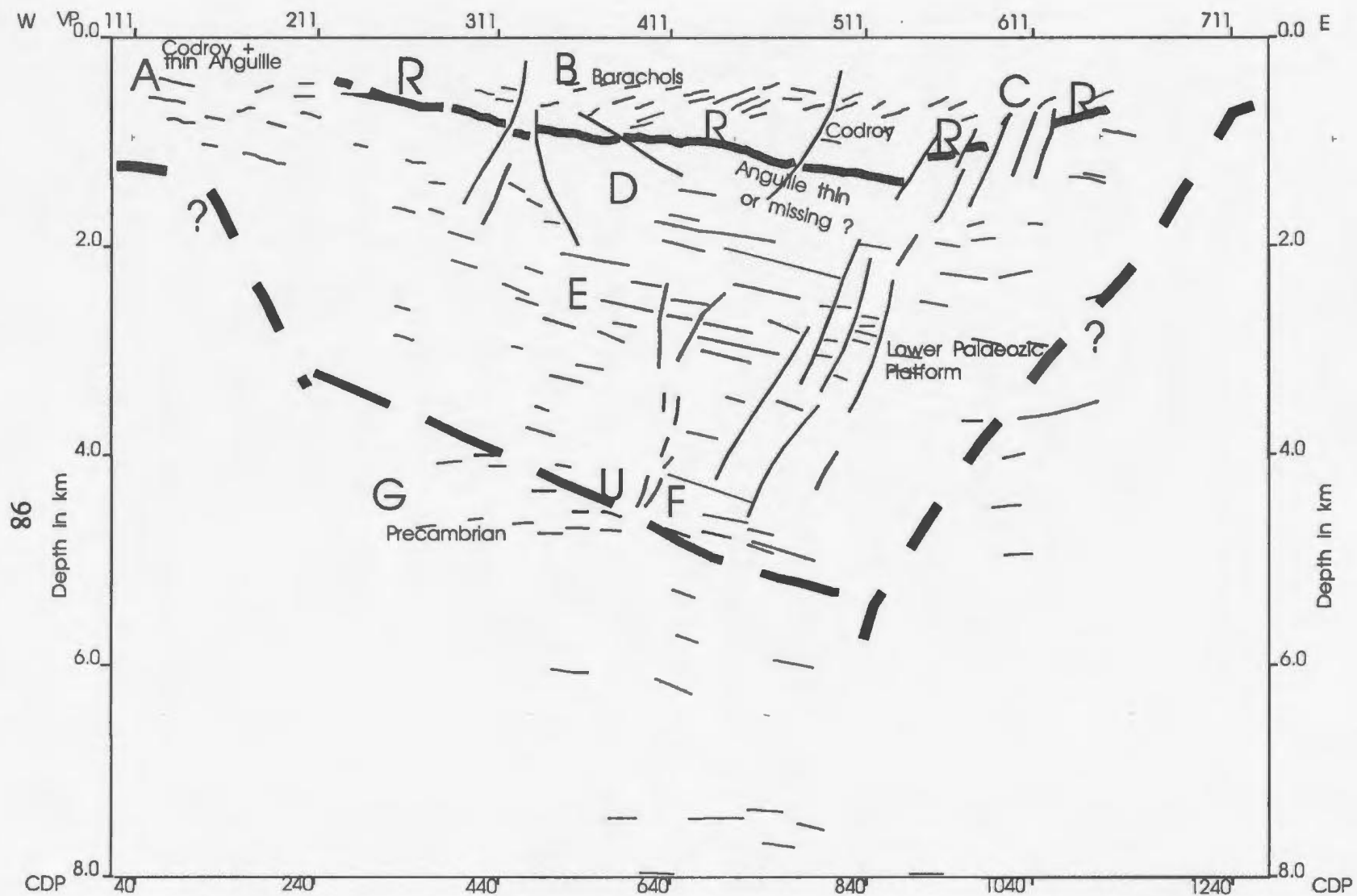


Figure 4.5. Model B - "R" as the Codroy-Barachois upon Pre-late Devonian/Carboniferous basement with or without Decollement.

Palaeozoic from Precambrian basement. The highly reflective nature of "E" suggests sediments above crystalline basement rather than intra-crystalline basement reflectivity, though some southeast dips in Grenville basement are observed in Lithoprobe data in deep seismic data in the area (Quinlan et al., 1992). From the magnetic field data (Fig. 2.7) it is evident, as discussed previously, that the Grenville basement is at great depth. From the discussion of the gravity effect of model A, it would be recalled that the gravity effect of Barachois/Codroy, separated from basement at reflector "R" is less than 9.2 mGal. This is less than the observed low, suggesting that basement (Lower Palaeozoic or Grenville) does not immediately underlie reflector "R". Structural relationships of "B" and "C" reflectors to "R" require some basal detachment. In both models A and B, it is possible that the Crabbes Brook Fault may represent the outcrop expression of the detachment zone because "R" approaches the surface close to the mapped location of the Crabbes Fault. Outcrop in this section of the seismic line is poor and it is impossible to verify this idea without some more research especially deep drilling.

Model B has less integrity because erosional truncation at the top of the Lower Palaeozoic ("D" and "E") below Carboniferous strata cannot be seen in the seismic profile.

4.4.4 Model C - A non-marine downlap within a half graben

Model C, which is non-marine downlap within a half graben (Figure 4.6), is based

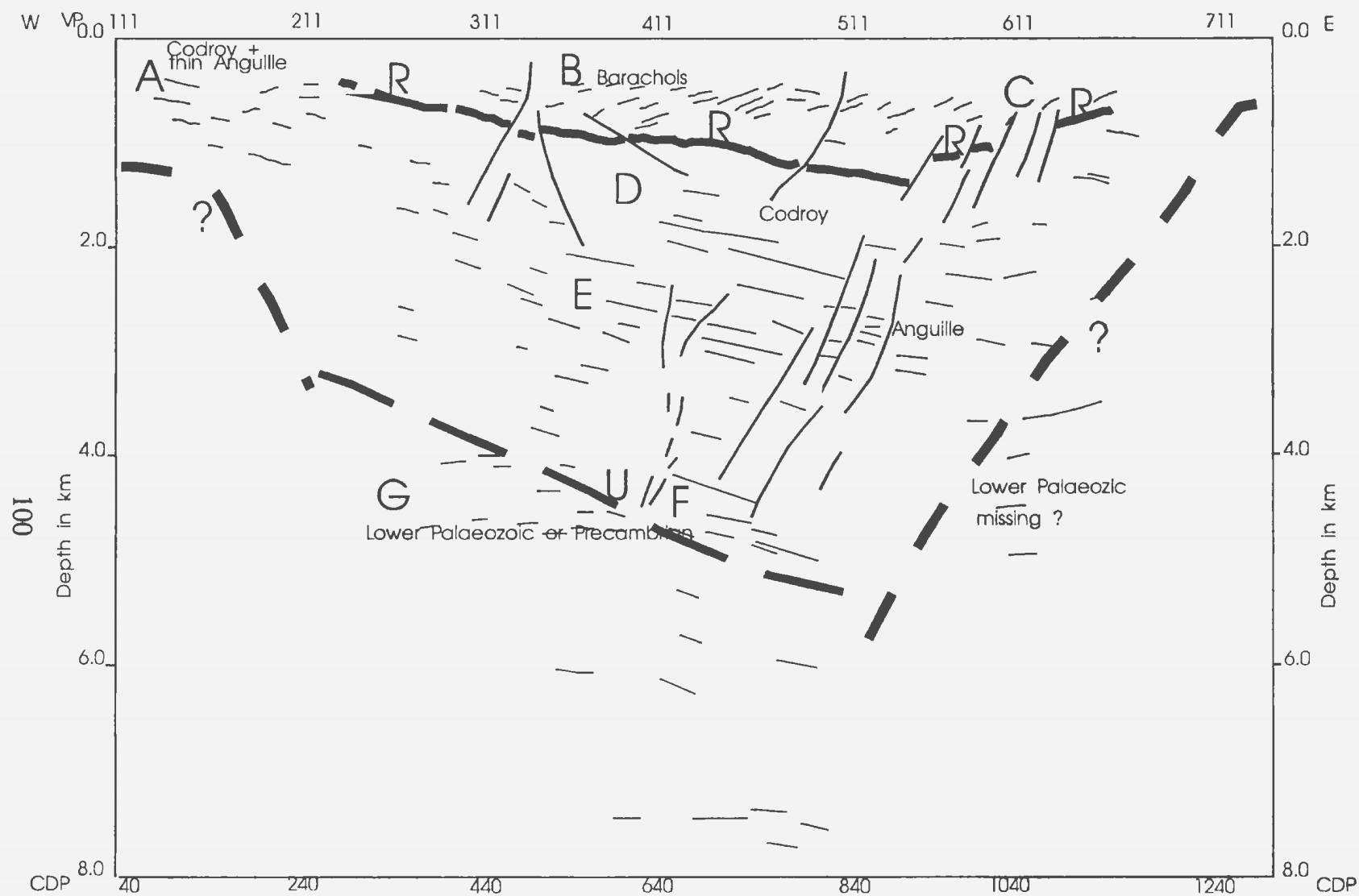


Figure 4.6. Model C - Non-marine downlap within a half graben.

on Reflector "R" as marking Crabbes limestone, the top of Viséan marine sedimentation in the basin (Hall et al., 1992). In this model package "D" would be marine Codroy Group comprising evaporites, thin limestone and fine grained grey and red beds of the Codroy Road Formation and Jeffrey's Village Members. The implication here would be that the Codroy Group (package "D") would overly the Anguille Group (package "E"). It is unlikely that "E" is lower Palaeozoic strata conserved in a down-faulted outlier beneath the basin because erosional truncation at the top of "E" is missing. "E" rests unconformably on either Lower Palaeozoic or Precambrian crystalline basement "G", though the possibility that Lower Palaeozoic is present at "F" cannot be ruled out. The low reflective package between "E" and "F" appears to be conformable with "F". But, this is not very clear from the seismic profile, therefore "F" may be or may be not Lower Palaeozoic.

In this model Codroy Group would be approximately 1.2 km thick overlying 1.0 km of Anguille. The Anguille is a full graben as in model A, bounded by faults on either side. However, the faults that define this graben cannot be placed exactly on the seismic profile because of the many minor faults that cut the whole section.

Packages "B" and "C" are interpreted as non-marine sediments that infilled a half-graben nestled east of the Long Range Fault and south of the Steel Mountain anorthosite. One of the predominant features of these packages ("B and "C") is the west dipping reflectors that intercept "R" at some points and may imply stratigraphic downlap. The downlap dipped at angles generally less than 20° for the reflectors.

This dip is a permissible repose for an offlapping sedimentary wedge deposited on a large alluvial fan (Hall et al., 1992).

Timing of the half-graben formation is not certain, but could have occurred during deposition of Windsor subzone C and even younger, since the Crabbes Limestone is likely not younger than early subzone C (Mamet, 1968; Knight 1983). The half-graben evolved from late Viséan through Westphalian as indicated by the age of the local coals (Hacquebard, 1972; Knight, 1983; Solomon, 1986). The east trending events with post-Codroy movements identified from seismic and potential fields data in offshore Bay St. George (Kilfoil, 1988) may suggest a linked subsidence history of onshore and offshore of the subbasin. The fault system, though complex, suggests that the basin may have been opened by strike slip movements but, later deformed by compressional forces.

The Barachois Group, though dominated by sandstones, contains some intervals dominated by shale and coal measures. Therefore, this could be imaged by the folded reflectors (Barachois syncline) in the middle of the seismic profile (VP 501 to 511). The east dipping packages would then consist of thick sandstone dominated sequences separated by fine grained (shale/mudstone/sandstone) intervals, a few tens to a hundred metres thick (the strongly imaged, westward dipping reflectors), reflecting pulses of basin subsidence coupled with relative uplift of source areas (Heward, 1978; Blair and Bilodeau, 1988). As the half graben grew wider and the source terrane retreated, the basin formed a complex floodplain of rivers and swampy to forested

overbank areas (coal bearing Barachois) (Hall et al., 1992).

Chapter 5: Conclusions

Reprocessing of this seismic profile has yielded significant results. In previous processing DMO was not at all applied to the data, therefore it can be concluded that DMO is a powerful tool in improving data quality. In the current project, more features have been unveiled especially unconformity "U", clear distinction of the reflection packages ("A" to "G") and clear identification of faults (see figures 3.20 and 4.1). It is now easier to interpret the seismic profile. There is a clue now that the basin may be limited downwards by "U". The clear distinction of the packages ("A" to "G") have made it easier to place boundaries between the different possible rock units.

There is no new data, either seismic or potential fields or drill hole data, that has been acquired in this area since this seismic line was interpreted by Hall et al. (1992). The unveiling of unconformity "U" has made it possible to constrain the basin downwards. "U" could be either Lower Palaeozoic/Precambrian boundary or Carboniferous/Lower Palaeozoic boundary or even Carboniferous/Precambrian boundary. Reflector "R" is most likely to be a décollement being imaged within the Carboniferous rocks. Therefore, models A and B are more likely than C. Model B requires a thick Lower Palaeozoic sequence in order that Grenville basement be deep enough to satisfy the magnetic field character. Since there is no surface evidence of any Lower Palaeozoic in this area, model B is regarded as somewhat less likely than model A. Moreover, the gravity anomaly map favours model A.

The structure of the basin from the current study is that of half graben as modelled

by Kilfoil (1988), Miller et al. (1990) and Hall et al. (1992). But, the depth and width extent of the basin is still uncertain. From the models, it appears that the basin could be as shallow as 2 km or as deep as 5 km. This contrasts with the 2-4 km models of Kilfoil (1988).

More research, especially deep drill holes and seismic reflection data, is needed to verify the above findings.

References

- Bell, W.A. 1948. Early Carboniferous Strata of St. George's Bay area. Geological Survey of Canada, Memoir 314, 112 p.
- Belt, E.S. 1969. Newfoundland Carboniferous Stratigraphy and its relation to the Maritimes Ireland. In Kay M. (Ed), Symposium on Stratigraphy and Structure Bearing on Continental Drift in the Northern American Ocean, Gander Meeting, 1967, AAPG, Memoir 12, p 734 - 753.
- Biondi, B. and Ronen, J. 1987. Dip Moveout in Shot Profiles, Geophysics, 52, p 1473-1482.
- Blair, T.C. and Bilodeau, W.L. 1988. Development of the tectonic cyclotherms in rift, pull-apart and foreland basins: Sedimentary response to episodic tectonism. Geology, 16, p 517-520.
- Dobrin, M.B., and Savit, C. H. 1988. Introduction to Geophysical Prospecting. New York, McGraw-Hill, 897p.
- Durling, P.W. and Marillier, F.J.Y. 1990. Structural trends and basement rock subdivisions in the western Gulf of St. Lawrence, northern Appalachians. Atlantic Geology 26, p 79-95.
- _____ 1993. Structural elements of the Magdalen Basin, Gulf of St. Lawrence, from seismic reflection data; in Research, Part D; Geological Survey of Canada, Paper 93-1D, p 147-154.
- Hacquebard, P.A. 1972. The Carboniferous of Eastern Canada. In Comptes Rendus,

7e Congrès International de Stratigraphie et de Géologie du Carbonifère,
Krefeld, Bd, 1, p 69-90.

- Hall, J., Langdon, G., Roberts, B., Hawkins, D., Fagan, A., Knight, I and Kilfoil, G. 1992. Reflection seismic imaging of the Carboniferous St. George coalfield, Western Newfoundland: a reappraisal of Palaeozoic stratigraphic thickness. *Bulletin of Canadian Petroleum Geology*, 40, p 321-334.
- Heward, P.A. 1978. Aluvial fan sequence and megasequence models: with examples from Westphalian D- Stephanian B coalfields, northern Spain: In A.D. Mial (ed). *Fluvial sedimentology*. Canadian Society of Petroleum Geologists, Memoir 5, p 669-702.
- Kilfoil, G.J. 1988. An integrated gravity, magnetic and seismic interpretation of the Carboniferous Bay St. George subbasin, western Newfoundland. Unpublished M.Sc. thesis, Memorial University of Newfoundland, 168 p.
- Kilfoil, G.J. and Bruce, P.A. 1991. Gridded Aeromagnetic data. 200 m grid cell (Ver.1.0), Newfoundland by 1:250000 NTS, map area, Newfoundland Dept. of Mines and Energy, Open File, Newfoundland (2063).
- Kleyn, A.H. 1984. *Seismic reflection interpretation*. London, Elsevier Applied Science Publishers, 269 p.
- Knight, I. 1982. Geology map of the Carboniferous Bay St. George subbasin, western Newfoundland, Map 82-1, Mineral Development Division, Newfoundland and Labrador Department of Mines and Energy.

- _____. 1983. Geology of the Carboniferous Bay St. George Subbasin, western Newfoundland, Memoir 1, Mineral Development Division, Newfoundland and Labrador Department of Mines and Energy, 358 p.
- Langdon, G. 1991. Current research into the western Newfoundland Carboniferous - Onshore and offshore. CERR, unpublished report.
- Langdon, G.S. and Hall, J. Carboniferous tectonics, Basin development and styles of deformation in the Cabot Strait. In prep.
- Larner, K.L., Gibson, B.R., Chambers, R. and Wiggins, R.A. 1979. Simultaneous estimation of the residual static and cross-dip corrections. *Geophysics*, 44, p 1175.
- Mamet, B.L. 1968. Sur une Microfaune du Viséan Supérieur de terre Neuve. *Naturaliste Canadien*, 95, p 1357-1372.
- Miller, H., Kilfoil, G.J., and Peavy, S.T. 1990. An integrated geophysical interpretation Carboniferous Bay St. George Subbasin, western Newfoundland. *Bulletin of Canadian Petroleum Geology*, 38, p 320-331.
- Murthy, G.S. and Rao, K.V. 1976. Palaeomagnetism of Steel Mountain and Indian Head anorthosites from western Newfoundland. *Canadian Journal of Earth Sciences*, 13 p 75-83.
- Neidell, N. and Taner, M.T. 1971. Semblance and other coherency measures for multichannel Data. *Geophysics*, 36, p 482-497.
- Peavy, S.T. 1985. A gravity and magnetic interpretation of the Bay St. George

- Carboniferous Subbasin in western Newfoundland. Unpublished M.Sc. thesis, Memorial University of Newfoundland, 207 p.
- Quinlan, G.M., Hall, J., Williams, H., Wright, J., Colman-Sadd, S.P., O'Brien, S.J., Stockmal, G.S. and Marillier, F. 1992. Lithoprobe onshore reflection transects across the Newfoundland Appalachians. *Canadian Journal of Earth Sciences*, 29, p 1865-1877.
- Rietsch, E. 1980. Estimation of the signal-to-noise ratio of seismic data with an application to stacking. *Geophysical prospecting*, 28, p 531-550.
- Riley, G.C. 1962. Stephenville map-area, Newfoundland. *Geophysical Survey of Canada, Memoir 232*, 72 p.
- Robinson, E.A. 1983. *Seismic Velocity Analysis and the Convolutional Model*. Boston, International Human Resources Development Corporation, 290 p.
- Schillcreff, S. and Williams, H. 1979. Geology of the Stephenville Map area, Newfoundland. In: *Current Research, Part A. Geological Survey of Canada, Paper 79-1A*, p 327-332.
- Solomon, S. 1986. Sedimentary and Fossil-fuel potential of the Upper Carboniferous Barachois Group, western Newfoundland. Unpublished M.Sc. thesis, Memorial University of Newfoundland, 256 p.
- Spector, A. 1969. Report on Interpretation of aeromagnetic data, St. George's Bay, Newfoundland. British Newfoundland Exploration Limited. Unpublished report, open file PB (157), Newfoundland and Labrador Department of Mines

and Energy.

STARPAK Processing Manual, 1989.

Stuart, C.J. and Caughey, C.A. 1977. Seismic facies and sedimentology of terrigenous Pleistocene deposits in Northwest and Central Gulf of Mexico. In: C.E. Payton (Ed). The seismic Stratigraphy - applications to hydrocarbon exploration, AAPG, Memoir 26, p 249-275.

Telford, W.M., Geldart, L.P. and Sheriff, R.E. 1990. Applied Geophysics. New York, Cambridge University Press, pp 770.

Vernall, P. 1954. Gravity Survey of the Bay St. George area, Southwest Newfoundland. Geological survey of Newfoundland, Unpublished report, Open file 12B (63).

Wiggins, R. A., Larner, K.L. and Wisecup, R.D. 1976. residual static analysis as a general linear inverse problem. Geophysics, 41, p 922.

Williams, H. 1978. Tectonic Lithofacies map of the Appalachian Orogen. Memorial University of Newfoundland, Map 1.

_____ 1985. Geology, Stephenville Map area, Newfoundland. Geological Survey Of Canada, Map 1579A (1:1,000,000).

Wilson, J.T. 1962. Cabot fault, an Appalachian equivalent of San Andreas and Great Glen Faults and some implications for continental displacement. Nature, 195, p. 135-138.

Yilmaz, O. 1987. Seismic Data Processing. Investigations in Geophysics volume 2,

Society of Exploration Geophysicists.

Appendix A

This appendix contains the values used to calculate field statics corrections and elevation values.

Abbreviations are as follows; t_i is the intercept time (ms); v_b is the velocity of the bedrock (km/s); z_w is the thickness of the weathered layer (m); E_s is the elevation (m) and T_d is the static correction (ms).

Appendix A

Table A.1. FIELD STATICS SPECIFICATIONS.

station	ti	vb	zw	Es	Td
101	5	3.6	6.013	124	5.886
103	10	3.6	12.03	124.5	4.411
105	13	3.6	15.63	124.9	3.498
107	15	3.6	18.04	125.3	2.852
109	15	3.6	18.04	125.8	2.713
111	15	3.6	18.04	126.2	2.602
113	15	3.6	18.04	126.7	2.463
115	15	3.6	18.04	127.1	2.352
117	15	3.6	18.04	127.5	2.241
119	16	3.6	19.24	128	1.835
121	18	3.6	21.65	128.2	1.245
123	20	3.6	24.05	127.5	0.905
125	25	3.6	30.07	126.8	-0.24
127	27	3.6	32.47	125.7	-0.47
129	29	3.6	34.88	124.5	-0.67
131	28	3.6	33.67	123.3	-0.07
133	25	3.6	30.07	122.1	1.068
135	23	3.6	27.66	120.9	1.936
137	22	3.6	26.46	119.7	2.537
139	21	3.625	25.18	118.5	3.046
141	20	3.625	23.98	117.3	3.646
143	19	3.625	22.78	116.9	4.025
145	18	3.625	21.58	116.6	4.376
147	18	3.625	21.58	116.3	4.459
149	18	3.625	21.58	115.9	4.57
151	19	3.65	22.71	115.6	4.291
153	20	3.65	23.91	115.2	4.13
155	22	3.65	26.3	114.9	3.672
157	24	3.65	28.69	114.6	3.214
159	26	3.65	31.08	114.2	2.783
161	29	3.7	34.47	113.9	1.838
163	32	3.7	38.04	112.6	1.37
165	35	3.725	41.49	109.5	1.266
167	38	3.75	44.92	107.4	0.878

Appendix A

Table A.1. FIELD STATICS SPECIFICATIONS.

169	41	3.8	48.22	109.8	-0.84
171	44	3.85	51.49	112.1	-2.53
173	46	3.9	53.58	114.3	-3.9
175	47	4	54.27	115.3	-4.89
177	47	4.05	54.05	116.4	-5.38
179	45	4.125	51.45	117.4	-5.35
181	41	4.2	48.63	118.5	-4.71
183	38	4.3	42.93	118.6	-4.18
185	35	4.35	39.41	118.7	-3.45
187	31	4.45	34.7	118.8	-2.54
189	28	4.525	31.21	118.9	-1.84
191	25	4.6	27.76	119	-1.11
193	22	4.675	24.34	119.1	-0.35
195	19	4.75	20.95	119.2	0.421
197	17	4.8	18.7	119.3	0.941
199	16	4.85	17.56	119.4	1.149
201	14	4.9	15.34	119.5	1.686
203	14	4.9	15.34	120.4	1.503
205	14	4.925	15.32	121.2	1.298
207	14	4.925	15.32	122	1.136
209	15	4.9	16.43	122.8	0.689
211	17	4.85	18.66	123.7	-0.06
213	19	4.775	20.92	124.5	-0.74
215	22	4.65	24.37	125.3	-1.63
217	24	4.5	26.79	126.2	-2.15
219	26	4.3	29.37	127	-2.51
221	28	4.15	31.96	127.8	-2.93
223	29	4	33.49	129	-3.12
225	30	3.8	35.28	130.3	-3.17
227	30	3.675	35.76	131.5	-3.12
229	30	3.45	36.82	132.7	-2.72
231	29	3.25	36.79	133.2	-1.91
233	27	3.1	35.34	133.4	-0.91
235	25	3	33.54	133.7	-0.16
237	22	2.9	30.38	134	0.803

Appendix A

Table A.1. FIELD STATICS SPECIFICATIONS.

239	20	2.825	28.32	134.3	1.422
241	17	2.8	24.29	134.6	2.03
243	14	2.8	20	134.2	2.785
245	13	2.8	18.58	133.9	3.096
247	12	2.8	17.15	133.6	3.408
249	12	2.8	17.15	133.2	3.551
251	12	2.8	17.15	132.9	3.658
253	15	2.8	21.43	132.6	3.152
255	17	2.8	24.29	132.2	2.887
257	19	2.8	27.15	131.9	2.586
259	19	2.8	27.15	131.6	2.693
261	19	2.8	27.15	131.5	2.729
263	17	2.8	24.29	131.3	3.208
265	15	2.8	21.43	131.1	3.688
267	10	2.8	14.29	130.9	4.78
269	8	2.8	11.43	131	5.153
271	8	2.8	11.43	131	5.153
273	8	2.8	11.43	131	5.153
275	8	2.8	11.43	131.1	5.117
277	8	2.8	11.43	131.2	5.081
279	8	2.8	11.43	131.4	5.01
281	7	2.8	10	131.6	5.143
283	7	2.8	10	131.8	5.071
285	7	2.8	10	132.4	4.857
287	7	2.8	10	132.9	4.678
289	9	2.8	12.86	133.5	4.056
291	12	2.8	17.15	134	3.265
293	15	2.8	21.43	134.6	2.438
295	15	2.8	21.43	134.5	2.474
297	15	2.8	21.43	133.8	2.724
299	16	2.8	22.86	133.1	2.77
301	16	2.8	22.86	132.4	3.02
303	16	2.8	22.86	133.3	2.698
305	16	2.8	22.86	134.4	2.305
307	16	2.8	22.86	135.5	1.913

Appendix A

Table A.1. FIELD STATICS SPECIFICATIONS.

309	16	2.8	22.86	136.7	1.484
311	18	2.85	25.27	137.8	0.513
313	23	2.85	32.28	138.9	-0.92
315	26	2.85	36.5	140.1	-1.97
317	27	2.85	37.9	141.2	-2.56
319	28	2.85	39.3	142.4	-3.19
321	28	2.9	38.67	143.8	-3.86
323	28	2.9	38.67	144.6	-4.14
325	28	2.9	38.67	145.4	-4.41
327	28	2.95	38.09	146.3	-4.88
329	28	3	37.57	147.1	-5.29
331	28	3.05	37.09	147.8	-5.66
333	27	3.1	35.34	148.3	-5.72
335	25	3.125	32.54	148.8	-5.47
337	22	3.15	28.48	149.3	-4.98
339	18	3.15	23.3	149.8	-4.19
341	17	3.175	21.89	150.3	-4.14
343	16	3.2	20.5	150.6	-4.03
345	14	3.2	17.93	150.8	-3.61
347	10	3.2	16.65	150.9	-3.4
349	12	3.2	15.37	150.4	-3.01
351	10	3.2	12.81	150	-2.4
353	9	3.2	11.53	149.5	-2.01
355	7	3.2	8.967	149.1	-1.4
357	5	3.2	6.405	148.6	-0.76
359	3	3.2	3.843	148.2	-0.16
361	2	3.225	2.549	147.9	0.167
363	2	3.225	2.549	148.1	0.105
365	1	3.225	1.275	148.3	0.285
367	0	3.25	0	148.4	0.492
369	0	3.25	0	151	-0.31
371	0	3.25	0	153	-0.92
373	0	3.3	0	154.3	-1.3
375	0	3.3	0	155.6	-1.7
377	0	3.3	0	156.8	-2.06

Appendix A

Table A.1. FIELD STATICS SPECIFICATIONS.

379	0	3.3	0	156.8	-2.06
381	0	3.3	0	158.1	-2.45
383	0	3.3	0	159.4	-2.85
385	0	3.33	0	160.4	-3.12
387	0	3.33	0	161.5	-3.45
389	1	3.33	1.251	162.5	-4
391	3	3.33	3.752	163.6	-4.83
393	4	3.33	5.003	164.6	-5.38
395	5	3.33	6.254	165.7	-5.96
397	5	3.33	6.254	166.7	-6.26
399	5	3.33	6.254	167.6	-6.53
401	5	3.33	6.254	168.4	-6.77
403	5	3.33	6.254	169.2	-7.01
405	5	3.33	6.254	170.3	-7.34
407	5	3.33	6.254	171.3	-7.65
409	4	3.33	5.003	172.3	-7.7
411	3	3.33	3.752	173.3	-7.75
413	2	3.33	2.501	174.4	-7.83
415	4	3.33	5.003	175.4	-8.63
417	7	3.33	8.755	176.4	-9.68
419	6	3.33	7.504	177.4	-9.73
421	6	3.33	7.504	177.9	-9.88
423	5	3.33	6.254	178.3	-9.75
425	4	3.33	5.003	178.4	-9.53
427	4	3.33	5.003	178.6	-9.59
429	4	3.33	5.003	178.7	-9.62
431	4	3.33	5.003	178.6	-9.59
433	4	3.33	5.003	178.2	-9.47
435	4	3.33	5.003	177.9	-9.38
437	4	3.33	5.003	177.5	-9.26
439	4	3.33	5.003	177.2	-9.17
441	4	3.33	5.003	176.8	-9.05
443	5	3.33	6.254	176.5	-9.21
445	6	3.33	7.504	176.4	-9.43
447	7	3.33	8.755	176.4	-9.68

Appendix A

Table A.1. FIELD STATICS SPECIFICATIONS.

449	8	3.33	10.01	176.3	-9.9
451	9	3.33	11.26	176.3	-10.1
453	9	3.33	11.26	176.2	-10.1
455	10	3.33	12.51	176.1	-10.3
457	10	3.33	12.51	176.1	-10.3
459	10	3.33	12.51	175.8	-10.2
461	10	3.33	12.51	175.6	-10.2
463	10	3.33	12.51	175.3	-10.1
465	12	3.33	15.01	176.5	-11
467	14	3.33	17.51	177.7	-11.8
469	14	3.33	17.51	178.9	-12.2
471	14	3.33	17.51	180.1	-12.5
473	14	3.33	17.51	181.4	-12.9
475	14	3.33	17.51	182.6	-13.3
477	14	3.33	17.51	183.8	-13.6
479	13	3.33	16.26	185	-13.8
481	12	3.33	15.01	186.2	-13.9
483	11	3.33	13.76	187.4	-14
485	10	3.33	12.51	188.2	-14
487	9	3.33	11.26	188.4	-13.8
489	8	3.33	10.01	188.4	-13.5
491	7	3.33	8.755	188.4	-13.3
493	6	3.33	7.504	188.3	-13
495	5	3.33	6.254	188.3	-12.8
497	6	3.33	7.504	188.3	-13
499	7	3.33	8.755	188.2	-13.2
501	7	3.33	8.755	186.8	-12.8
503	7	3.33	8.755	185.4	-12.4
505	7	3.33	8.755	184.4	-12.1
507	7	3.33	8.755	183.4	-11.8
509	7	3.33	8.755	182.4	-11.5
511	6	3.33	7.504	181.5	-11
513	5	3.33	6.254	180.5	-10.4
515	4	3.33	5.003	179.5	-9.86
517	4	3.33	5.003	178.5	-9.56

Appendix A

Table A.1. FIELD STATICS SPECIFICATIONS.

519	2	3.33	2.501	177.5	-8.76
521	0	3.33	0	176.5	-7.96
523	0	3.33	0	175.5	-7.66
525	0	3.33	0	174.8	-7.45
527	0	3.33	0	174.2	-7.27
529	0	3.33	0	175.5	-7.66
531	0	3.33	0	177.5	-8.26
533	0	3.33	0	178.7	-8.62
535	0	3.33	0	179.7	-8.92
537	0	3.33	0	180.8	-9.25
539	0	3.33	0	181.9	-9.58
541	1	3.33	1.251	183	-10.2
543	2	3.33	2.501	184.1	-10.7
545	4	3.33	5.003	185.4	-11.6
547	5	3.33	6.254	186.6	-12.2
549	7	3.33	8.755	186.3	-12.6
551	10	3.33	12.51	185.9	-13.3
553	12	3.33	15.01	185.5	-13.7
555	11	3.33	13.76	183.6	-12.8
557	10	3.33	12.51	181.7	-12
559	10	3.33	12.51	179.8	-11.4
561	10	3.33	12.51	177.9	-10.9
563	12	3.33	15.01	176	-10.8
565	14	3.33	17.51	175	-11
567	17	3.33	21.26	175.9	-12
569	18	3.33	22.51	172.9	-11.4
571	14	3.33	17.51	171.9	-10.1
573	10	3.33	12.51	171.7	-9.01
575	12	3.33	15.01	173.9	-10.2
577	13	3.33	16.26	176.1	-11.1
579	13	3.33	16.26	178.4	-11.8
581	12	3.33	15.01	180.6	-12.2
583	11	3.33	13.76	182.8	-12.6
585	10	3.33	12.51	184.3	-12.8
587	8	3.33	10.01	185.5	-12.7

Appendix A

Table A.1. FIELD STATICS SPECIFICATIONS.

589	6	3.33	7.504	186	-12.3
591	7	3.33	8.755	186.5	-12.7
593	8	3.33	10.01	187	-13.1
595	6	3.33	7.504	187.6	-12.8
597	5	3.33	6.254	188.1	-12.7
599	3	3.33	3.752	188.6	-12.3
601	2	3.33	2.501	189.3	-12.3
603	2	3.33	2.501	190.1	-12.5
605	5	3.33	6.254	191.3	-13.7
607	3	3.33	3.752	192.5	-13.5
609	2	3.33	2.501	193.7	-13.6
611	3	3.33	3.752	195	-14.3
613	4	3.33	5.003	196.2	-14.9
615	5	3.33	6.254	197.5	-15.5
617	6	3.33	7.504	198.7	-16.1
619	6	3.33	7.504	199.5	-16.4
621	7	3.33	8.755	199.9	-16.7
623	7	3.33	8.755	200.4	-16.9
625	8	3.33	10.01	201.6	-17.5
627	8	3.33	10.01	202.9	-17.9
629	7	3.33	8.755	204.2	-18
631	7	3.33	8.755	205.4	-18.4
633	10	3.33	12.51	206.7	-19.5
635	12	3.33	15.01	206.8	-20.1
637	10	3.33	12.51	206.8	-19.6
639	7	3.33	8.755	206.8	-18.8
641	0	3.33	0	206.8	-17.1
643	0	3.33	0	206.9	-17.1
645	0	3.33	0	206.4	-16.9
647	0	3.33	0	206	-16.8
649	0	3.33	0	205.6	-16.7
651	0	3.33	0	205.8	-16.8
653	0	3.33	0	206.4	-16.9
655	0	3.33	0	207	-17.1
657	0	3.33	0	207.6	-17.3

Appendix A

Table A.1. FIELD STATICS SPECIFICATIONS.

659	0	3.33	0	208.2	-17.5
661	0	3.33	0	208.8	-17.7
663	0	3.33	0	209.4	-17.8
665	0	3.33	0	210.1	-18
667	0	3.33	0	210.7	-18.2
669	0	3.33	0	211.3	-18.4
671	1	3.33	1.251	211.7	-18.8
673	3	3.33	3.752	212.1	-19.4
675	5	3.33	6.254	212.5	-20
677	7	3.33	8.755	212.9	-20.6
679	10	3.33	12.51	213.3	-21.5
681	15	3.33	18.76	213.6	-22.8
683	18	3.33	22.51	213.5	-23.6
685	20	3.33	25.01	214.3	-24.3
687	22	3.33	27.52	215.1	-25
689	25	3.33	31.27	216	-26.1
691	31	3.33	38.77	216.4	-27.7
693	40	3.33	50.03	216.9	-30.1
695	70	3.33	87.55	217.2	-37.7
697	74	3.33	92.55	217.4	-38.7
699	75	3.33	93.8	217.6	-39
701	76	3.33	95.05	217.7	-39.3
703	76	3.33	95.05	217.9	-39.4
705	75	3.33	93.8	218.5	-39.3
707	73	3.33	91.3	219.2	-39
709	72	3.33	90.05	219.9	-39
711	70	3.33	87.55	220.5	-38.7
713	68	3.33	85.05	221.2	-38.4
715	67	3.33	83.8	221.9	-38.3
717	67	3.33	83.8	221.8	-38.3
719	67	3.33	83.8	221.5	-38.2
721	67	3.33	83.8	221.1	-38.1
723	67	3.33	83.8	220	-37.8
725	67	3.33	83.8	216.9	-36.8
727	67	3.33	83.8	213.8	-35.9

Appendix A

Table A.1. FIELD STATICS SPECIFICATIONS.

729	67	3.33	83.8	210.7	-35
731	67	3.33	83.8	207.5	-34
733	67	3.33	83.8	207	-33.9
735	67	3.33	83.8	200.3	-31.8

Appendix B

DMO Theory

The impulse response in time-space coordinates of the DMO operator derived by Biondi and Ronen (1987) is an ellipse:

$$\left(\frac{t}{t_1}\right)^2 + \left(\frac{x - x_1}{x_1}\right)^2 = 1 \quad (\text{B.1})$$

where t_1 is the location of the impulse and x represents full offset. The above equation is only part of the operator, no amplitude information is included in it. Amplitude information is ignored at this point due to its uncertainty. It would be expensive to perform DMO using equation B.1. Therefore, a change of variables has to be made that transforms equation B.1.

Let $x = \exp(p)$, $x_0 = \exp(p_0)$

$t = \exp(s)$, $t_0 = \exp(s_0)$, then:

$$(\exp(s - s_0))^2 + (\exp(p - p_0) - 1)^2 = 1 \quad (\text{B.2})$$

Equation B.2 is more pleasing than equation B.1 because the form of the curve does not change with (s_0, p_0) , therefore convolution applies and a fast algorithm could be written.

Appendix B

But, the change of variables involves a logarithmic stretch which will usually increase the size of the shot record. The amount of increase is dependent on the frequency and wavenumber content of the data, and also on the start time and near offset. The transformation makes time zero and offset zero to map to infinity in the p and s domains. There must be a non-zero start time and a non-zero offset. DMO in shot records is a compromise. The offset direction is log transformed so vectoring could be used, and the time axis is left as it is, to avoid additional data to process. The reason x axis is chosen to be transformed is that normalised wavenumbers for a moved-out shot tend to be lower as compared to the normalised frequencies, therefore this direction would be less sensitive to the transformation.

After log transforming x axis, equation B.1 becomes:

$$\left(\frac{t}{t_i}\right)^2 + (\exp(p - p_0) - 1)^2 = 1 \quad (\text{B.3})$$

If p is made the subject of the formula in equation B.3, the following expression is obtained:

$$p = p_i + \log \left(1 \pm \sqrt{1 - \left(\frac{t}{t_i}\right)^2} \right) \quad (\text{B.4})$$

Appendix B

A plot of equation B.4 is shown in figure B.1. Figure B.2 shows the plot of the same equation with different p_0 's and t_0 's. Note that the form of the curve does not change with p_0 , rather it changes with t_0 .

Equation B.3 can now be used to produce an algorithm that will perform DMO. Consider the following integral;

$$g(t, p) = \int_t^{\infty} A f(s, p - \log [1 - \sqrt{1 - (\frac{t}{s})^2}] ds + \int_t^{\infty} B f(s, p - \log [1 + \sqrt{1 - (\frac{t}{s})^2}]) ds \quad (B.5)$$

where $f(t, p)$ is the stretched NMO-corrected shot record, $g(t, p)$ is the stretched zero offset section and A and B are arbitrary functions to be determined. It is hoped that this integral will give the proper t-p relationship by substituting a delta function at some location for the function f, i.e let $f(s, p) = \Delta(s - t_0) * \Delta(p - p_0)$, and solve the integral:

$$g(t, p) = \int_t^{\infty} A \Delta(s - t_0) * \Delta(p - p_0 - \ln [1 - \sqrt{1 - (t/s)^2}]) ds$$

Appendix B

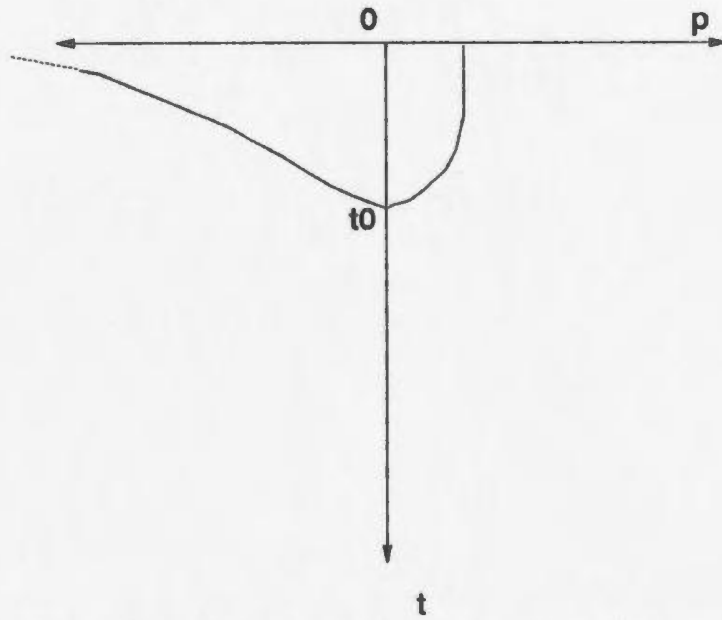


Figure B.1. Plot of equation B.4. P_0 was set to zero for this plot (Blondi and Ronen, 1987).

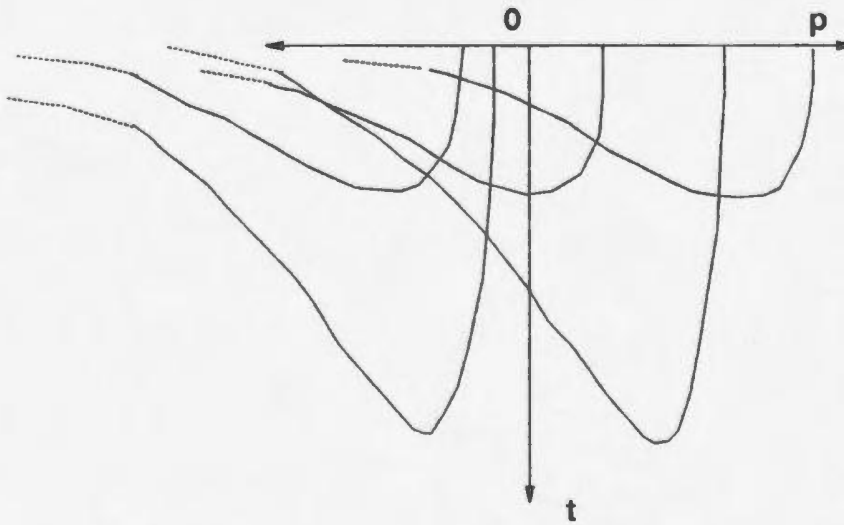


Figure B.2. Plot of equation B.4 for different values for P_0 's and t_0 's (Blondi and Ronen, 1987).

Appendix B

$$+ \int_t^{\infty} B \Delta(s - t_0) * \Delta(p - p_0 - \ln[1 + \sqrt{1 - (t/s)^2}]) ds \quad (B.6)$$

By the definition of the delta function, the above integral will only have non-zero values

when s is equal to t_0 , and

$$p - p_0 - \log(1 - \sqrt{1 - (t/s)^2}) = 0 \quad (B.7)$$

and

$$p - p_0 - \log(1 + \sqrt{1 - (t/s)^2}) = 0 \quad (B.8)$$

Substituting t_0 for s in the above equations, we arrive at equation B.4, the desired time response. Applying Fourier transform in p on the above equation the following expression is obtained:

$$g(t, k) = \int_t^{\infty} A f(s, k) e^{jk \ln(1 - \sqrt{1 - (t/s)^2})} ds$$

$$+ \int_t^{\infty} B f(s, k) e^{j k l n (1 + \sqrt{1 - (t/s)^2})} ds \quad (B.9)$$

There are no restrictions on the values of A and B because the amplitudes of DMO are uncertain. However, a convenient choice of A and B would be the derivatives of

$$\log (1 - \sqrt{1 - (t/s)^2}) \quad (B.10)$$

and

$$- \log (1 - \sqrt{1 + (t/s)^2}) \quad (B.11)$$

with respect to s.

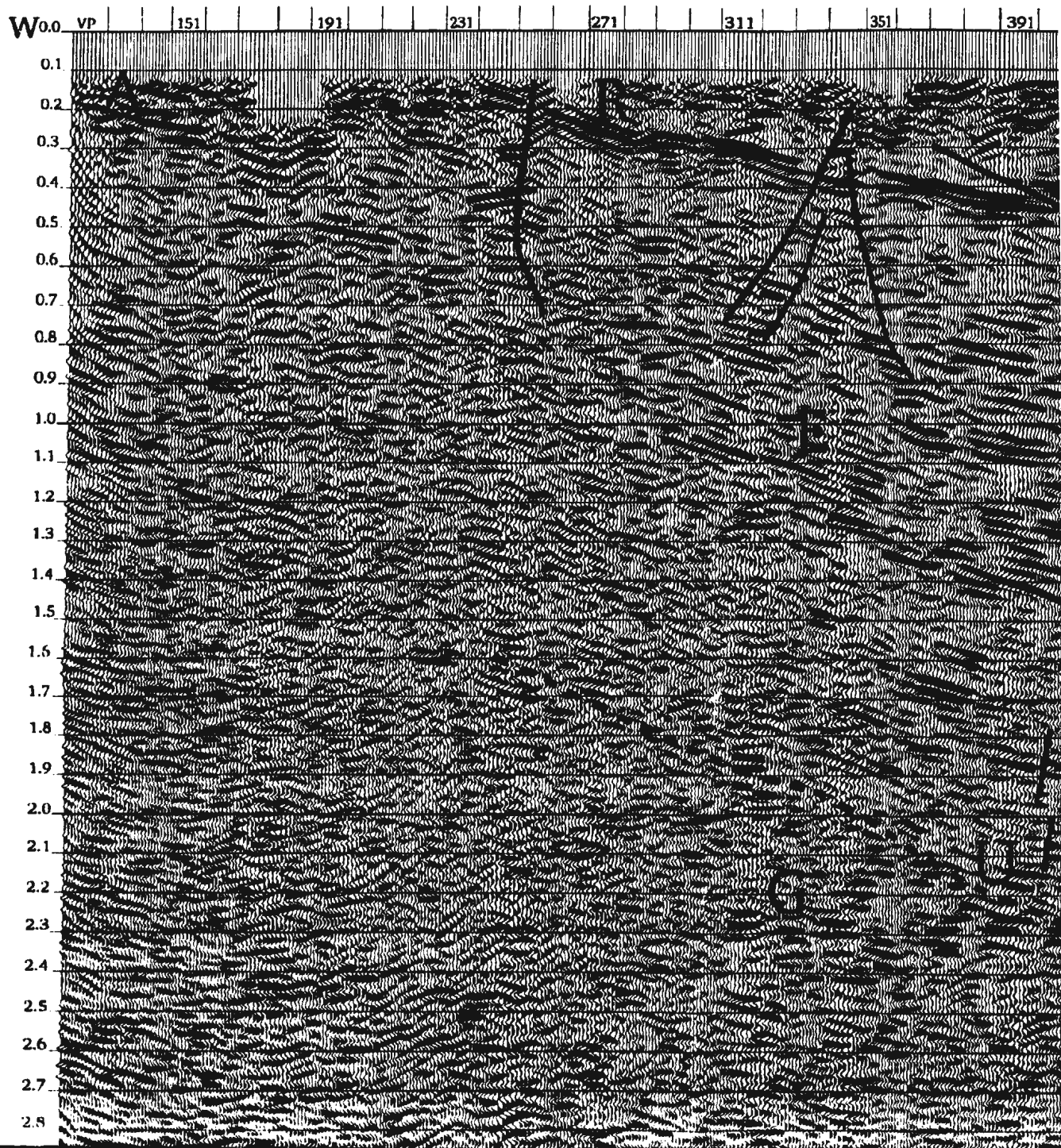
The final result after all the analytical computations is:

$$\begin{aligned} g(m\Delta t, k) = & \sum_{n=m}^{\infty} f(n\Delta t, k) [e^{j k l n (1 - \sqrt{1 - (\frac{m}{n} + 1)^2})} \\ & - e^{j k l n (1 - \sqrt{1 - (\frac{m}{n})^2})} - e^{j k l n (1 + \sqrt{1 - (\frac{m}{n+1})^2})} \\ & + e^{j k l n (1 + \sqrt{1 - \frac{m^2}{n^2}})}] \end{aligned} \quad (B.12)$$

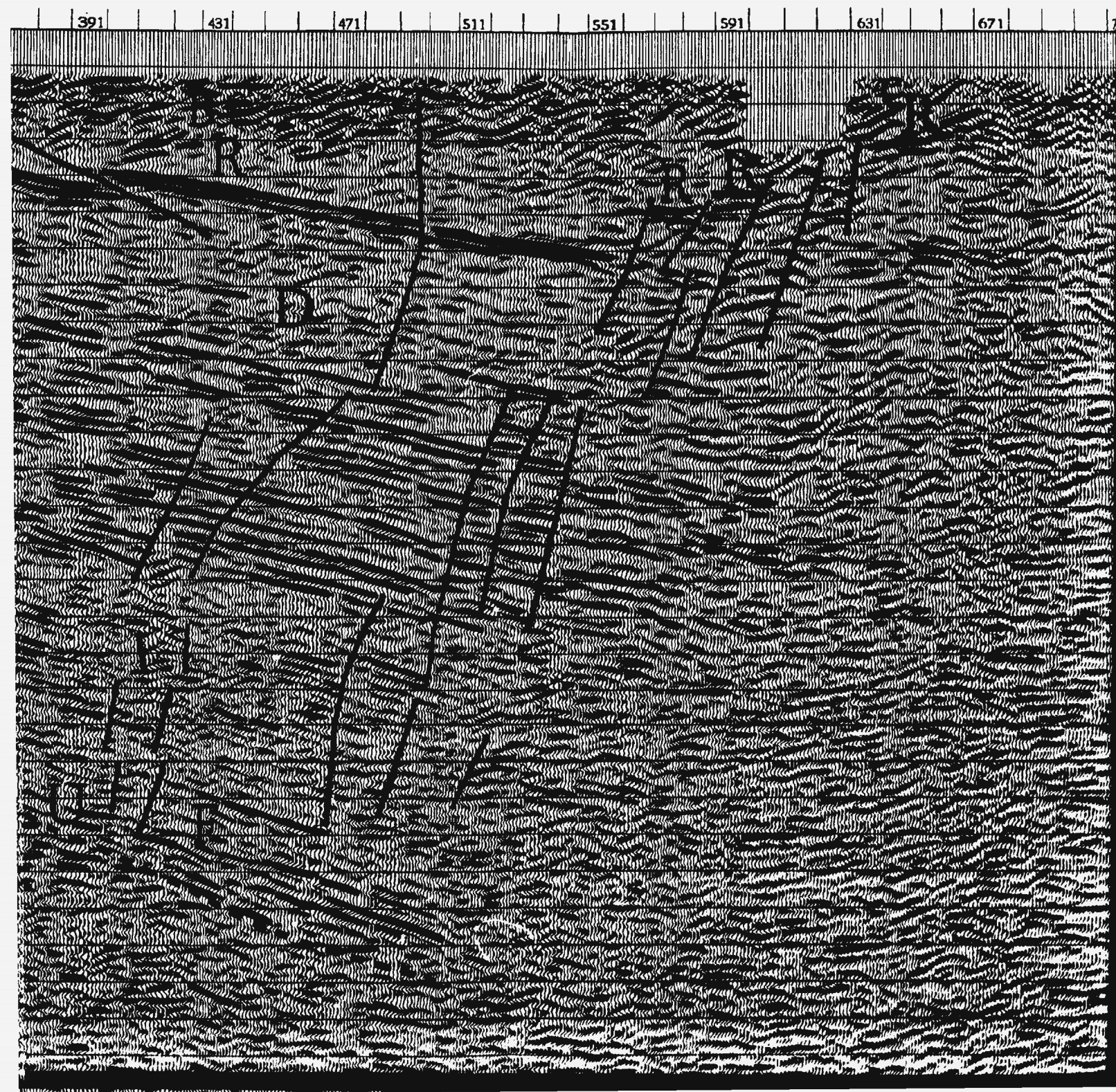
Appendix B

where $t = m * dt$ and $s = n * dt$. The above expression is the operator used to DMO in shot records.

Figure 4.2. Main re
of the seismic prof
reflection packages;
0.2 to 0.6 s TWT; th
unconformity "U" i



2. Main reflection packages, faults and unconformity
smic profile. Packages "A" to "G" mark the main
packages; "R" is a major reflector which extends from
s TWT; the faults are shown as vertical thin lines and
ity "U" is shown by a dashed line.



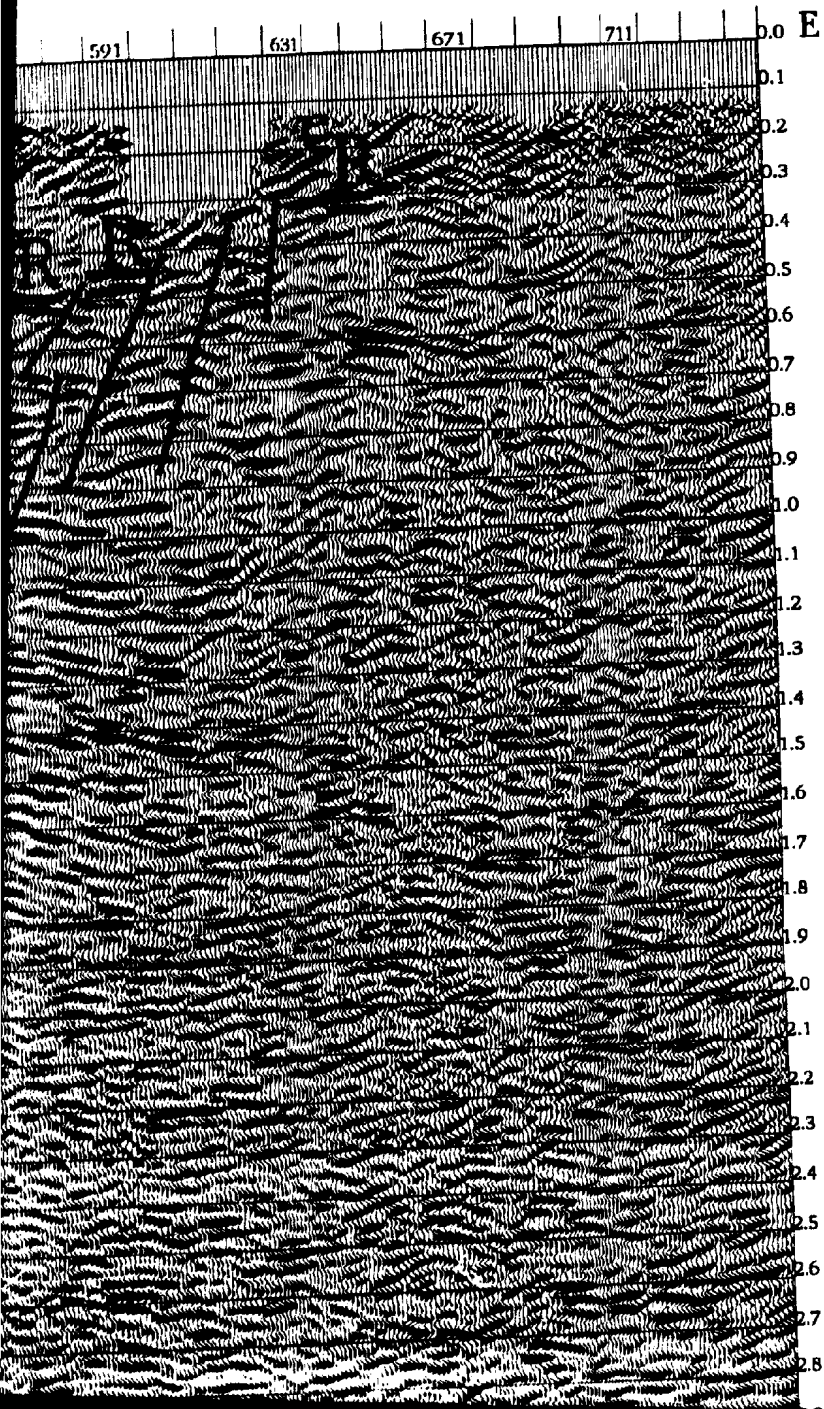
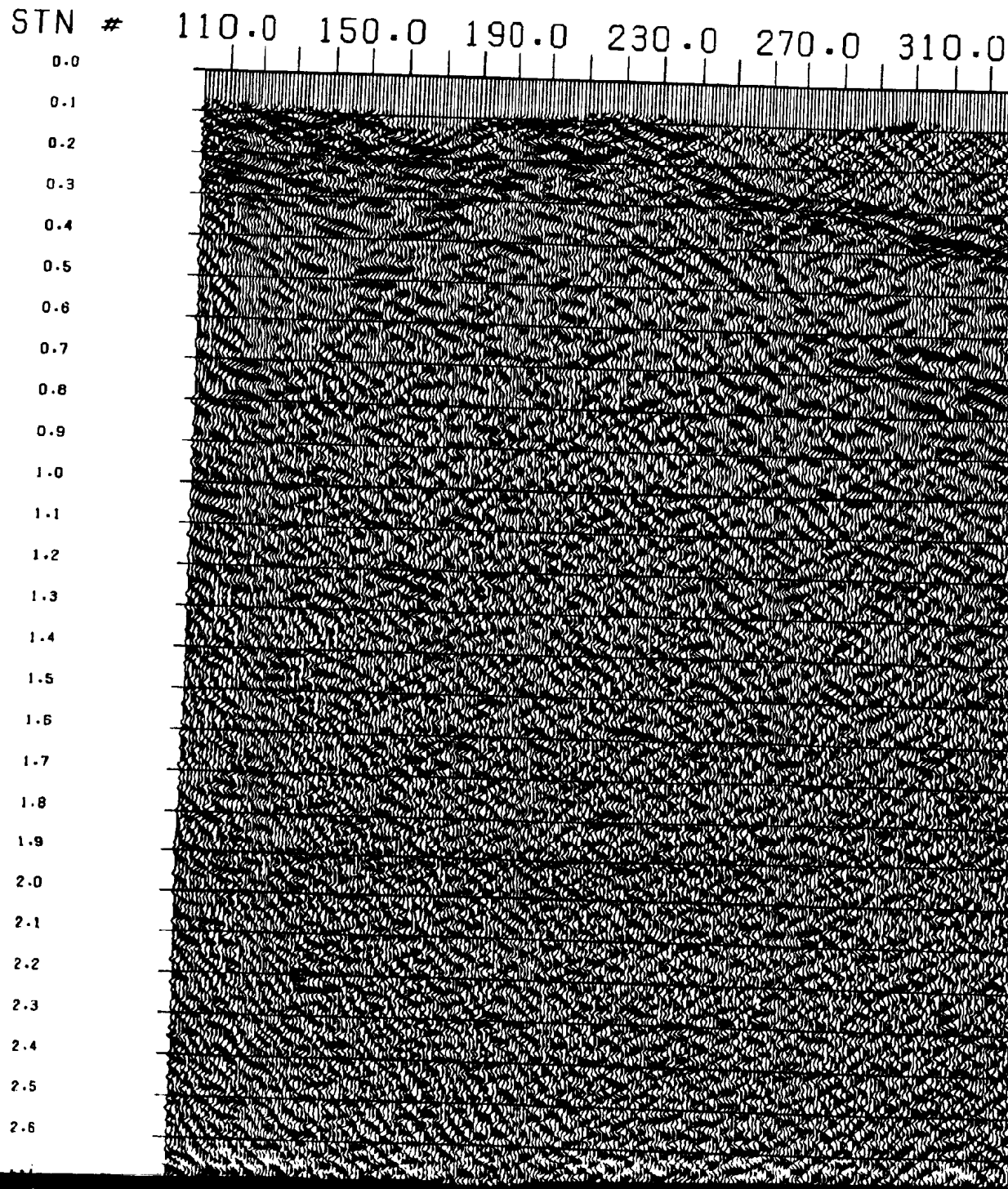
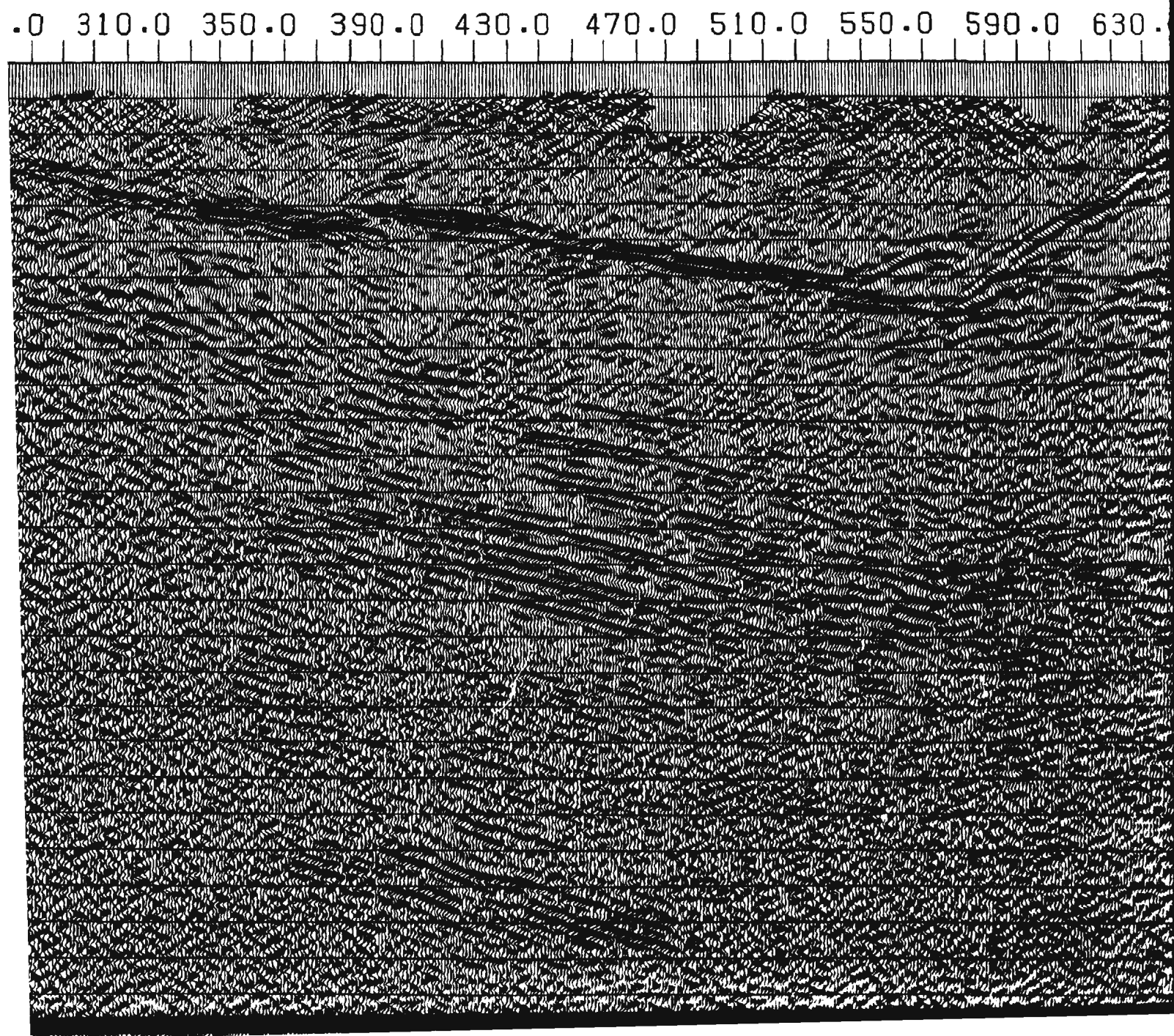


Figure 4.1. The seismic profile as processed previously. Note the difference in focus of events as compared to figure 3.21. In this section unconformity "U" cannot be identified. The demarcation between one package to the other is not clear.



previously. Note
to figure 3.21. In
identified. The
is not clear.



590.0 630.0 670.0 710.0

STN #

0.0

0.1

0.2

0.3

0.4

0.5

0.6

0.7

0.8

0.9

1.0

1.1

1.2

1.3

1.4

1.5

1.6

1.7

1.8

1.9

2.0

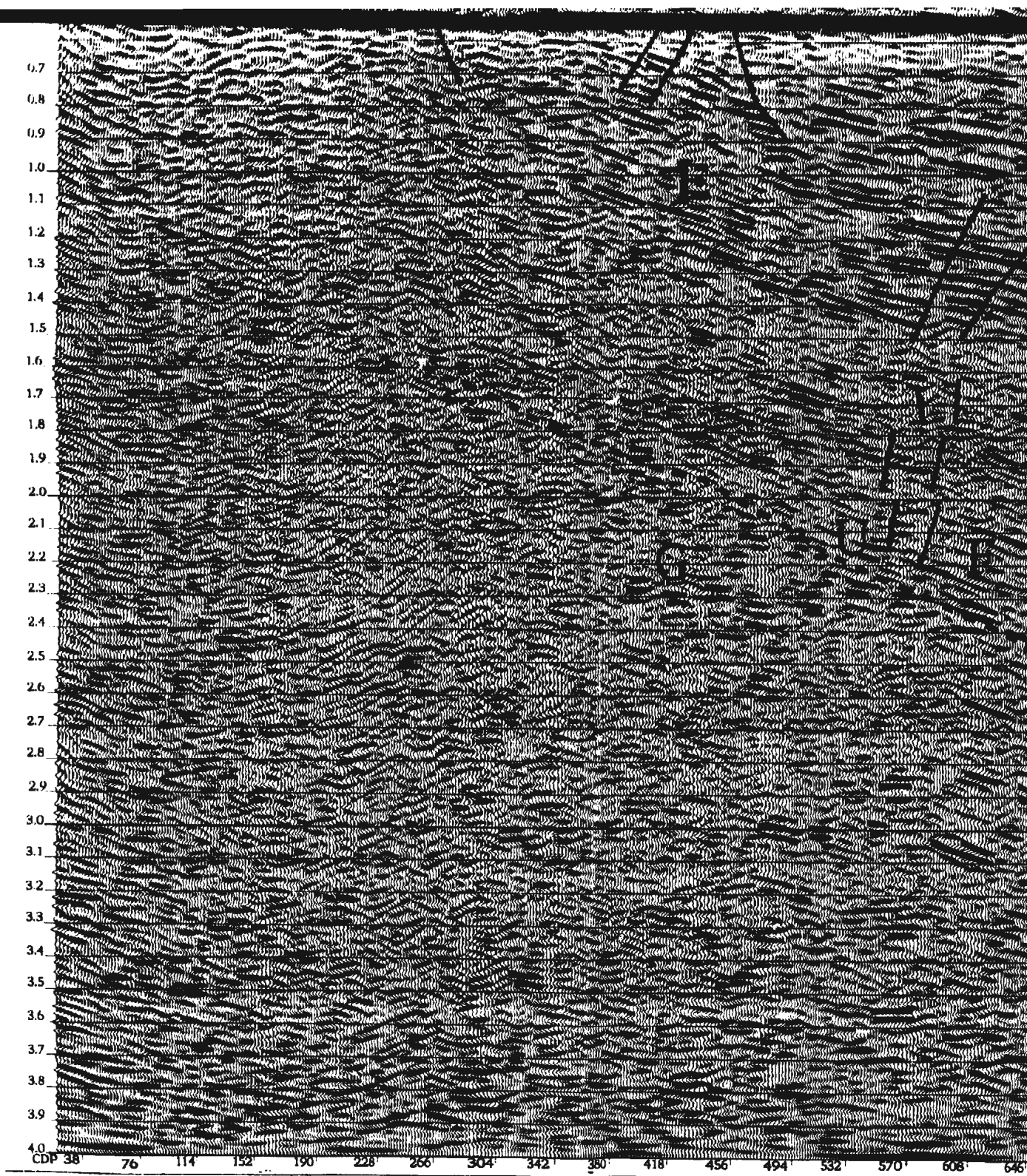
2.1

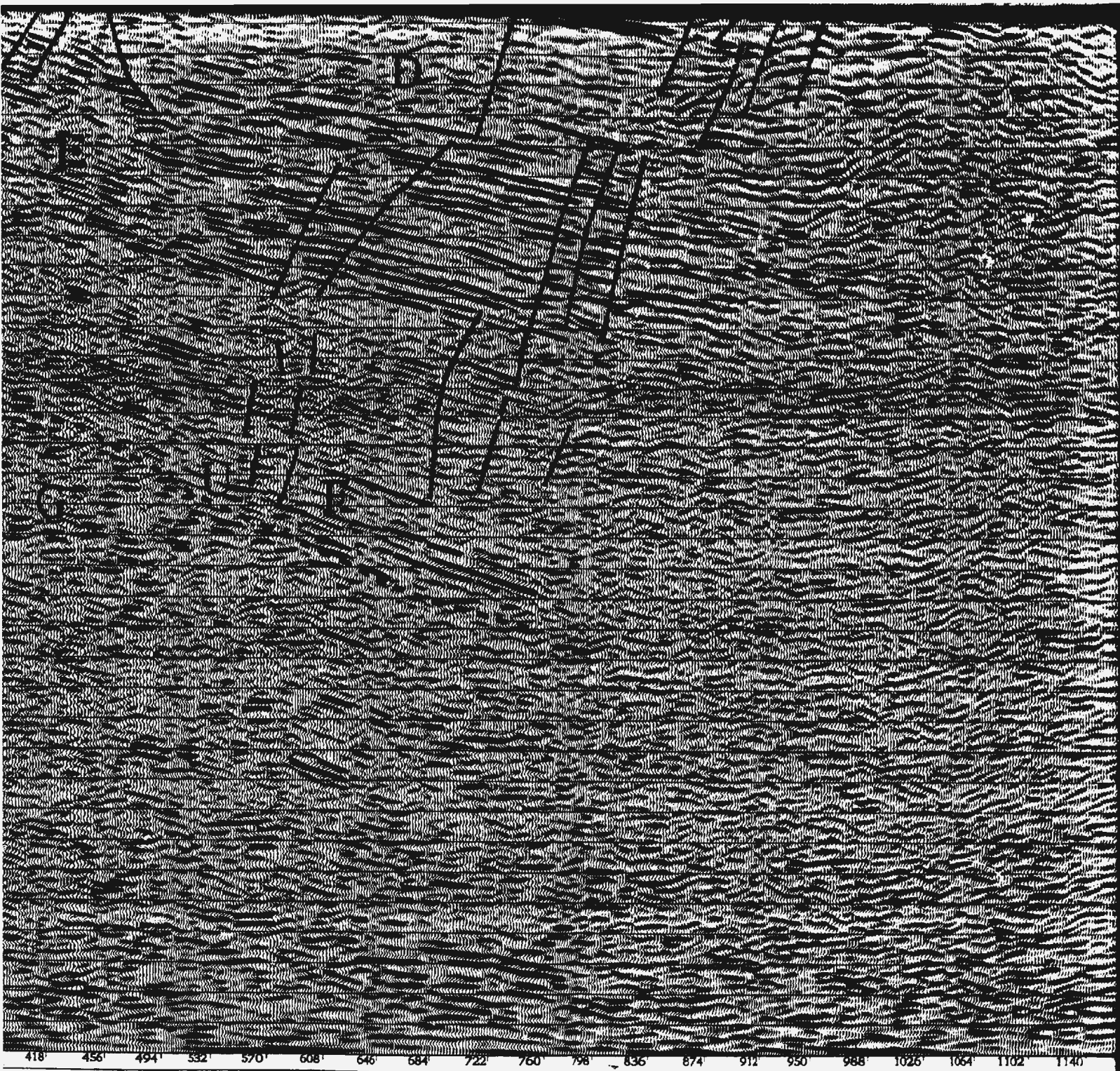
2.2

2.3

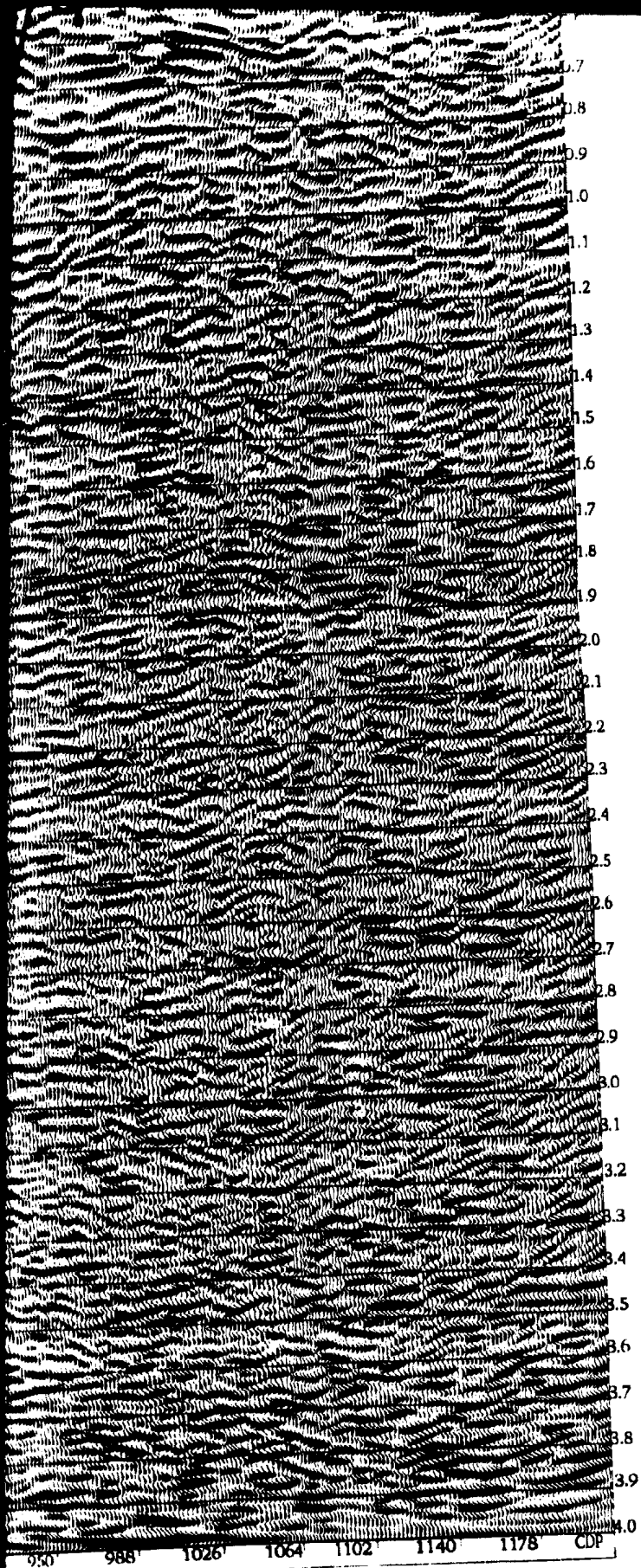
2.4

2.5

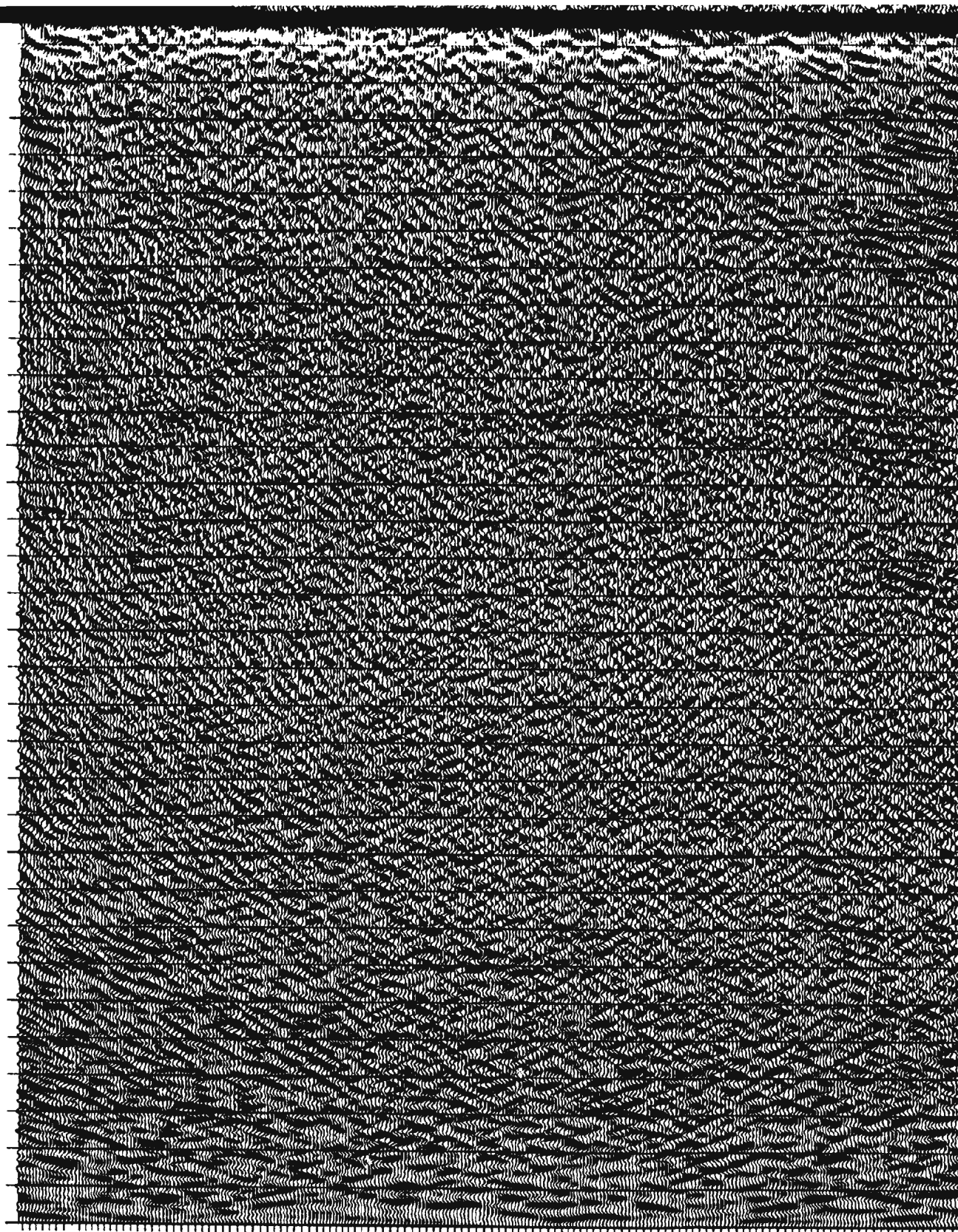


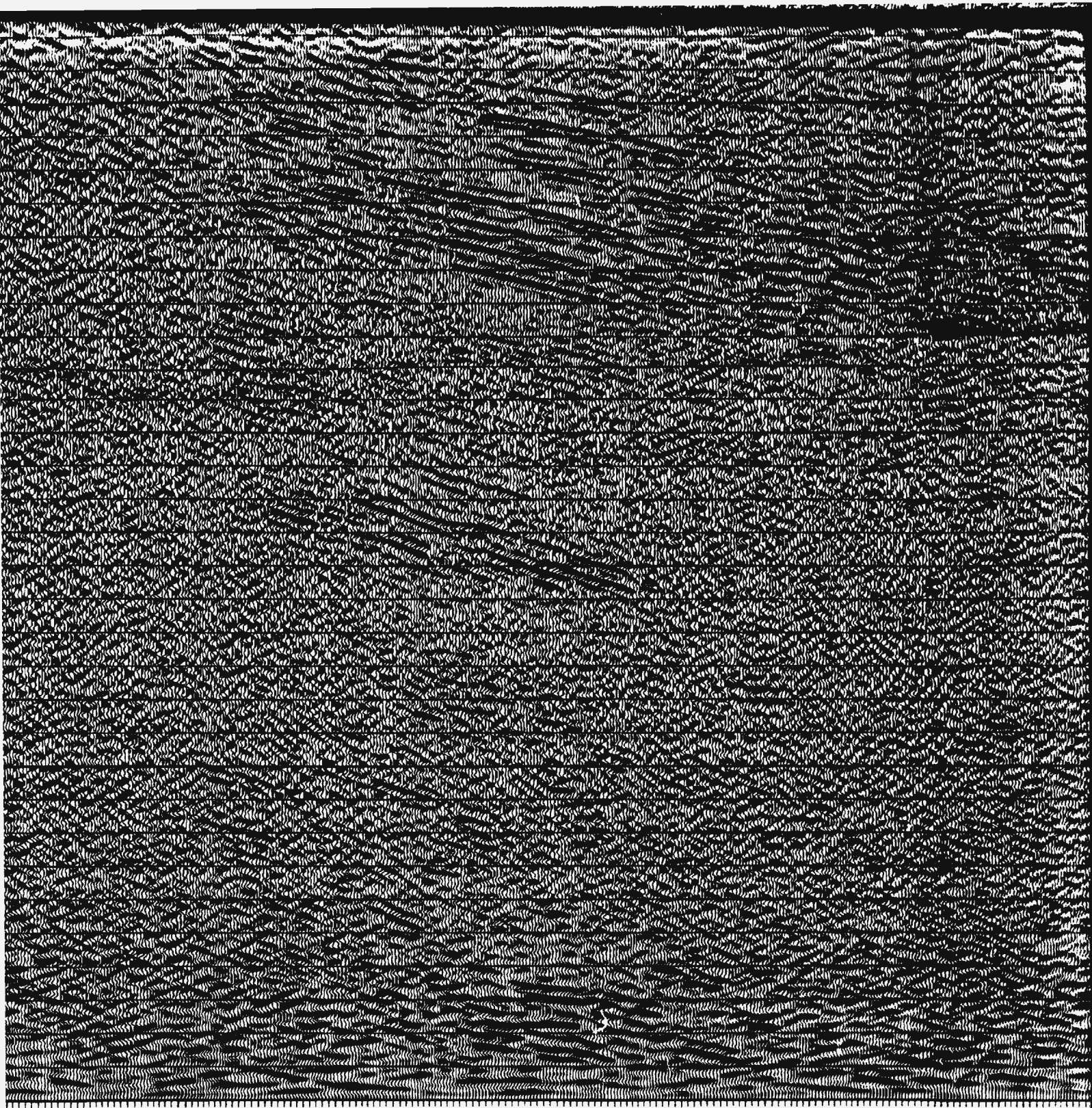


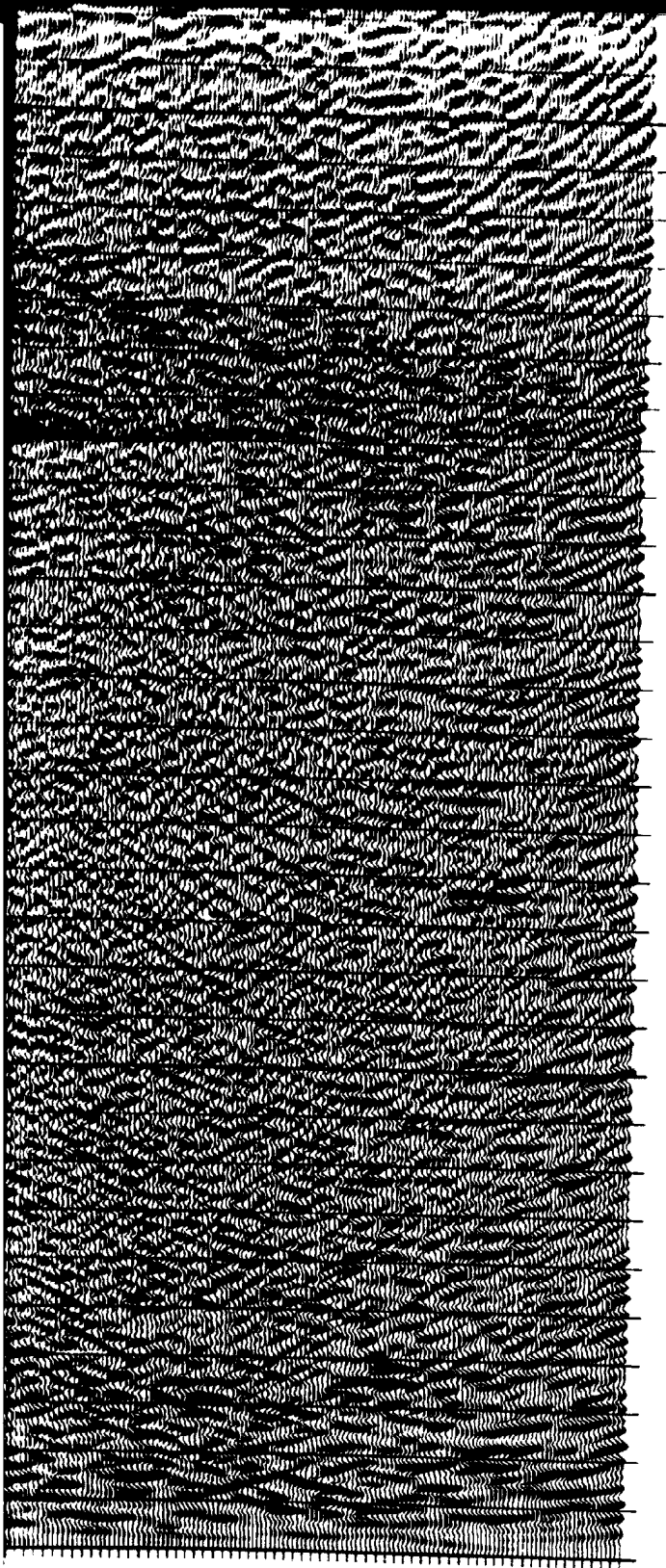
418 456 494 532 570 608 646 684 722 760 798 836 874 912 950 988 1026 1064 1102 1140



0.9
1.0
1.1
1.2
1.3
1.4
1.5
1.6
1.7
1.8
1.9
2.0
2.1
2.2
2.3
2.4
2.5
2.6
2.7
2.8
2.9
3.0
3.1
3.2
3.3
3.4
3.5
3.6
3.7
3.8
3.9
4.0







6.5

CDP

Figure 3.16.
stack proces

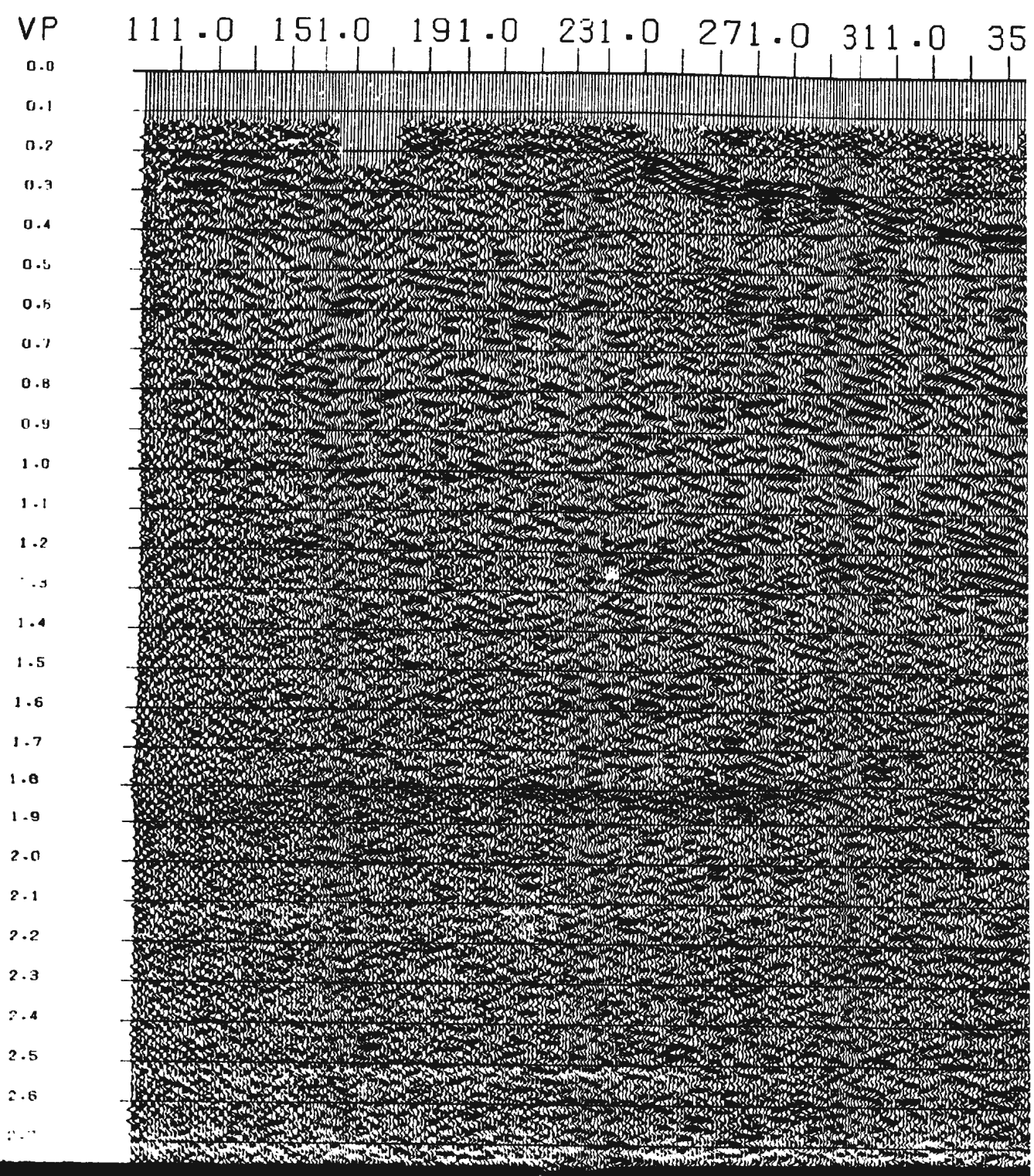
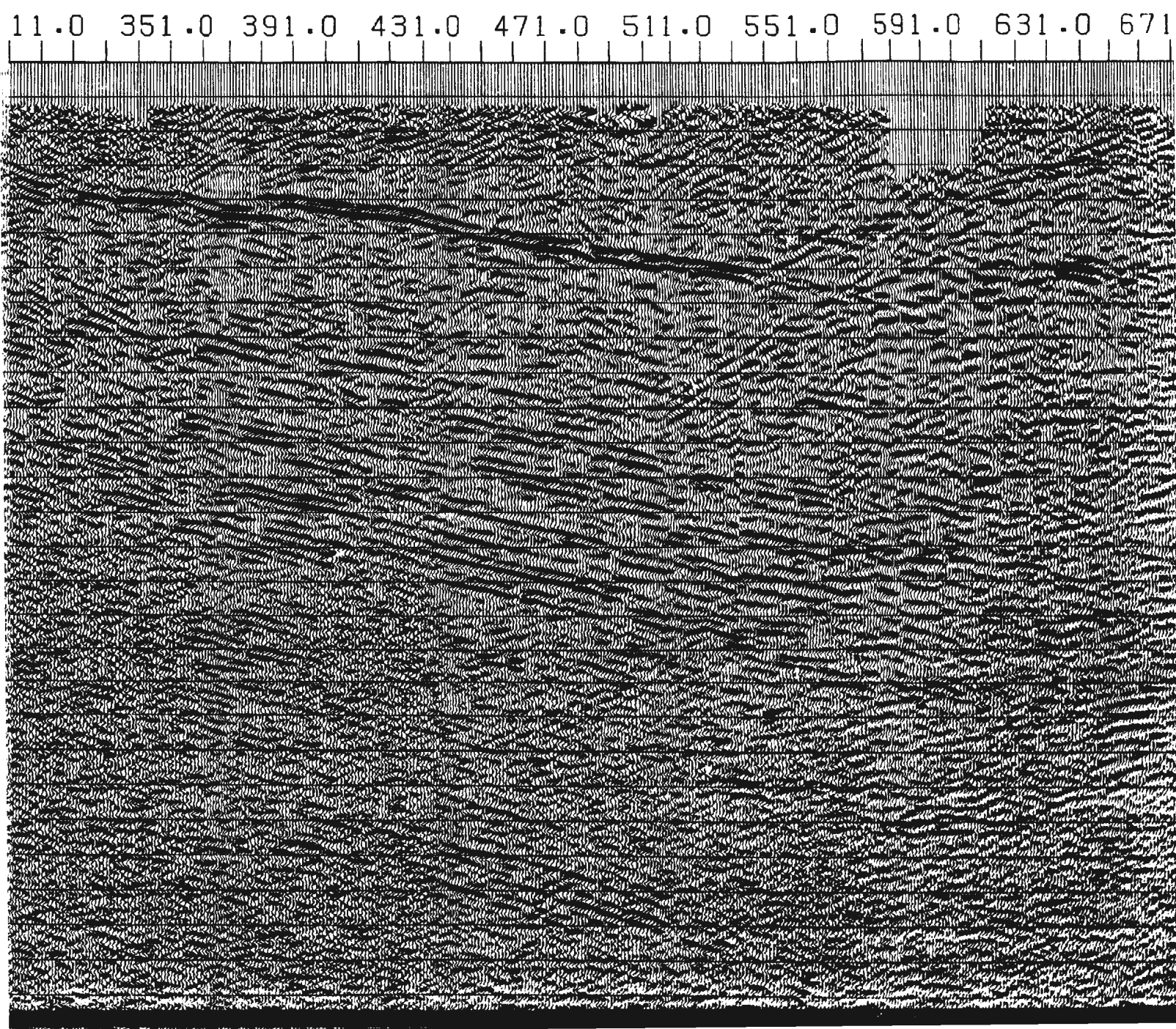


Figure 3.16. Stacked section after DMO correction, with no post stack processing.



1.0 591.0 631.0 671.0 711.0

VP

0.0
0.1
0.2
0.3
0.4
0.5
0.6
0.7
0.8
0.9
1.0
1.1
1.2
1.3
1.4
1.5
1.6
1.7
1.8
1.9
2.0
2.1
2.2
2.3
2.4
2.5
2.6

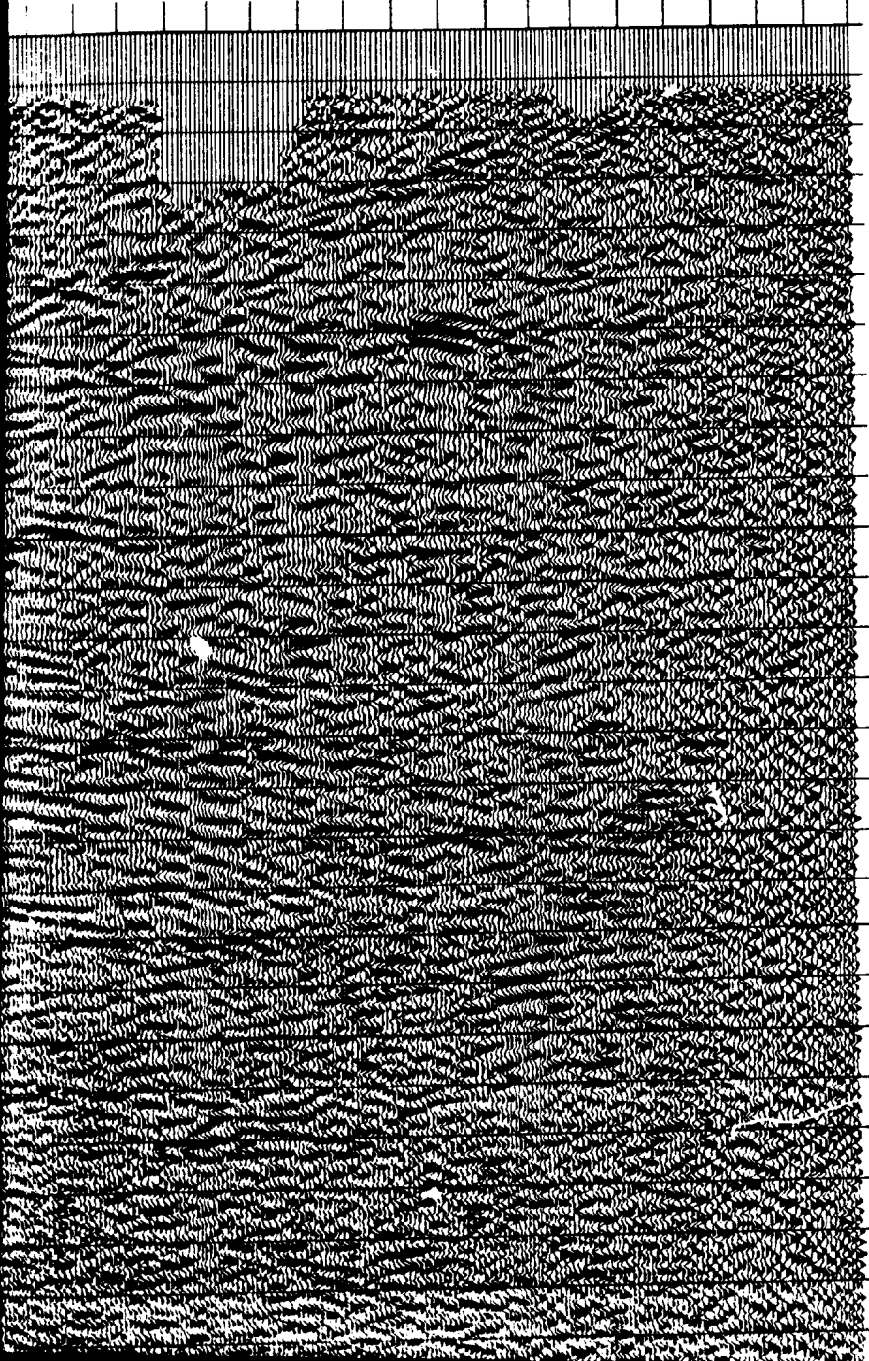
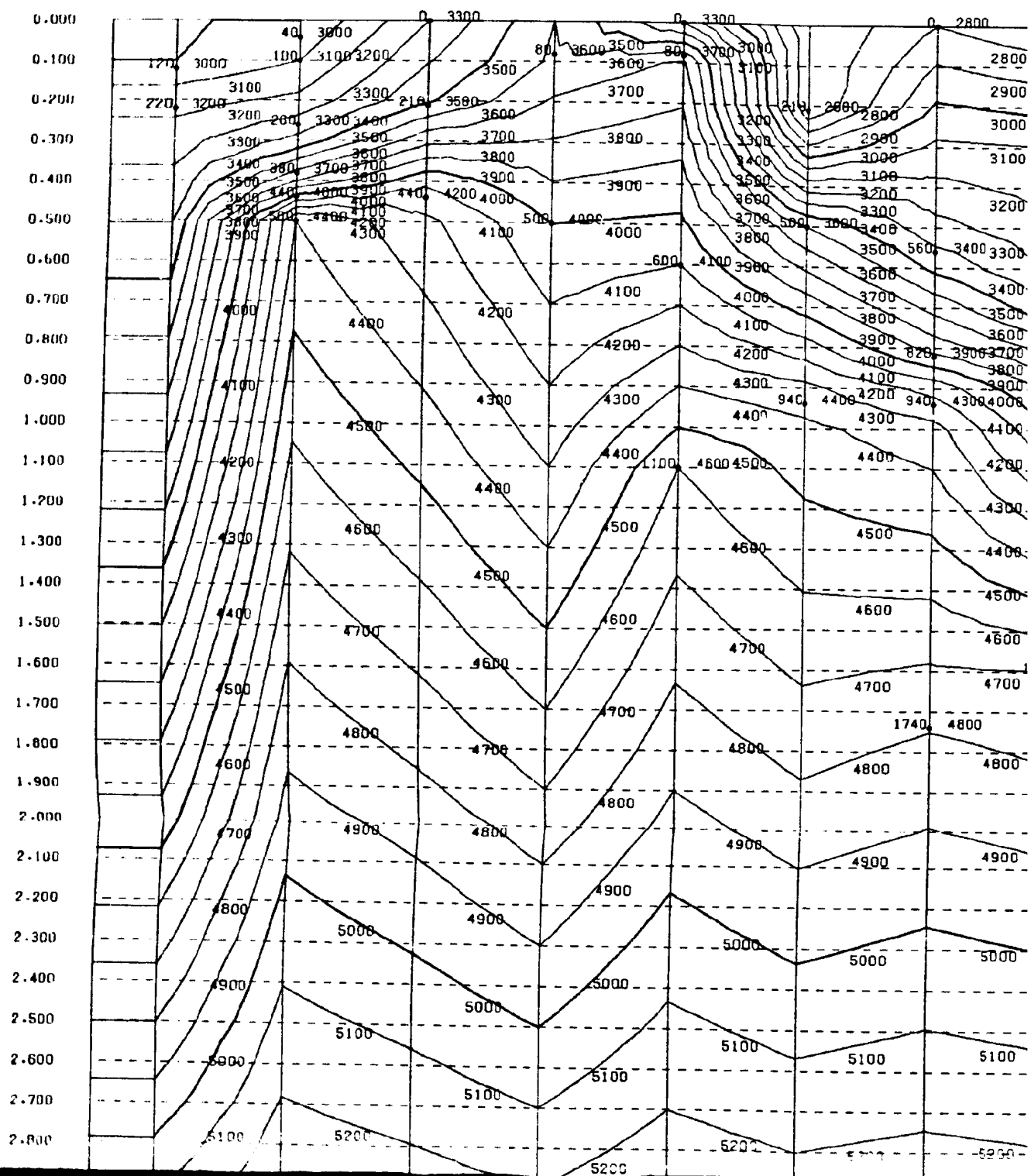
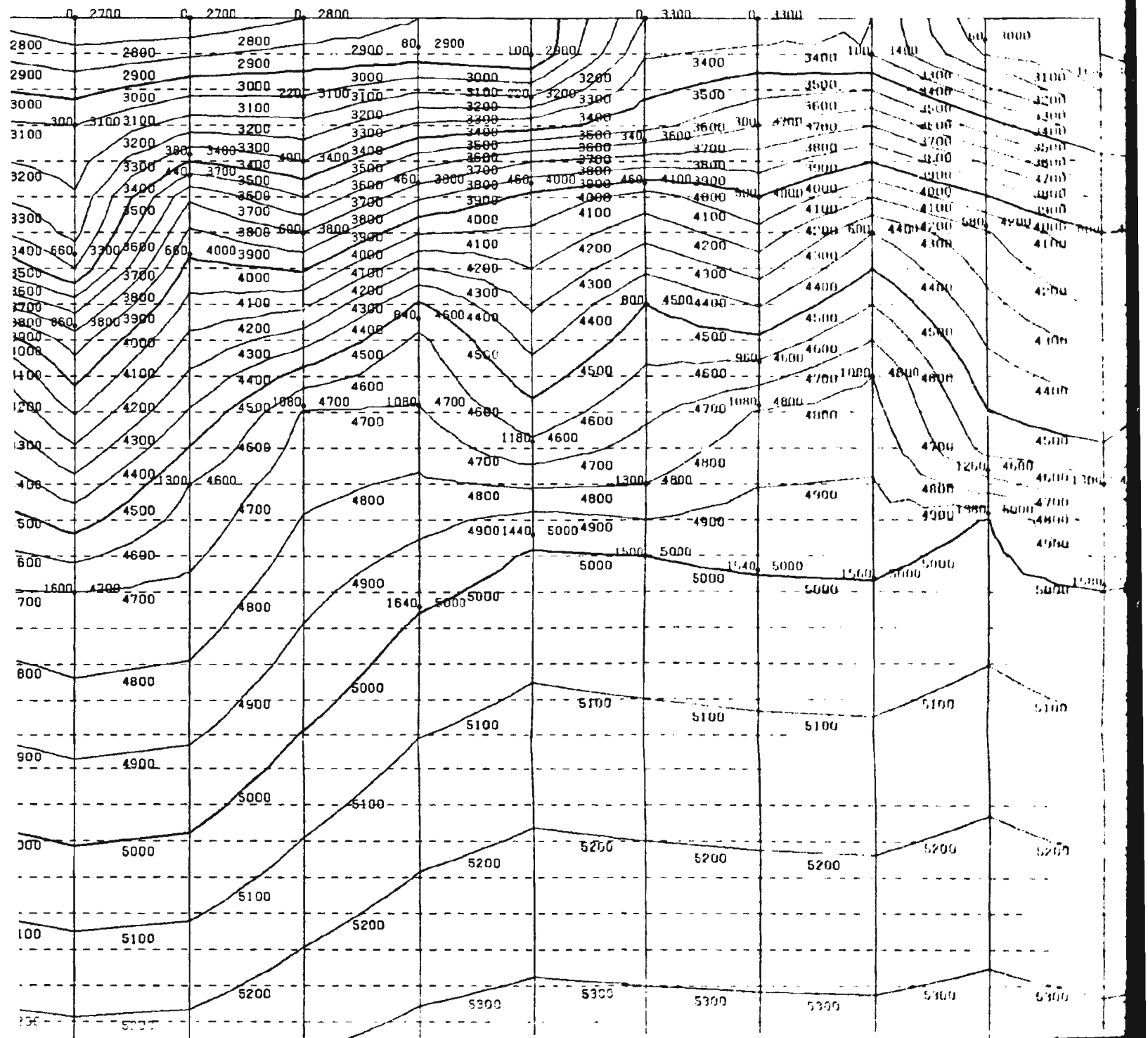
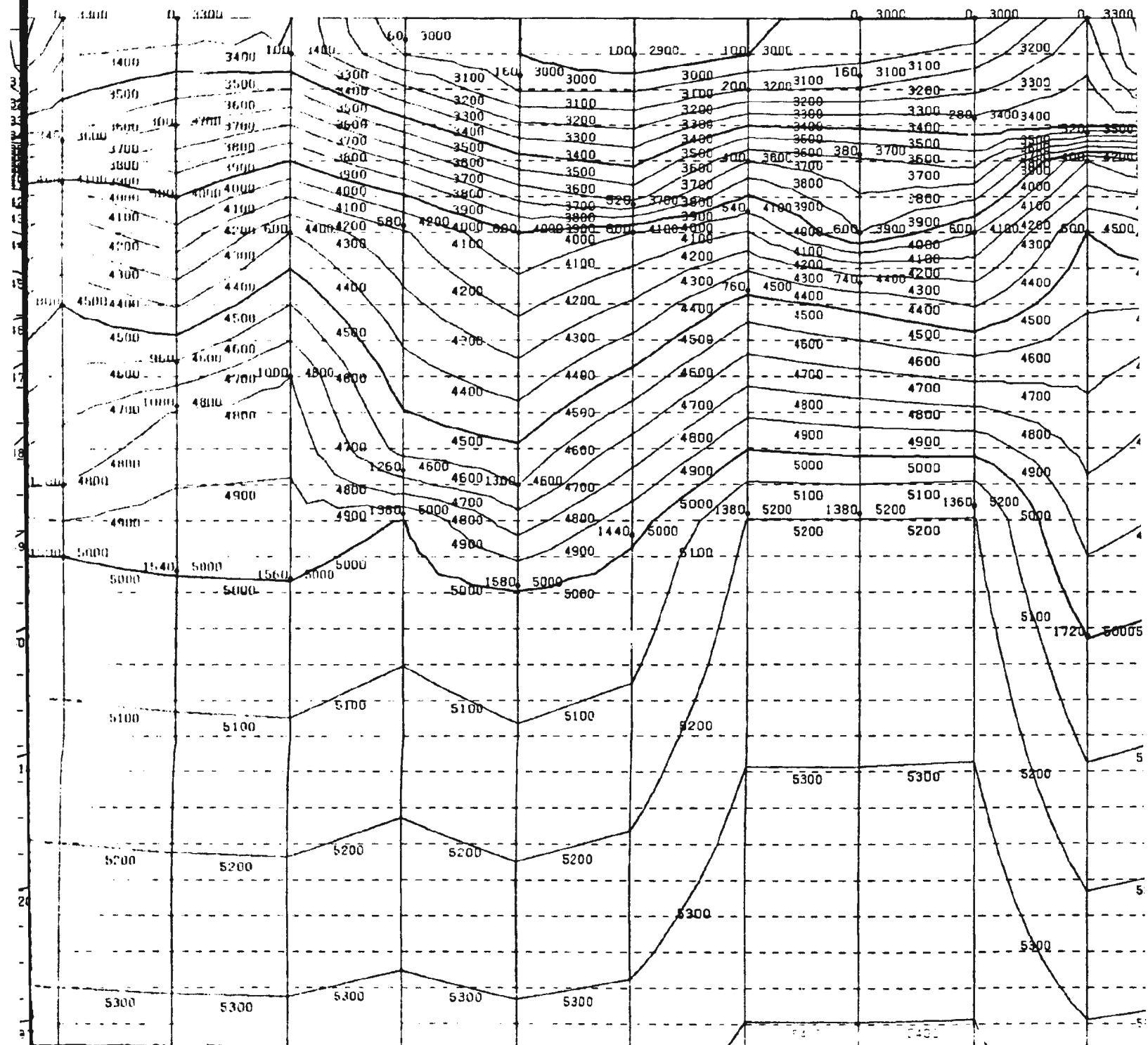


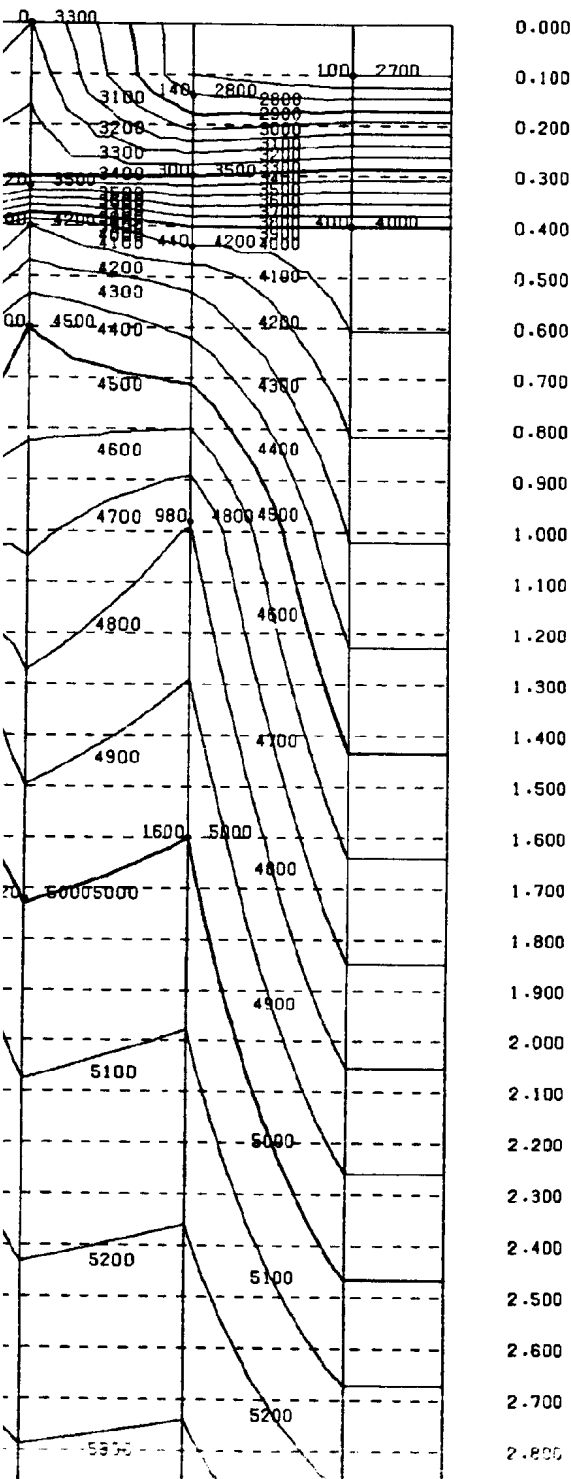
Figure 3.12. Velo



velocity field contours after DMO correction.



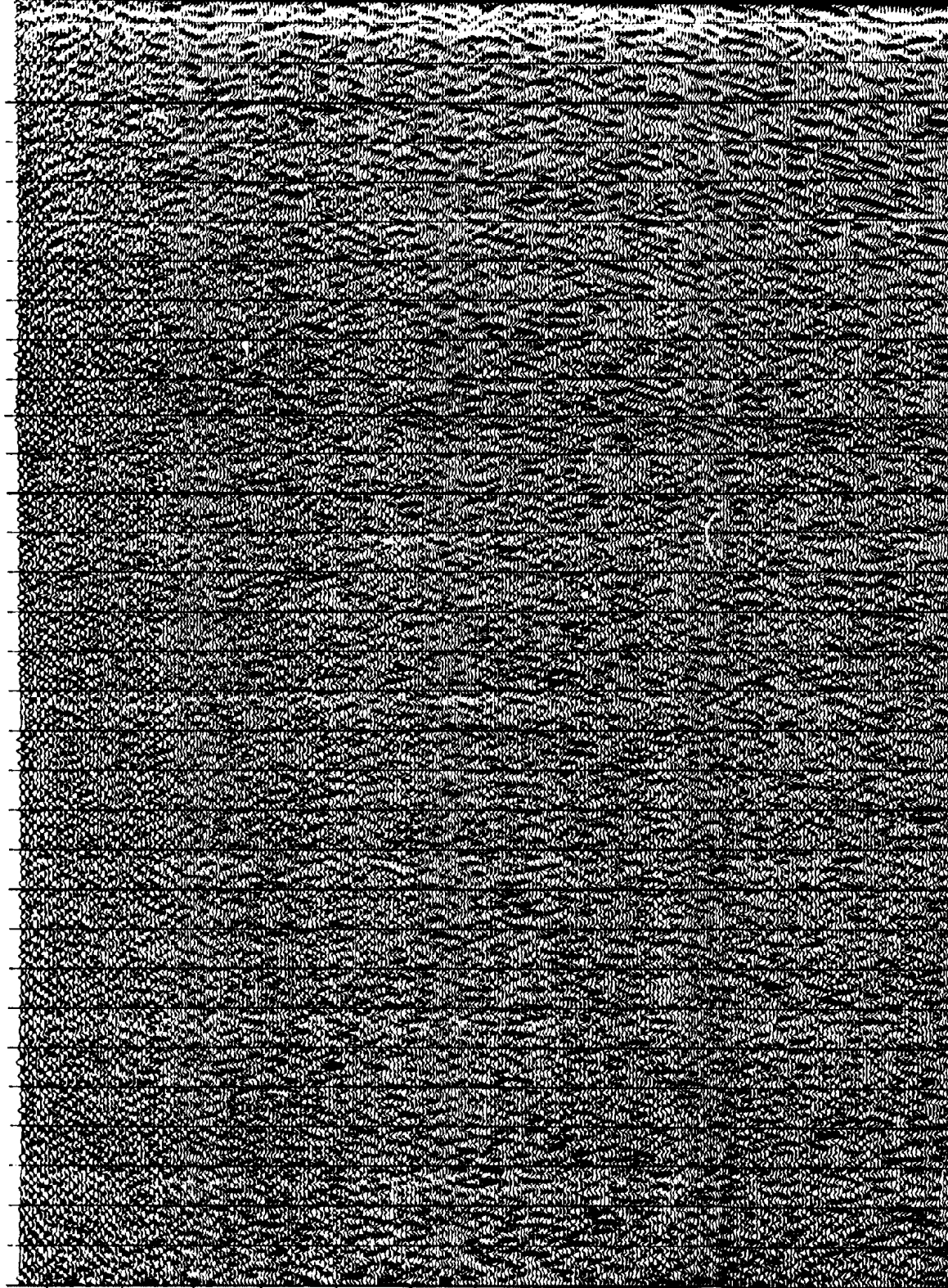




1

two trace sum

0.9
1.0
1.1
1.2
1.3
1.4
1.5
1.6
1.7
1.8
1.9
2.0
2.1
2.2
2.3
2.4
2.5
2.6
2.7
2.8
3.0
3.1
3.2
3.3
3.4
3.5
3.6
3.7
3.8
3.9
4.0



CDP

38

76

114

152

190

228

266

304

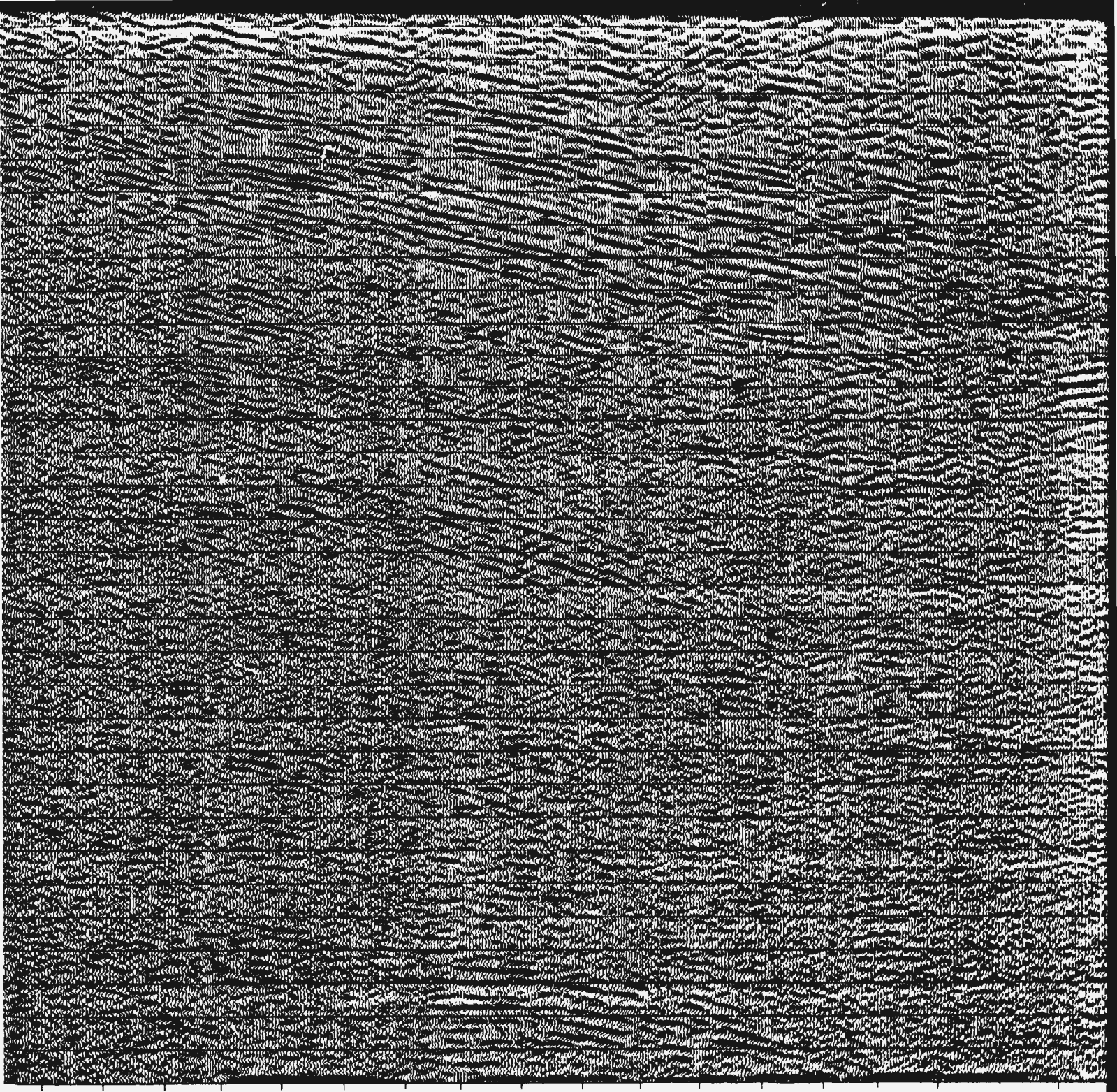
342

380

418

456

494



418

456

494

532

570

608

646

684

722

760

798

836

874

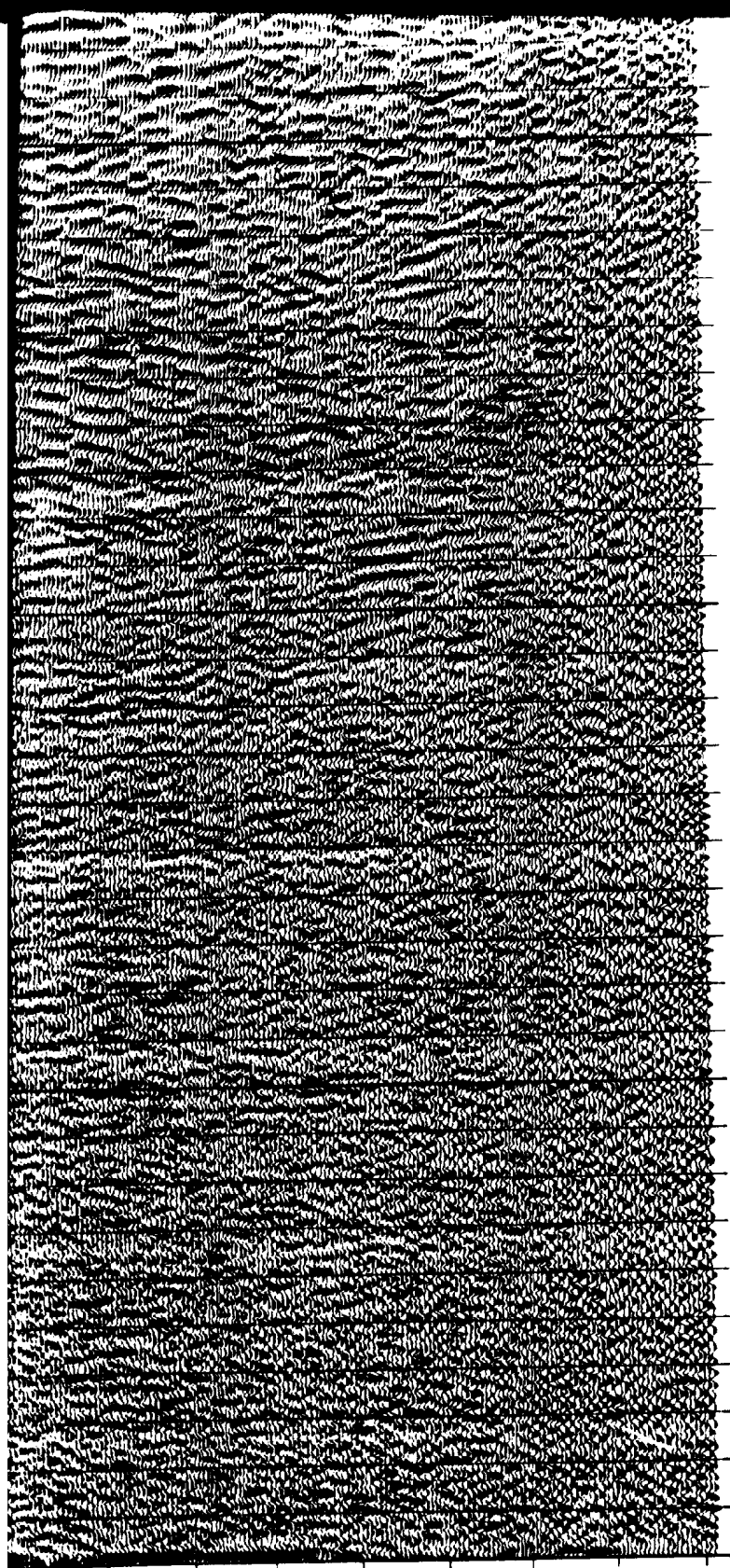
912

950

988

1026

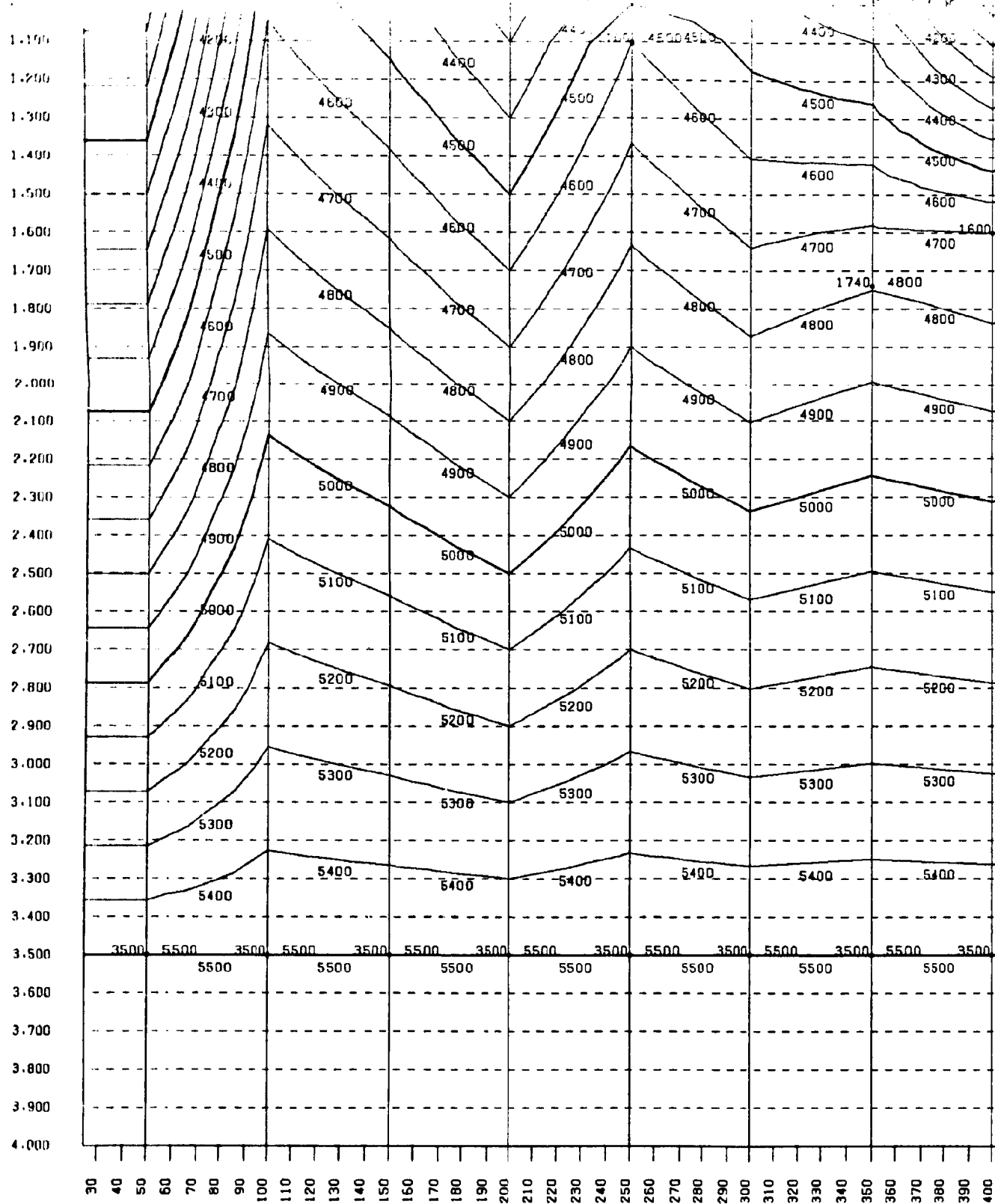
1064

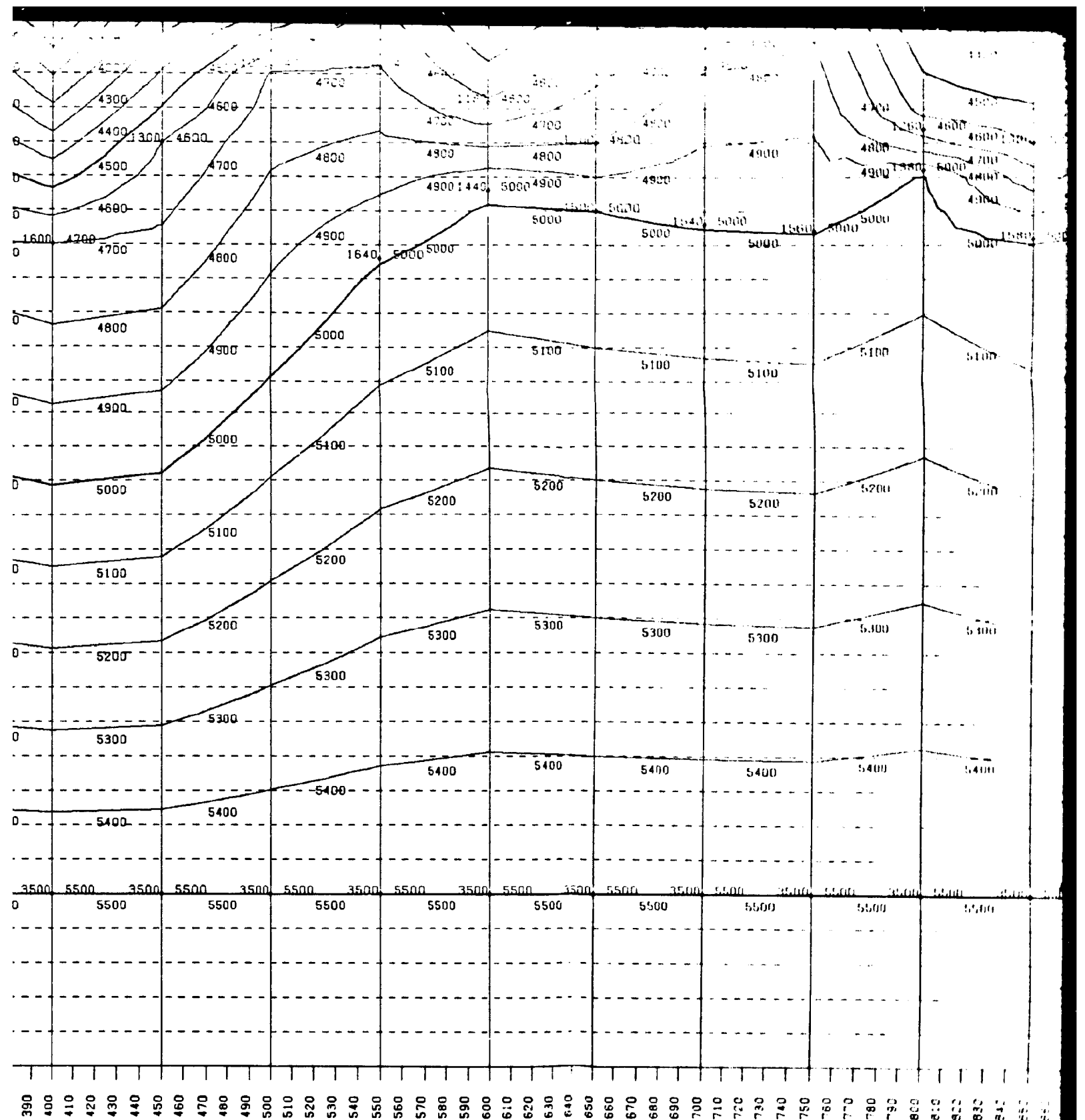


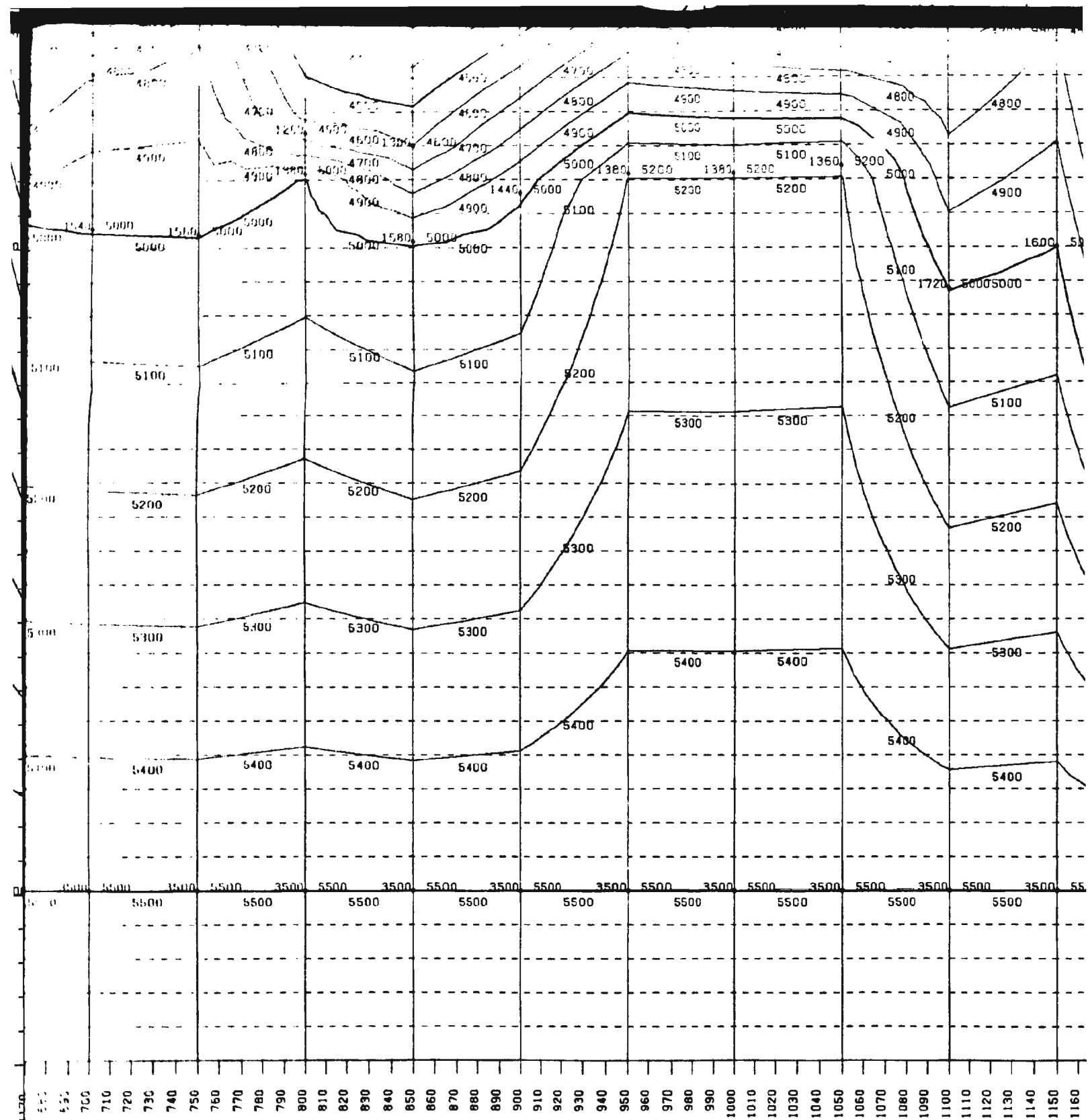
0.9
1.0
1.1
1.2
1.3
1.4
1.5
1.6
1.7
1.8
1.9
2.0
2.1
2.2
2.3
2.4
2.5
2.6
2.7
2.8
2.9
3.0
3.1
3.2
3.3
3.4
3.5
3.6
3.7
3.8
3.9
4.0

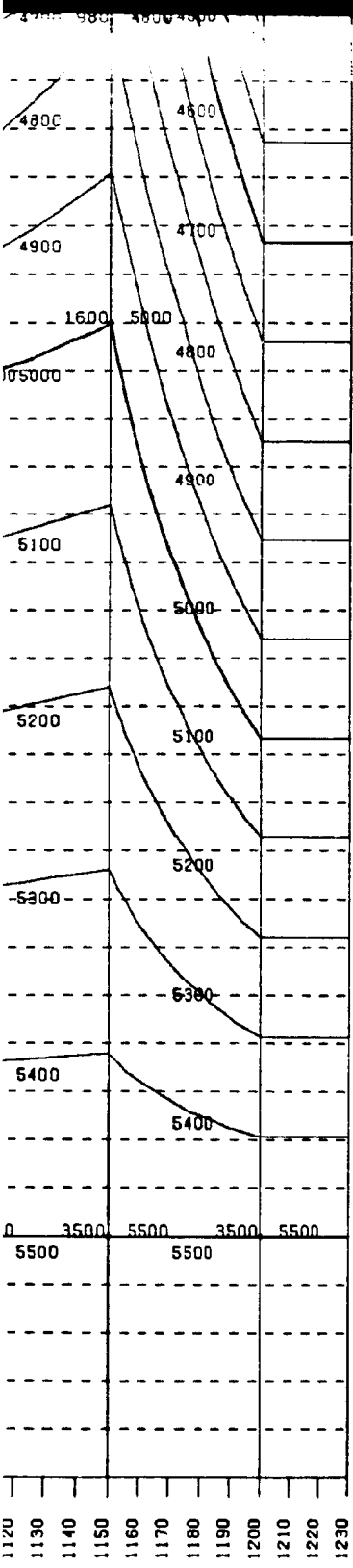
950
998
1026
1064
1102
1140
1178
1216

CDP



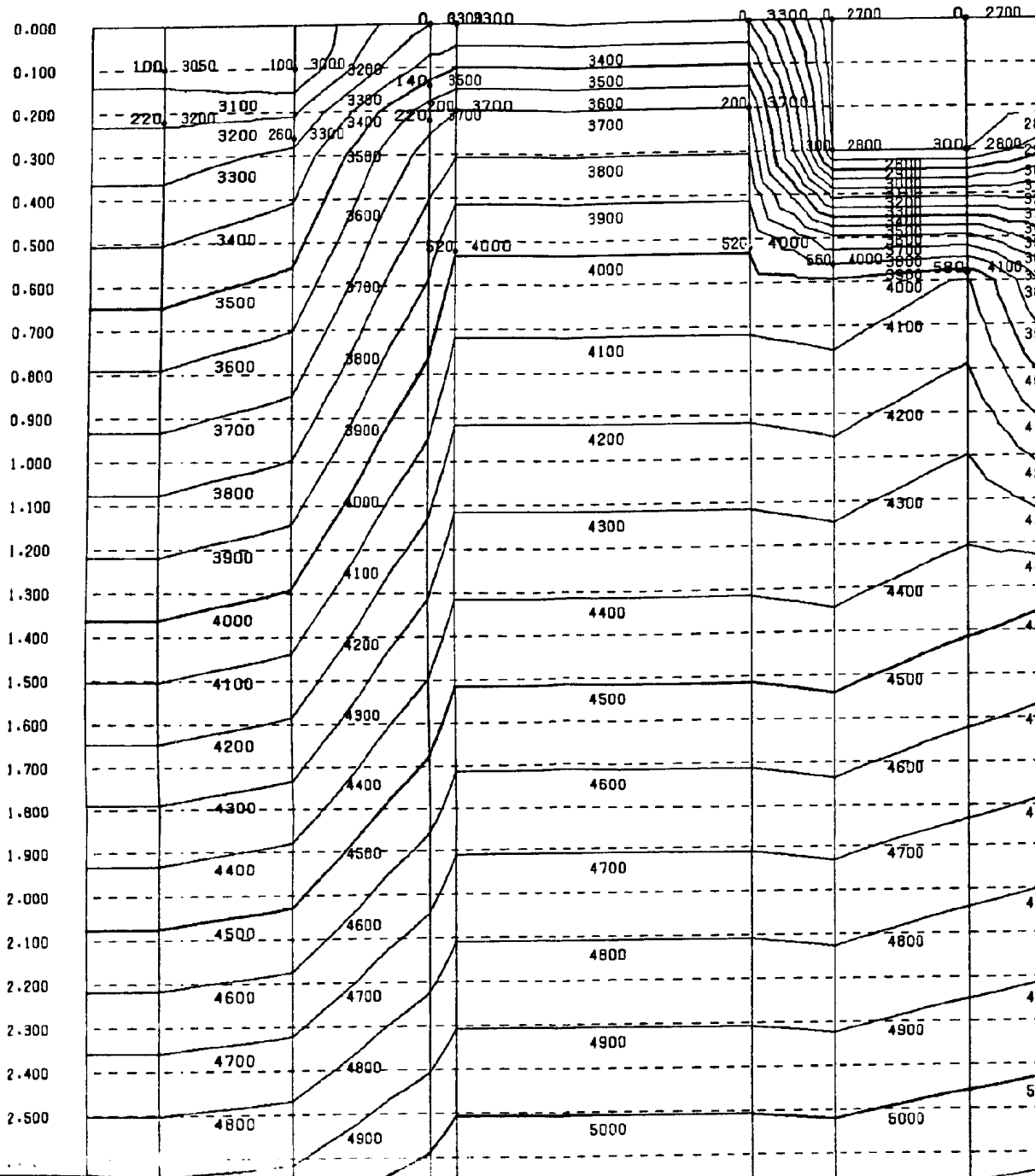




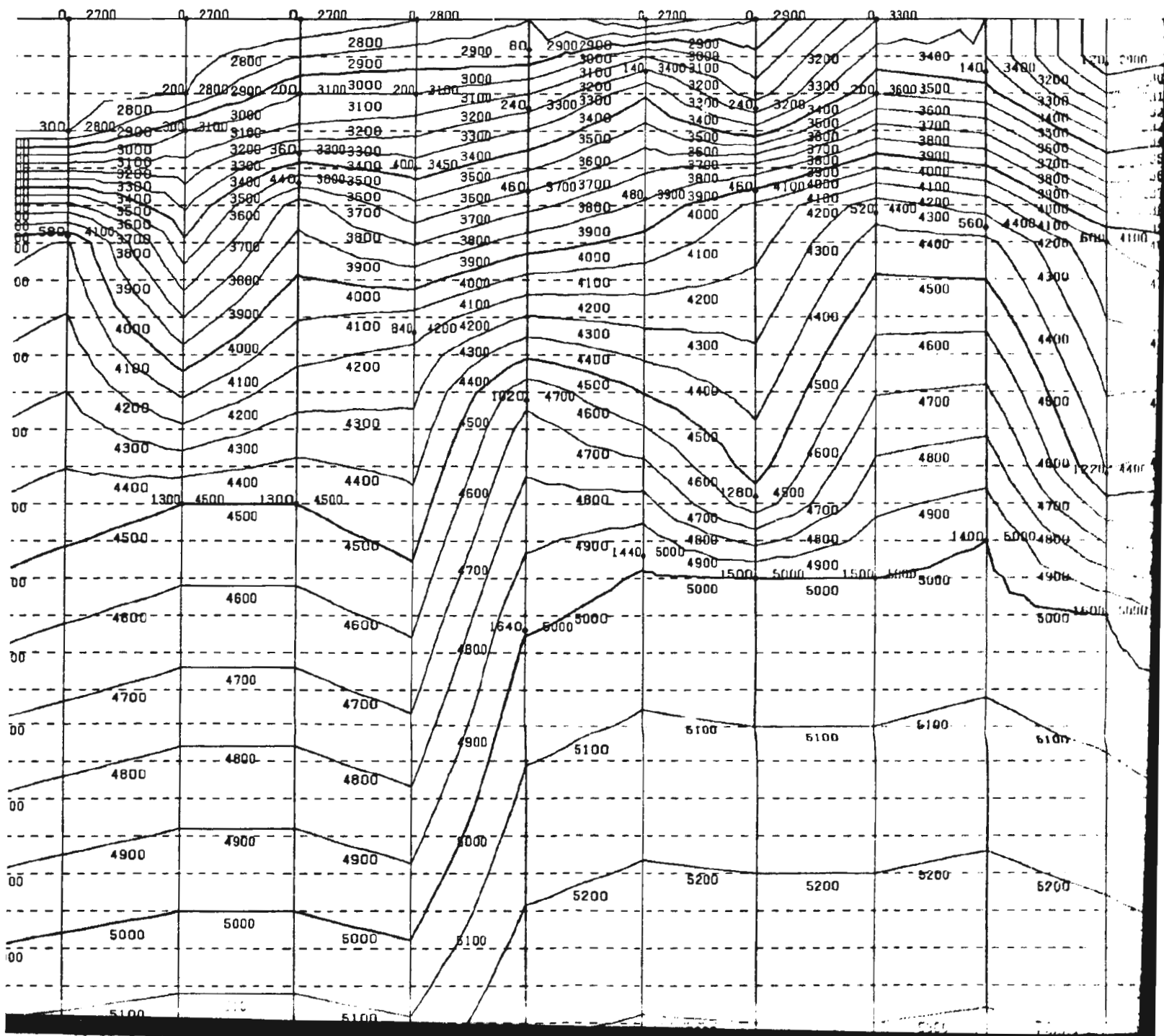


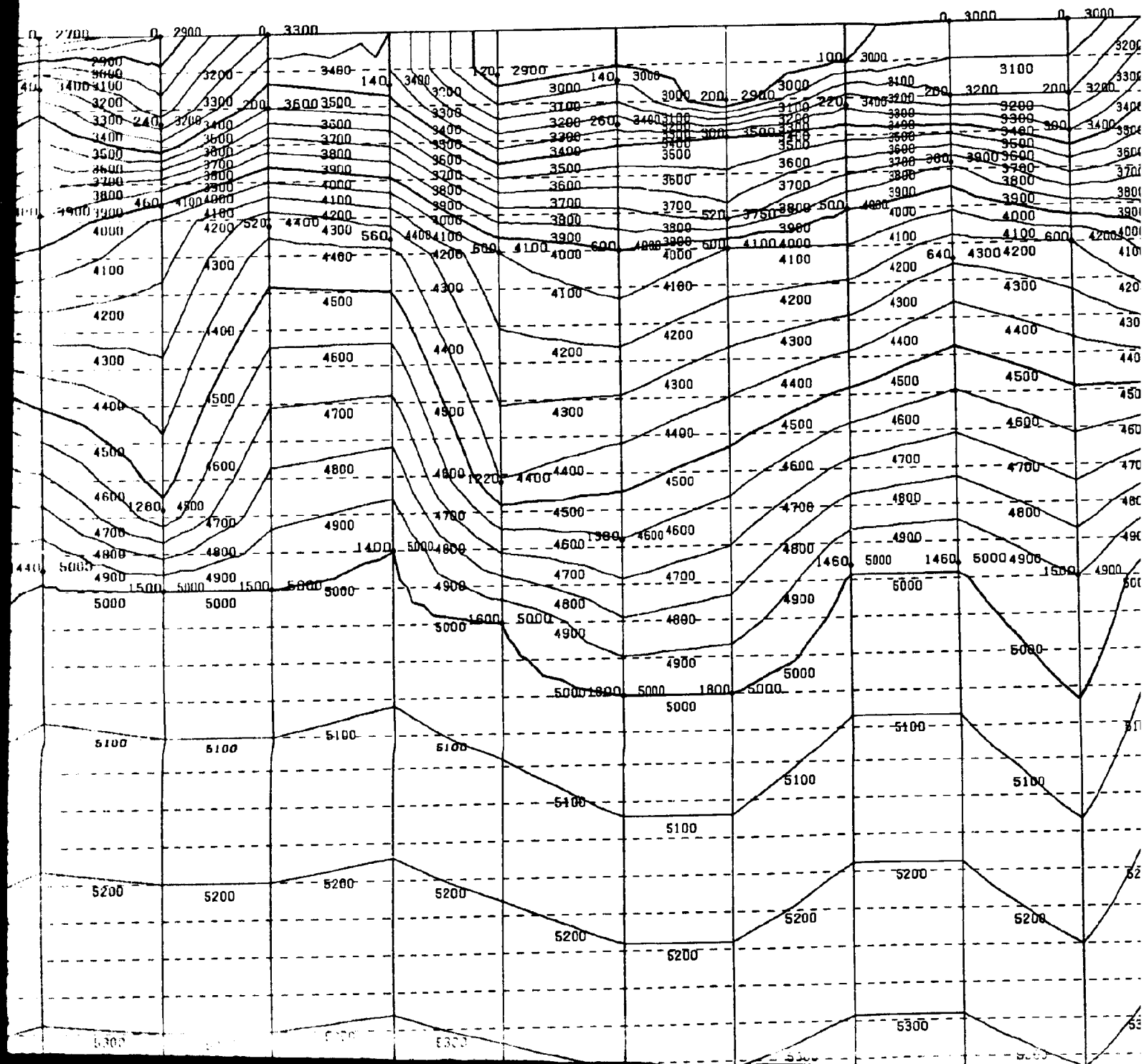
1.100
1.200
1.300
1.400
1.500
1.600
1.700
1.800
1.900
2.000
2.100
2.200
2.300
2.400
2.500
2.600
2.700
2.800
2.900
3.000
3.100
3.200
3.300
3.400
3.500
3.600
3.700
3.800
3.900
4.000

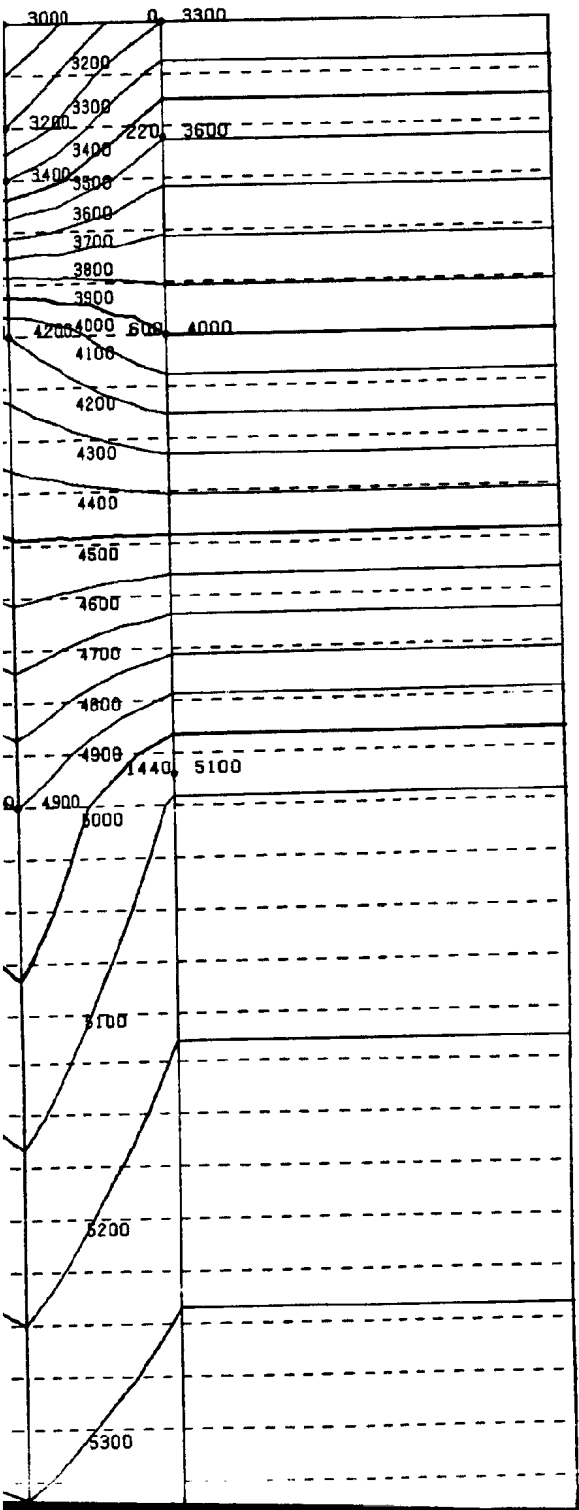
Figure 3.11. Velocity field



city field contours before DMO correction.





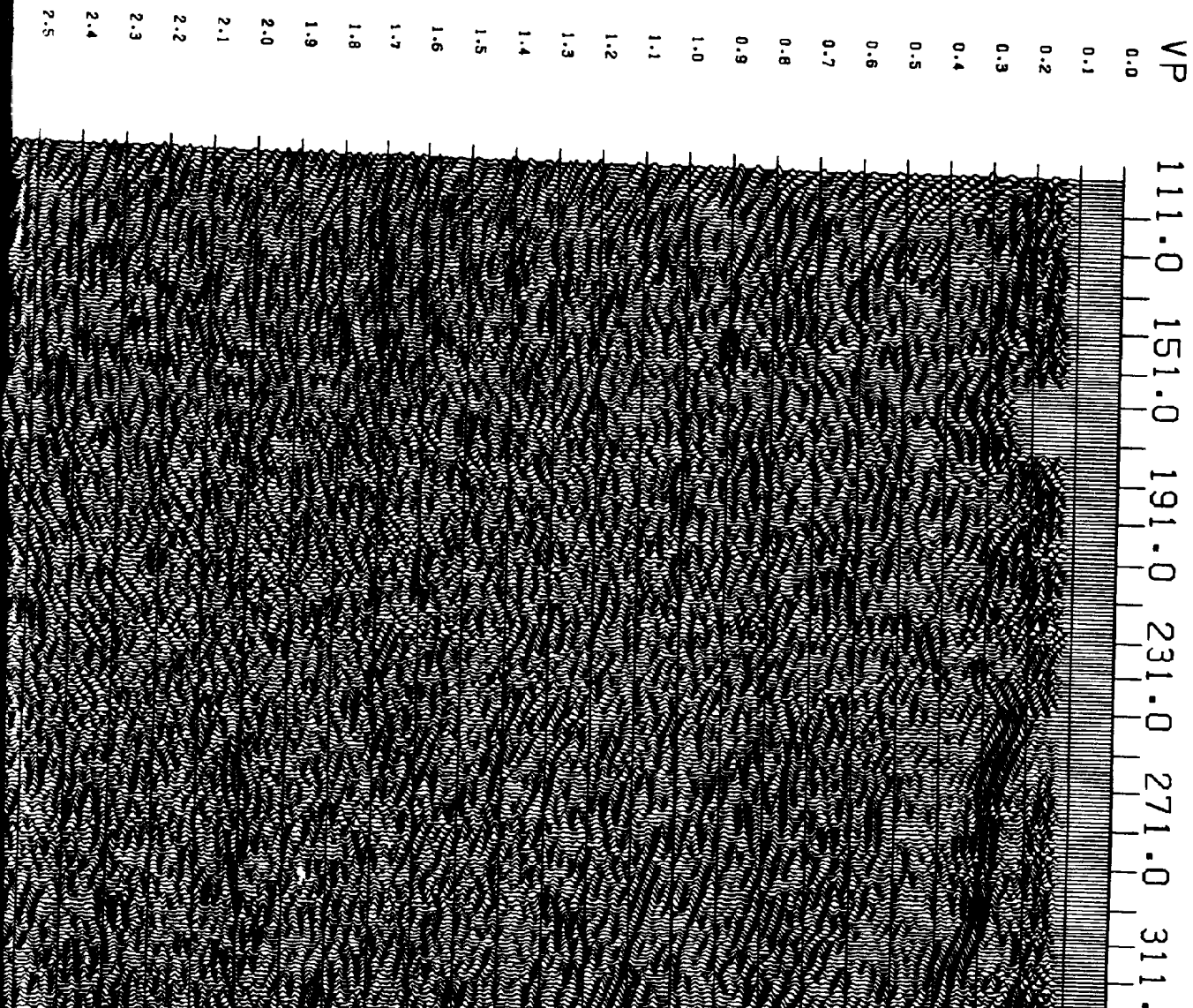


- 0.000
- 0.100
- 0.200
- 0.300
- 0.400
- 0.500
- 0.600
- 0.700
- 0.800
- 0.900
- 1.000
- 1.100
- 1.200
- 1.300
- 1.400
- 1.500
- 1.600
- 1.700
- 1.800
- 1.900
- 2.000
- 2.100
- 2.200
- 2.300
- 2.400
- 2.500
- 2.600
- 2.700
- 2.800

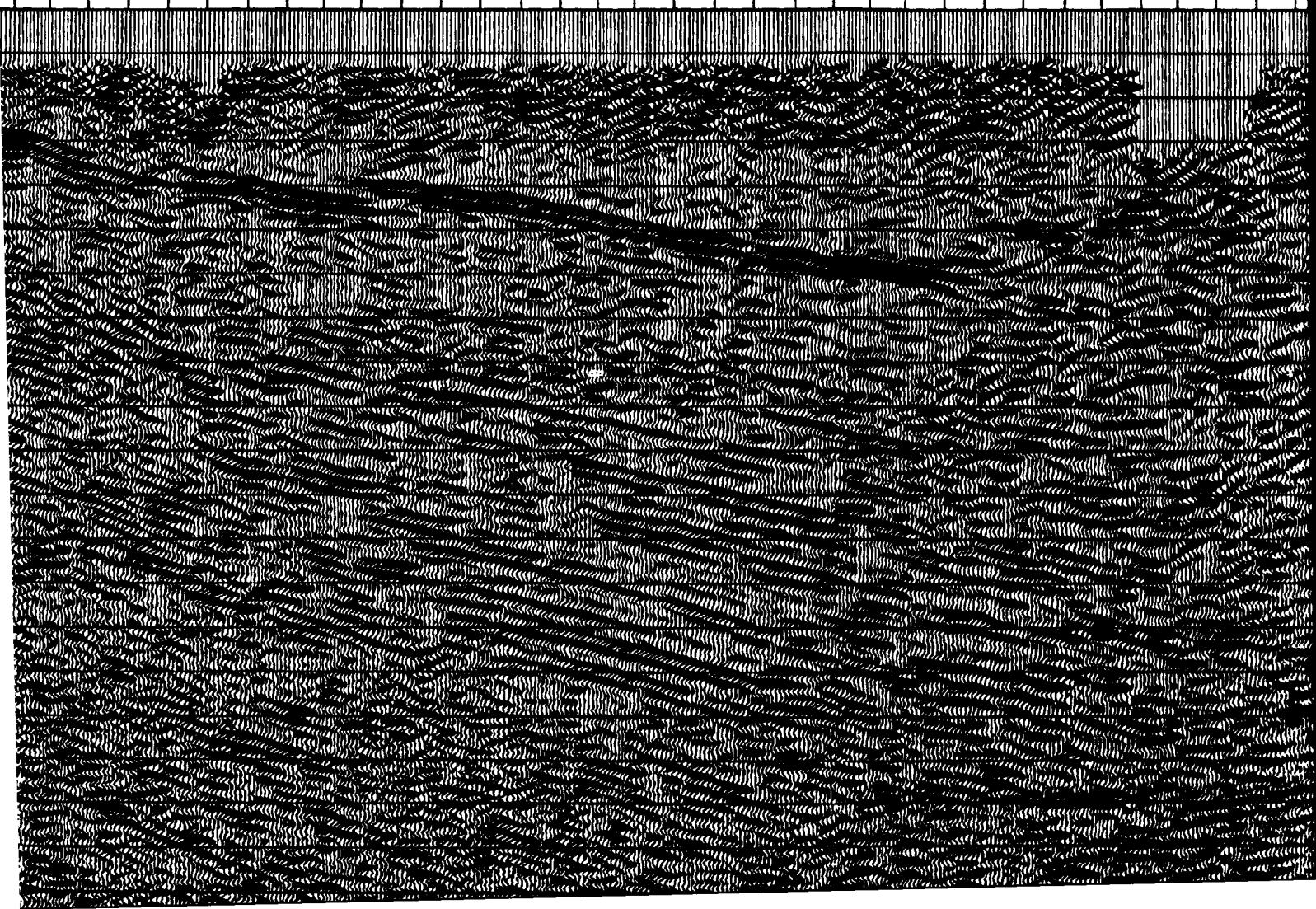
post-nmo

90

Figure 3.22. Final display of the processed profile. This is a 1:1 section if an average velocity of 4 km/s is assumed for the whole section.



311.0 351.0 391.0 431.0 471.0 511.0 551.0 591.0 631.0



CENTRE FOR
MEMORIAL UN

LINE:

S.P.

AREA:

TITLE

ACQUISITION

SHOT BY:

ENERGY SOURCE:
TYPE:
SWEEP LENGTH:
SWEEP LENGTH:
SOURCE ARRAY:
SHOTPOINT INTER

RECEIVING ARRANGEMENT:
FOLD OF RECORDING:
GROUP INTERVAL:
NUMBER OF GROUPS:
STATION CAP AT
GEOPHONES/GROUP:

INSTRUMENTATION:
RECORDING SYSTEM:
PRE-AMP GAIN:
FILTERS:
RECORD FORMAT:
RECORD LENGTH:
SAMPLE RATE:

PROCESSING

PROCESSED BY:

1. APPLICATION OF

2. APPLICATION OF

3. DNO CORRECTION

1.0 551.0 591.0 631.0 671.0 711.0

VP

0.0

0.1

0.2

0.3

0.4

0.5

0.6

0.7

0.8

0.9

1.0

1.1

1.2

1.3

1.4

1.5

1.6

1.7

1.8

1.9

2.0

2.1

2.2

2.3

2.4



1

FOR EARTH RESOURCES RESEARCH
UNIVERSITY OF NEWFOUNDLAND

LINE: ROBINSONS RIVER
(PASTURE ROAD)

L.P. 1 - 318

REA: BAY ST. GEORGE - WESTERN NPLD

ITLE: FINAL STACK

← W

ION

CAPILANO GEOPHYSICAL LTD.

ICE:

VIBROSEIS
20 HZ - 90 HZ, 500 MS TAPER
8 SECONDS
4 OVER 30 M, MOVE UP 8 M
40 M

RANGEMENT:

104 MAXIMUM

ECORDING:

20.0 METRES

IRVAL:

240

GROUPS:

26

P AT SP:

12

GROUP:

ION:

DPS V

SYSTEM:

48 DB

AIN:

HIGH CUT 128.0 HZ AT 72 DB

IMAT:

SSG Y, 240 CHANNEL

IGTH:

4 SECONDS

'E:

2 MS

NG

CENTRE FOR EARTH RESOURCES RESEARCH

MEMORIAL UNIVERSITY OF NEWFOUNDLAND

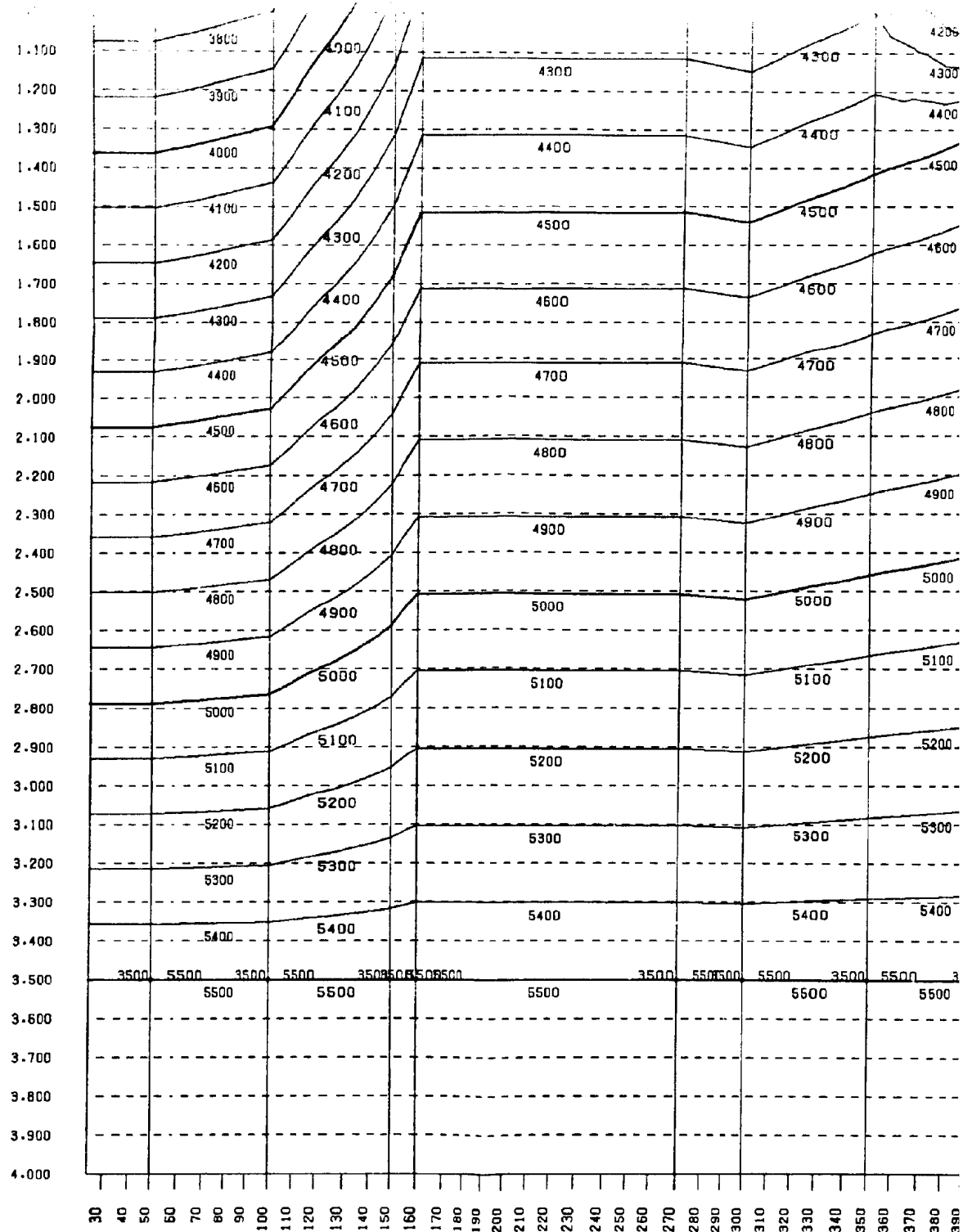
OF BINNING AND GEOMETRY:

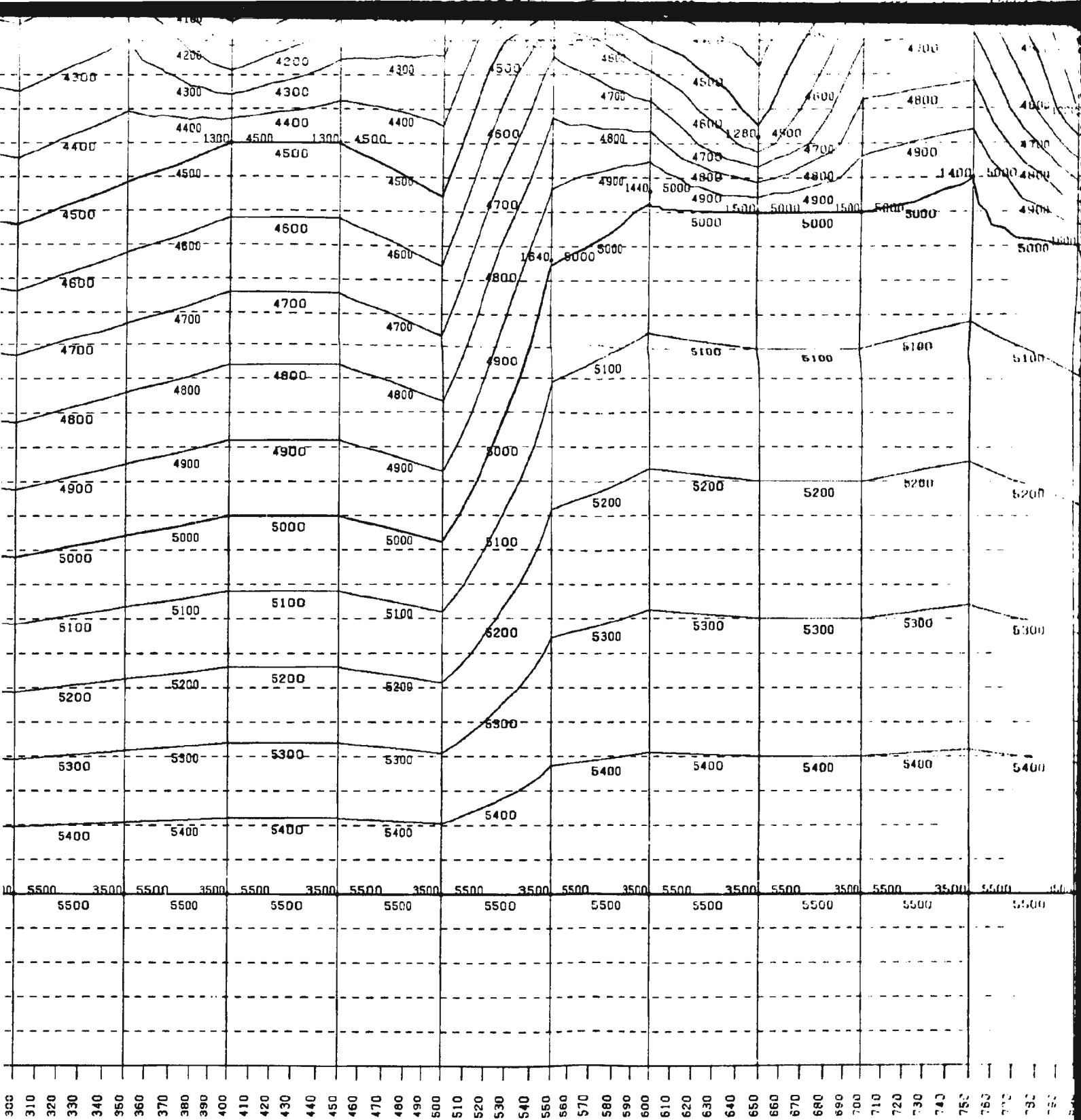
SURVEY DATA SUPPLIED BY CONTRACTOR

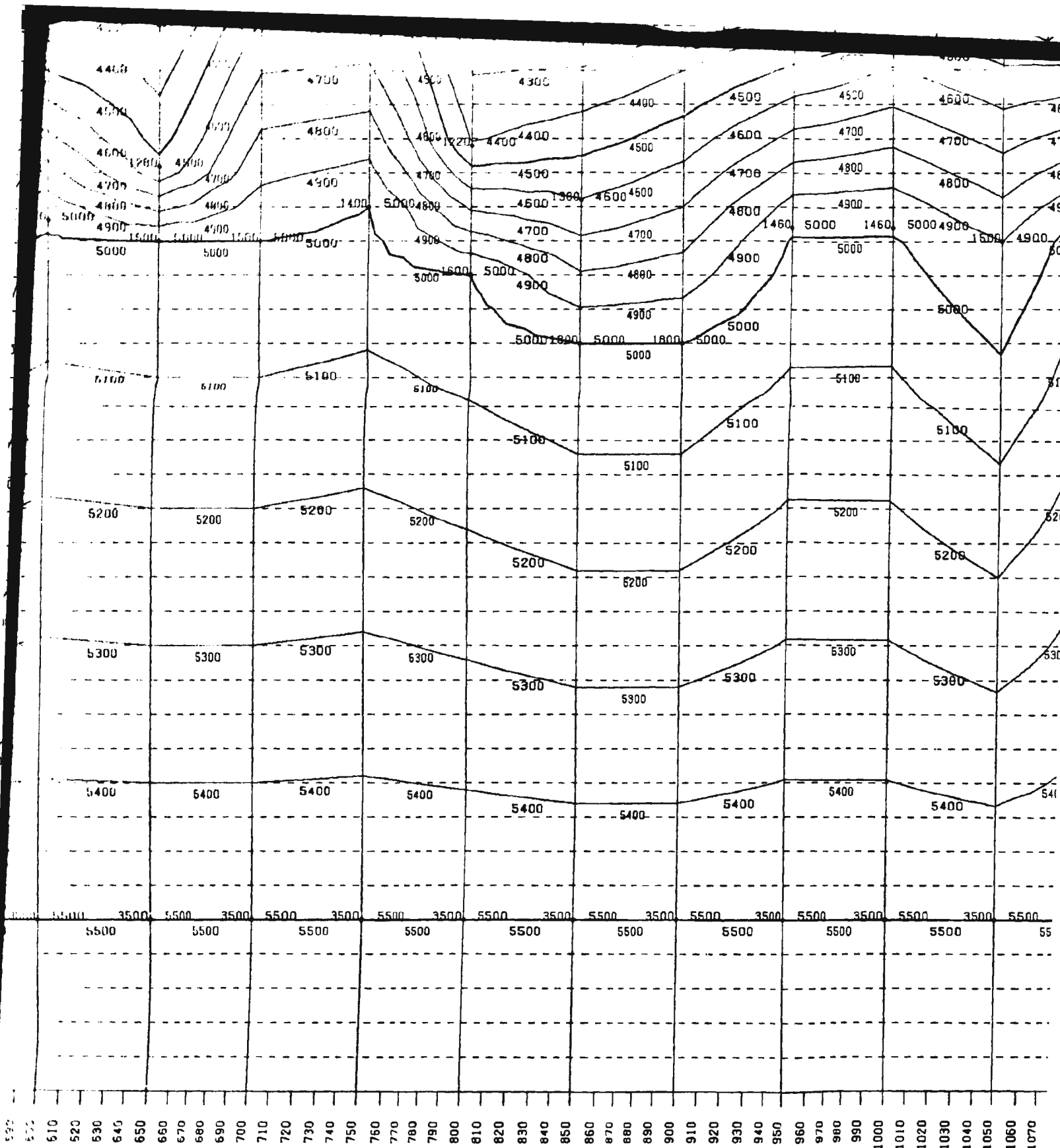
OF FIELD STATICS:

ELEVATION AND
REFRACTION STATICS
FROM FIRST BREAKS

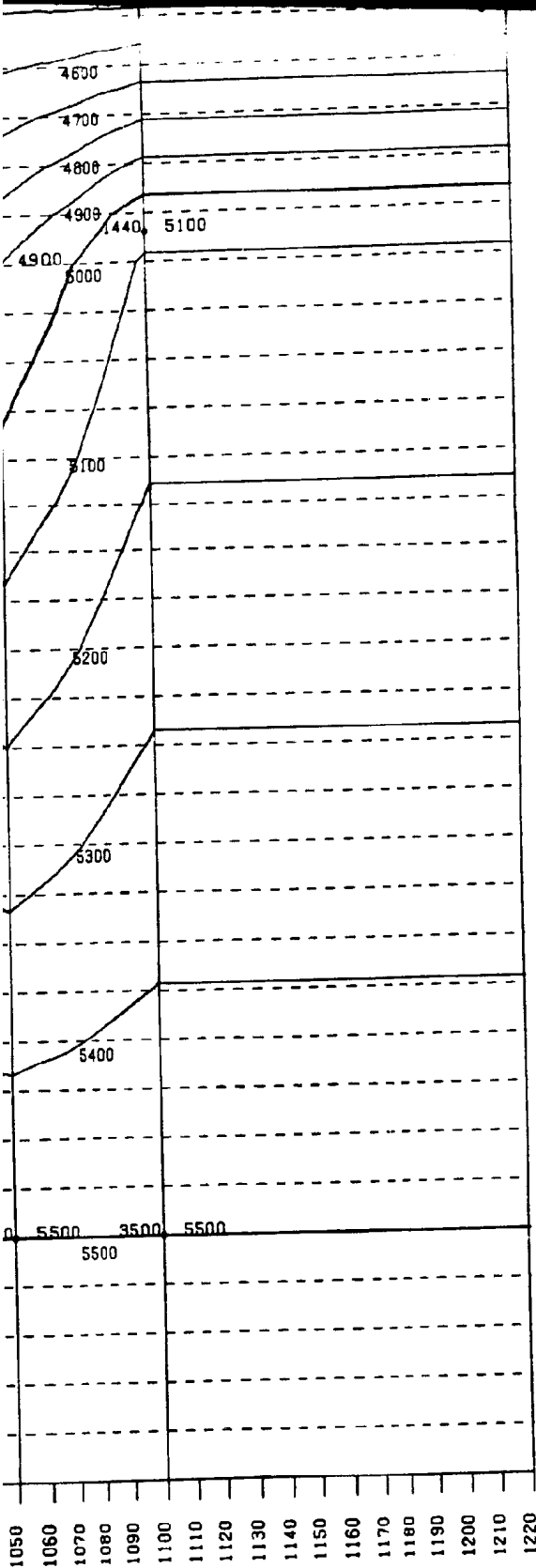
CTION:







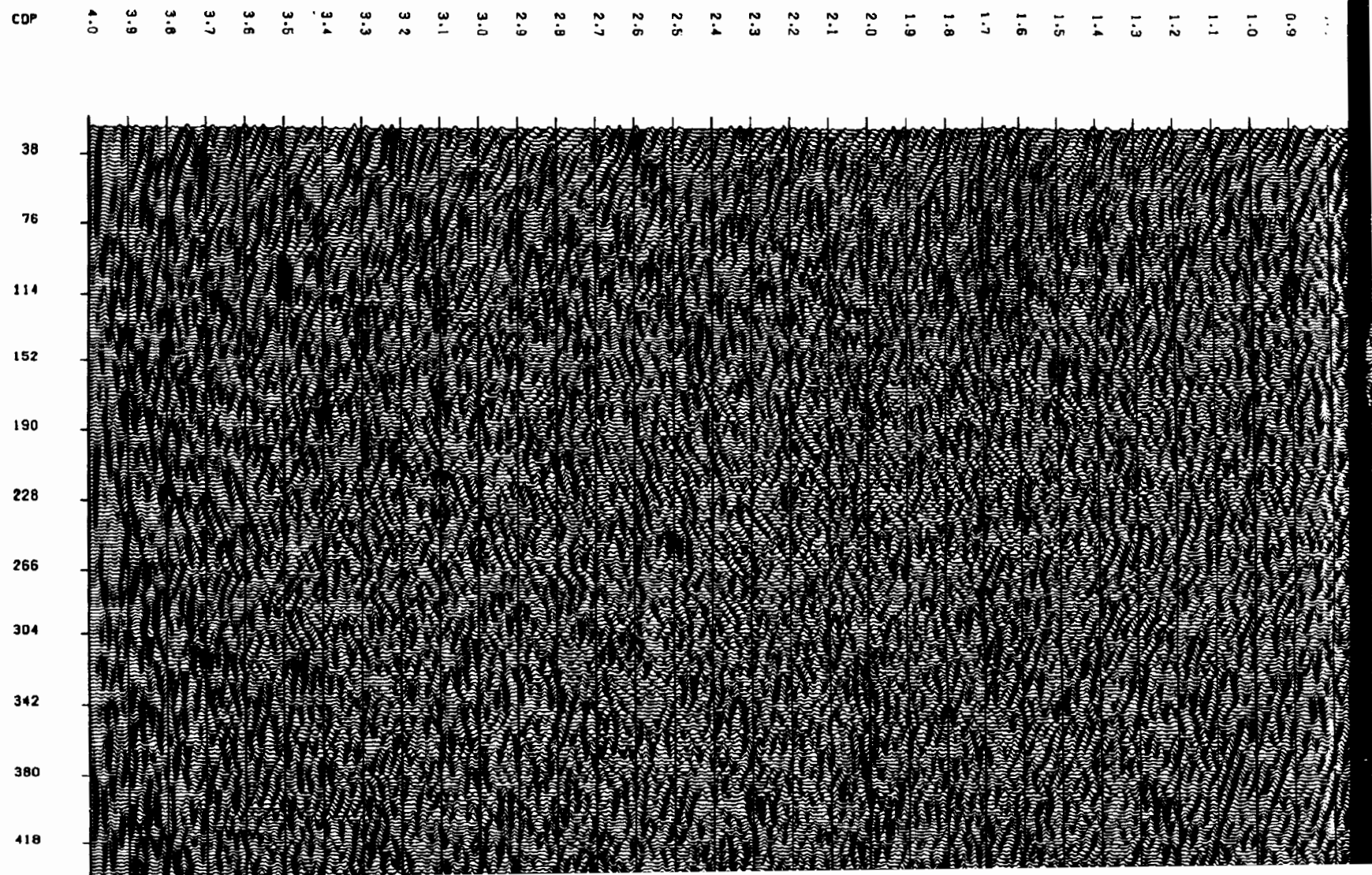
500 510 520 530 540 550 560 570 580 590 600 610 620 630 640 650 660 670 680 690 700 710 720 730 740 750 760 770 780 790 800 810 820 830 840 850 860 870 880 890 900 910 920 930 940 950 960 970 980 990 1000 1010 1020 1030 1040 1050 1060 1070

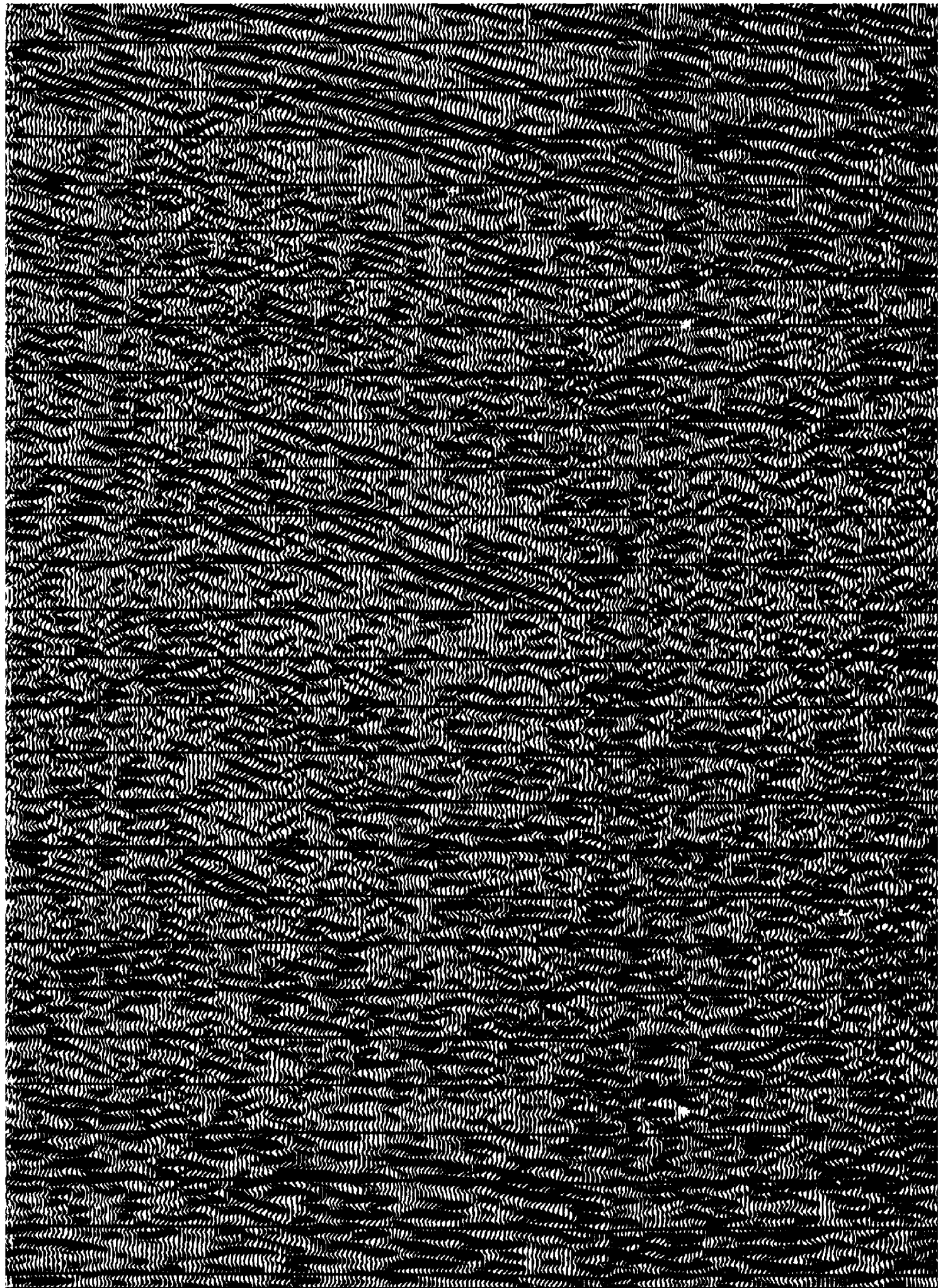


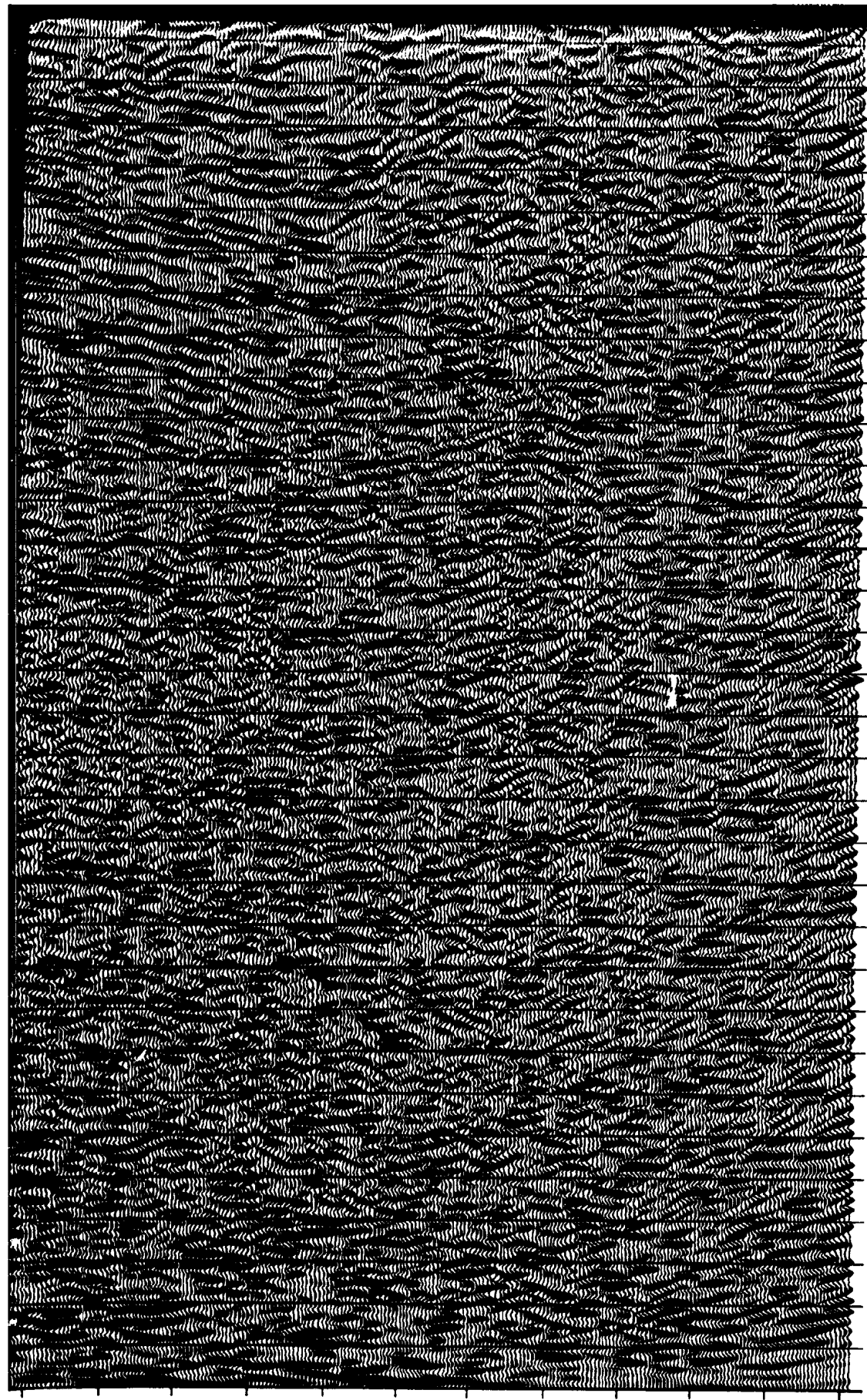
- 1.100
- 1.200
- 1.300
- 1.400
- 1.500
- 1.600
- 1.700
- 1.800
- 1.900
- 2.000
- 2.100
- 2.200
- 2.300
- 2.400
- 2.500
- 2.600
- 2.700
- 2.800
- 2.900
- 3.000
- 3.100
- 3.200
- 3.300
- 3.400
- 3.500
- 3.600
- 3.700
- 3.800
- 3.900
- 4.000

stack, mute applied post-nmo
Pre-stack agc, post agc
two trace sum

Figure 3.22. Final display
section if an average
whole section.







0.9
1.0
1.1
1.2
1.3
1.4
1.5
1.6
1.7
1.8
1.9
2.0
2.1
2.2
2.3
2.4
2.5
2.6
2.7
2.8
2.9
3.0
3.1
3.2
3.3
3.4
3.5
3.6
3.7
3.8
3.9
4.0

798
836
874
912
950
988
1026
1064
1102
1140
1178
1216

CDP

BY: CAPILANO GEOPHYSICAL LTD.

GY SOURCE:
PE: VIBROSEIS
EEP PARAMETERS: 20 HZ - 90 HZ, 500 MS TAPER
EEP LENGTH: 8 SECONDS
JRCE ARRAY: 4 OVER 30 M, MOVE UP 8 M
DTPOINT INTERVAL: 40 M

IVING ARRANGEMENT:
JD OF RECORDING: 104 MAXIMUM
JUP INTERVAL: 20.0 METRES
MNER OF GROUPS: 240
ATION GAP AT SP: 26
OPHONES/GROUP: 12

UMENTATION:
ORDING SYSTEM: DFS Y
I-AMP GAIN: 48 DB
TERS: HIGH CUT 128.0 HZ AT 72 DB
ORD FORMAT: SEC Y, 240 CHANNEL
ORD LENGTH: 4 SECONDS
APLE RATE: 2 MS

PROCESSING

ISSUED BY: CENTRE FOR EARTH RESOURCES RESEARCH
MEMORIAL UNIVERSITY OF NEWFOUNDLAND

PLICATION OF BINNING AND GEOMETRY: SURVEY DATA SUPPLIED BY CONTRACTOR

PLICATION OF FIELD STATICS: ELEVATION AND
REFRACTION STATICS
FROM FIRST BREAKS

MO CORRECTION:

DP GATHER: MAXIMUM FOLD 104

OTCR FILTER: REJECTION OF 90 HZ
APPLIED IN TIME DOMAIN

MO CORRECTION: VELOCITY DERIVATION
FROM MERVEL VELOCITY ANALYSES, CVNMO
AND CONSTANT VELOCITY STACKS (CVS)

BOYT MUTE: PICKED AND APPLIED ON
NMO CORRECTED GATHERS

RE-STACK AGC: 1000 MS WINDOW

DP STACK:
TYPE STANDARD MEAN AMPLITUDE CDP
COVERAGE 8000% - 10400%

RESIDUAL STATICS APPLICATION: FROM PICKED HORIZON
ON DMO CORRECTED STACK

US DEGREE FINITE DIFFERENCE MIGRATION:
BASED ON VELOCITY ANALYSIS AFTER DMO

HANDPASS FILTER: 0.0 S: 20 HZ TO 90 HZ AT 32 DB/OCT
3.0 S: 20 HZ TO 60 HZ AT 32 DB/OCT

COHERENCY FILTER:

AUTOMATIC GAIN CONTROL: AGC BALANCING WINDOW - 500 MS

PLAY

YE: 30/11/1992

STEM: VERSATEC ELECTROSTATIC PLOTTER #7236
IS 0 %
RTICAL SCALE 8 CM/SEC
RIZONTAL SCALE 14 TRACES/CM, 1:13900
LARITY NORMAL
TUM PLANE 100 METRES

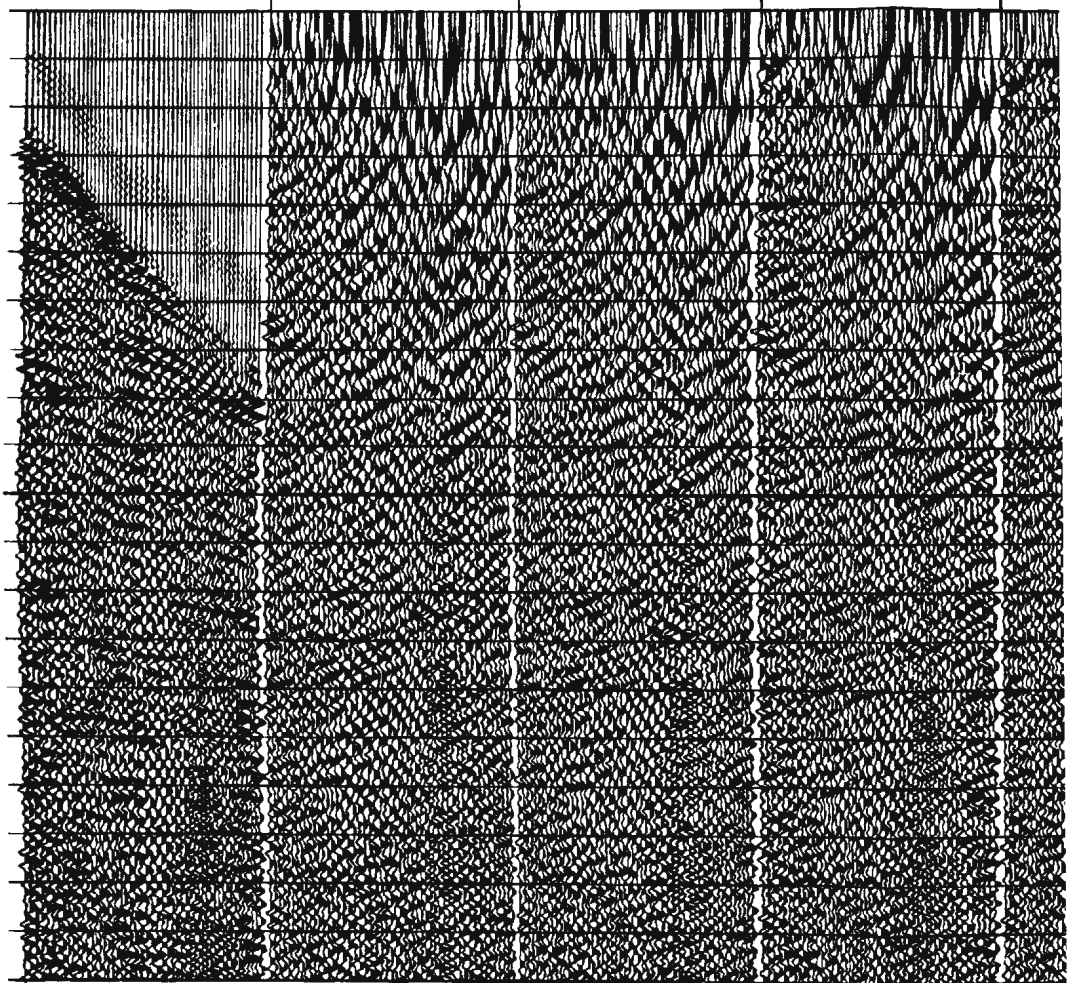


Fig 3.10. (d)

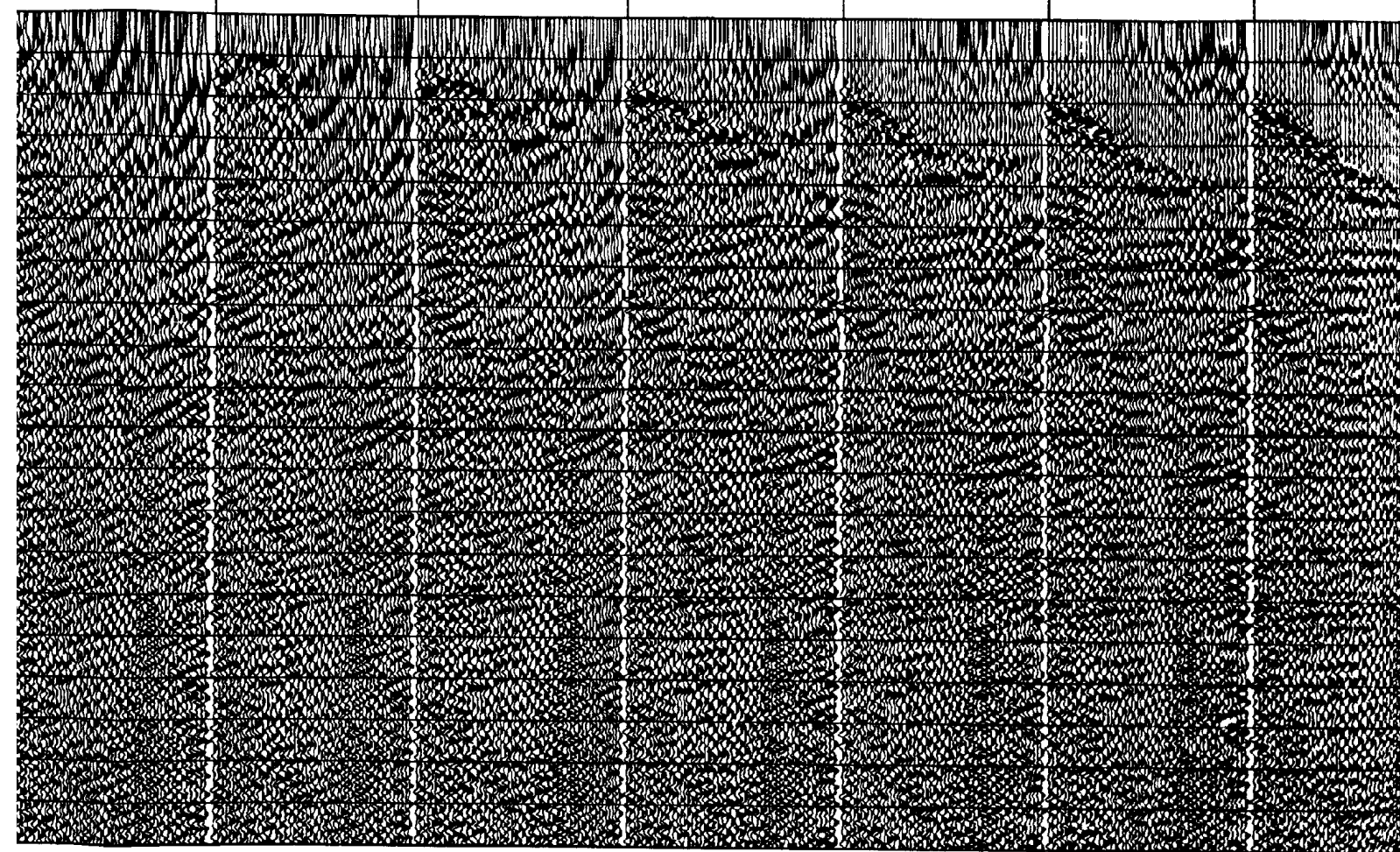
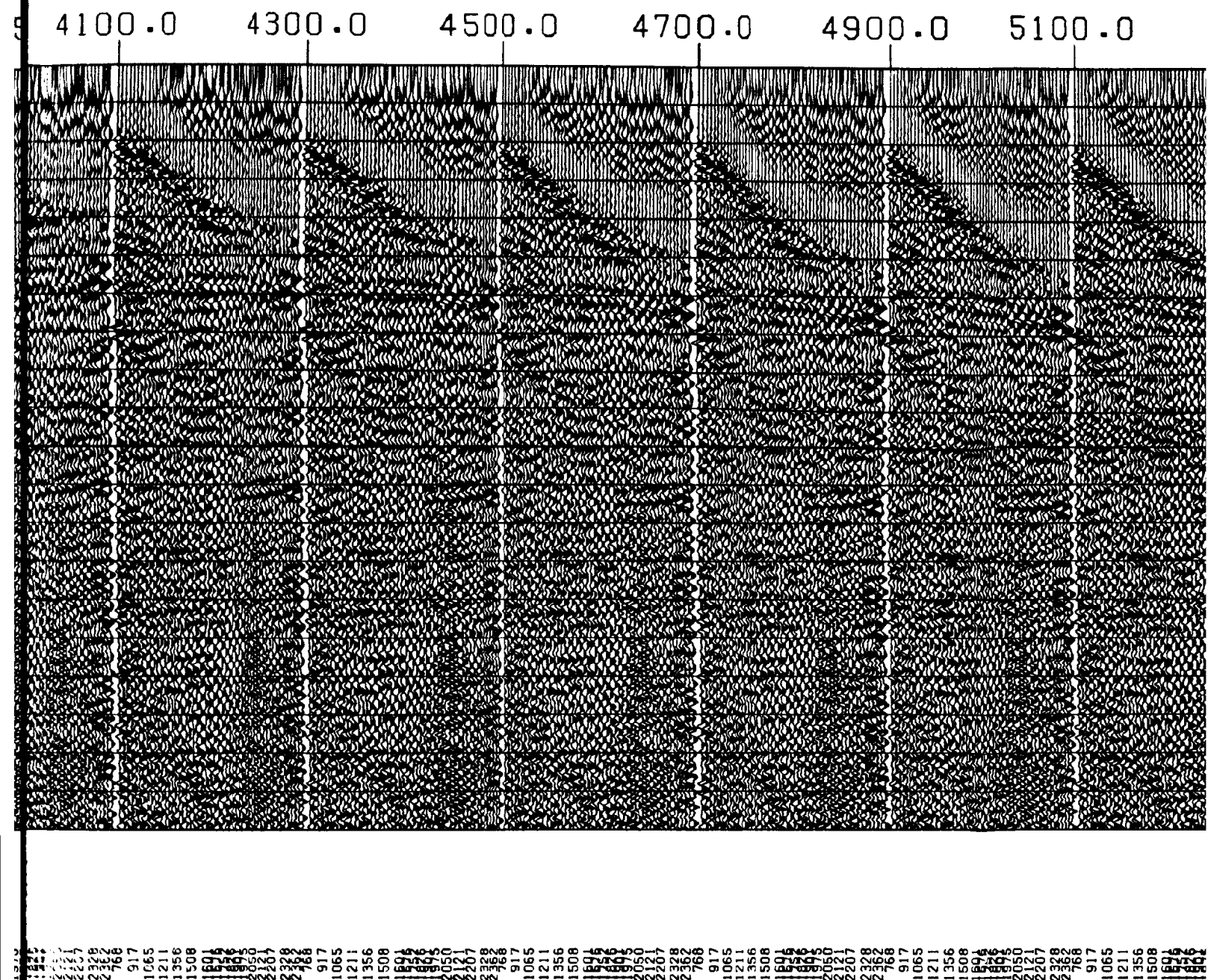
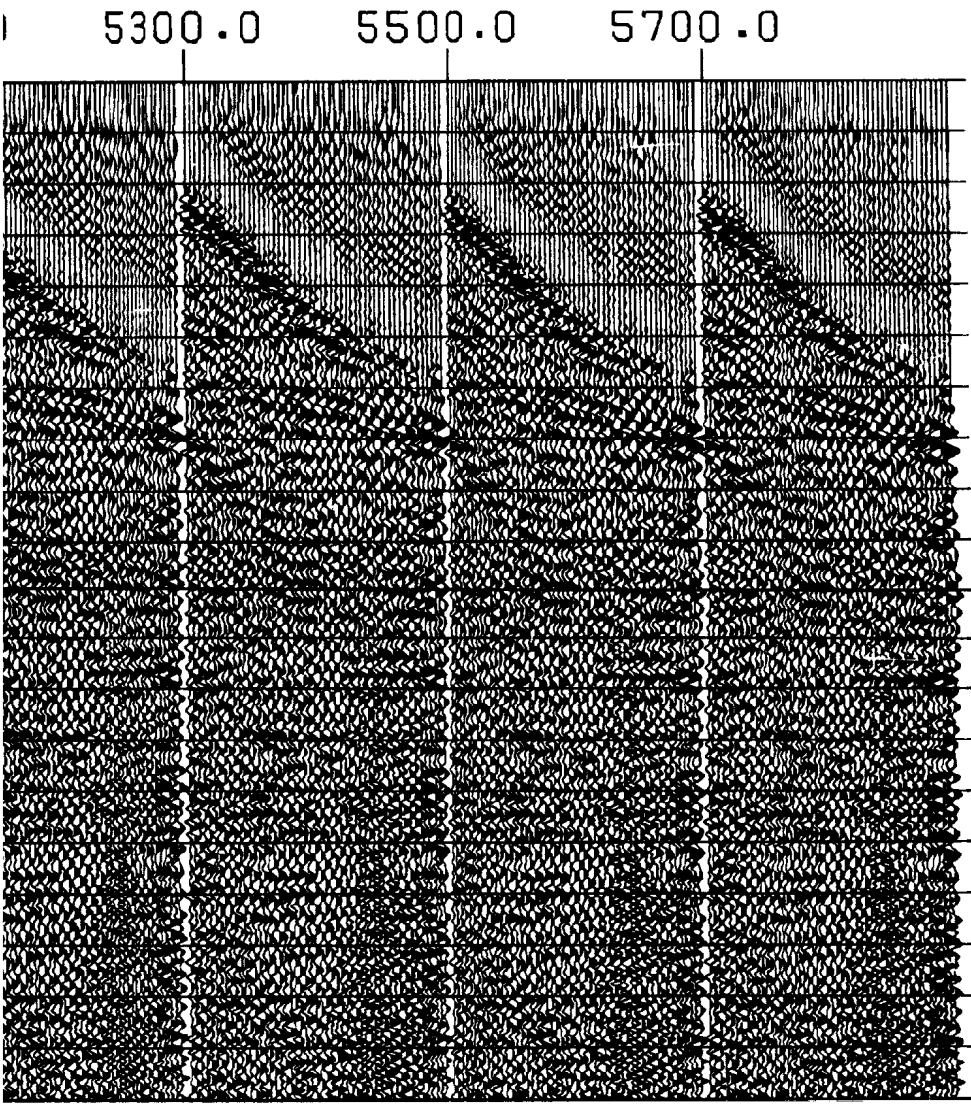
[illegible]

Fig 3.10. (cont.)





VEL

- 0.0
- 0.1
- 0.2
- 0.3
- 0.4
- 0.5
- 0.6
- 0.7
- 0.8
- 0.9
- 1.0
- 1.1
- 1.2
- 1.3
- 1.4
- 1.5
- 1.6
- 1.7
- 1.8
- 1.9
- 2.0

CDP

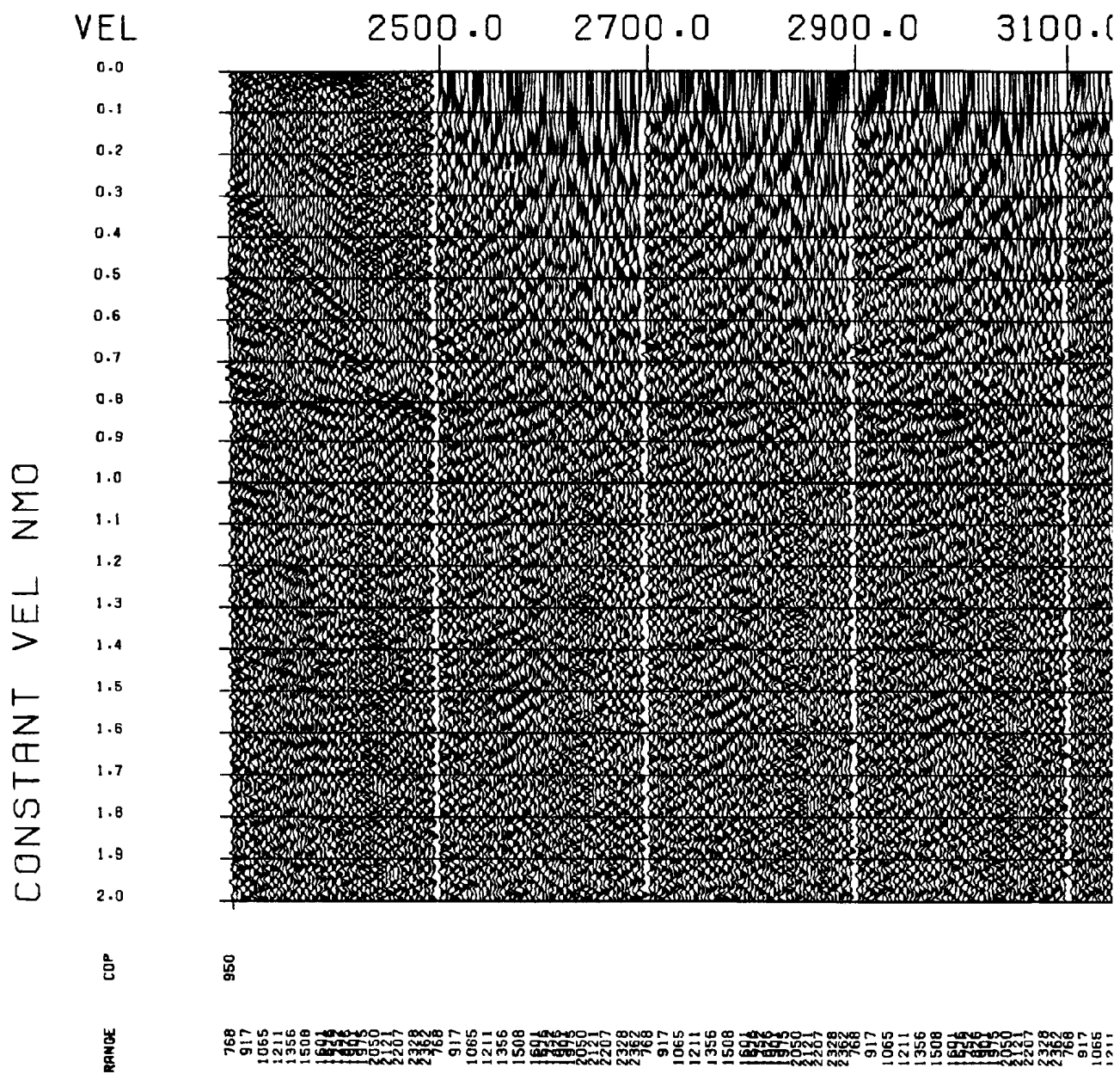
1356
1508
1694
1879
2065
2251
2437
2623
2809
2995
3181
3367
3553
3739
3925
4111
4297
4483
4669
4855
5041
5227
5413
5599
5785
5971
6157
6343
6529
6715
6901
7087
7273
7459
7645
7831
8017
8203
8389
8575
8761
8947
9133
9319
9505
9691
9877
10063
10249
10435
10621
10807
10993
11179
11365
11551
11737
11923
12109
12295
12481
12667
12853
13039
13225
13411
13597
13783
13969
14155
14341
14527
14713
14899
15085
15271
15457
15643
15829
16015
16201
16387
16573
16759
16945
17131
17317
17503
17689
17875
18061
18247
18433
18619
18805
18991
19177
19363
19549
19735
19921
20107
20293
20479
20665
20851
21037
21223
21409
21595
21781
21967
22153
22339
22525
22711
22897
23083
23269
23455
23641
23827
24013
24199
24385
24571
24757
24943
25129
25315
25501
25687
25873
26059
26245
26431
26617
26803
26989
27175
27361
27547
27733
27919
28105
28291
28477
28663
28849
29035
29221
29407
29593
29779
29965
30151
30337
30523
30709
30895
31081
31267
31453
31639
31825
32011
32197
32383
32569
32755
32941
33127
33313
33499
33685
33871
34057
34243
34429
34615
34801
34987
35173
35359
35545
35731
35917
36103
36289
36475
36661
36847
37033
37219
37405
37591
37777
37963
38149
38335
38521
38707
38893
39079
39265
39451
39637
39823
40009
40195
40381
40567
40753
40939
41125
41311
41497
41683
41869
42055
42241
42427
42613
42799
42985
43171
43357
43543
43729
43915
44101
44287
44473
44659
44845
45031
45217
45403
45589
45775
45961
46147
46333
46519
46705
46891
47077
47263
47449
47635
47821
48007
48193
48379
48565
48751
48937
49123
49309
49495
49681
49867
50053
50239
50425
50611
50797
50983
51169
51355
51541
51727
51913
52099
52285
52471
52657
52843
53029
53215
53401
53587
53773
53959
54145
54331
54517
54703
54889
55075
55261
55447
55633
55819
56005
56191
56377
56563
56749
56935
57121
57307
57493
57679
57865
58051
58237
58423
58609
58795
58981
59167
59353
59539
59725
59911
60097
60283
60469
60655
60841
61027
61213
61399
61585
61771
61957
62143
62329
62515
62701
62887
63073
63259
63445
63631
63817
64003
64189
64375
64561
64747
64933
65119
65305
65491
65677
65863
66049
66235
66421
66607
66793
66979
67165
67351
67537
67723
67909
68095
68281
68467
68653
68839
69025
69211
69397
69583
69769
69955
70141
70327
70513
70699
70885
71071
71257
71443
71629
71815
72001
72187
72373
72559
72745
72931
73117
73303
73489
73675
73861
74047
74233
74419
74605
74791
74977
75163
75349
75535
75721
75907
76093
76279
76465
76651
76837
77023
77209
77395
77581
77767
77953
78139
78325
78511
78697
78883
79069
79255
79441
79627
79813
80000
80186
80372
80558
80744
80930
81116
81302
81488
81674
81860
82046
82232
82418
82604
82790
82976
83162
83348
83534
83720
83906
84092
84278
84464
84650
84836
85022
85208
85394
85580
85766
85952
86138
86324
86510
86696
86882
87068
87254
87440
87626
87812
88000
88186
88372
88558
88744
88930
89116
89302
89488
89674
89860
90046
90232
90418
90604
90790
90976
91162
91348
91534
91720
91906
92092
92278
92464
92650
92836
93022
93208
93394
93580
93766
93952
94138
94324
94510
94696
94882
95068
95254
95440
95626
95812
96000
96186
96372
96558
96744
96930
97116
97302
97488
97674
97860
98046
98232
98418
98604
98790
98976
99162
99348
99534
99720
99906
100092
100278
100464
100650
100836
101022
101208
101394
101580
101766
101952
102138
102324
102510
102696
102882
103068
103254
103440
103626
103812
104000
104186
104372
104558
104744
104930
105116
105302
105488
105674
105860
106046
106232
106418
106604
106790
106976
107162
107348
107534
107720
107906
108092
108278
108464
108650
108836
109022
109208
109394
109580
109766
109952
110138
110324
110510
110696
110882
111068
111254
111440
111626
111812
112000
112186
112372
112558
112744
112930
113116
113302
113488
113674
113860
114046
114232
114418
114604
114790
114976
115162
115348
115534
115720
115906
116092
116278
116464
116650
116836
117022
117208
117394
117580
117766
117952
118138
118324
118510
118696
118882
119068
119254
119440
119626
119812
120000
120186
120372
120558
120744
120930
121116
121302
121488
121674
121860
122046
122232
122418
122604
122790
122976
123162
123348
123534
123720
123906
124092
124278
124464
124650
124836
125022
125208
125394
125580
125766
125952
126138
126324
126510
126696
126882
127068
127254
127440
127626
127812
128000
128186
128372
128558
128744
128930
129116
129302
129488
129674
129860
130046
130232
130418
130604
130790
130976
131162
131348
131534
131720
131906
132092
132278
132464
132650
132836
133022
133208
133394
133580
133766
133952
134138
134324
134510
134696
134882
135068
135254
135440
135626
135812
136000
136186
136372
136558
136744
136930
137116
137302
137488
137674
137860
138046
138232
138418
138604
138790
138976
139162
139348
139534
139720
139906
140092
140278
140464
140650
140836
141022
141208
141394
141580
141766
141952
142138
142324
142510
142696
142882
143068
143254
143440
143626
143812
144000
144186
144372
144558
144744
144930
145116
145302
145488
145674
145860
146046
146232
146418
146604
146790
146976
147162
147348
147534
147720
147906
148092
148278
148464
148650
148836
149022
149208
149394
149580
149766
149952
150138
150324
150510
150696
150882
151068
151254
151440
151626
151812
152000
152186
152372
152558
152744
152930
153116
153302
153488
153674
153860
154046
154232
154418
154604
154790
154976
155162
155348
155534
155720
155906
156092
156278
156464
156650
156836
157022
157208
157394
157580
157766
157952
158138
158324
158510
158696
158882
159068
159254
159440
159626
159812
160000
160186
160372
160558
160744
160930
161116
161302
161488
161674
161860
162046
162232
162418
162604
162790
162976
163162
163348
163534
163720
163906
164092
164278
164464
164650
164836
165022
165208
165394
165580
165766
165952
166138
166324
166510
166696
166882
167068
167254
167440
167626
167812
168000
168186
168372
168558
168744
168930
169116
169302
169488
169674
169860
170046
170232
170418
170604
170790
170976
171162
171348
171534
171720
171906
172092
172278
172464
172650
172836
173022
173208
173394
173580
173766
173952
174138
174324
174510
174696
174882
175068
175254
175440
175626
175812
176000
176186
176372
176558
176744
176930
177116
177302
177488
177674
177860
178046
178232
178418
178604
178790
178976
179162
179348
179534
179720
179906
180092
180278
180464
180650
180836
181022
181208
181394
181580
181766
181952
182138
182324
182510
182696
182882
183068
183254
183440
183626
183812
184000
184186
184372
184558
184744
184930
185116
185302
185488
185674
185860
186046
186232
186418
186604
186790
186976
187162
187348
187534
187720
187906
188092
188278
188464
188650
188836
189022
189208
189394
189580
189766
189952
190138
190324
190510
190696
190882
191068
191254
191440
191626
191812
192000
192186
192372
192558
192744
192930
193116
193302
193488
193674
193860
194046
194232
194418
194604
194790
194976
195162
195348
195534
195720
195906
196092
196278
196464
196650
196836
197022
197208
197394
197580
197766
197952
198138
198324
198510
198696
198882
199068
199254
199440
199626
199812
200000

RANGE

7

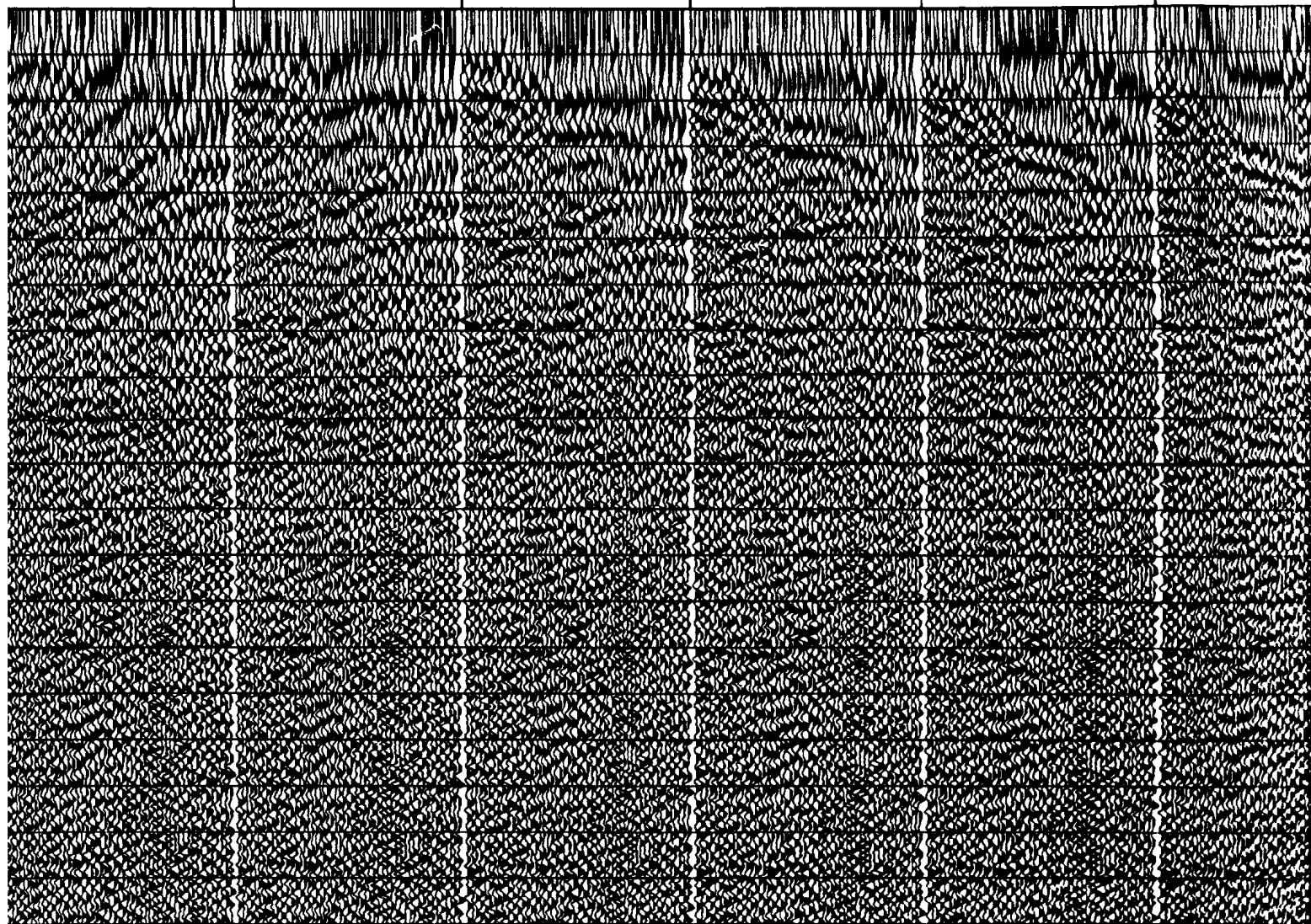
(a)

Figure 3.10. Constant velocity normal moveout (CVN CMP 950 after DMO correction. (a) Before DMO correction. (b) After DMO correction.



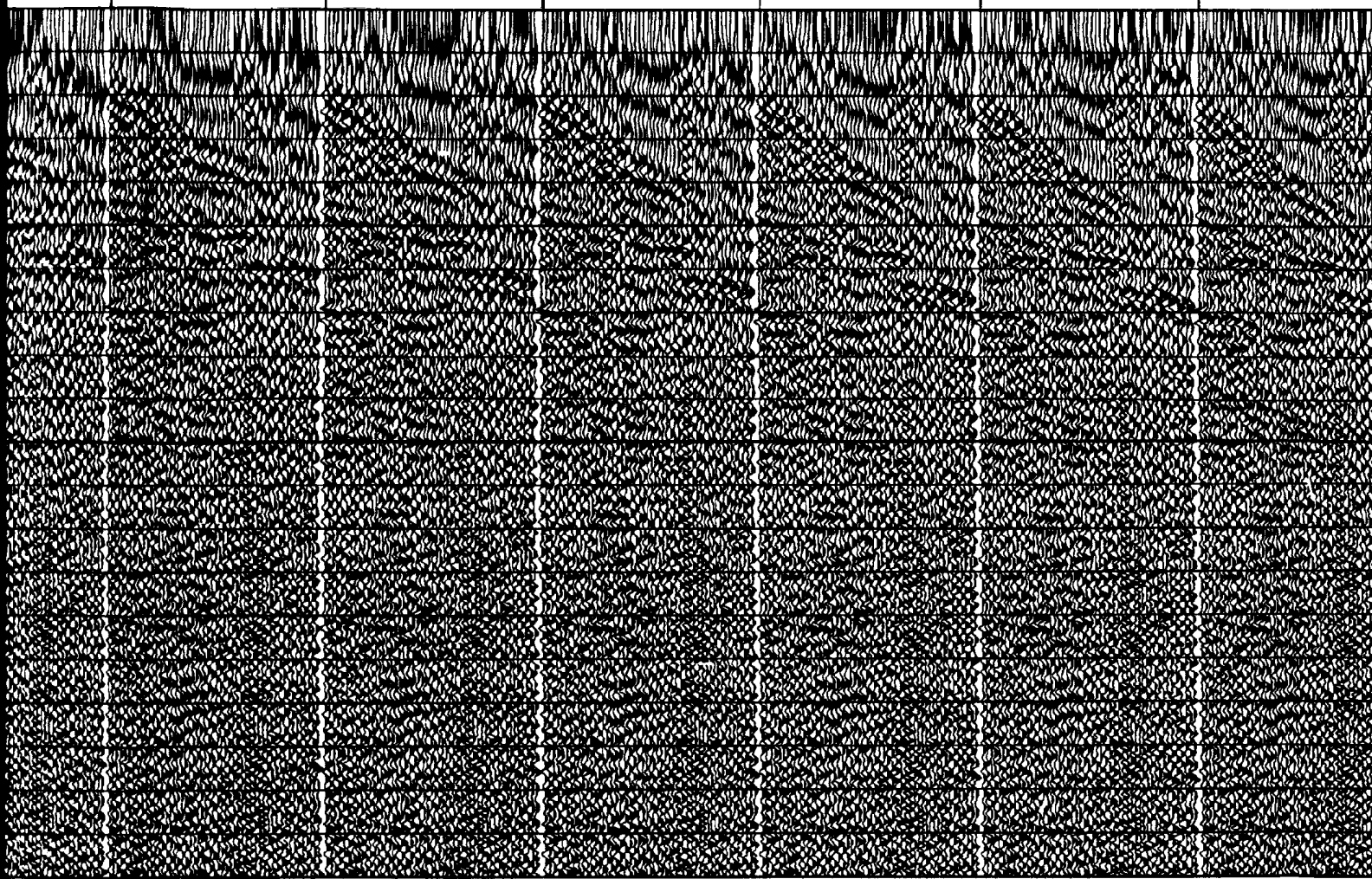
(VNMO) of
correction.

3100.0 3300.0 3500.0 3700.0 3900.0 4100.0 4300.0



917	1065	1211	1356	1508	1655	1802	1950	2097	2244	2391	2538	2685	2832	2979	3126	3273	3420	3567	3714	3861	4008	4155	4302	4449	4596	4743	4890	5037	5184	5331	5478	5625	5772	5919	6066	6213	6360	6507	6654	6801	6948	7095	7242	7389	7536	7683	7830	7977	8124	8271	8418	8565	8712	8859	9006	9153	9300	9447	9594	9741	9888	10035	10182	10329	10476	10623	10770	10917	11064	11211	11358	11505	11652	11799	11946	12093	12240	12387	12534	12681	12828	12975	13122	13269	13416	13563	13710	13857	14004	14151	14298	14445	14592	14739	14886	15033	15180	15327	15474	15621	15768	15915	16062	16209	16356	16503	16650	16797	16944	17091	17238	17385	17532	17679	17826	17973	18120	18267	18414	18561	18708	18855	19002	19149	19296	19443	19590	19737	19884	20031	20178	20325	20472	20619	20766	20913	21060	21207	21354	21501	21648	21795	21942	22089	22236	22383	22530	22677	22824	22971	23118	23265	23412	23559	23706	23853	24000	24147	24294	24441	24588	24735	24882	25029	25176	25323	25470	25617	25764	25911	26058	26205	26352	26499	26646	26793	26940	27087	27234	27381	27528	27675	27822	27969	28116	28263	28410	28557	28704	28851	28998	29145	29292	29439	29586	29733	29880	30027	30174	30321	30468	30615	30762	30909	31056	31203	31350	31497	31644	31791	31938	32085	32232	32379	32526	32673	32820	32967	33114	33261	33408	33555	33702	33849	33996	34143	34290	34437	34584	34731	34878	35025	35172	35319	35466	35613	35760	35907	36054	36201	36348	36495	36642	36789	36936	37083	37230	37377	37524	37671	37818	37965	38112	38259	38406	38553	38700	38847	38994	39141	39288	39435	39582	39729	39876	40023	40170	40317	40464	40611	40758	40905	41052	41199	41346	41493	41640	41787	41934	42081	42228	42375	42522	42669	42816	42963	43110	43257	43404	43551	43698	43845	43992	44139	44286	44433	44580	44727	44874	45021	45168	45315	45462	45609	45756	45903	46050	46197	46344	46491	46638	46785	46932	47079	47226	47373	47520	47667	47814	47961	48108	48255	48402	48549	48696	48843	48990	49137	49284	49431	49578	49725	49872	50019	50166	50313	50460	50607	50754	50901	51048	51195	51342	51489	51636	51783	51930	52077	52224	52371	52518	52665	52812	52959	53106	53253	53400	53547	53694	53841	53988	54135	54282	54429	54576	54723	54870	55017	55164	55311	55458	55605	55752	55899	56046	56193	56340	56487	56634	56781	56928	57075	57222	57369	57516	57663	57810	57957	58104	58251	58398	58545	58692	58839	58986	59133	59280	59427	59574	59721	59868	60015	60162	60309	60456	60603	60750	60897	61044	61191	61338	61485	61632	61779
-----	------	------	------	------	------	------	------	------	------	------	------	------	------	------	------	------	------	------	------	------	------	------	------	------	------	------	------	------	------	------	------	------	------	------	------	------	------	------	------	------	------	------	------	------	------	------	------	------	------	------	------	------	------	------	------	------	------	------	------	------	------	-------	-------	-------	-------	-------	-------	-------	-------	-------	-------	-------	-------	-------	-------	-------	-------	-------	-------	-------	-------	-------	-------	-------	-------	-------	-------	-------	-------	-------	-------	-------	-------	-------	-------	-------	-------	-------	-------	-------	-------	-------	-------	-------	-------	-------	-------	-------	-------	-------	-------	-------	-------	-------	-------	-------	-------	-------	-------	-------	-------	-------	-------	-------	-------	-------	-------	-------	-------	-------	-------	-------	-------	-------	-------	-------	-------	-------	-------	-------	-------	-------	-------	-------	-------	-------	-------	-------	-------	-------	-------	-------	-------	-------	-------	-------	-------	-------	-------	-------	-------	-------	-------	-------	-------	-------	-------	-------	-------	-------	-------	-------	-------	-------	-------	-------	-------	-------	-------	-------	-------	-------	-------	-------	-------	-------	-------	-------	-------	-------	-------	-------	-------	-------	-------	-------	-------	-------	-------	-------	-------	-------	-------	-------	-------	-------	-------	-------	-------	-------	-------	-------	-------	-------	-------	-------	-------	-------	-------	-------	-------	-------	-------	-------	-------	-------	-------	-------	-------	-------	-------	-------	-------	-------	-------	-------	-------	-------	-------	-------	-------	-------	-------	-------	-------	-------	-------	-------	-------	-------	-------	-------	-------	-------	-------	-------	-------	-------	-------	-------	-------	-------	-------	-------	-------	-------	-------	-------	-------	-------	-------	-------	-------	-------	-------	-------	-------	-------	-------	-------	-------	-------	-------	-------	-------	-------	-------	-------	-------	-------	-------	-------	-------	-------	-------	-------	-------	-------	-------	-------	-------	-------	-------	-------	-------	-------	-------	-------	-------	-------	-------	-------	-------	-------	-------	-------	-------	-------	-------	-------	-------	-------	-------	-------	-------	-------	-------	-------	-------	-------	-------	-------	-------	-------	-------	-------	-------	-------	-------	-------	-------	-------	-------	-------	-------	-------	-------	-------	-------	-------	-------	-------	-------	-------	-------	-------	-------	-------	-------	-------	-------	-------	-------	-------	-------	-------	-------	-------	-------	-------	-------	-------	-------	-------	-------	-------	-------	-------	-------	-------	-------	-------	-------	-------	-------	-------	-------	-------	-------	-------	-------	-------	-------	-------	-------	-------	-------	-------	-------	-------	-------	-------	-------	-------	-------	-------	-------	-------	-------	-------	-------	-------	-------	-------

4100.0 4300.0 4500.0 4700.0 4900.0 5100.0 5300.0



1065 1211 1356 1508 1654 1800 1946 2092 2238 2384 2530 2676 2822 2968 3114 3260 3406 3552 3698 3844 3990 4136 4282 4428 4574 4720 4866 5012 5158 5304 5450 5596 5742 5888 6034 6180 6326 6472 6618 6764 6910 7056 7202 7348 7494 7640 7786 7932 8078 8224 8370 8516 8662 8808 8954 9100 9246 9392 9538 9684 9830 9976 10122 10268 10414 10560 10706 10852 11000 11146 11292 11438 11584 11730 11876 12022 12168 12314 12460 12606 12752 12898 13044 13190 13336 13482 13628 13774 13920 14066 14212 14358 14504 14650 14796 14942 15088 15234 15380 15526 15672 15818 15964 16110 16256 16402 16548 16694 16840 16986 17132 17278 17424 17570 17716 17862 18008 18154 18300 18446 18592 18738 18884 19030 19176 19322 19468 19614 19760 19906 20052 20198 20344 20490 20636 20782 20928 21074 21220 21366 21512 21658 21804 21950 22096 22242 22388 22534 22680 22826 22972 23118 23264 23410 23556 23702 23848 23994 24140 24286 24432 24578 24724 24870 25016 25162 25308 25454 25600 25746 25892 26038 26184 26330 26476 26622 26768 26914 27060 27206 27352 27498 27644 27790 27936 28082 28228 28374 28520 28666 28812 28958 29104 29250 29396 29542 29688 29834 29980 30126 30272 30418 30564 30710 30856 31002 31148 31294 31440 31586 31732 31878 32024 32170 32316 32462 32608 32754 32900 33046 33192 33338 33484 33630 33776 33922 34068 34214 34360 34506 34652 34798 34944 35090 35236 35382 35528 35674 35820 35966 36112 36258 36404 36550 36696 36842 36988 37134 37280 37426 37572 37718 37864 38010 38156 38302 38448 38594 38740 38886 39032 39178 39324 39470 39616 39762 39908 40054 40200 40346 40492 40638 40784 40930 41076 41222 41368 41514 41660 41806 41952 42098 42244 42390 42536 42682 42828 42974 43120 43266 43412 43558 43704 43850 43996 44142 44288 44434 44580 44726 44872 45018 45164 45310 45456 45602 45748 45894 46040 46186 46332 46478 46624 46770 46916 47062 47208 47354 47500 47646 47792 47938 48084 48230 48376 48522 48668 48814 48960 49106 49252 49398 49544 49690 49836 49982 50128 50274 50420 50566 50712 50858 51004 51150 51296 51442 51588 51734 51880 52026 52172 52318 52464 52610 52756 52902 53048 53194 53340 53486 53632 53778 53924 54070 54216 54362 54508 54654 54800 54946 55092 55238 55384 55530 55676 55822 55968 56114 56260 56406 56552 56698 56844 56990 57136 57282 57428 57574 57720 57866 58012 58158 58304 58450 58596 58742 58888 59034 59180 59326 59472 59618 59764 59910 60056 60202 60348 60494 60640 60786 60932 61078 61224 61370 61516 61662 61808 61954 62100 62246 62392 62538 62684 62830 62976 63122 63268 63414 63560 63706 63852 63998 64144 64290 64436 64582 64728 64874 65020 65166 65312 65458 65604 65750 65896 66042 66188 66334 66480 66626 66772 66918 67064 67210 67356 67502 67648 67794 67940 68086 68232 68378 68524 68670 68816 68962 69108 69254 69400 69546 69692 69838 69984 70130 70276 70422 70568 70714 70860 71006 71152 71298 71444 71590 71736 71882 72028 72174 72320 72466 72612 72758 72904 73050 73196 73342 73488 73634 73780 73926 74072 74218 74364 74510 74656 74802 74948 75094 75240 75386 75532 75678 75824 75970 76116 76262 76408 76554 76700 76846 76992 77138 77284 77430 77576 77722 77868 78014 78160 78306 78452 78598 78744 78890 79036 79182 79328 79474 79620 79766 79912 80058 80204 80350 80496 80642 80788 80934 81080 81226 81372 81518 81664 81810 81956 82102 82248 82394 82540 82686 82832 82978 83124 83270 83416 83562 83708 83854 83999 84145 84291 84437 84583 84729 84875 85021 85167 85313 85459 85605 85751 85897 86043 86189 86335 86481 86627 86773 86919 87065 87211 87357 87503 87649 87795 87941 88087 88233 88379 88525 88671 88817 88963 89109 89255 89401 89547 89693 89839 90000 90146 90292 90438 90584 90730 90876 91022 91168 91314 91460 91606 91752 91898 92044 92190 92336 92482 92628 92774 92920 93066 93212 93358 93504 93650 93796 93942 94088 94234 94380 94526 94672 94818 94964 95110 95256 95402 95548 95694 95840 95986 96132 96278 96424 96570 96716 96862 97008 97154 97300 97446 97592 97738 97884 98030 98176 98322 98468 98614 98760 98906 99052 99198 99344 99490 99636 99782 99928 100074 100220 100366 100512 100658 100804 100950 101096 101242 101388 101534 101680 101826 101972 102118 102264 102410 102556 102702 102848 102994 103140 103286 103432 103578 103724 103870 104016 104162 104308 104454 104600 104746 104892 105038 105184 105330 105476 105622 105768 105914 106060 106206 106352 106498 106644 106790 106936 107082 107228 107374 107520 107666 107812 107958 108104 108250 108396 108542 108688 108834 108980 109126 109272 109418 109564 109710 109856 110002 110148 110294 110440 110586 110732 110878 111024 111170 111316 111462 111608 111754 111900 112046 112192 112338 112484 112630 112776 112922 113068 113214 113360 113506 113652 113798 113944 114090 114236 114382 114528 114674 114820 114966 115112 115258 115404 115550 115696 115842 115988 116134 116280 116426 116572 116718 116864 117010 117156 117302 117448 117594 117740 117886 118032 118178 118324 118470 118616 118762 118908 119054 119200 119346 119492 119638 119784 119930 120076 120222 120368 120514 120660 120806 120952 121098 121244 121390 121536 121682 121828 121974 122120 122266 122412 122558 122704 122850 122996 123142 123288 123434 123580 123726 123872 124018 124164 124310 124456 124602 124748 124894 125040 125186 125332 125478 125624 125770 125916 126062 126208 126354 126500 126646 126792 126938 127084 127230 127376 127522 127668 127814 127960 128106 128252 128398 128544 128690 128836 128982 129128 129274 129420 129566 129712 129858 130004 130150 130296 130442 130588 130734 130880 131026 131172 131318 131464 131610 131756 131902 132048 132194 132340 132486 132632 132778 132924 133070 133216 133362 133508 133654 133800 133946 134092 134238 134384 134530 134676 134822 134968 135114 135260 135406 135552 135698 135844 135990 136136 136282 136428 136574 136720 136866 137012 137158 137304 137450 137596 137742 137888 138034 138180 138326 138472 138618 138764 138910 139056 139202 139348 139494 139640 139786 139932 140078 140224 140370 140516 140662 140808 140954 141100 141246 141392 141538 141684 141830 141976 142122 142268 142414 142560 142706 142852 142998 143144 143290 143436 143582 143728 143874 144020 144166 144312 144458 144604 144750 144896 145042 145188 145334 145480 145626 145772 145918 146064 146210 146356 146502 146648 146794 146940 147086 147232 147378 147524 147670 147816 147962 148108 148254 148400 148546 148692 148838 148984 149130 149276 149422 149568 149714 149860 150006 150152 150298 150444 150590 150736 150882 151028 151174 151320 151466 151612 151758 151904 152050 152196 152342 152488 152634 152780 152926 153072 153218 153364 153510 153656 153802 153948 154094 154240 154386 154532 154678 154824 154970 155116 155262 155408 155554 155700 155846 155992 156138 156284 156430 156576 156722 156868 157014 157160 157306 157452 157598 157744 157890 158036 158182 158328 158474 158620 158766 158912 159058 159204 159350 159496 159642 159788 159934 160080 160226 160372 160518 160664 160810 160956 161102 161248 161394 161540 161686 161832 161978 162124 162270 162416 162562 162708 162854 163000 163146 163292 163438 163584 163730 163876 164022 164168 164314 164460 164606 164752 164898 165044 165190 165336 165482 165628 165774 165920 166066 166212 166358 166504 166650 166796 166942 167088 167234 167380 167526 167672 167818 167964 168110 168256 168402 168548 168694 168840 168986 169132 169278 169424 169570 169716 169862 170008 170154 170300 170446 170592 170738 170884 171030 171176 171322 171468 171614 171760 171906 172052 172198 172344 172490 172636 172782 172928 173074 173220 173366 173512 173658 173804 173950 174096 174242 174388 174534 174680 174826 174972 175118 175264 175410 175556 175702 175848 175994 176140 176286 176432 176578 176724 176870 177016 177162 177308 177454 177600 177746 177892 178038 178184 178330 178476 178622 178768 178914 179060 179206 179352 179498 179644 179790 179936 180082 180228 180374 180520 180666 180812 180958 181104 181250 181396 181542 181688 181834 181980 182126 182272 182418 182564 182710 182856 183002 183148 183294 183440 183586 183732 183878 184024 184170 184316 184462 184608 184754 184900 185046 185192 185338 185484 185630 185776 185922 186068 186214 186360 186506 186652 186798 186944 187090 187236 187382 187528 187674 187820 187966 188112 188258 188404 188550 188696 188842 188988 189134 189280 189426 189572 189718 189864 190010 190156 190302 190448 190594 190740 190886 191032 191178 191324 191470 191616 191762 191908 192054 192200 192346 192492 192638 192784 192930 193076 193222 193368 193514 193660 193806 193952 194098 194244 194390 194536 194682 194828 194974 195120 195266 195412 195558 195704 195850 195996 196142 196288 196434 196580 196726 196872 197018 197164 197310 197456 197602 197748 197894 198040 198186 198332 198478 198624 198770 198916 199062 199208 199354 199500 199646 199792 200000

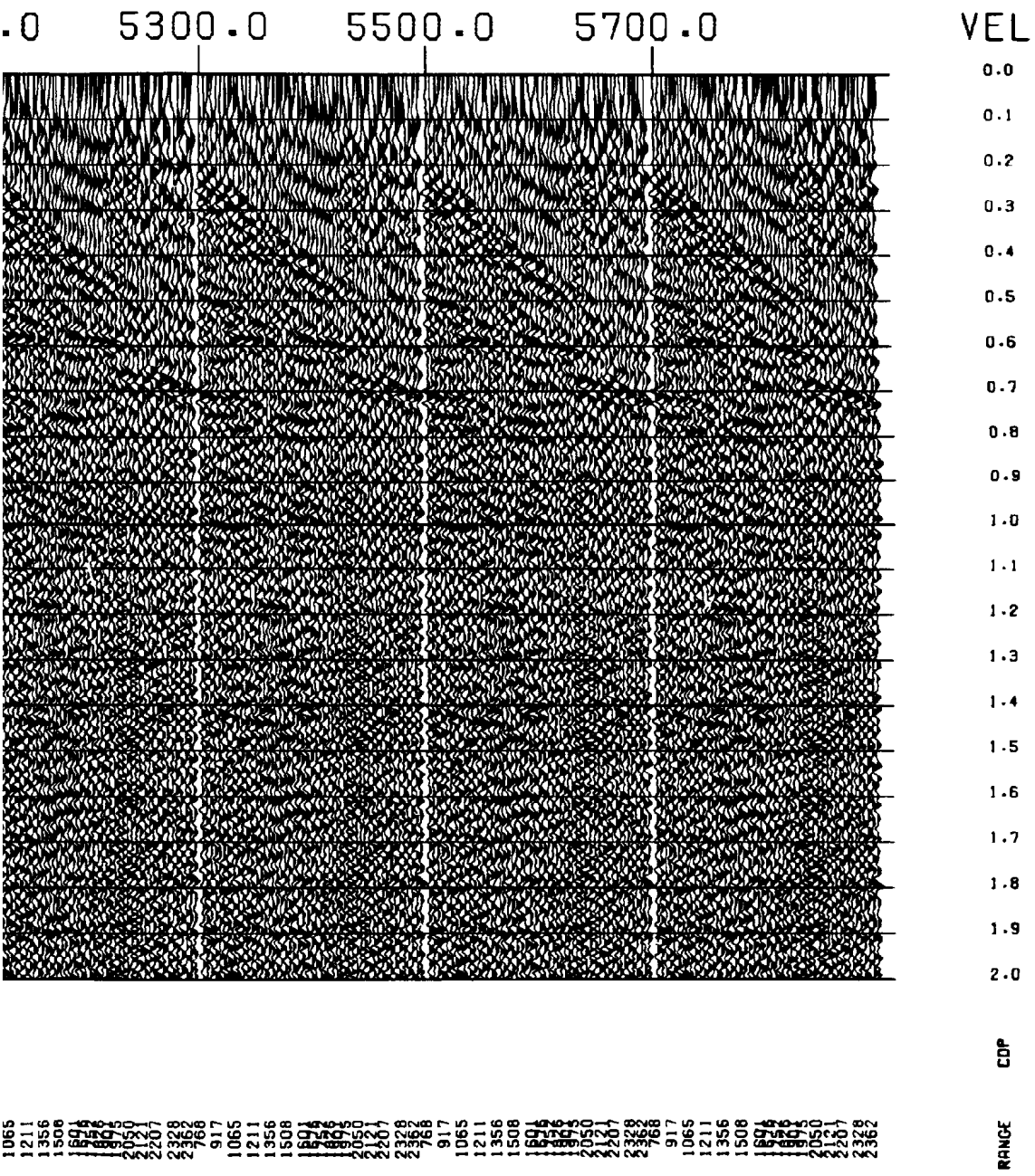
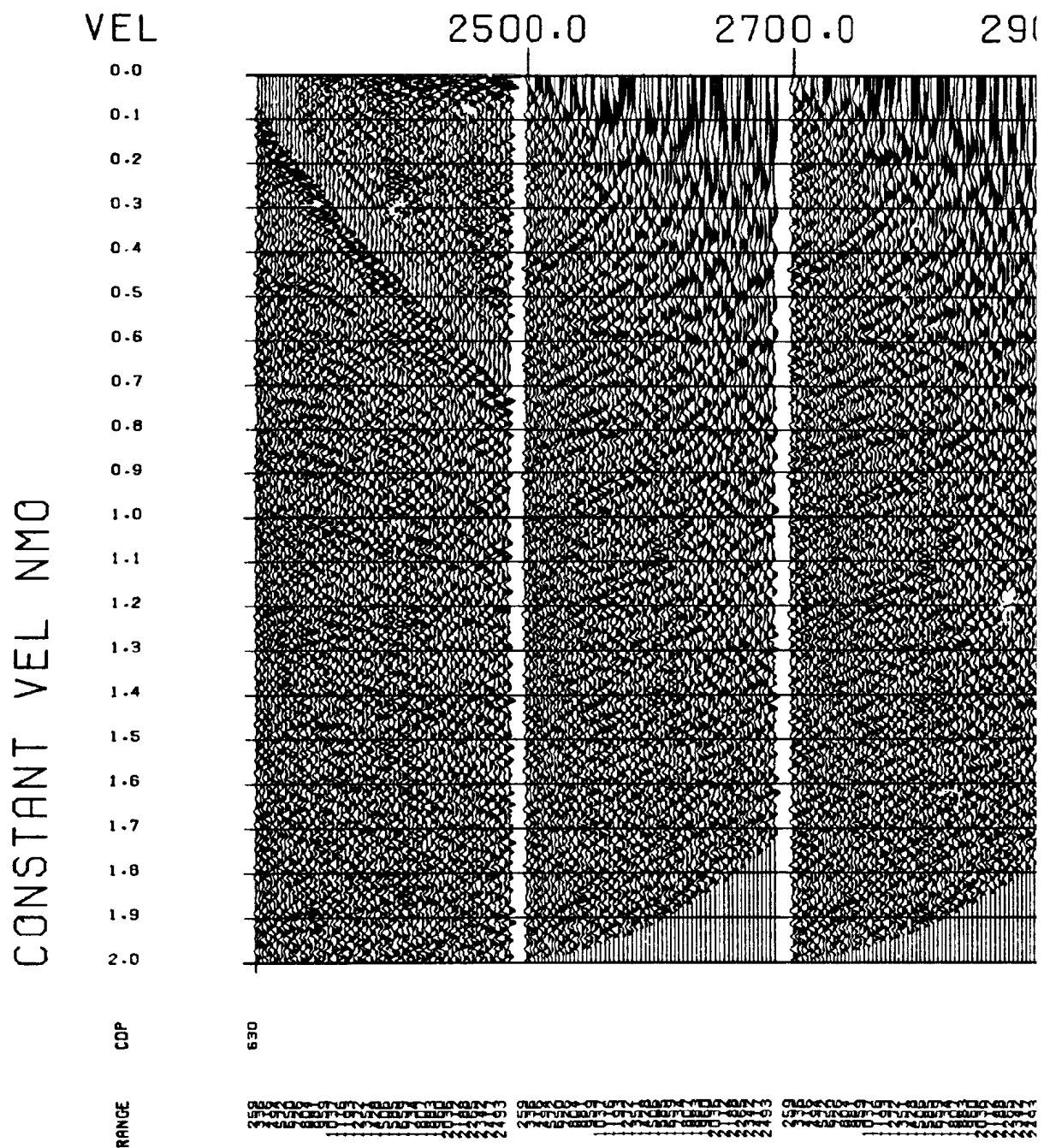
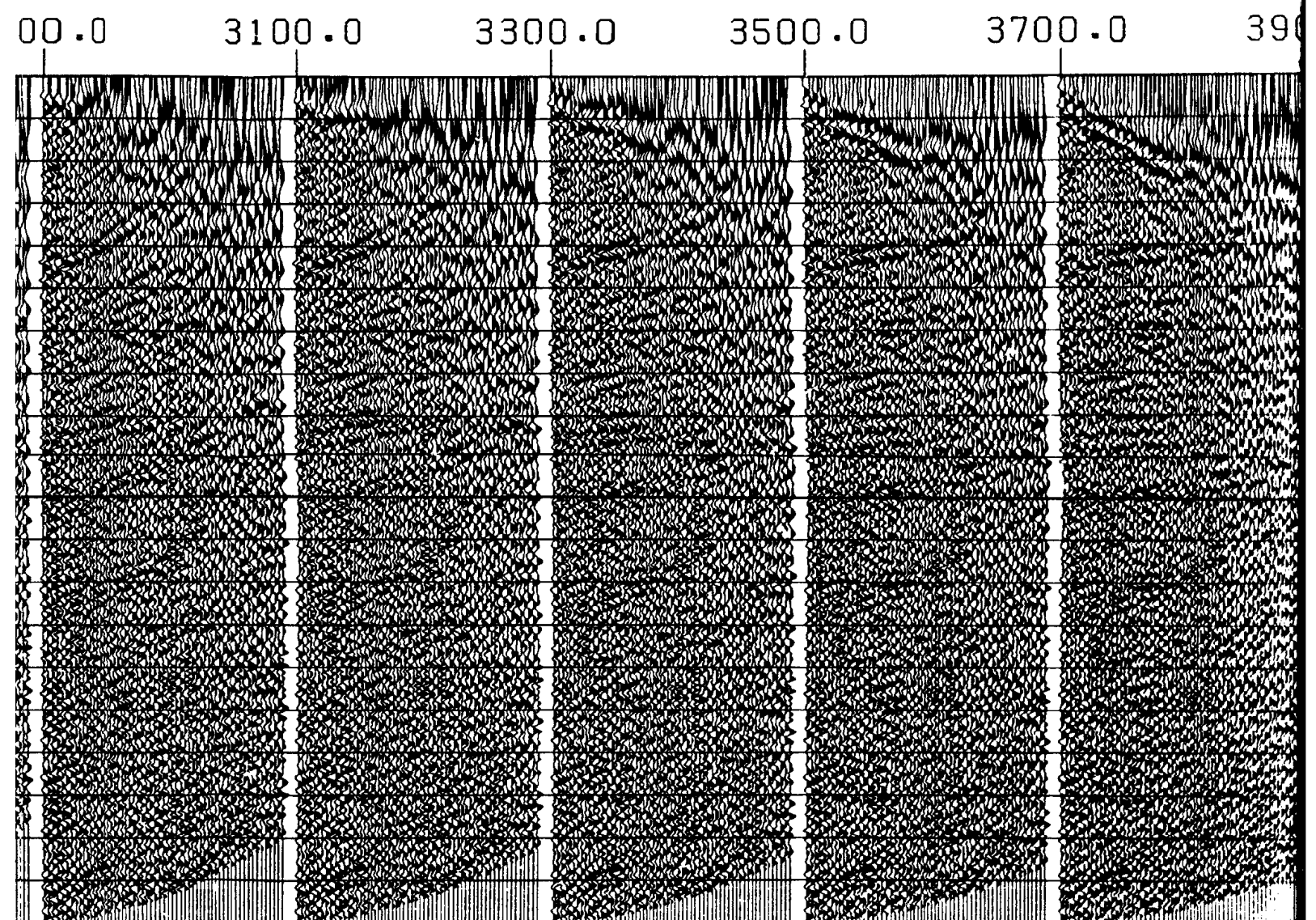


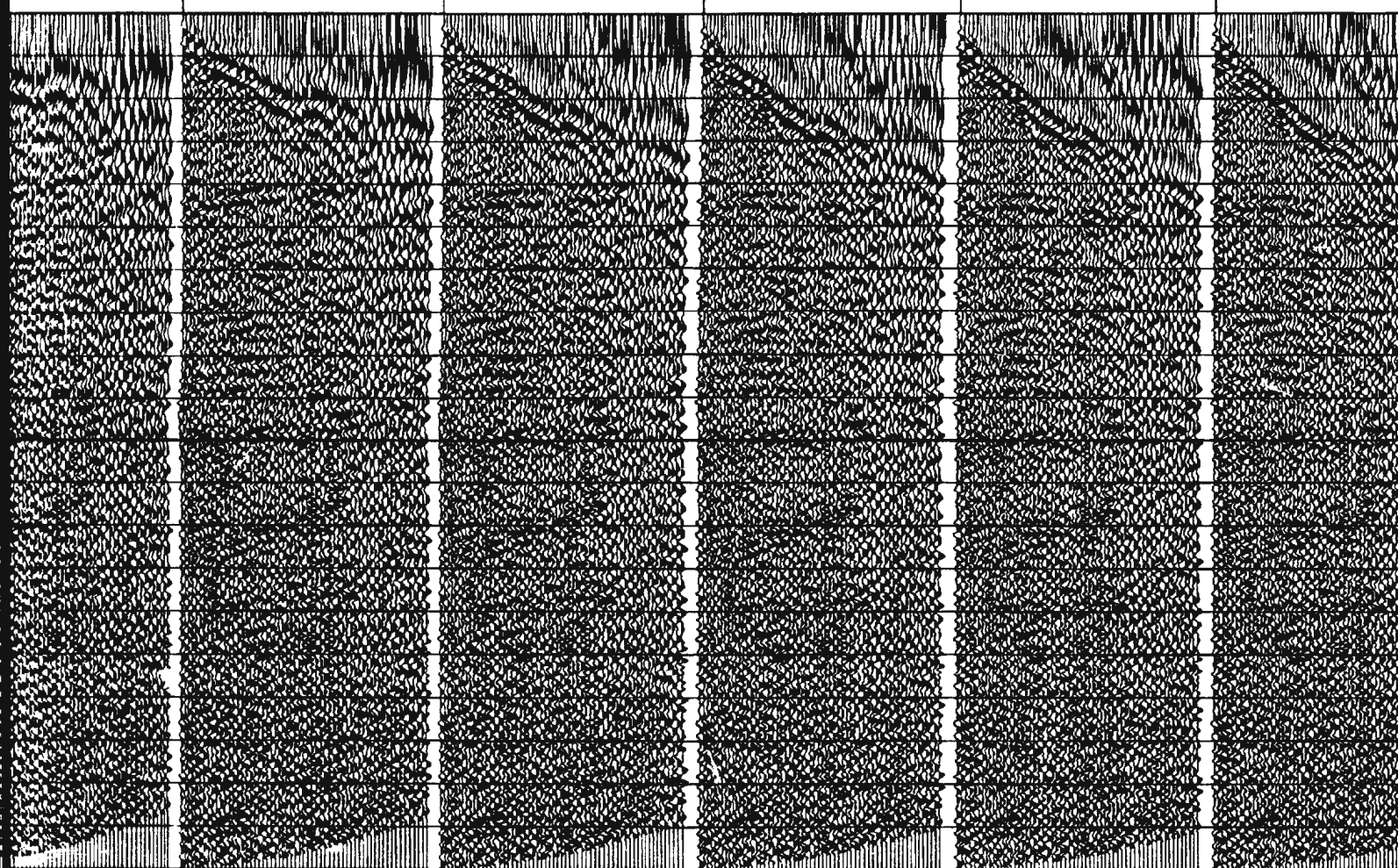
Figure 3.8. Constant velocity normal moved
CMP 630 before DMO correction.



out (CVNMO) of

[illegible]

4500.0

[illegible]

5300.0

5500.0

5700.0

VEL

0.0

0.1

0.2

0.3

0.4

0.5

0.6

0.7

0.8

0.9

1.0

1.1

1.2

1.3

1.4

1.5

1.6

1.7

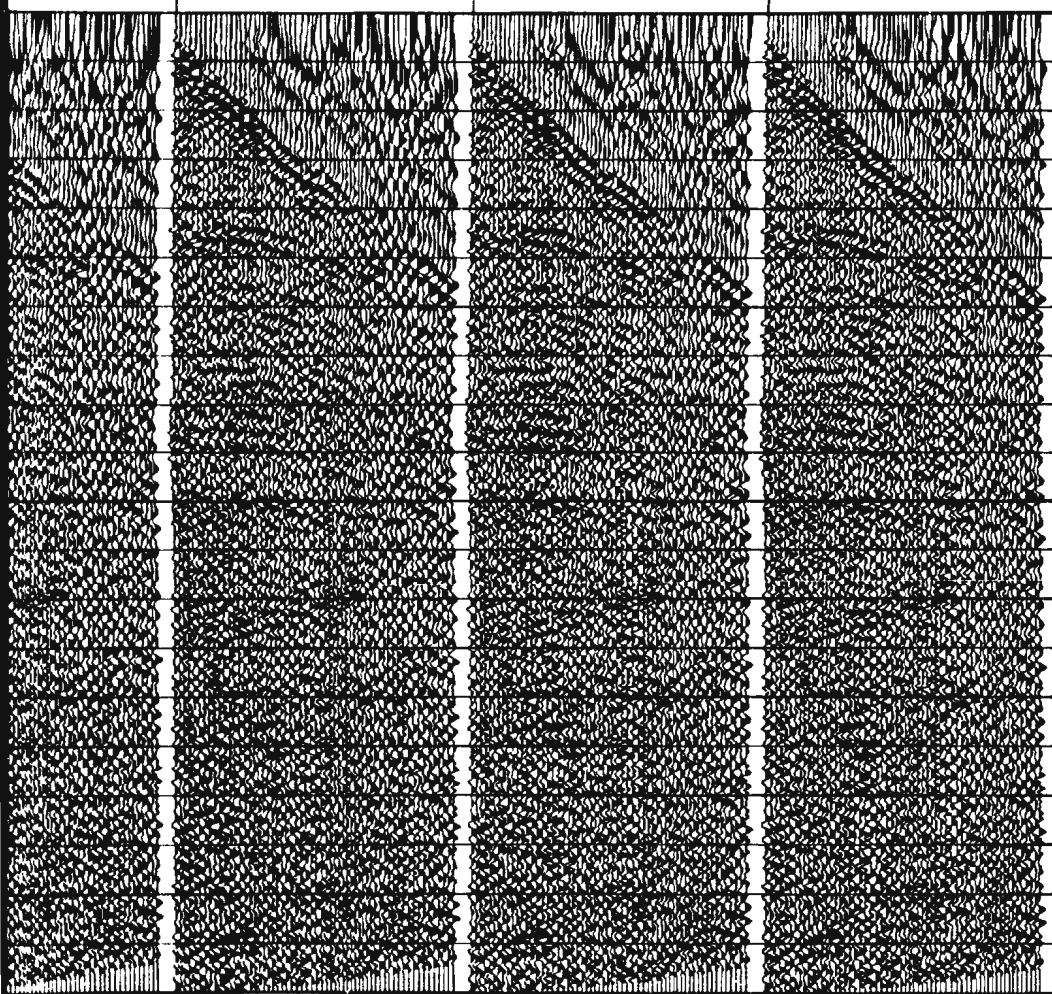
1.8

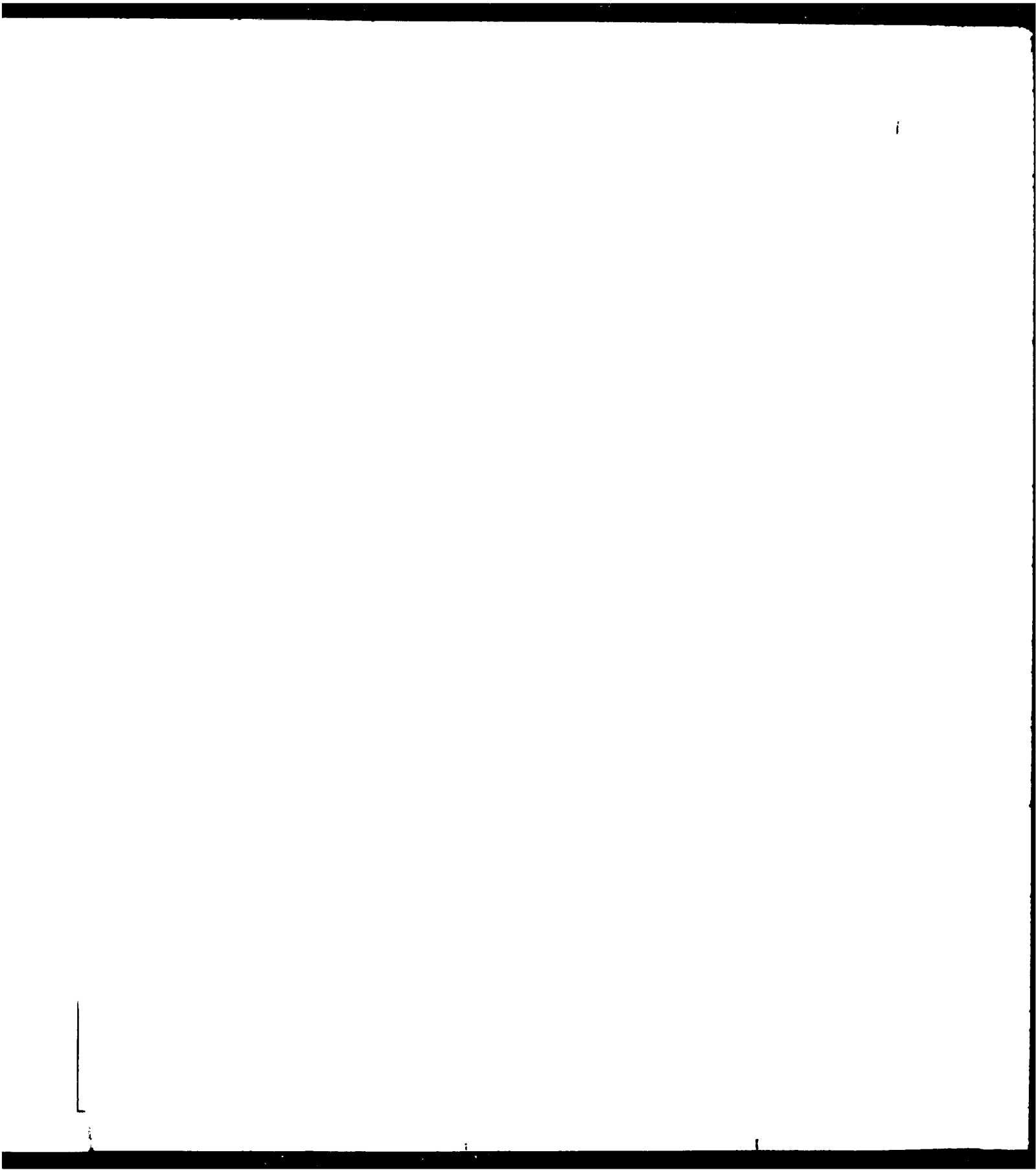
1.9

2.0

COP

RANGE





ROBINSONS RIVER LINE, 1989
CONSTANT VELOCITY STACK - VEL = 5500 M/S

CDP 0.0 0.1 0.2 0.3 0.4 0.5 0.6 0.7 0.8 0.9 1.0 1.1 1.2 1.3 1.4 1.5 1.6 1.7 1.8 1.9 2.0

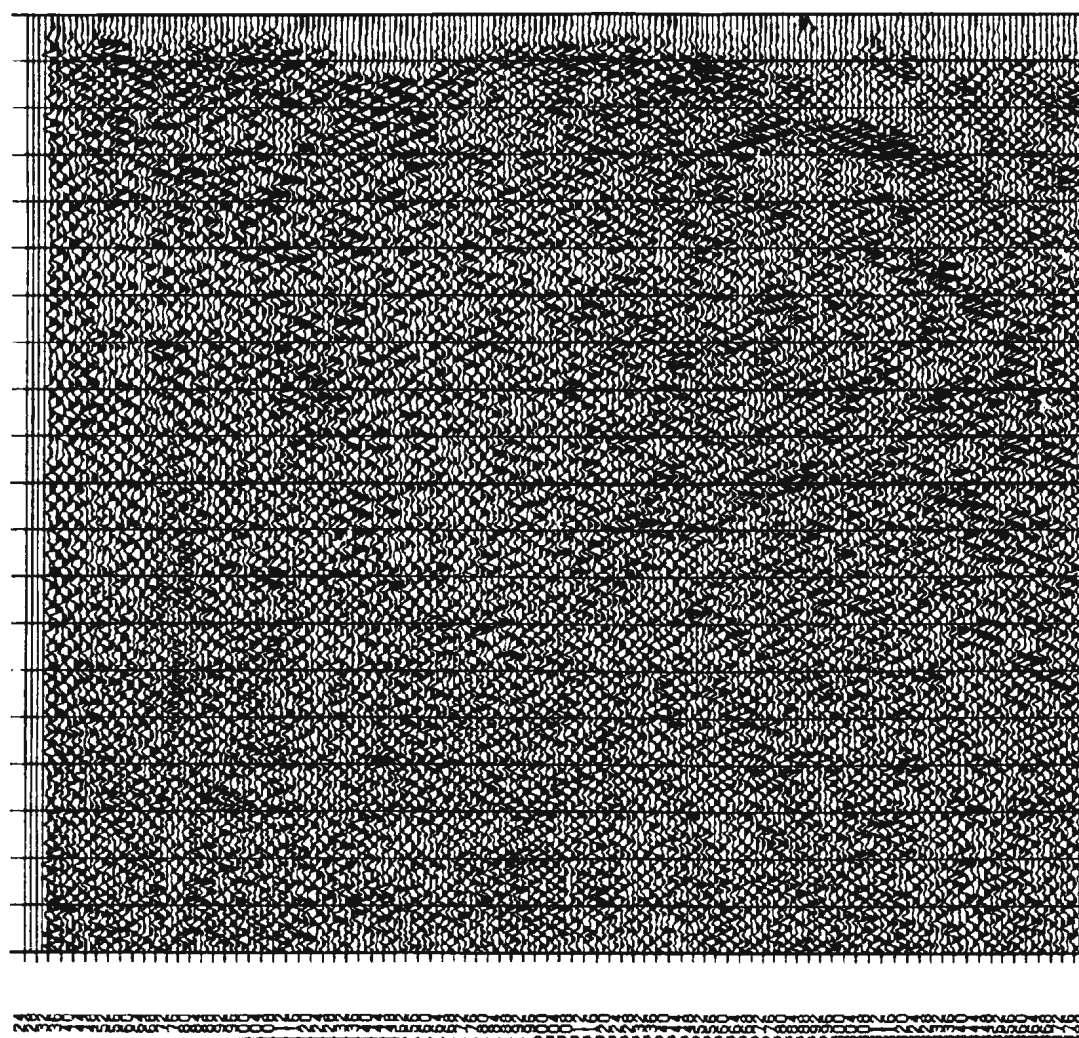
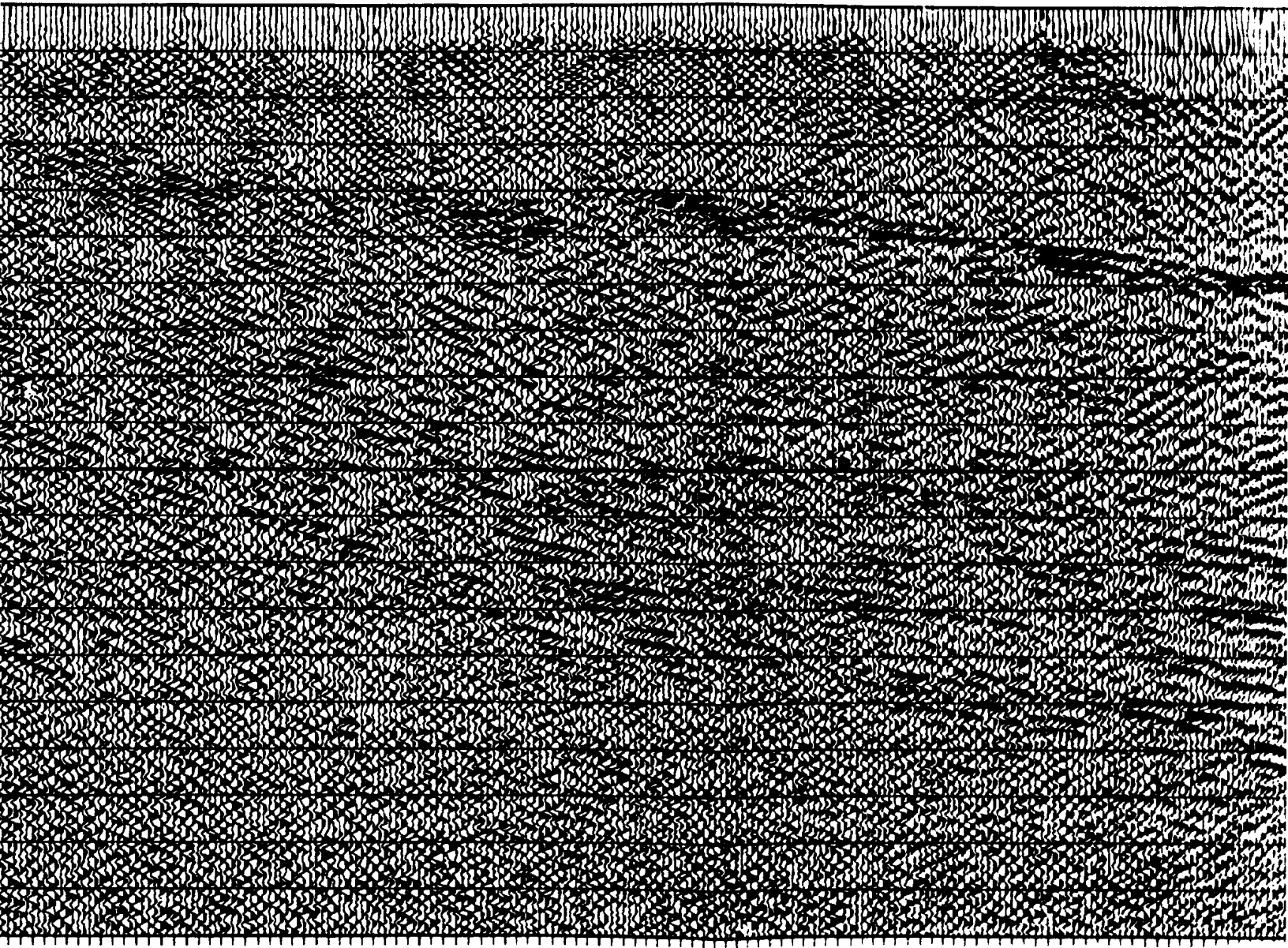
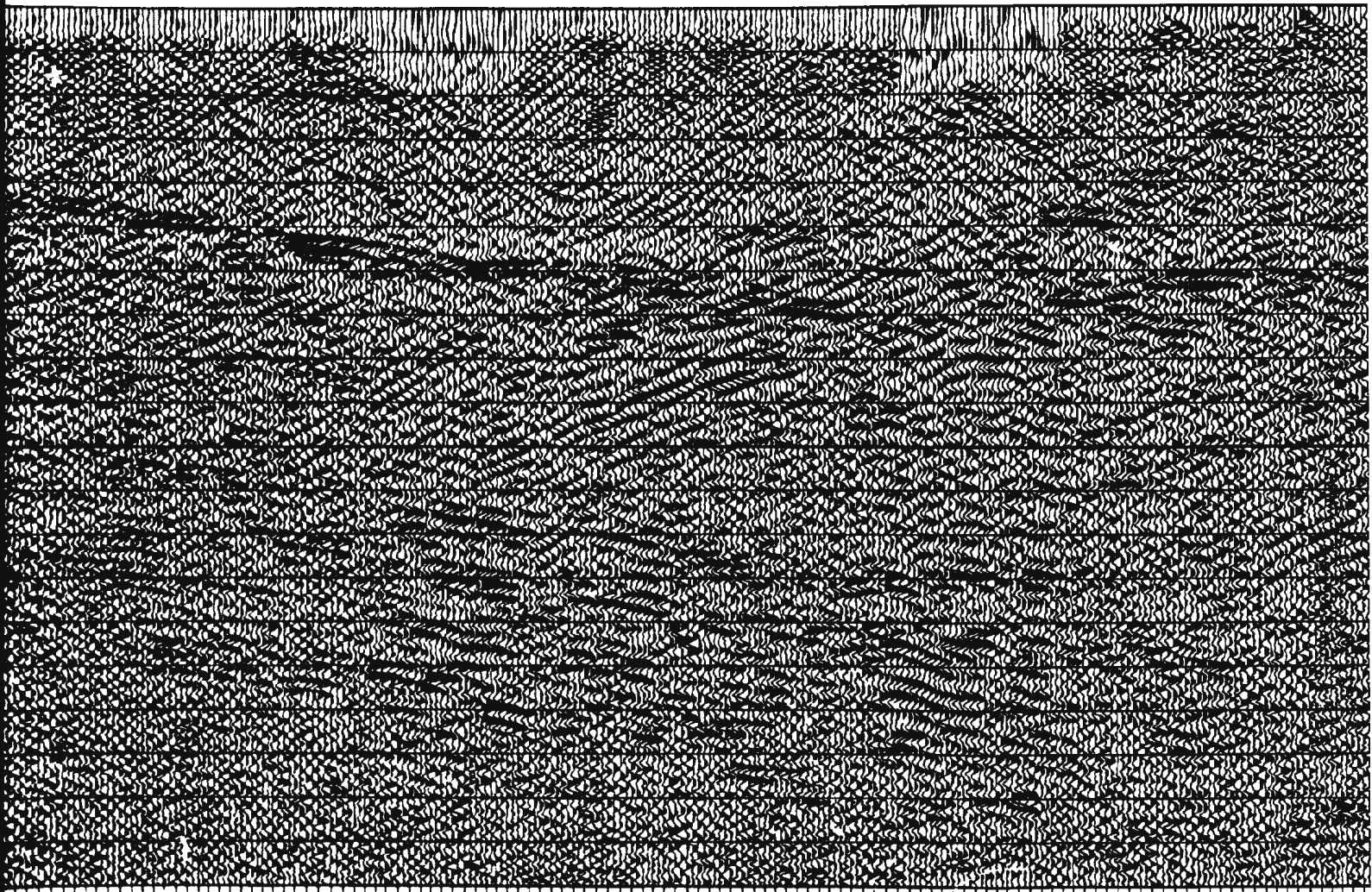
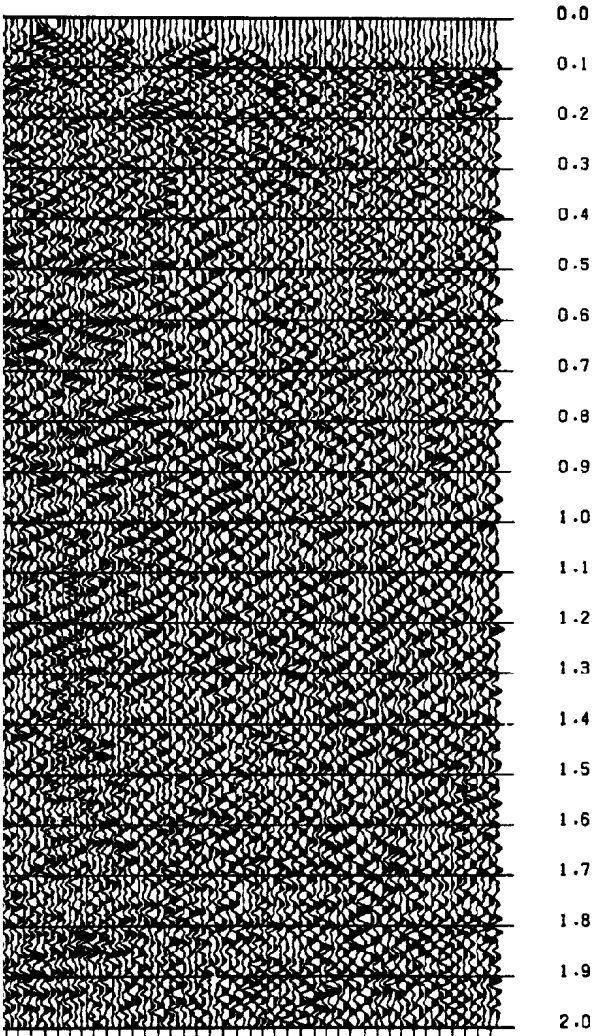


Figure 3.7 (t). Constant velocity stack of 5500 m/s.



17





CDP

CDP

ROBINSONS RIVER LINE, 1989
CONSTANT VELOCITY STACK - VEL = 5300 M/S

0.0
0.1
0.2
0.3
0.4
0.5
0.6
0.7
0.8
0.9
1.0
1.1
1.2
1.3
1.4
1.5
1.6
1.7
1.8
1.9
2.0

CDP

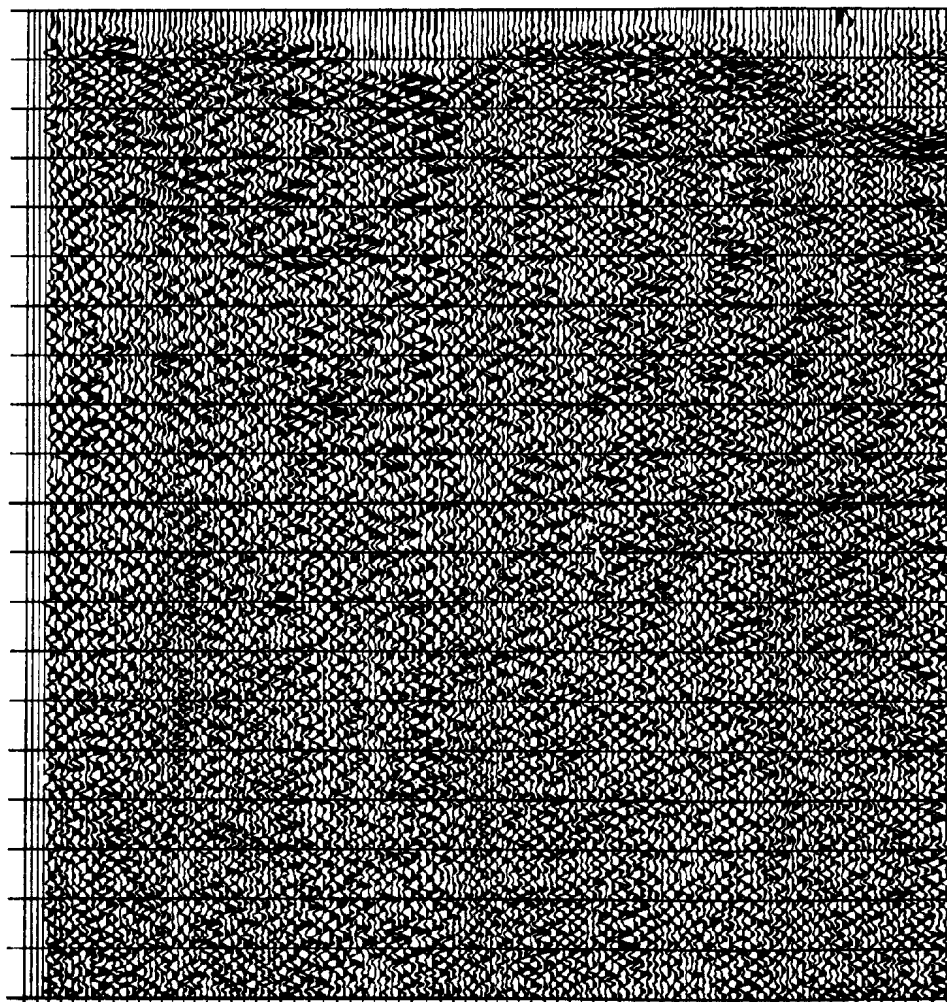
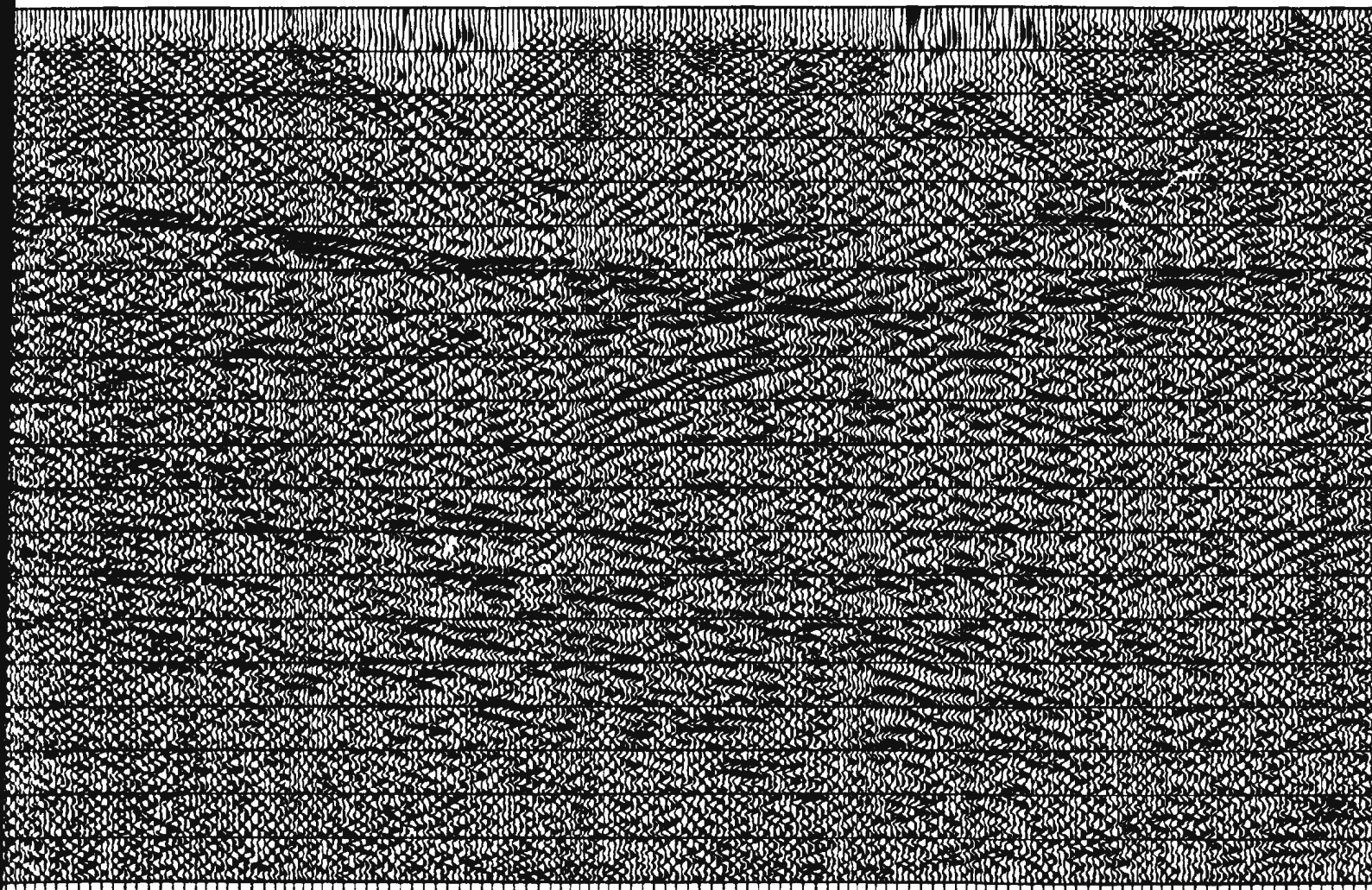


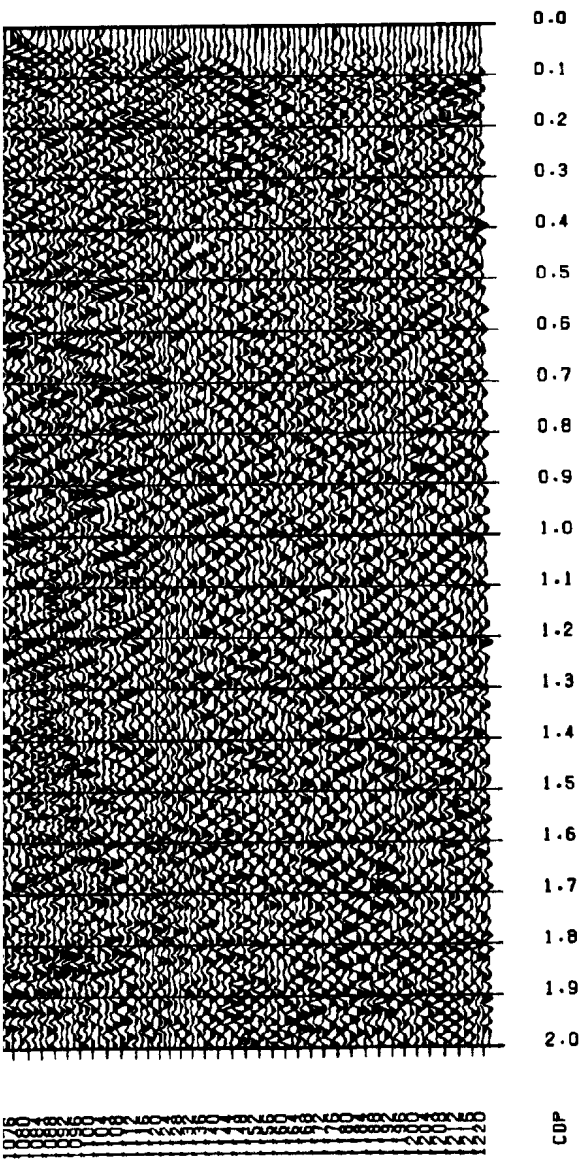
Figure 3.7 (s). Constant velocity

This image is a dense, black and white halftone pattern. It consists of a fine, regular grid of small dots or pixels, creating a textured, grainy appearance. The pattern is uniform across the entire frame, with no discernible figures, text, or other objects. It resembles a high-resolution scan of a textured surface or a heavily degraded digital image.

[illegible]

T





ROBINSONS RIVER LINE, 1989
CONSTANT VELOCITY STACK - VEL = 5100 M/S

0.0
0.1
0.2
0.3
0.4
0.5
0.6
0.7
0.8
0.9
1.0
1.1
1.2
1.3
1.4
1.5
1.6
1.7
1.8
1.9
2.0

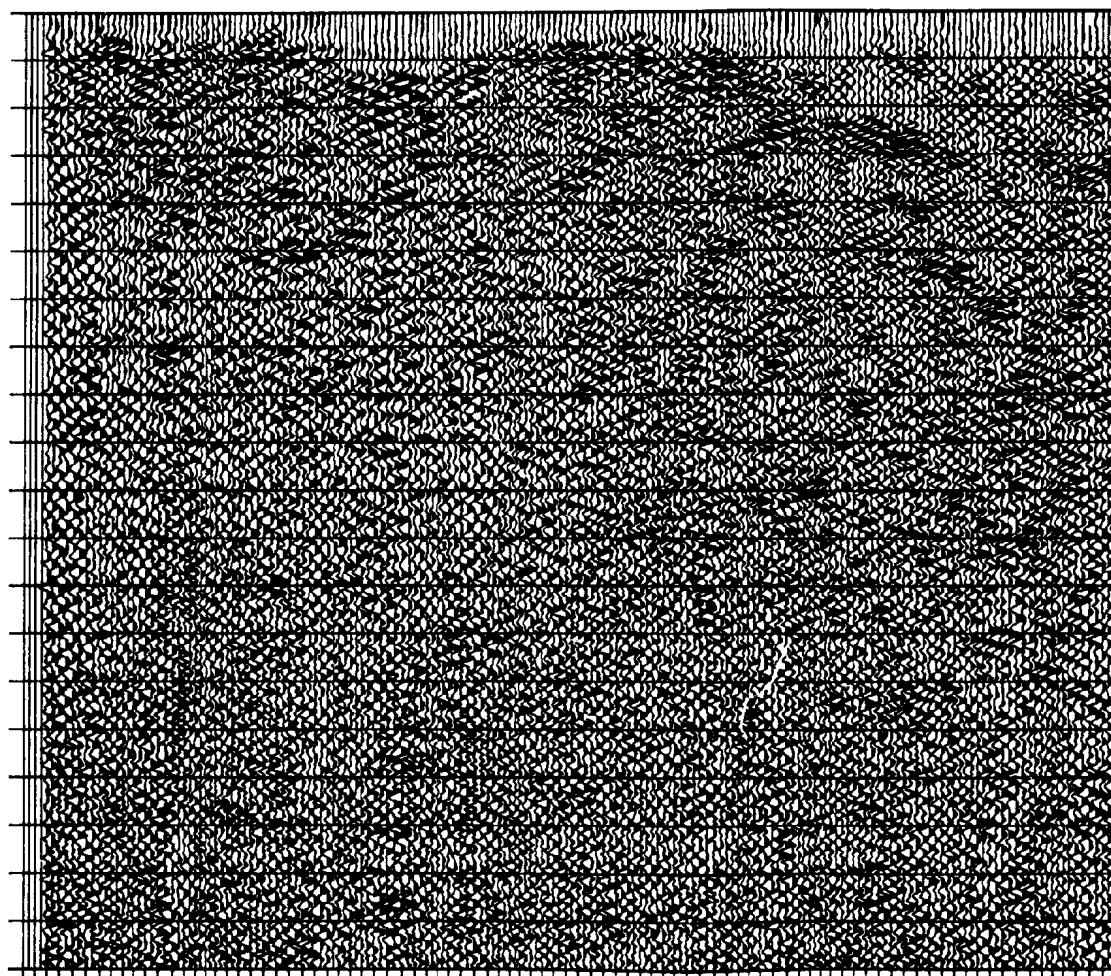
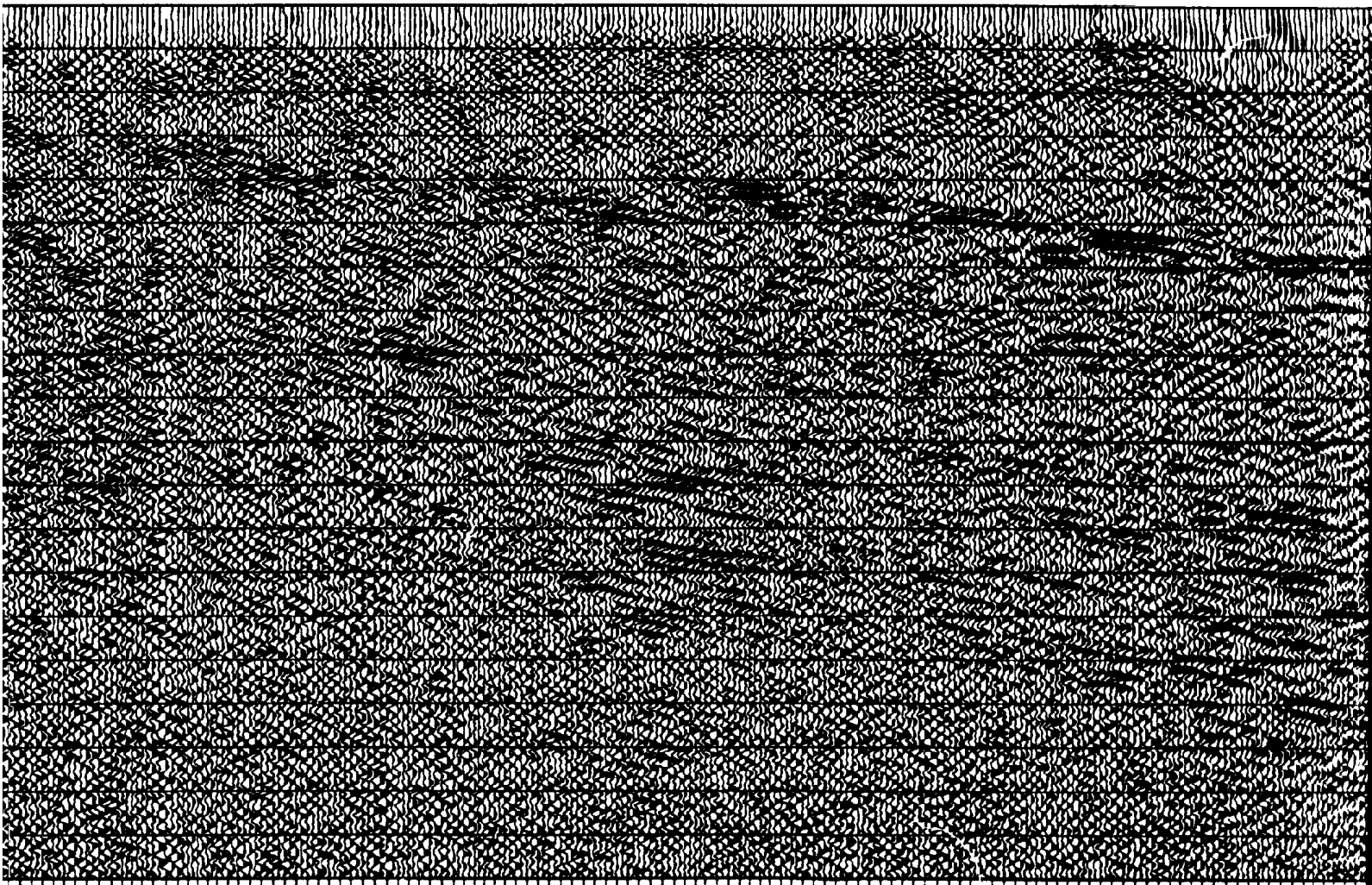
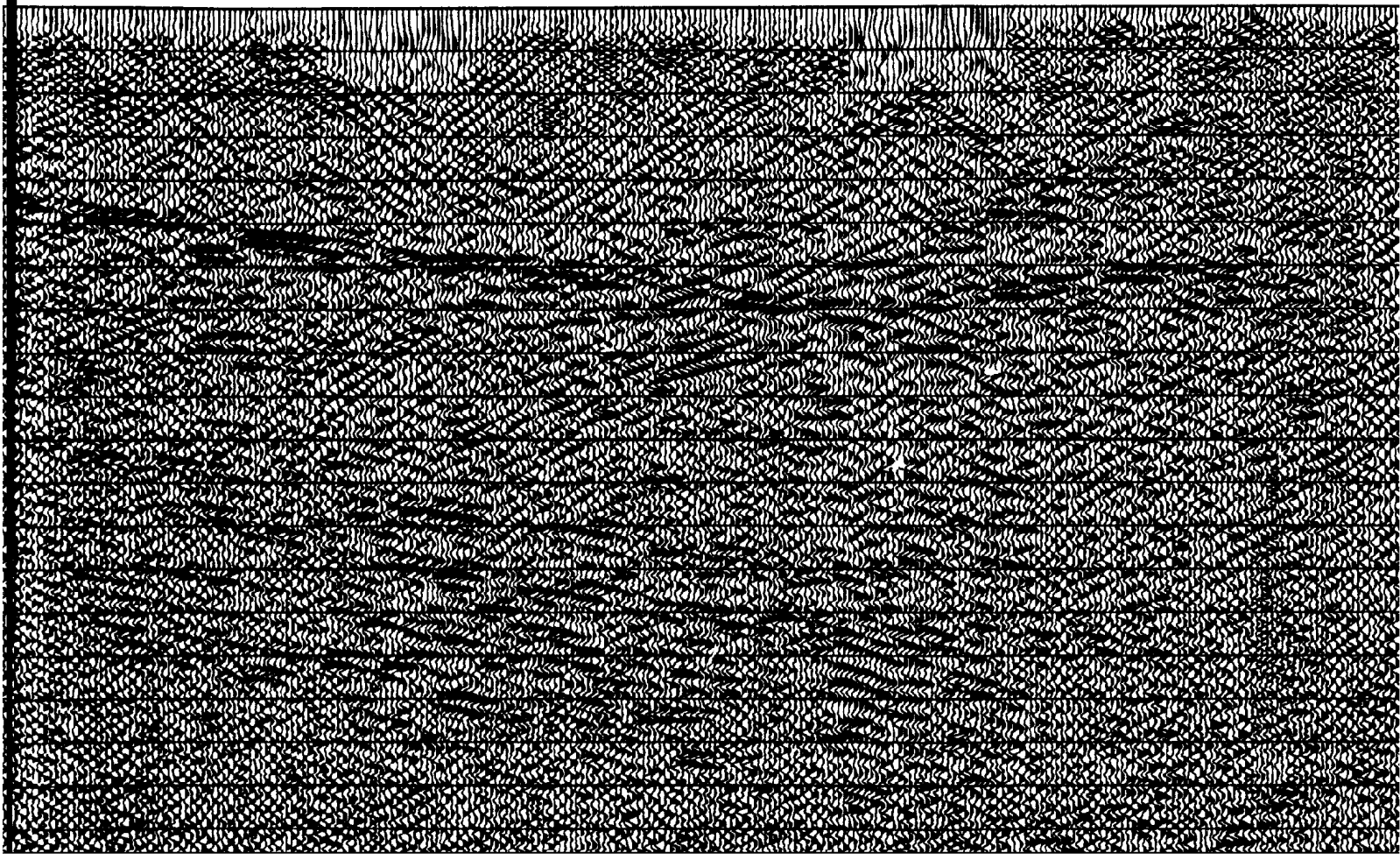


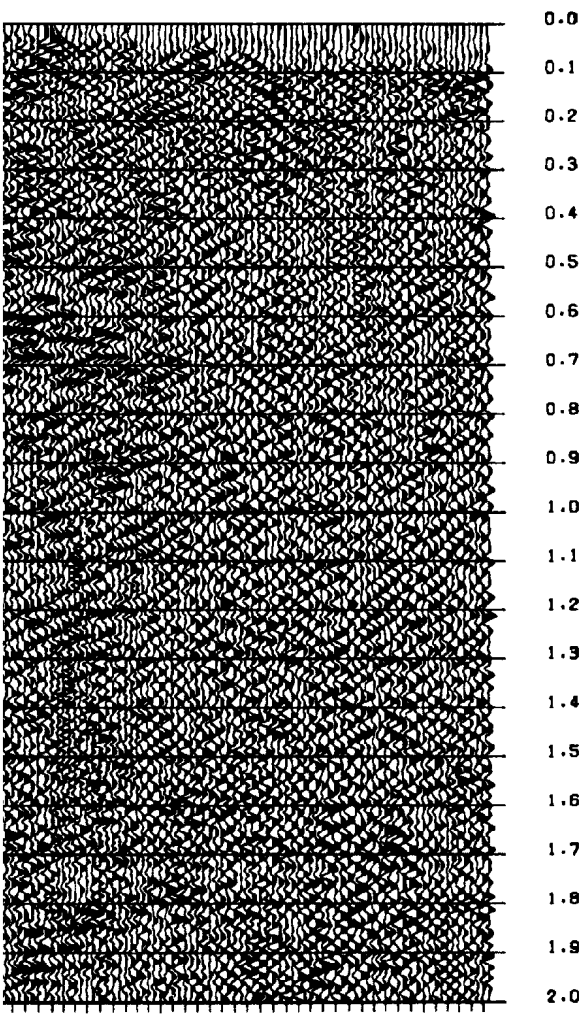
Figure 3.7 (r). Constant velocity stack of 5100

stack of 5100 m/s.



- T -





0.0
0.1
0.2
0.3
0.4
0.5
0.6
0.7
0.8
0.9
1.0
1.1
1.2
1.3
1.4
1.5
1.6
1.7
1.8
1.9
2.0

CDP

7
ROBINSONS RIVER LINE, 1989
CONSTANT VELOCITY STACK - VEL = 4900 M/S

0.0
0.1
0.2
0.3
0.4
0.5
0.6
0.7
0.8
0.9
1.0
1.1
1.2
1.3
1.4
1.5
1.6
1.7
1.8
1.9
2.0

CDP

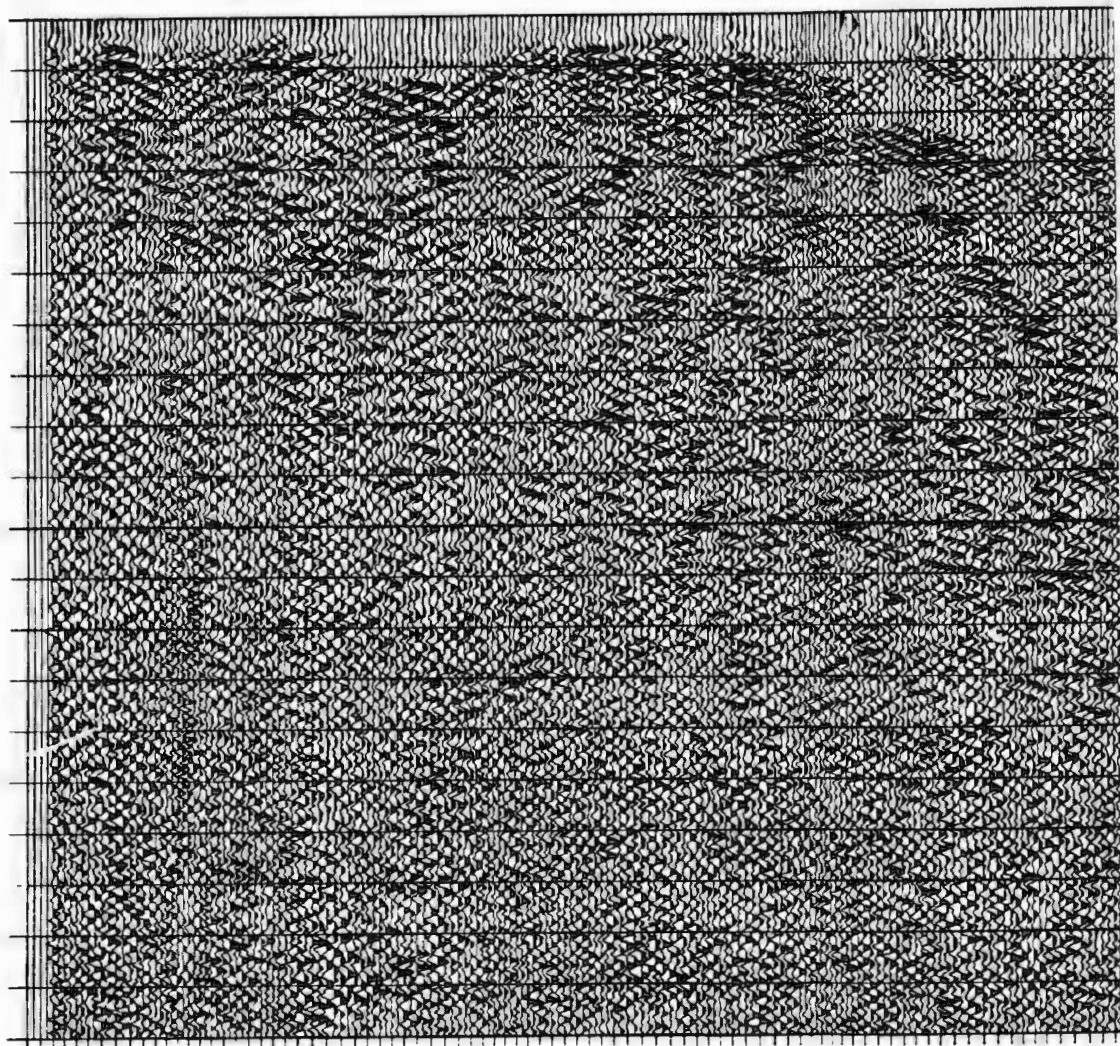
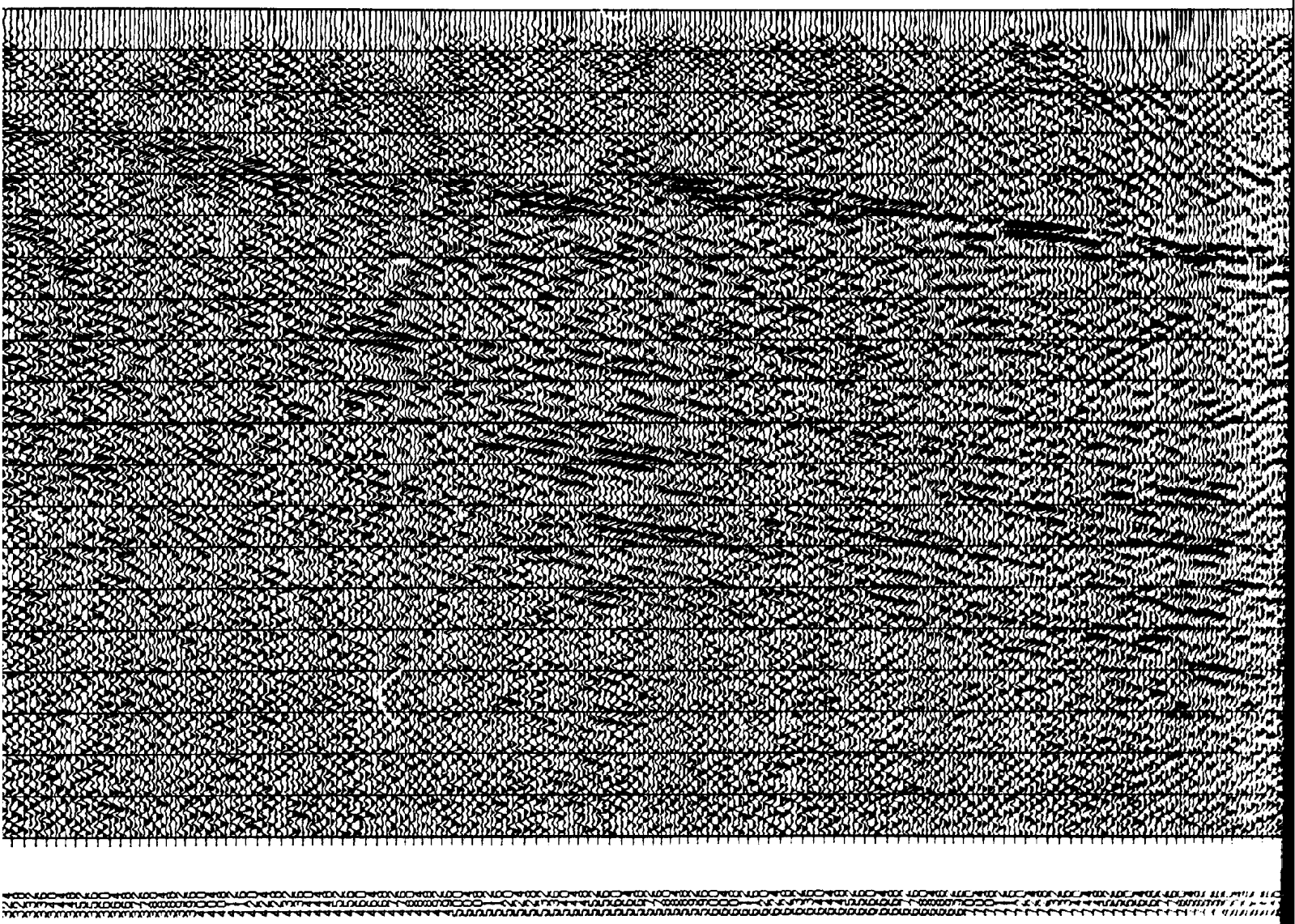


Figure 3.7 (q). Constant velocity stack events at depth start stacking at same

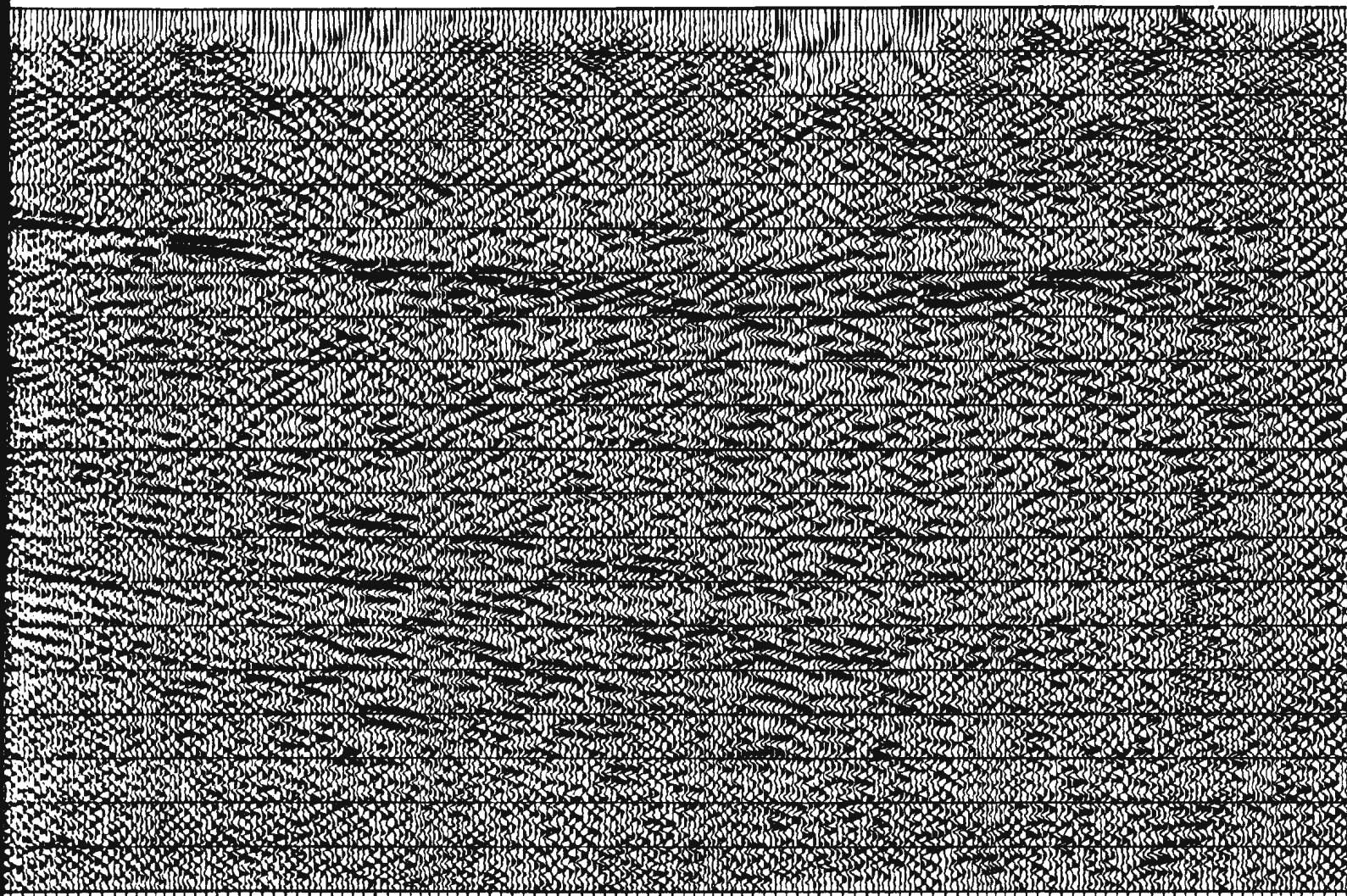
velocity stack of 4900 m/s. Note that
ing at same velocity.

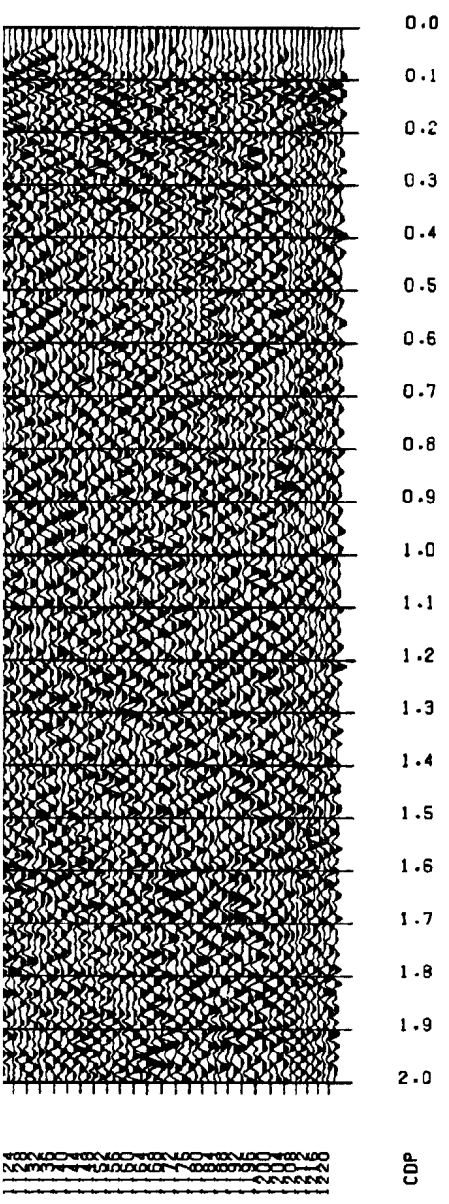


1

1

9





ROBINSONS RIVER LINE, 1989
CONSTANT VELOCITY STACK - VEL = 4700 M/S

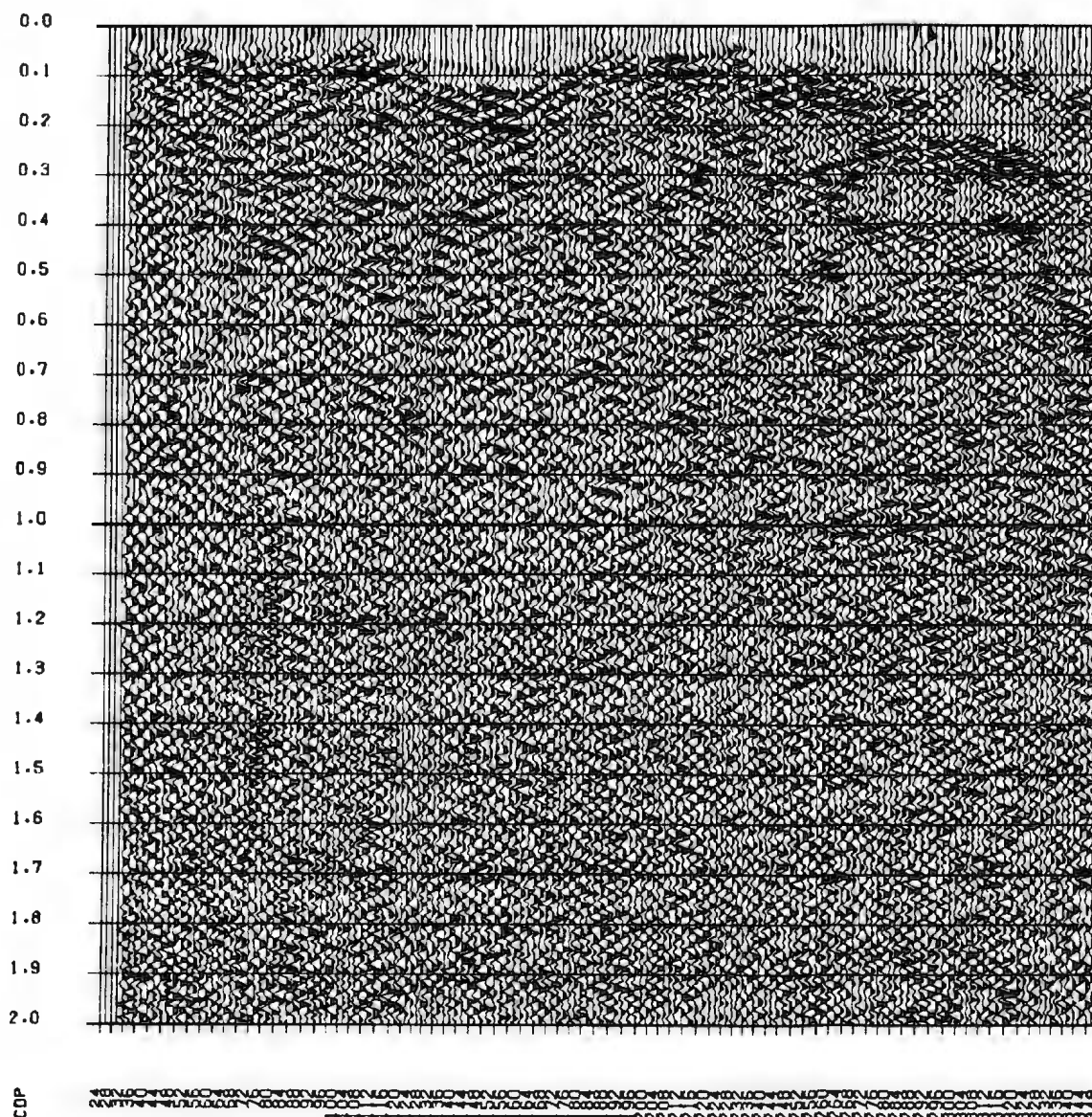
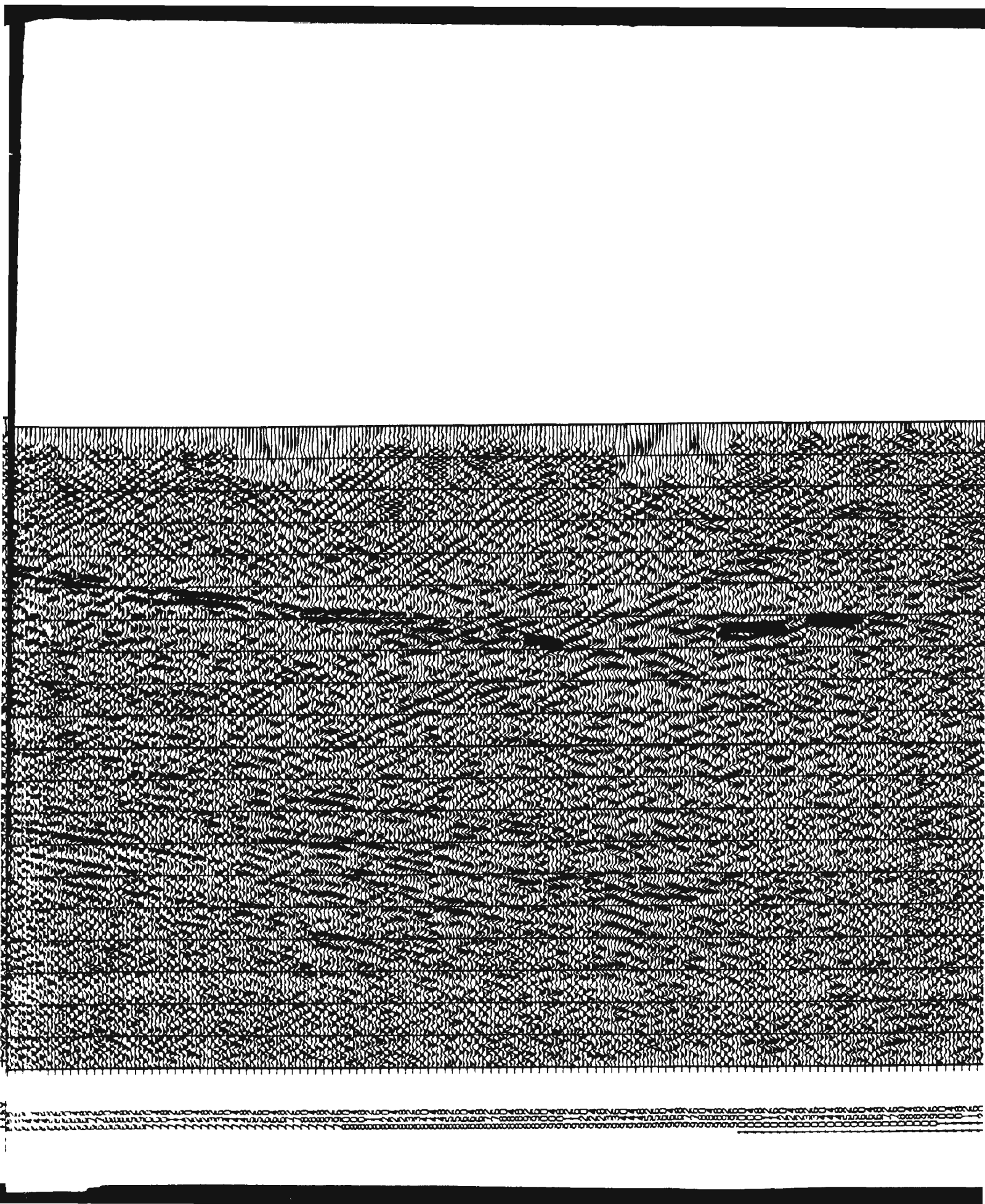


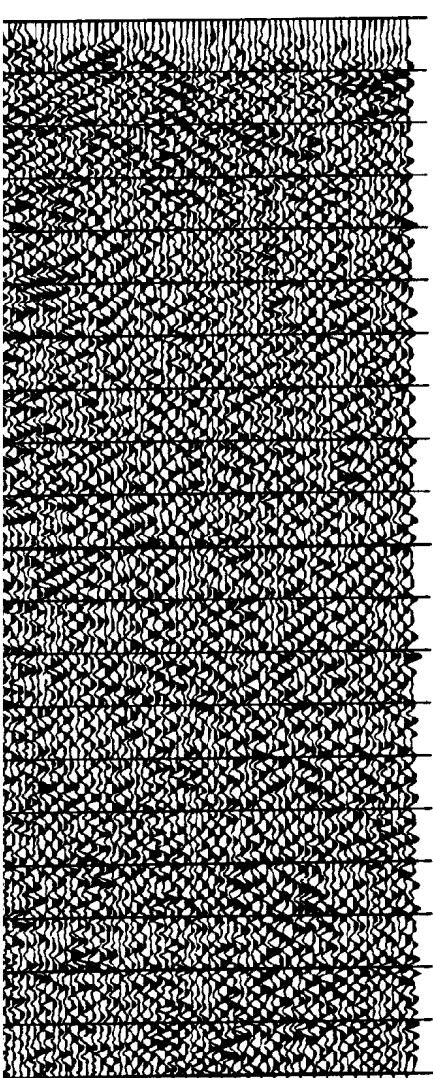
Figure 3.7 (p). Constant velocity stack indicate velocity picks.

This image shows a highly textured, black and white surface, likely the cover or endpaper of an old book. The texture is dense and irregular, with many small, dark, and light patches creating a mottled appearance. A vertical strip of lighter, more uniform material runs along the right edge, possibly indicating a hinge or a different section of the book's binding. The overall effect is one of age and wear.

[illegible]



- - -



0.0
0.1
0.2
0.3
0.4
0.5
0.6
0.7
0.8
0.9
1.0
1.1
1.2
1.3
1.4
1.5
1.6
1.7
1.8
1.9
2.0

CDP

ROBINSONS RIVER LINE, 1989
 CONSTANT VELOCITY STACK - VEL = 4500 M/S

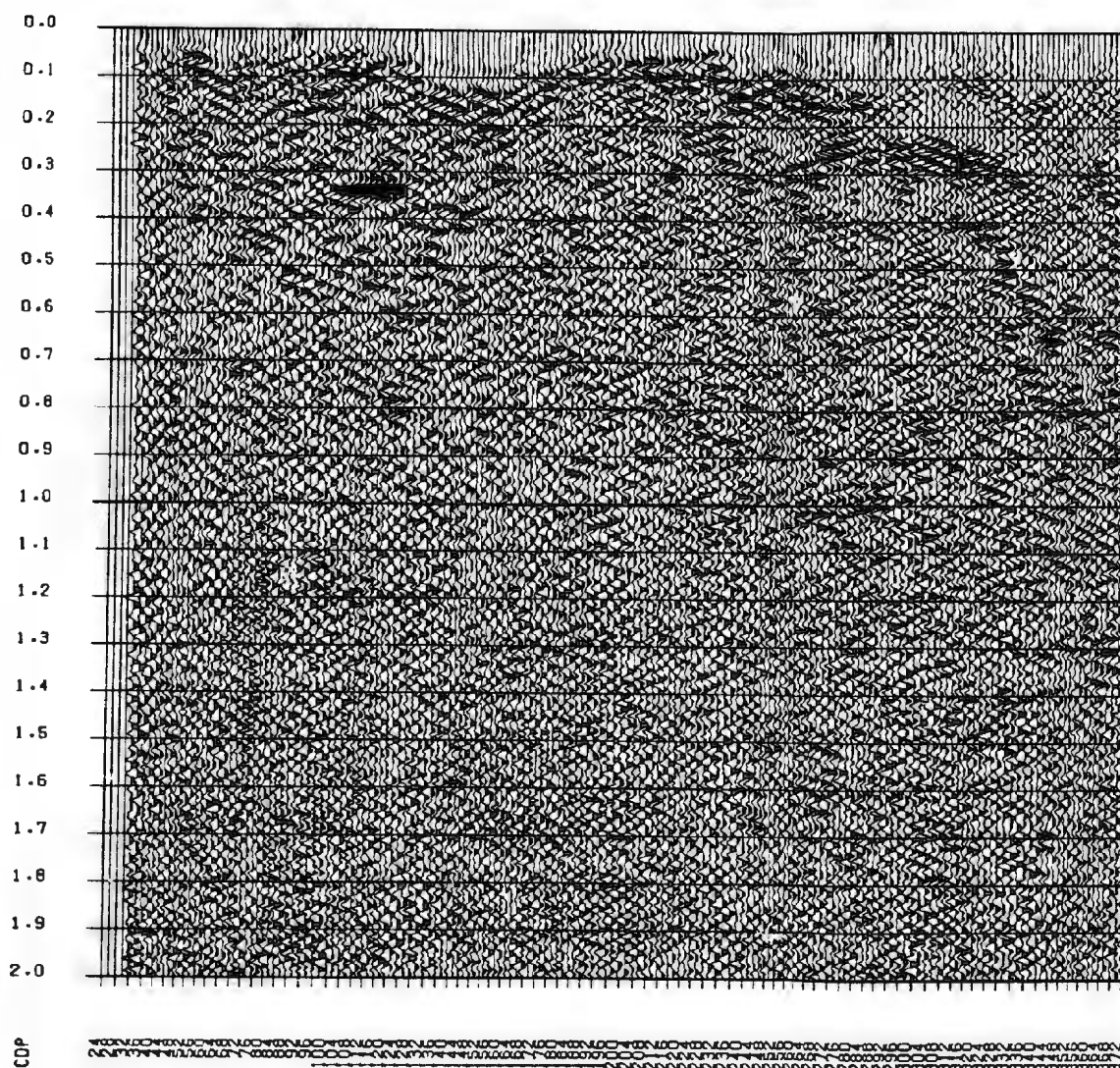
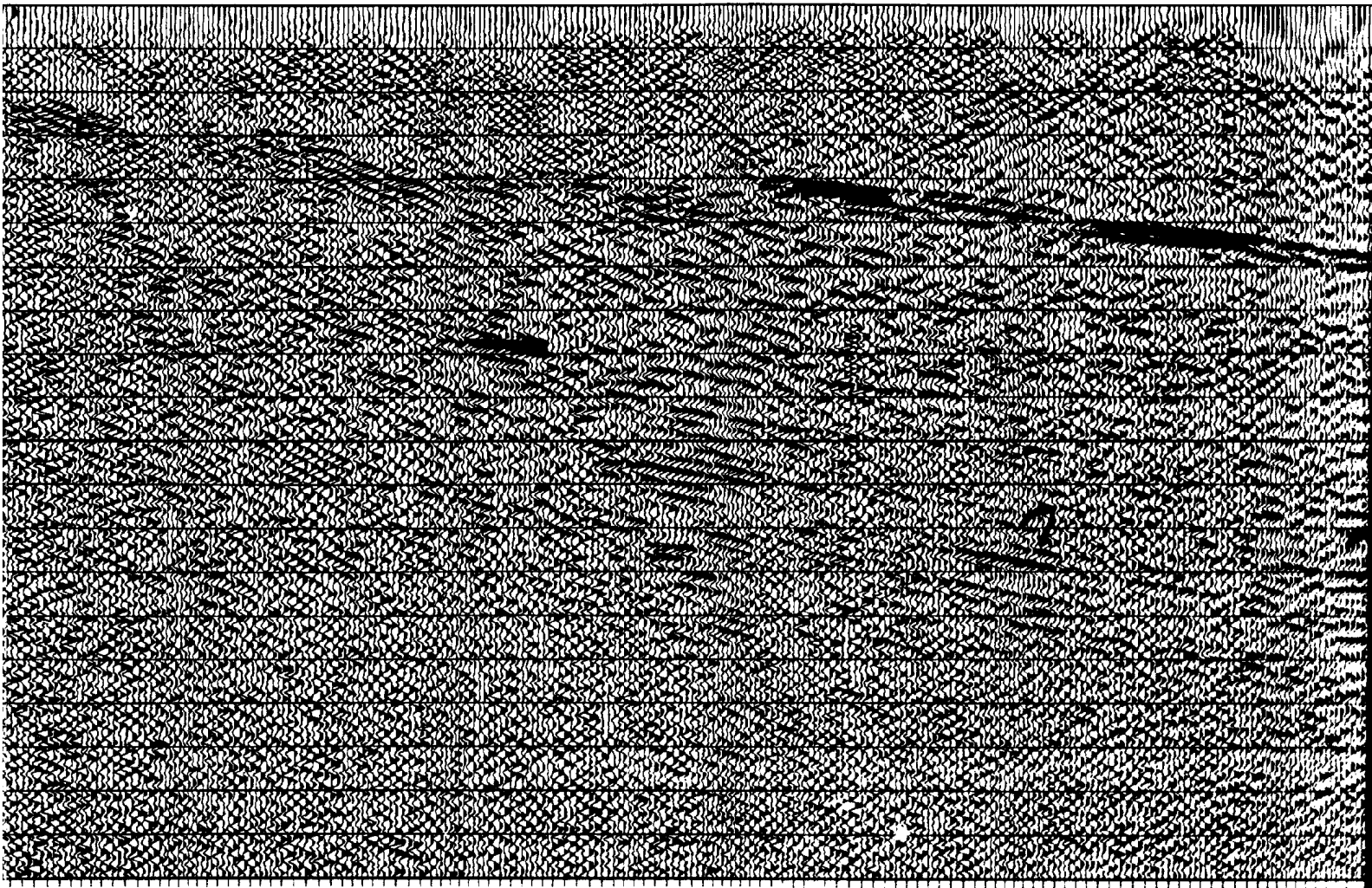
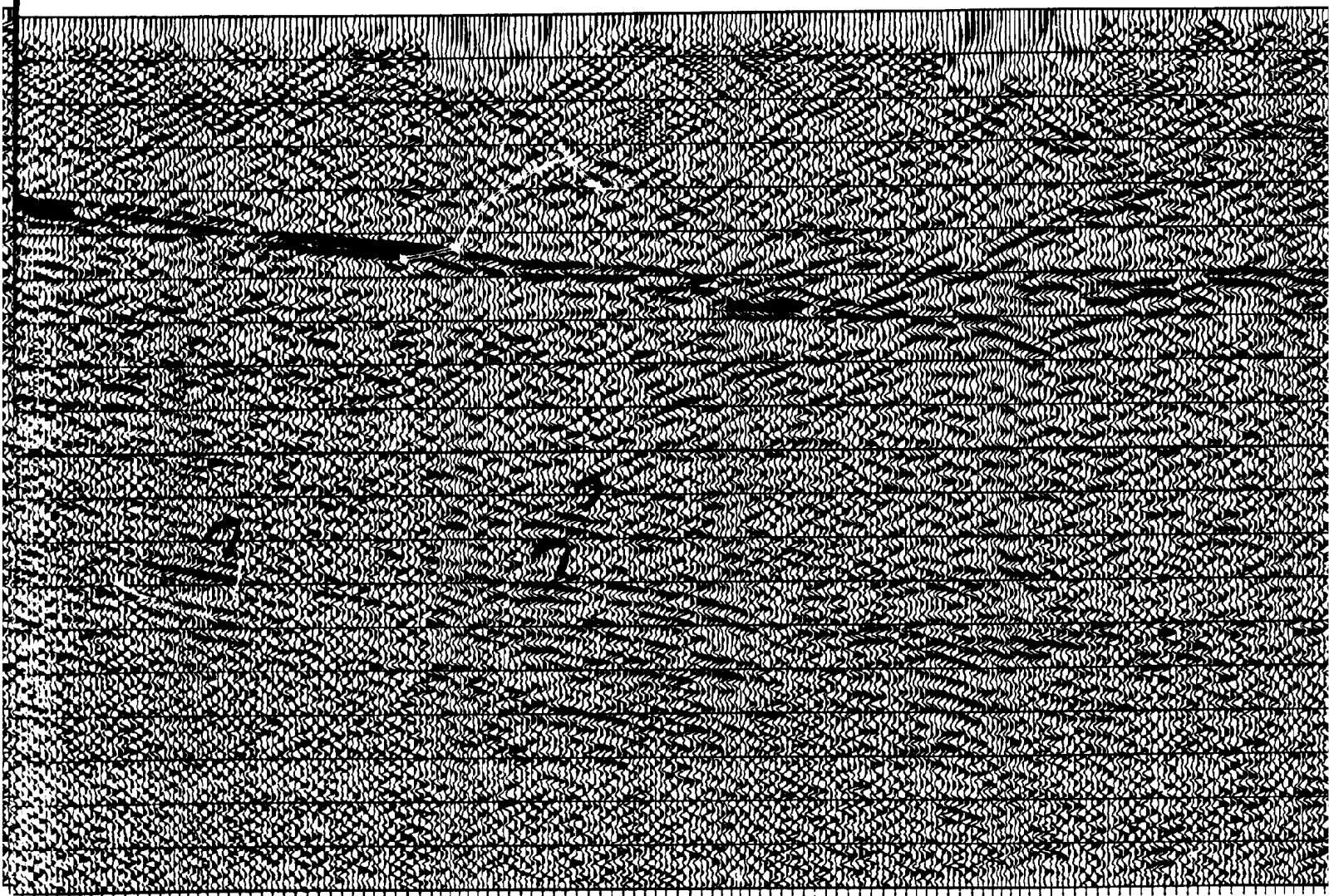


Figure 3.7 (o). Constant velocity stack. The marks indicate velocity picks.

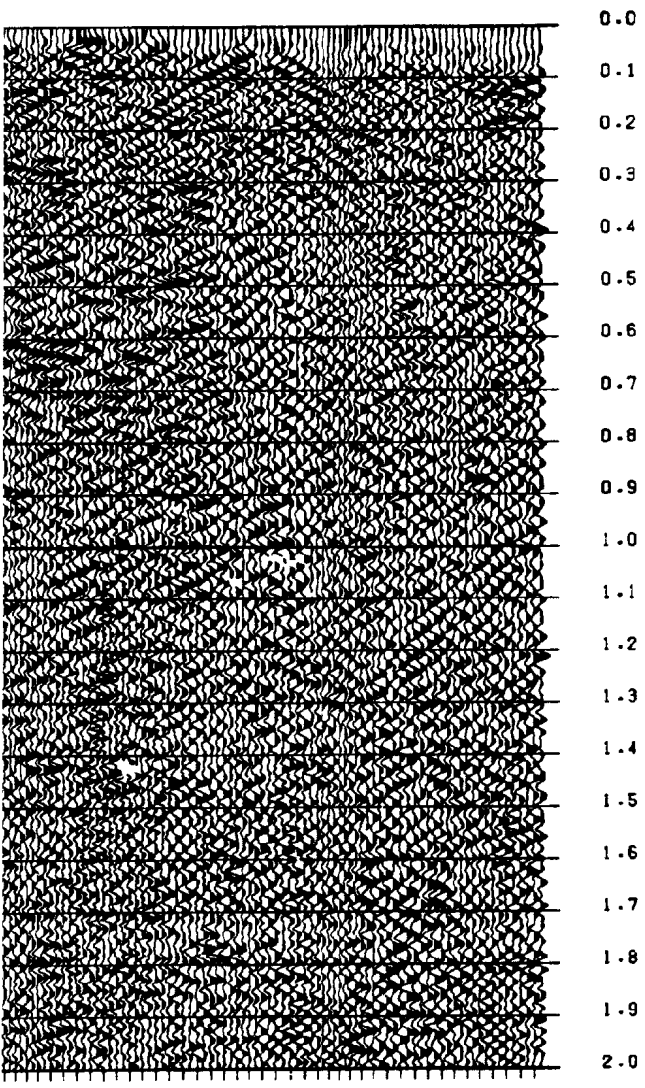
(o). Constant velocity stack of 4500 m/s, blue cate velocity picks.



1



2



0.0 0.1 0.2 0.3 0.4 0.5 0.6 0.7 0.8 0.9 1.0 1.1 1.2 1.3 1.4 1.5 1.6 1.7 1.8 1.9 2.0

0.0
0.1
0.2
0.3
0.4
0.5
0.6
0.7
0.8
0.9
1.0
1.1
1.2
1.3
1.4
1.5
1.6
1.7
1.8
1.9
2.0

0.0
0.1
0.2
0.3
0.4
0.5
0.6
0.7
0.8
0.9
1.0
1.1
1.2
1.3
1.4
1.5
1.6
1.7
1.8
1.9
2.0

ROBINSONS RIVER LINE, 1989
CONSTANT VELOCITY STACK - VEL = 4300 M/S

0.0
0.1
0.2
0.3
0.4
0.5
0.6
0.7
0.8
0.9
1.0
1.1
1.2
1.3
1.4
1.5
1.6
1.7
1.8
1.9
2.0

CDP

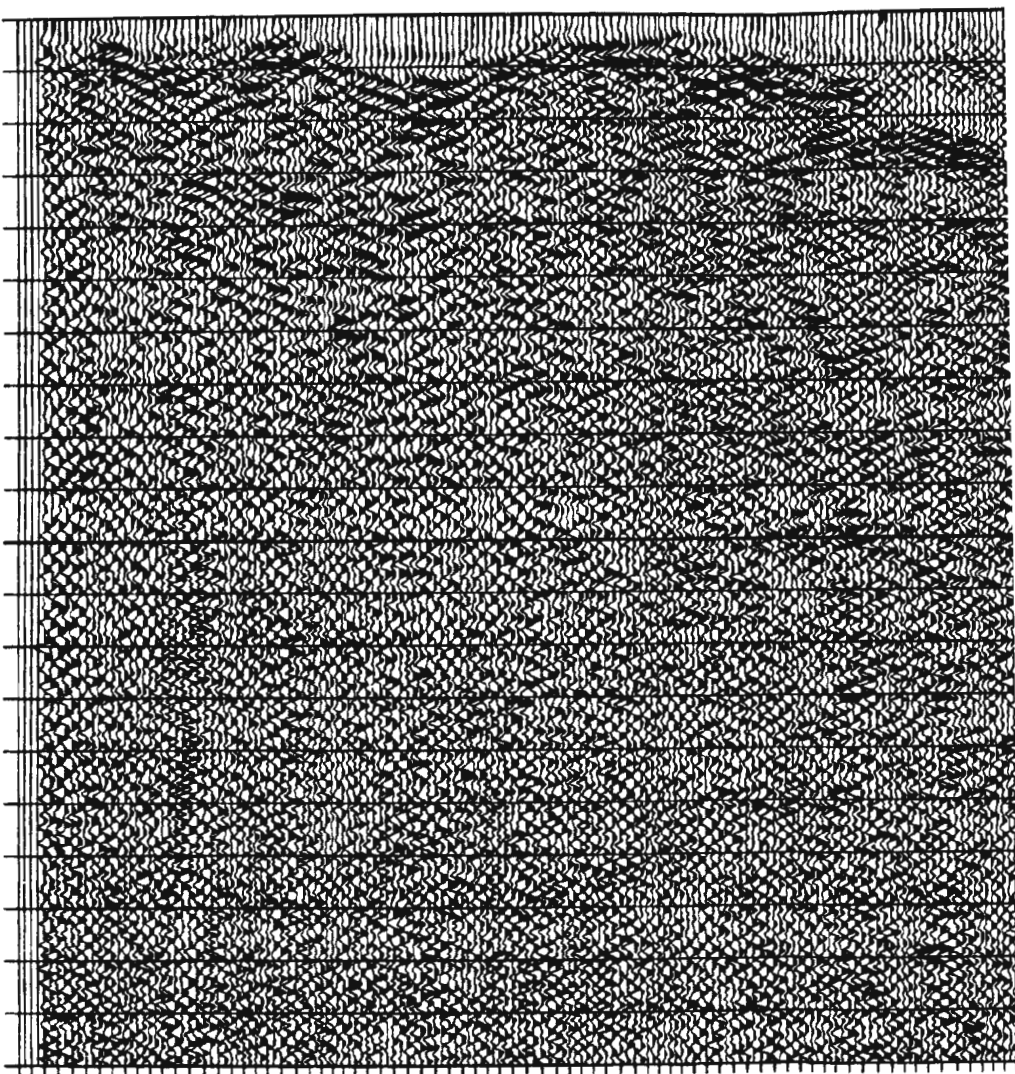
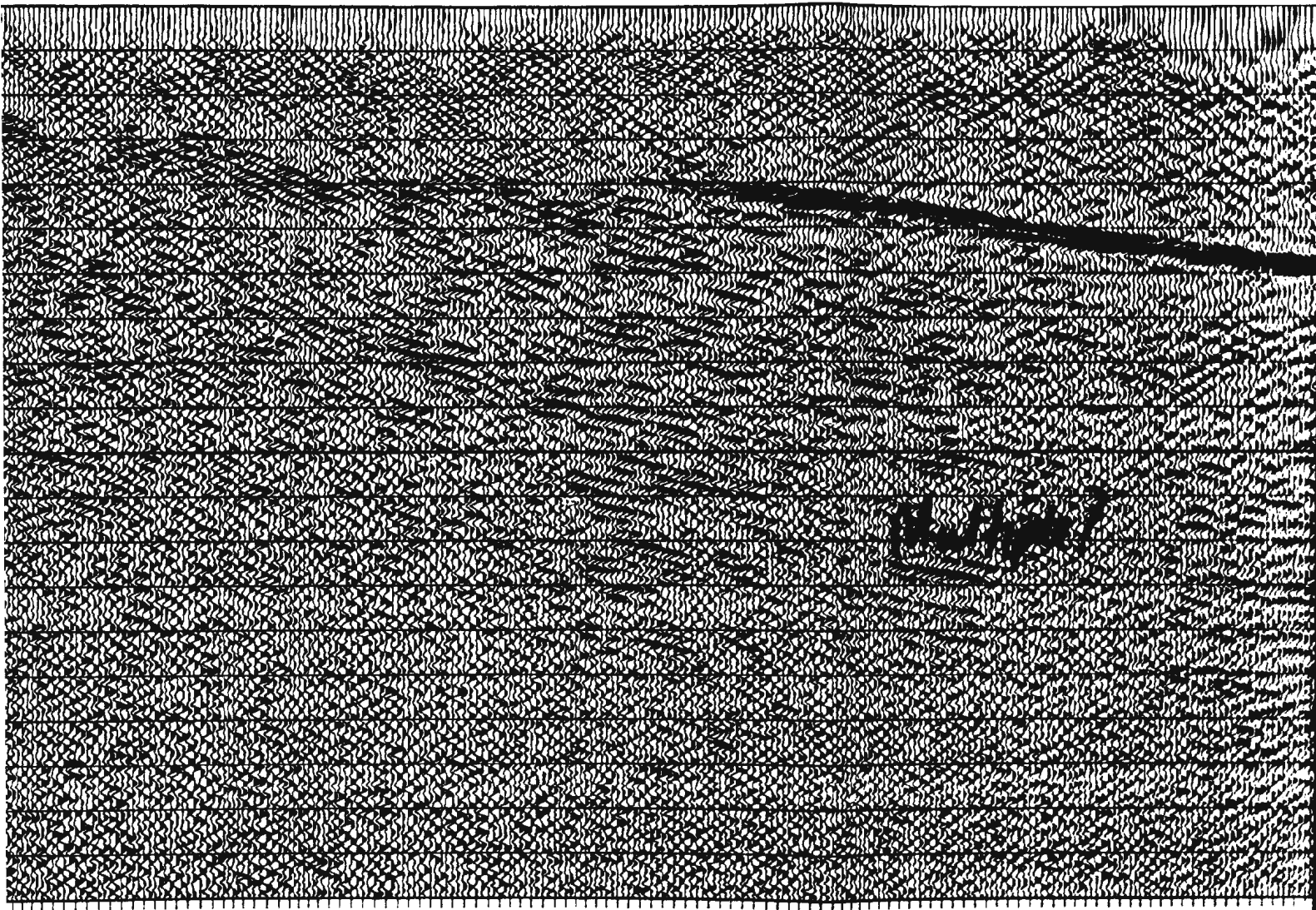


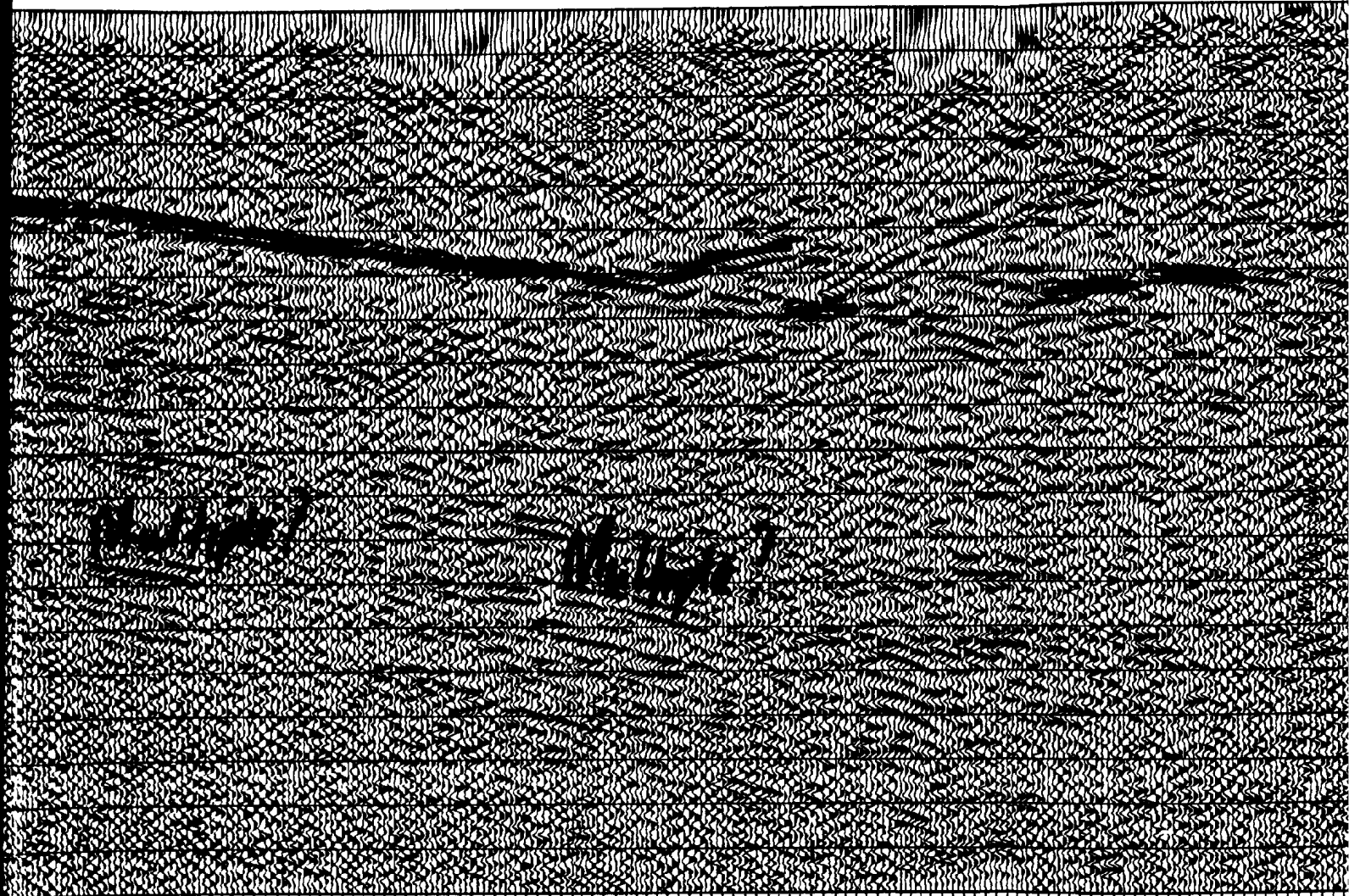
Figure 3.7 (n). Constant vel
marks indicate velocity pic
multiples at CMPs 800 to 9

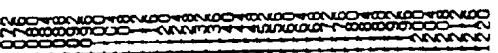
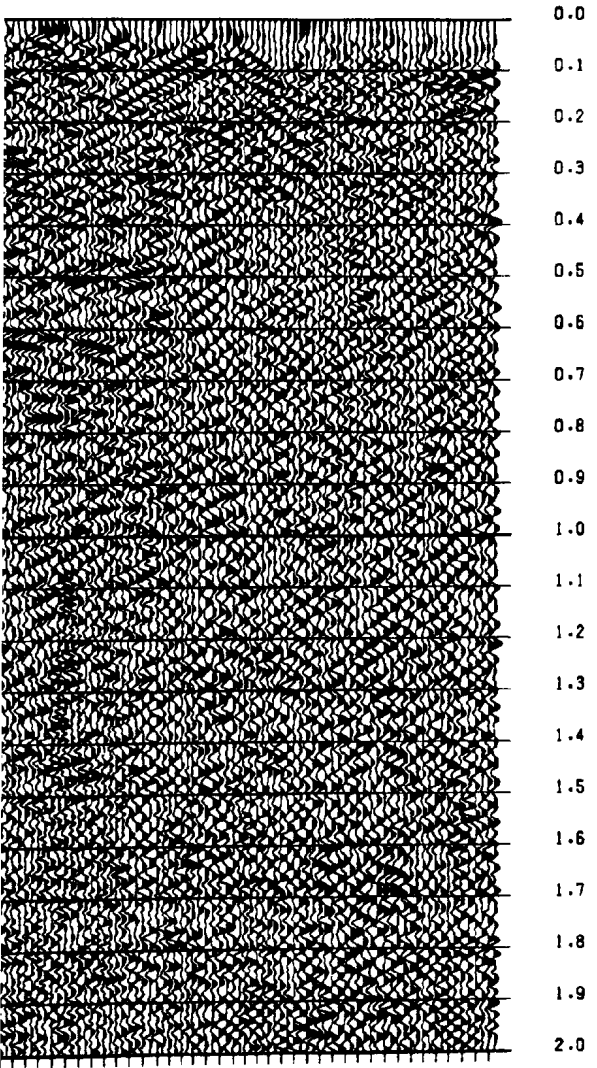
velocity stack of 4300 m/s, blue
picks. Notice the likelihood of
900, TWT 1.3 s.



0 100 200 300 400 500 600 700 800 900 1000 1100 1200 1300 1400 1500 1600 1700 1800 1900 2000 2100 2200 2300 2400 2500 2600 2700 2800 2900 3000 3100 3200 3300 3400 3500 3600 3700 3800 3900 4000 4100 4200 4300 4400 4500 4600 4700 4800 4900 5000 5100 5200 5300 5400 5500 5600 5700 5800 5900 6000 6100 6200 6300 6400 6500 6600 6700 6800 6900 7000 7100 7200 7300 7400 7500 7600 7700 7800 7900 8000 8100 8200 8300 8400 8500 8600 8700 8800 8900 9000 9100 9200 9300 9400 9500 9600 9700 9800 9900 10000

1





CDP

ROBINSONS RIVER LINE, 1989
CONSTANT VELOCITY STACK - VEL = 4100 M/S

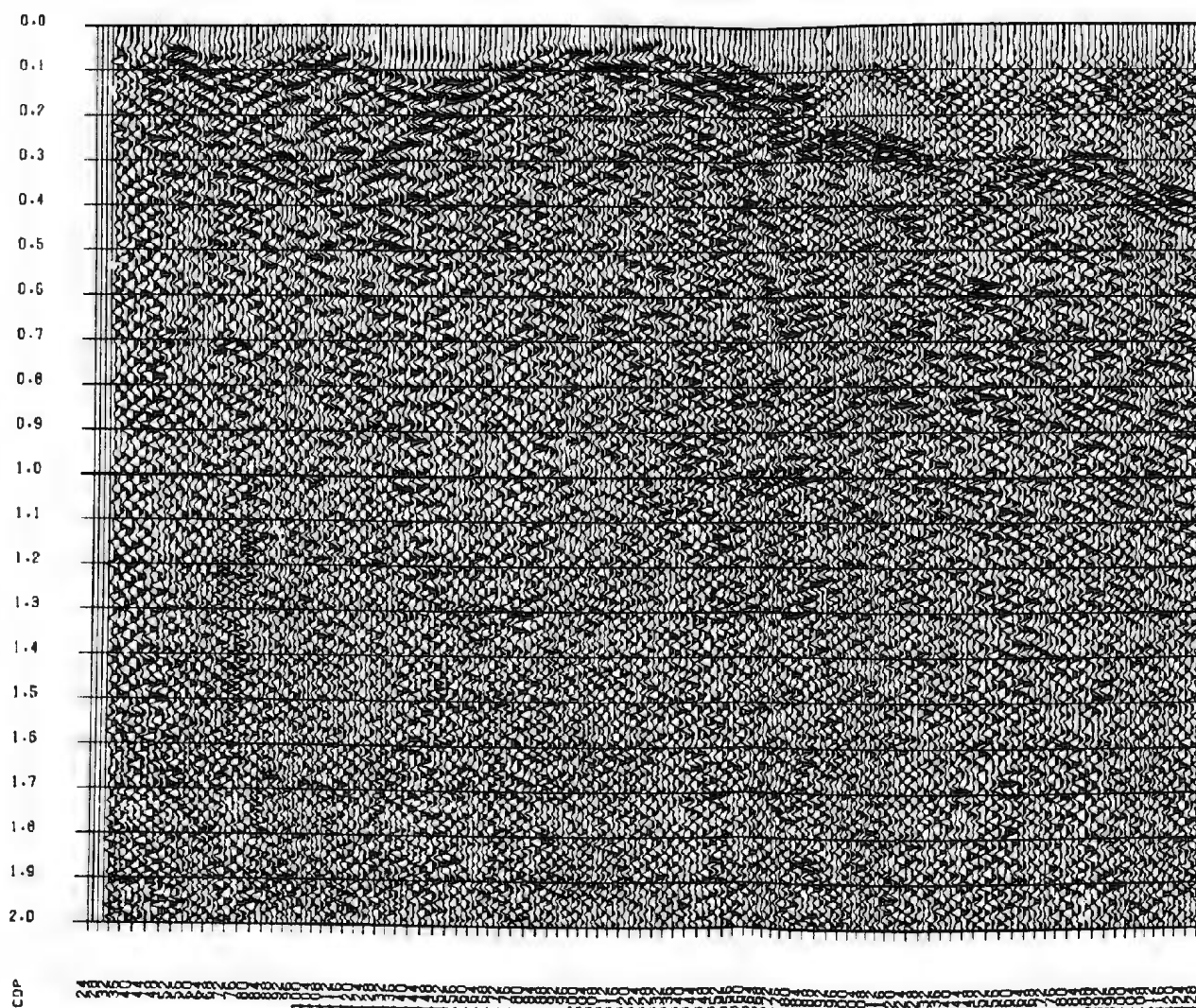
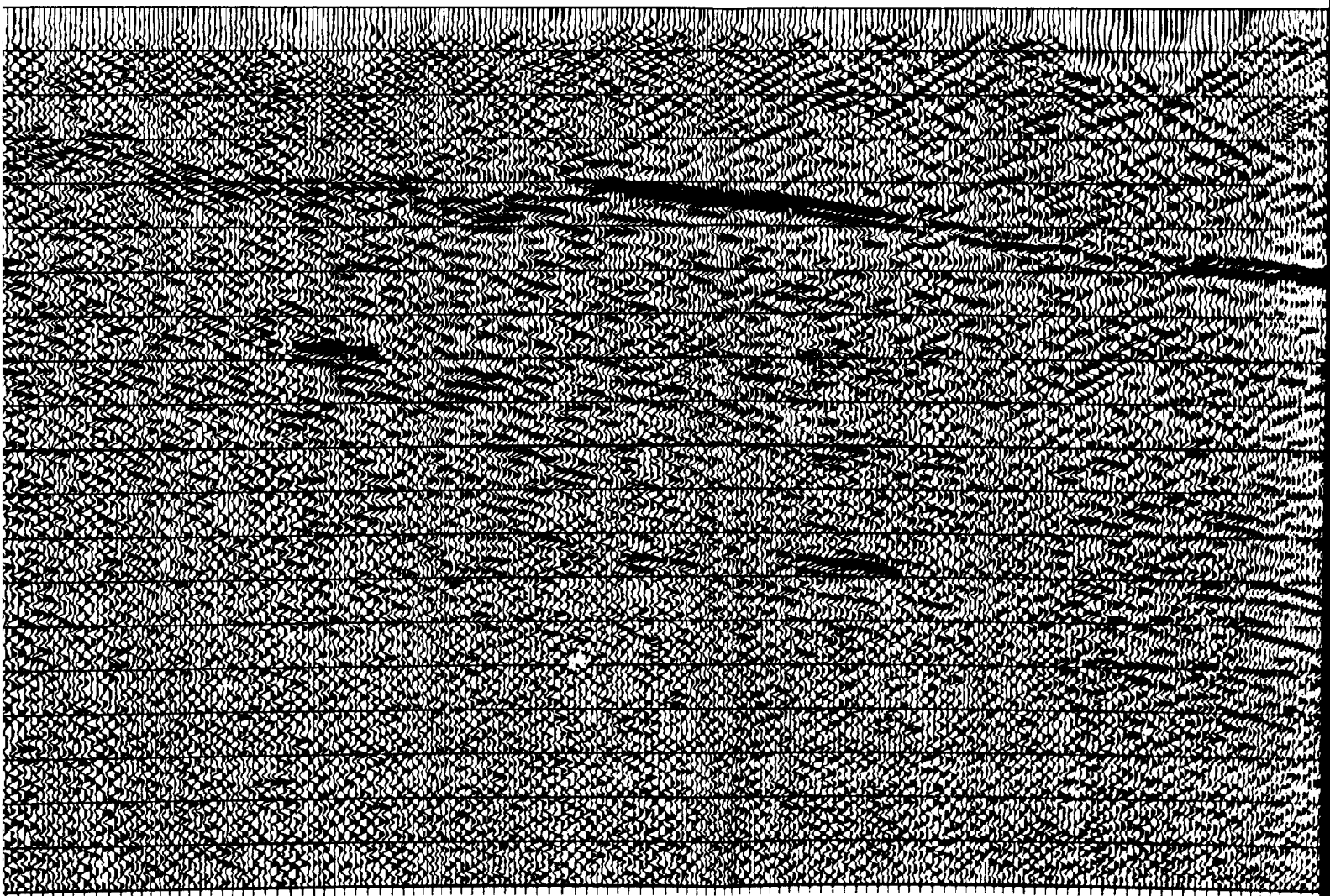


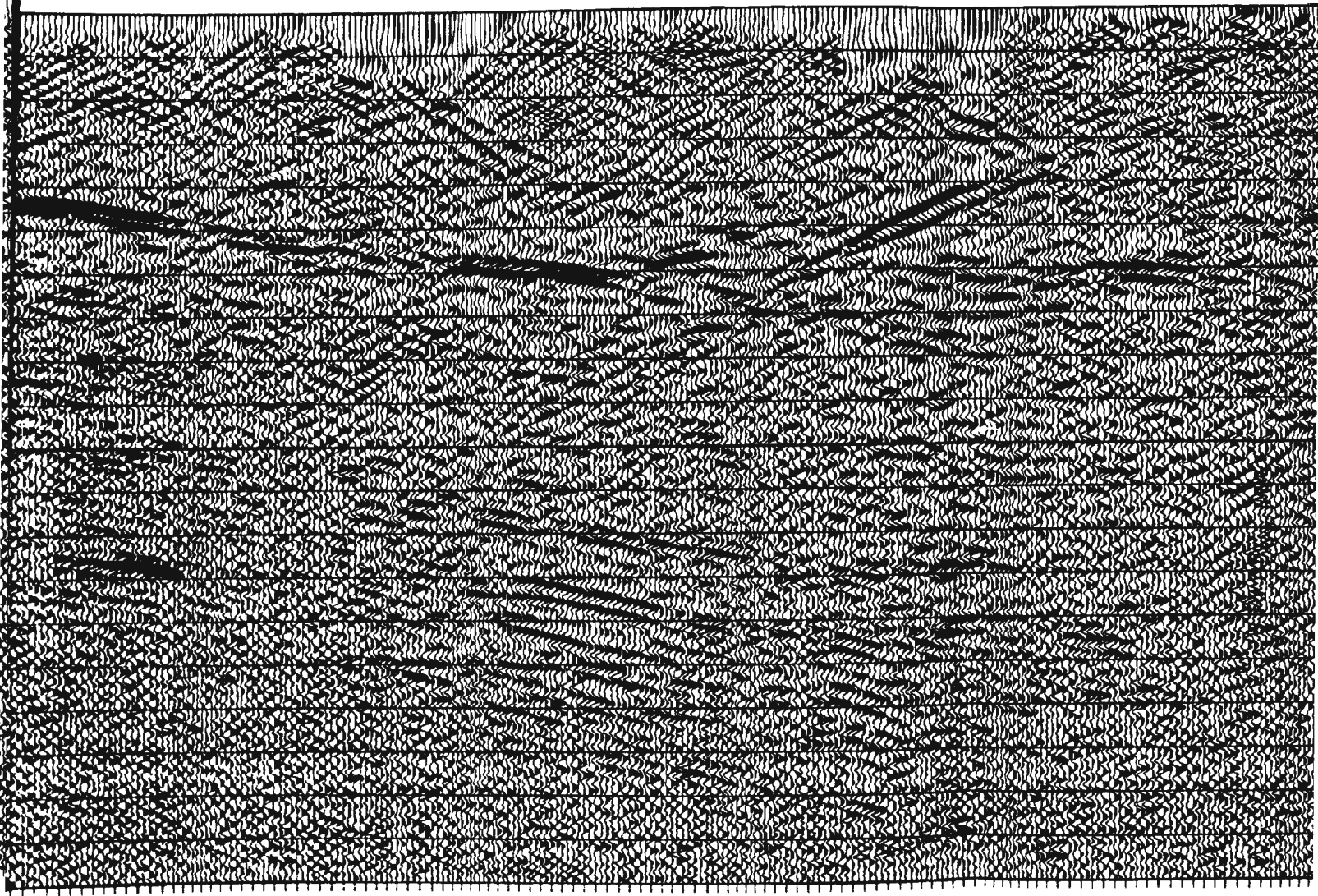
Figure 3.7 (m). Constant velocity stack of 4100 marks indicate velocity picks.

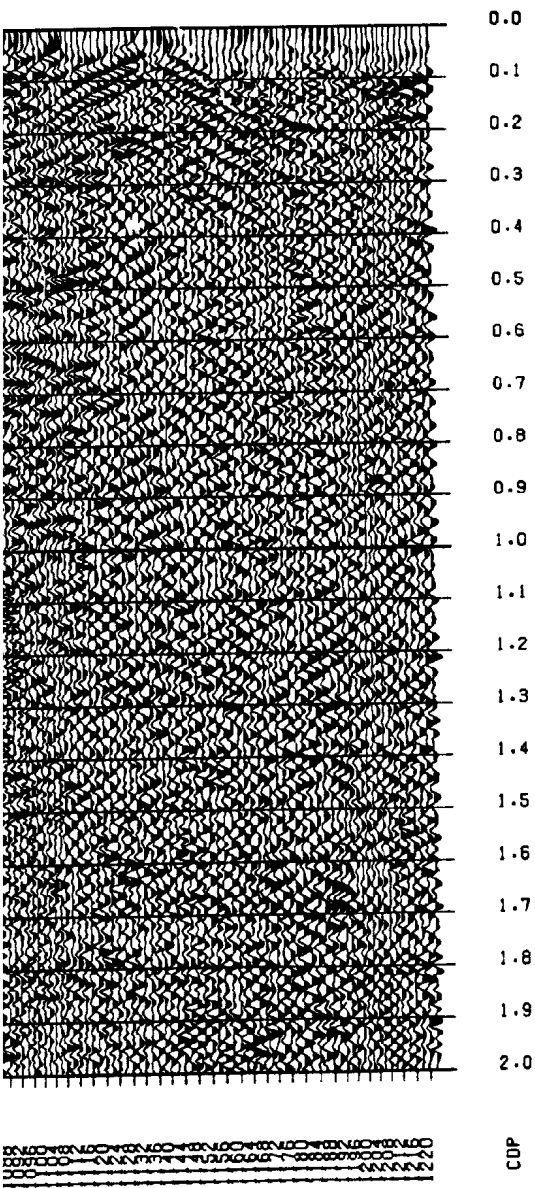
y stack of 4100 m/s, blue



100 200 300 400 500 600 700 800 900 1000 1100 1200 1300 1400 1500 1600 1700 1800 1900 2000 2100 2200 2300 2400 2500 2600 2700 2800 2900 3000 3100 3200 3300 3400 3500 3600 3700 3800 3900 4000 4100 4200 4300 4400 4500 4600 4700 4800 4900 5000 5100 5200 5300 5400 5500 5600 5700 5800 5900 6000 6100 6200 6300 6400 6500 6600 6700 6800 6900 7000 7100 7200 7300 7400 7500 7600 7700 7800 7900 8000 8100 8200 8300 8400 8500 8600 8700 8800 8900 9000 9100 9200 9300 9400 9500 9600 9700 9800 9900 10000

1. 7





7
ROBINSONS RIVER LINE, 1989
CONSTANT VELOCITY STACK - VEL = 3900 M/S

0.0
0.1
0.2
0.3
0.4
0.5
0.6
0.7
0.8
0.9
1.0
1.1
1.2
1.3
1.4
1.5
1.6
1.7
1.8
1.9
2.0

CDP

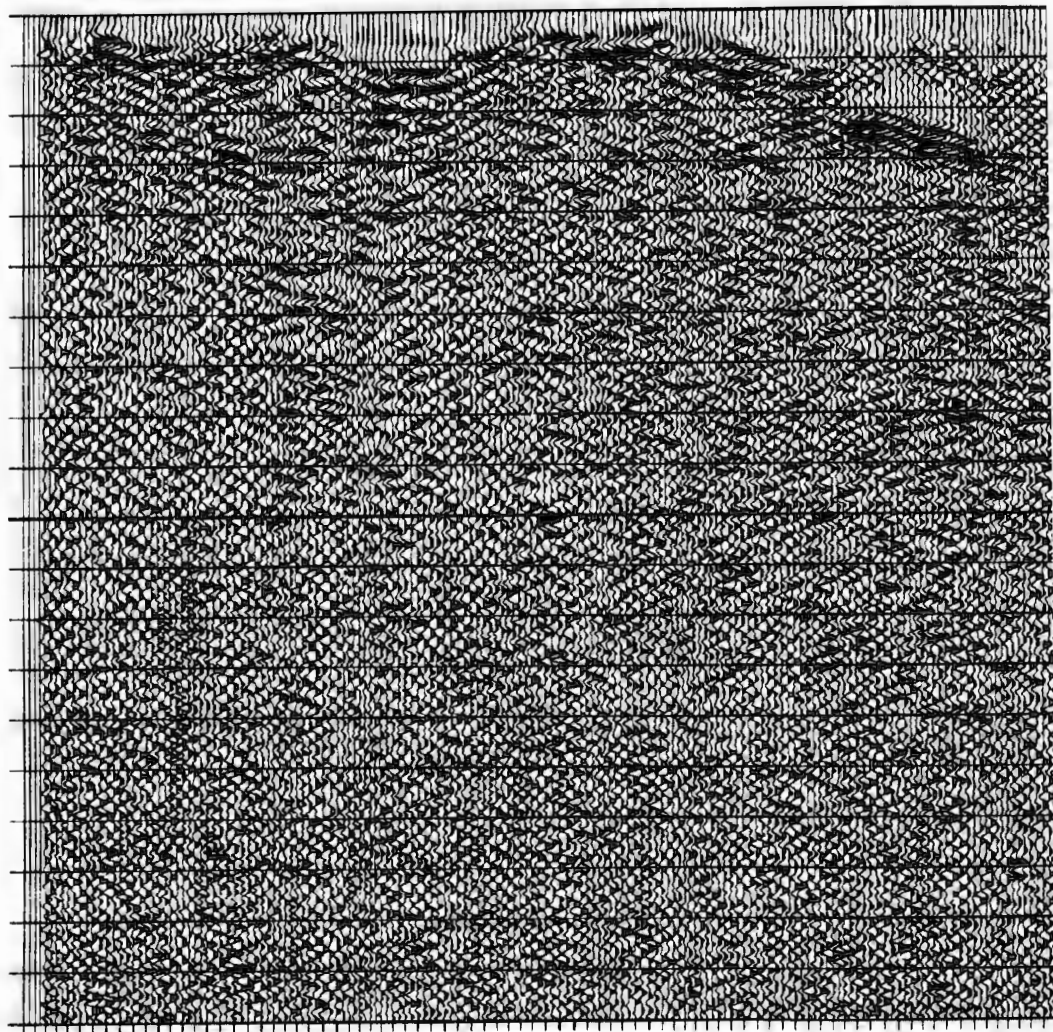
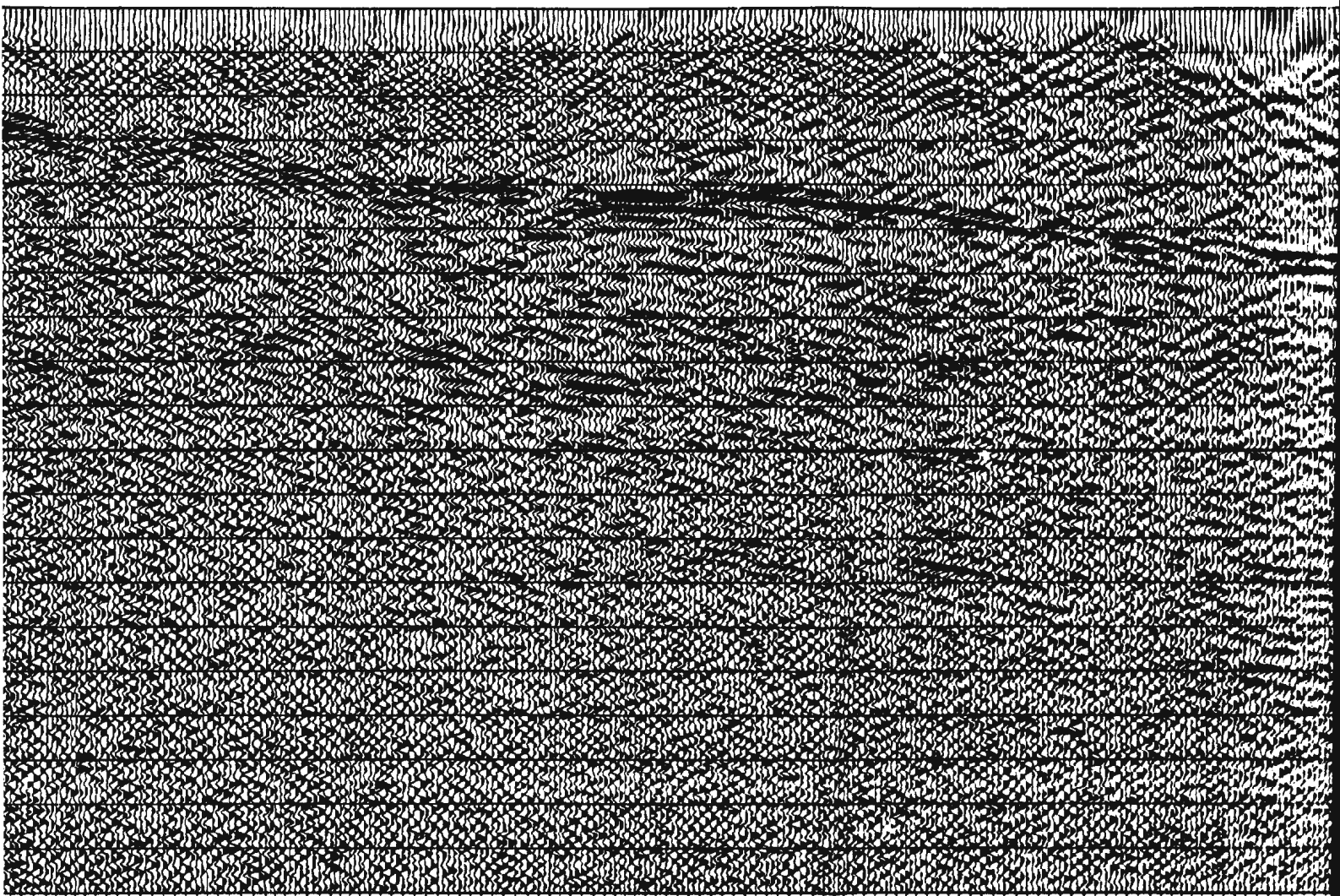
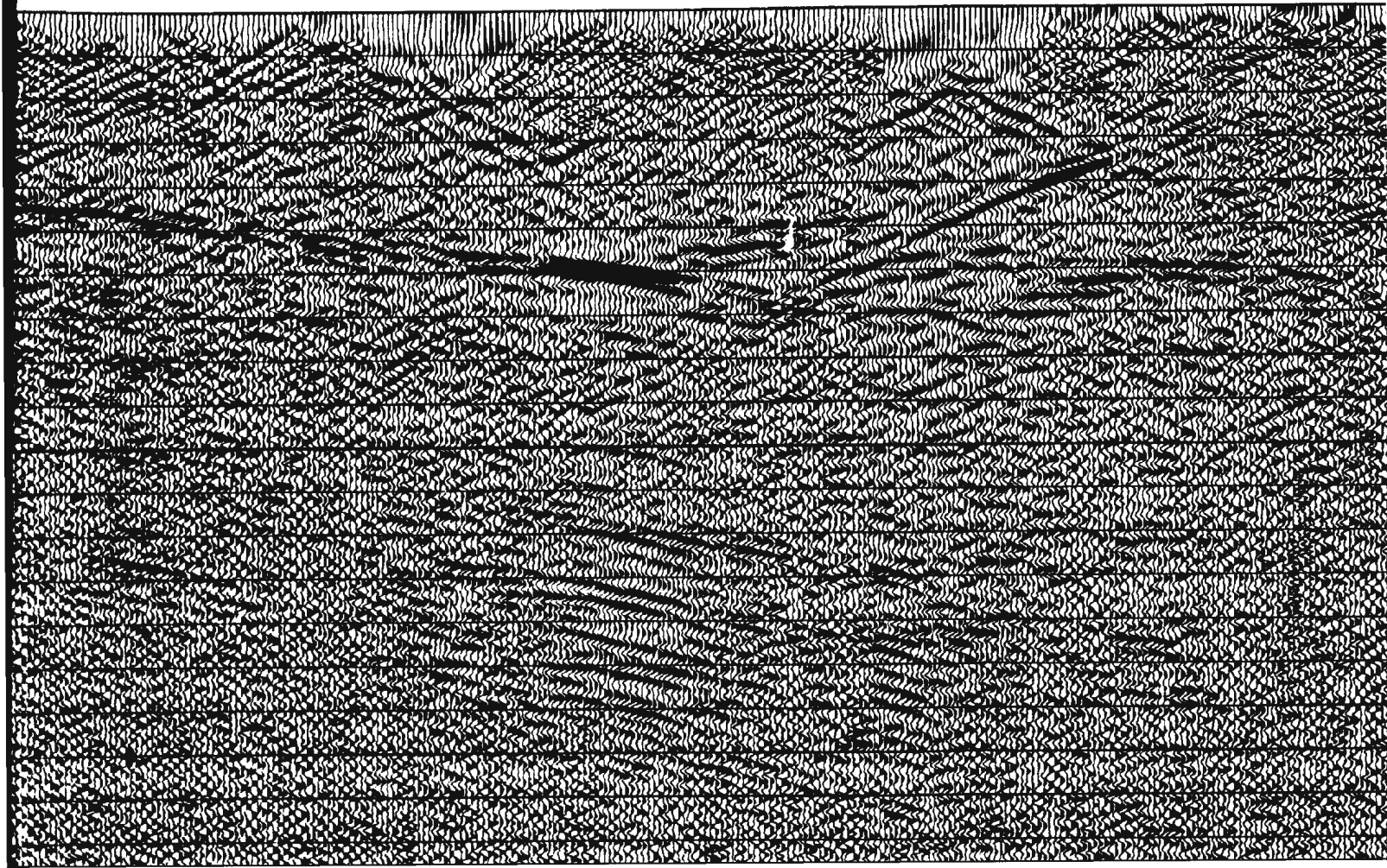


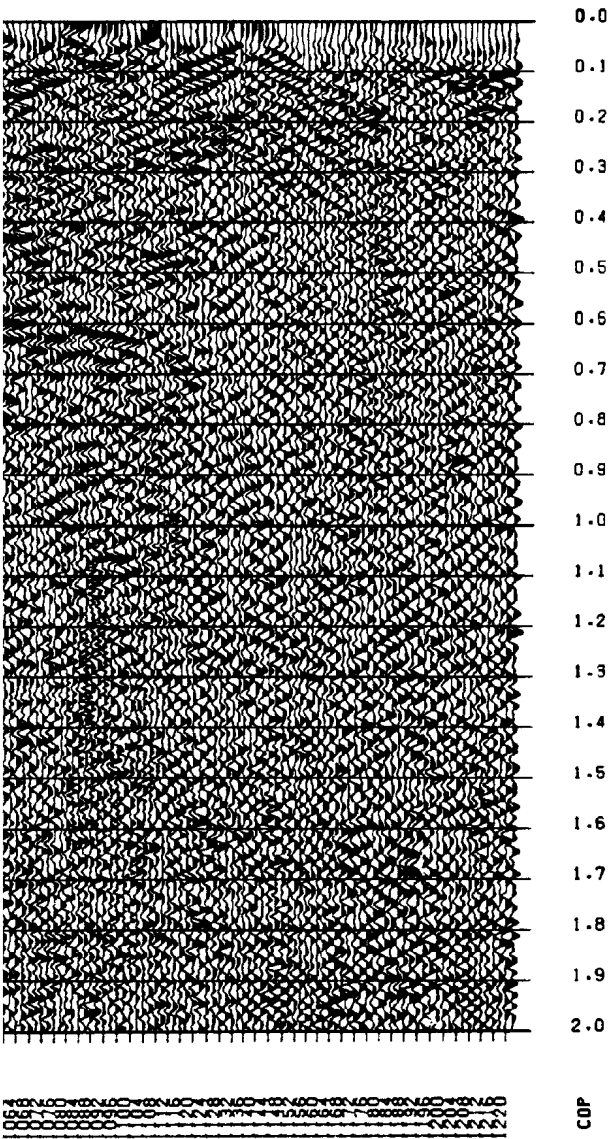
Figure 3.7 (l). Constant velocity stack. The marks indicate velocity processing.

1

[illegible]

1. 7





ROBINSONS RIVER LINE, 1989
CONSTANT VELOCITY STACK - VEL = 3700 M/S

0.0
0.1
0.2
0.3
0.4
0.5
0.6
0.7
0.8
0.9
1.0
1.1
1.2
1.3
1.4
1.5
1.6
1.7
1.8
1.9
2.0

CDP

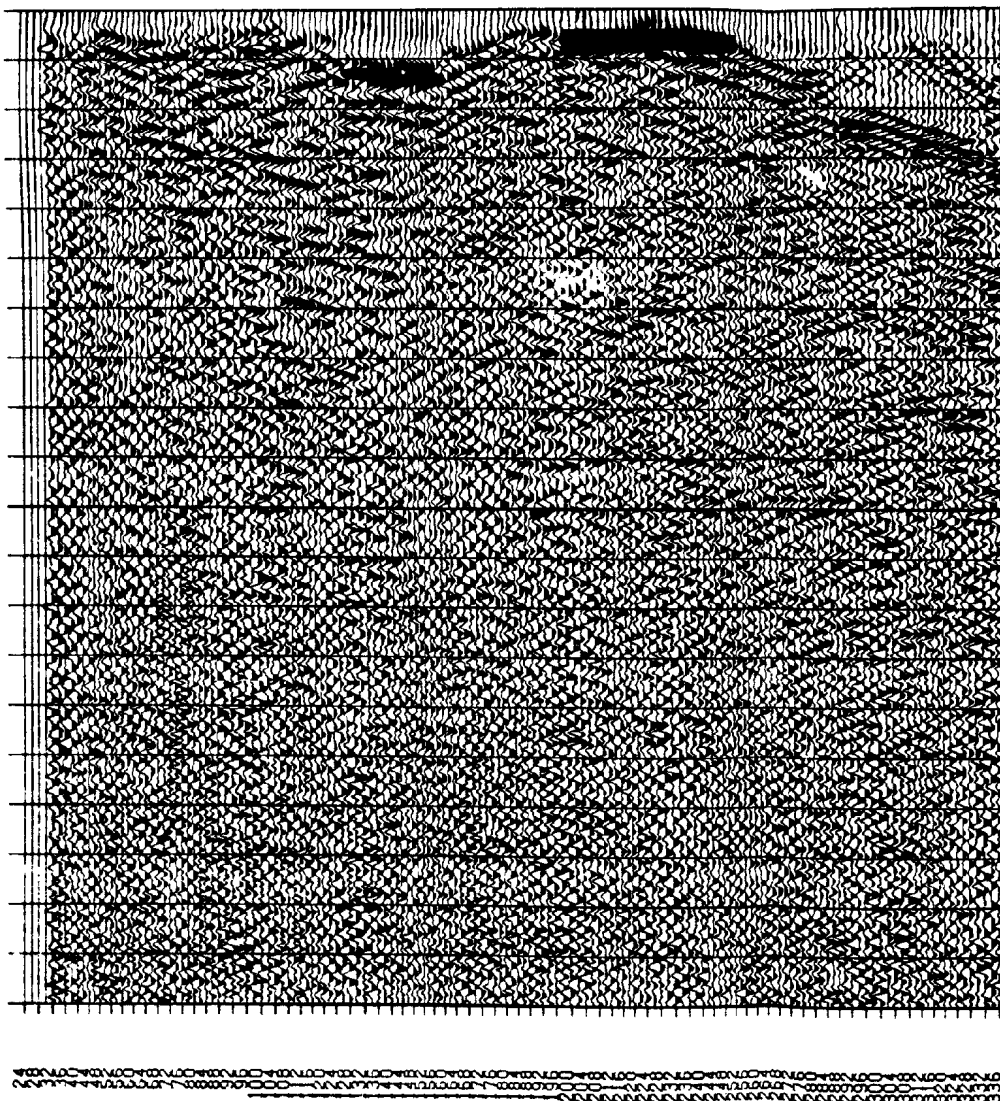
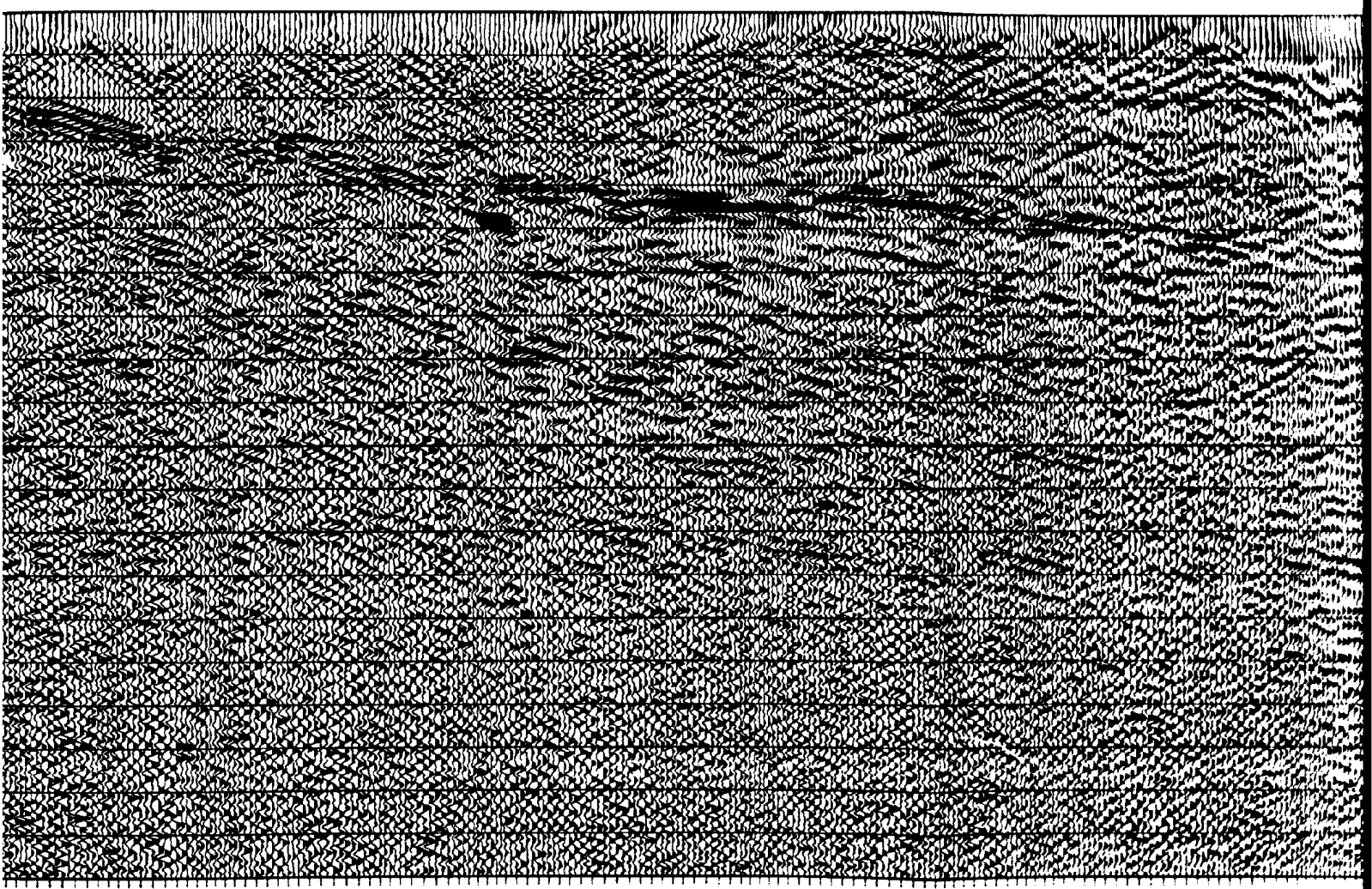


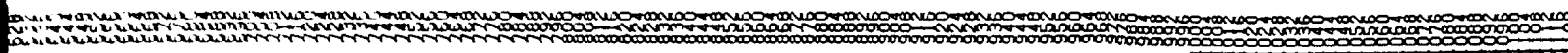
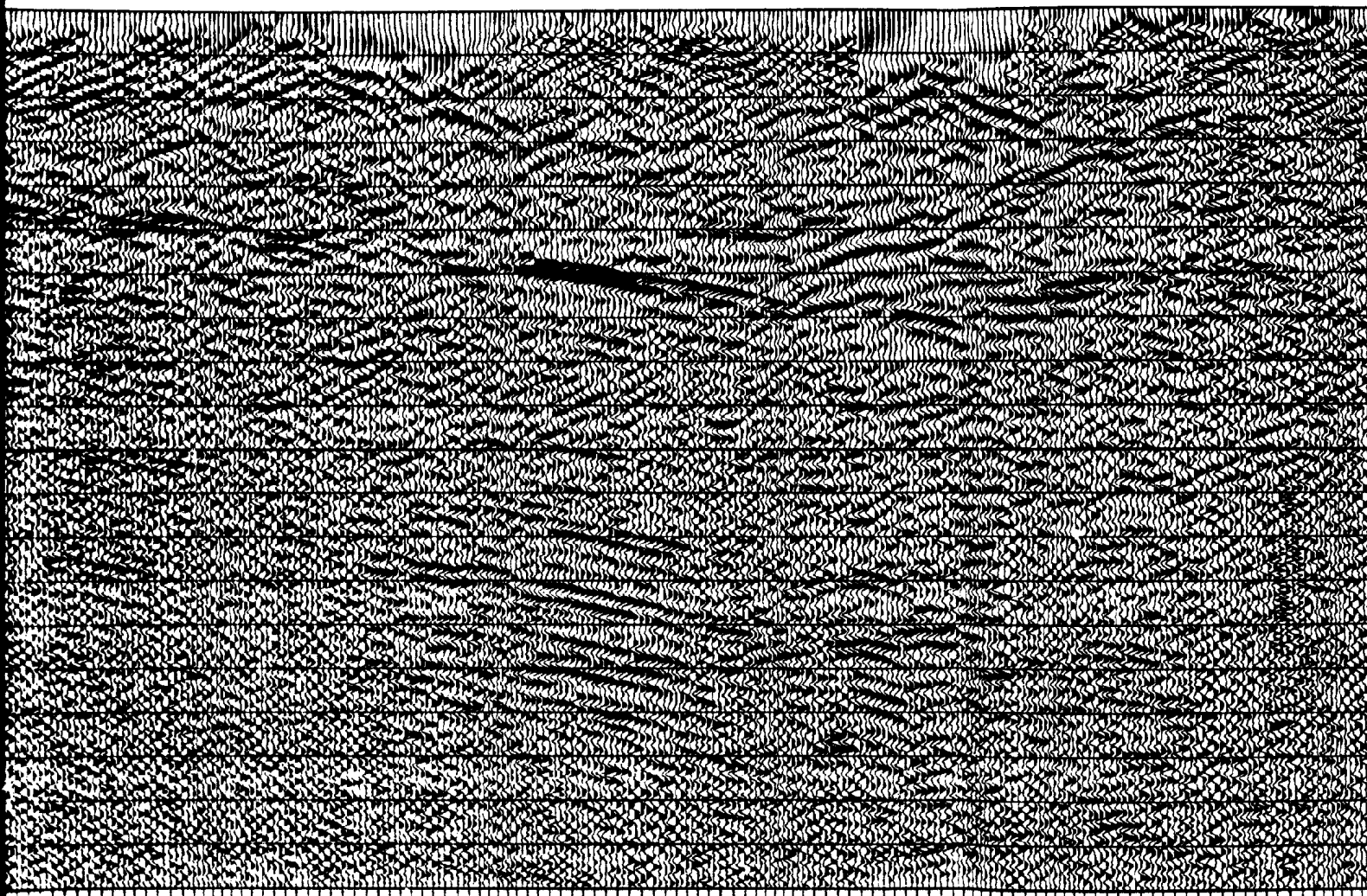
Figure 3.7 (k). Constant velocity marks indicate velocity pick

Constant velocity stack of 3700 m/s, blue
velocity picks.



SEISMIC DATA VISUALIZATION

7



7
ROBINSONS RIVER LINE, 1989
CONSTANT VELOCITY STACK - VEL = 3500 M/S

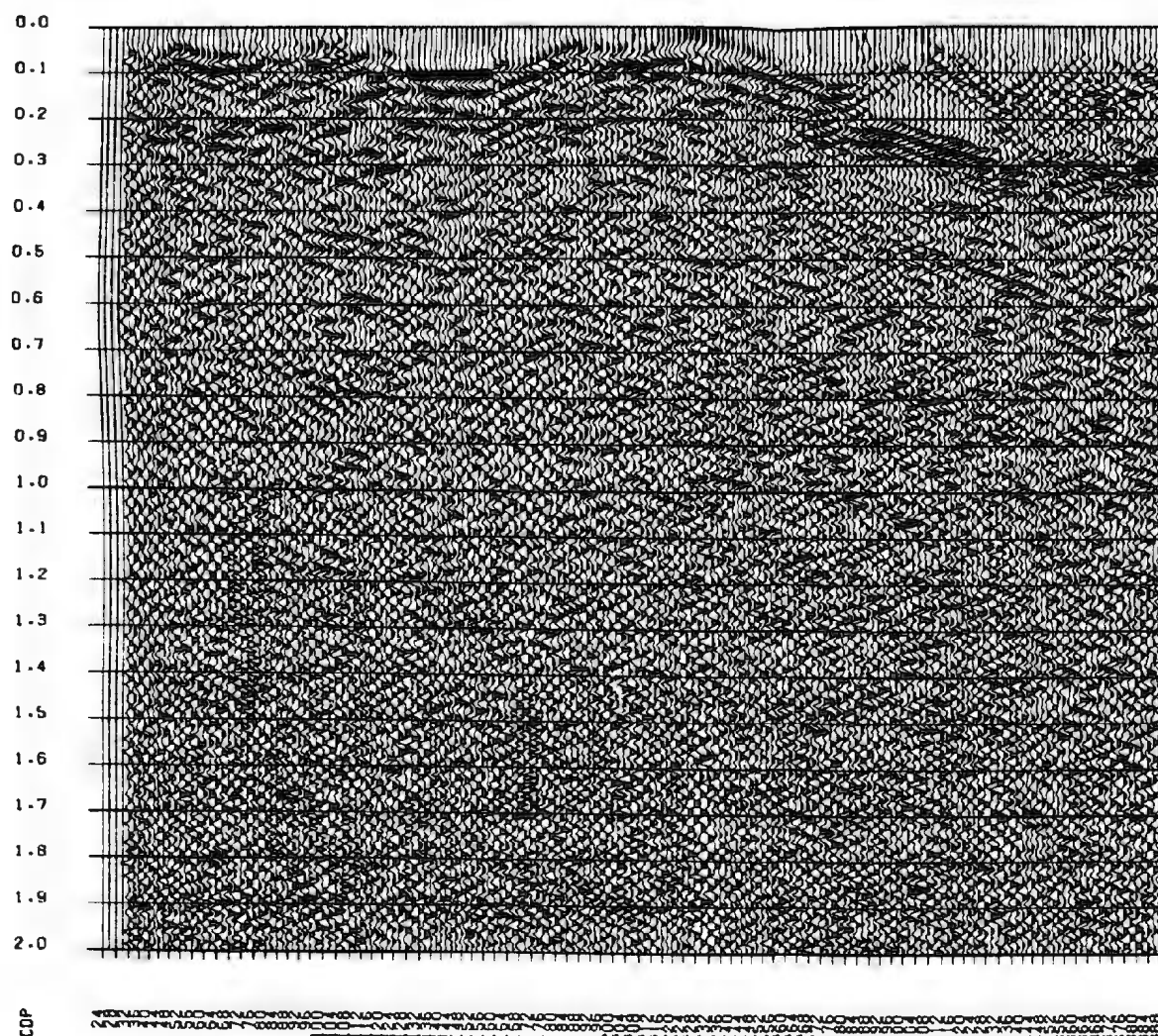
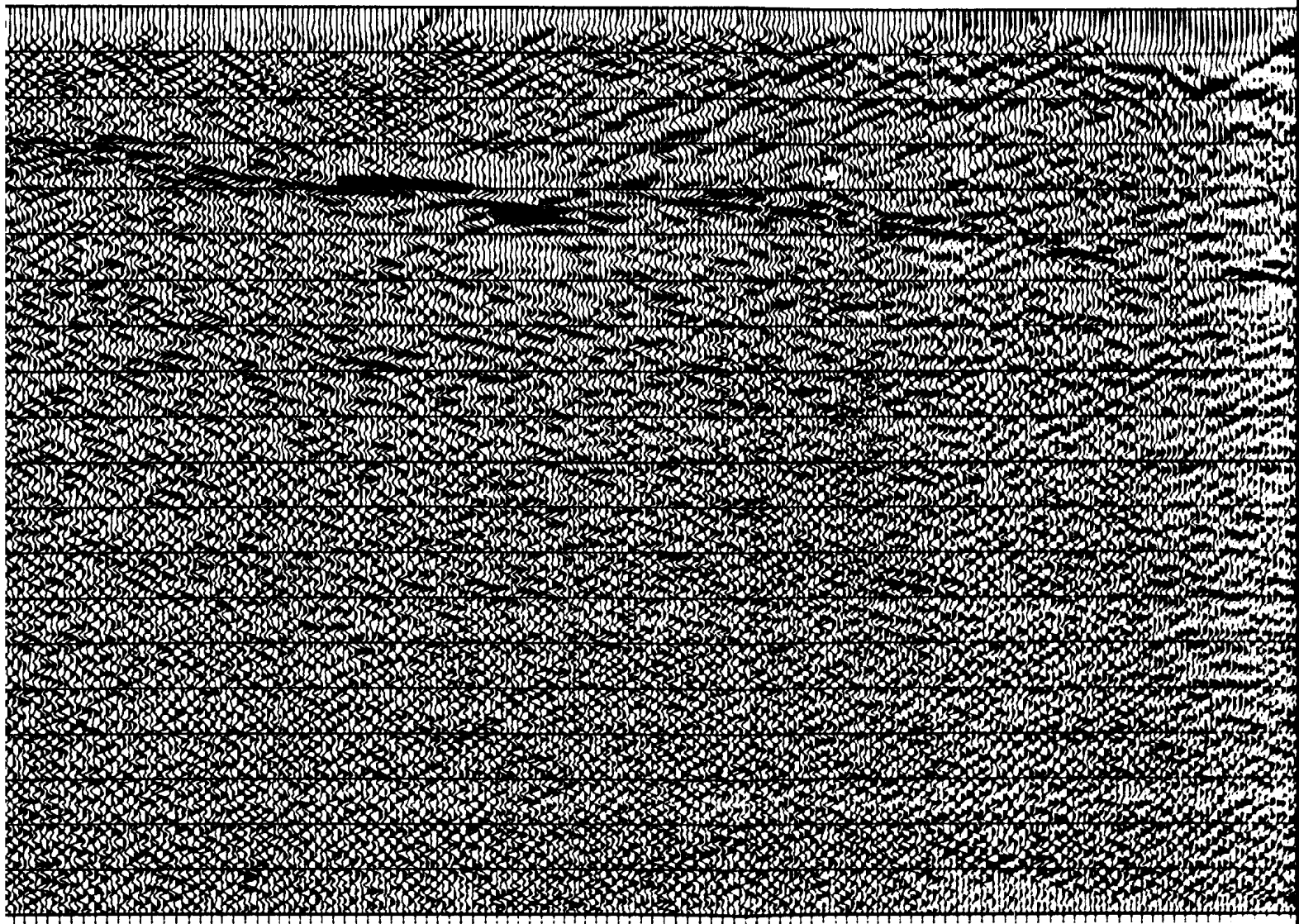


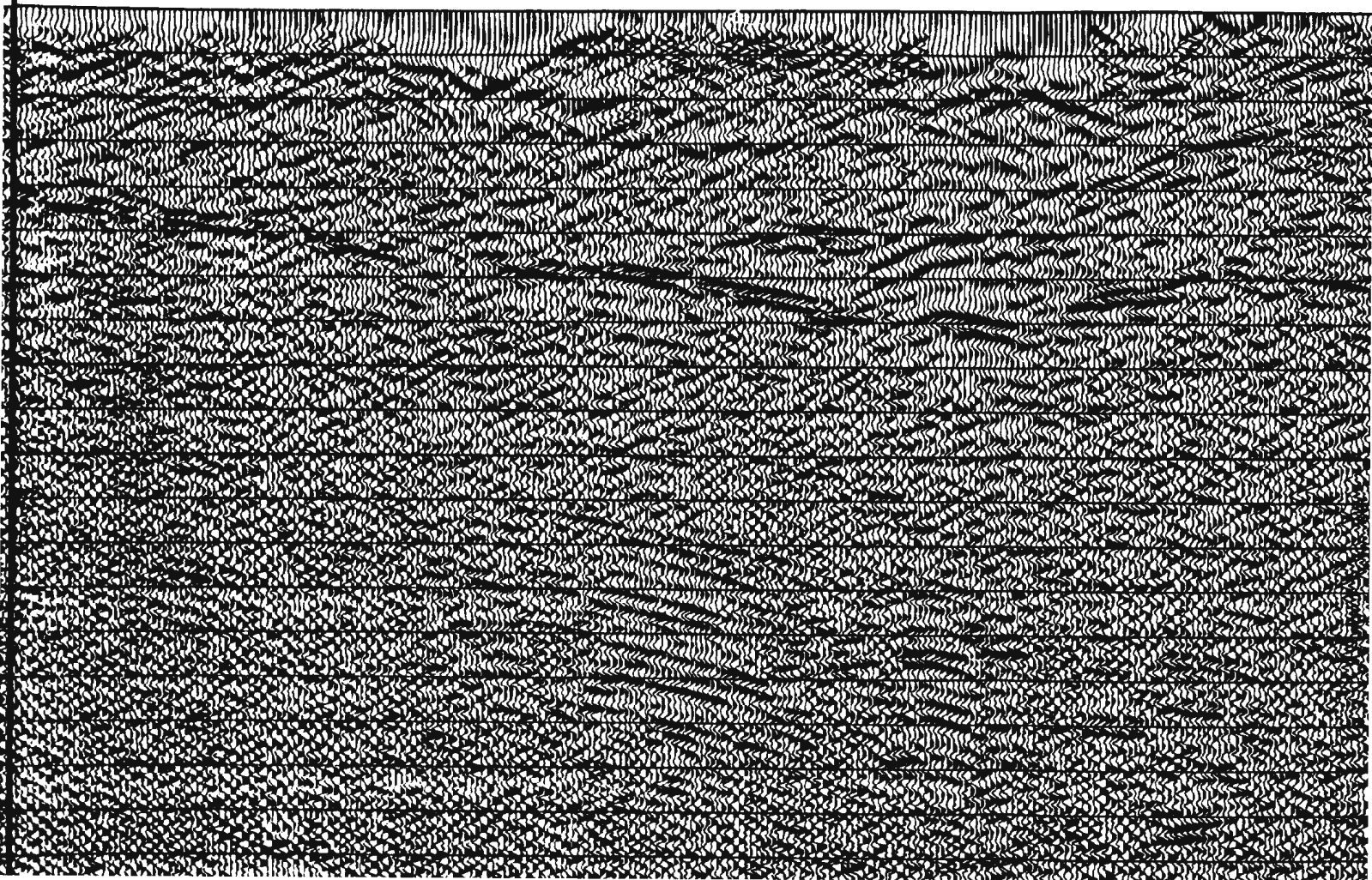
Figure 3.7 (j). Constant velocity stack. Small marks indicate velocity picks.

velocity stack of 3500 m/s, blue
picks.



Velocity stack of 3500 m/s, blue picks.

7



3.0

COP

ROBINSONS RIVER LINE, 1989
CONSTANT VELOCITY STACK - VEL = 3300 M/S

0.0
0.1
0.2
0.3
0.4
0.5
0.6
0.7
0.8
0.9
1.0
1.1
1.2
1.3
1.4
1.5
1.6
1.7
1.8
1.9
2.0

CDP

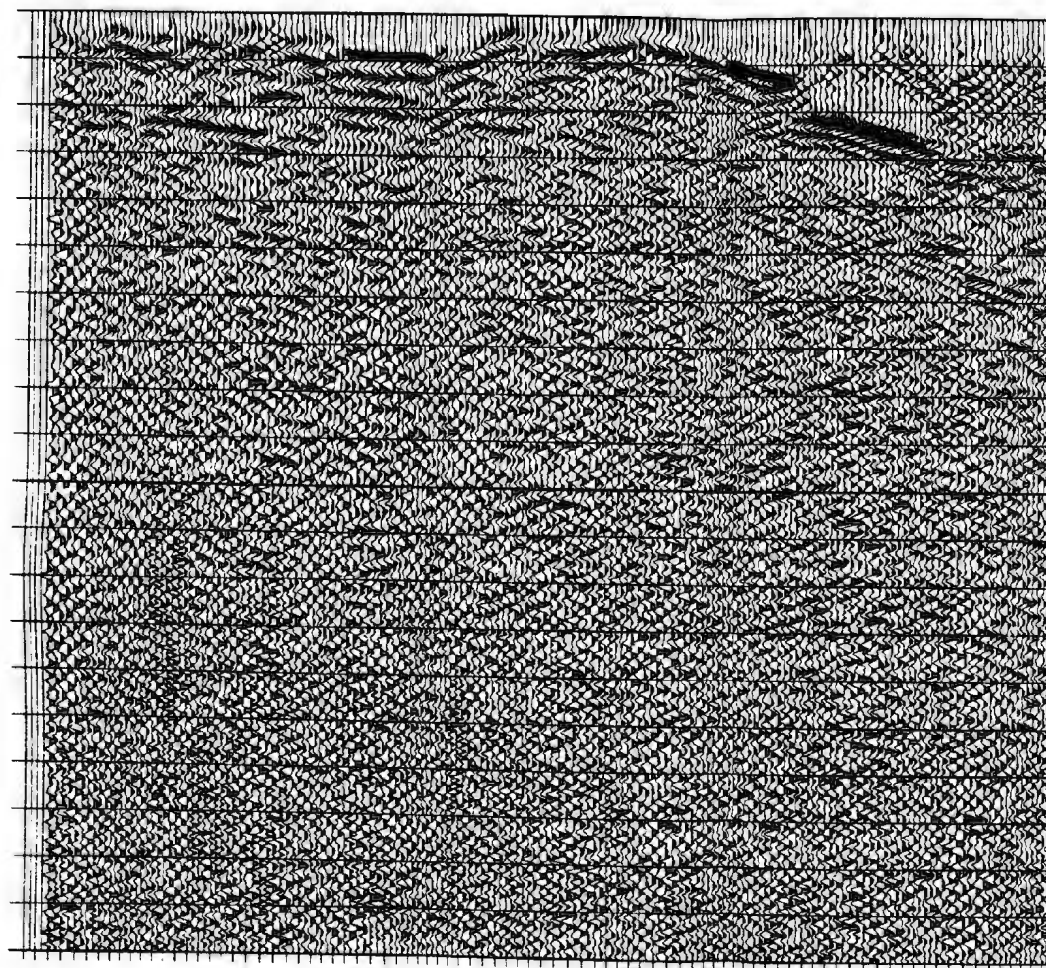
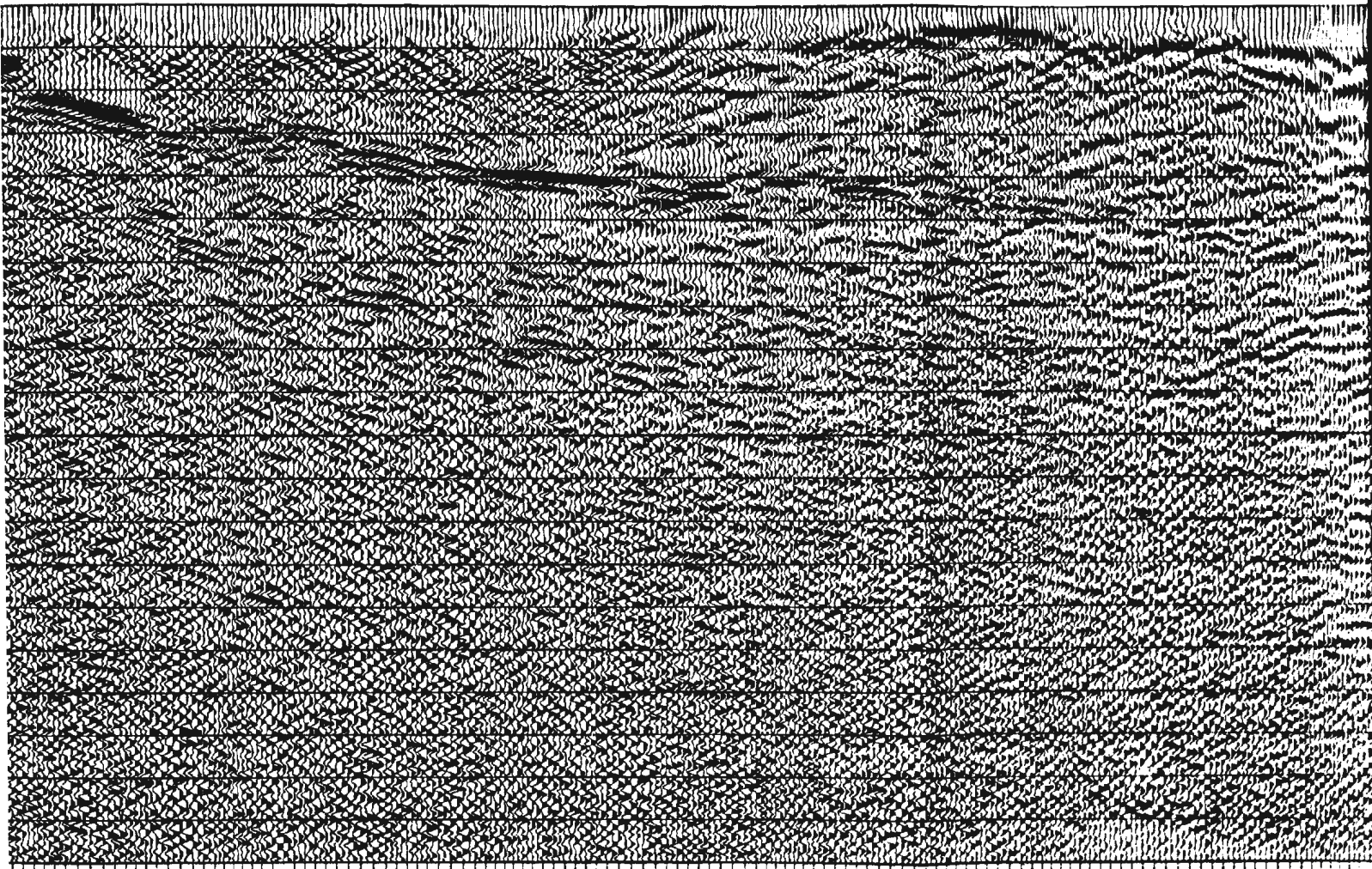
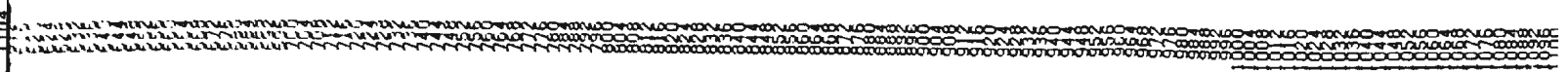
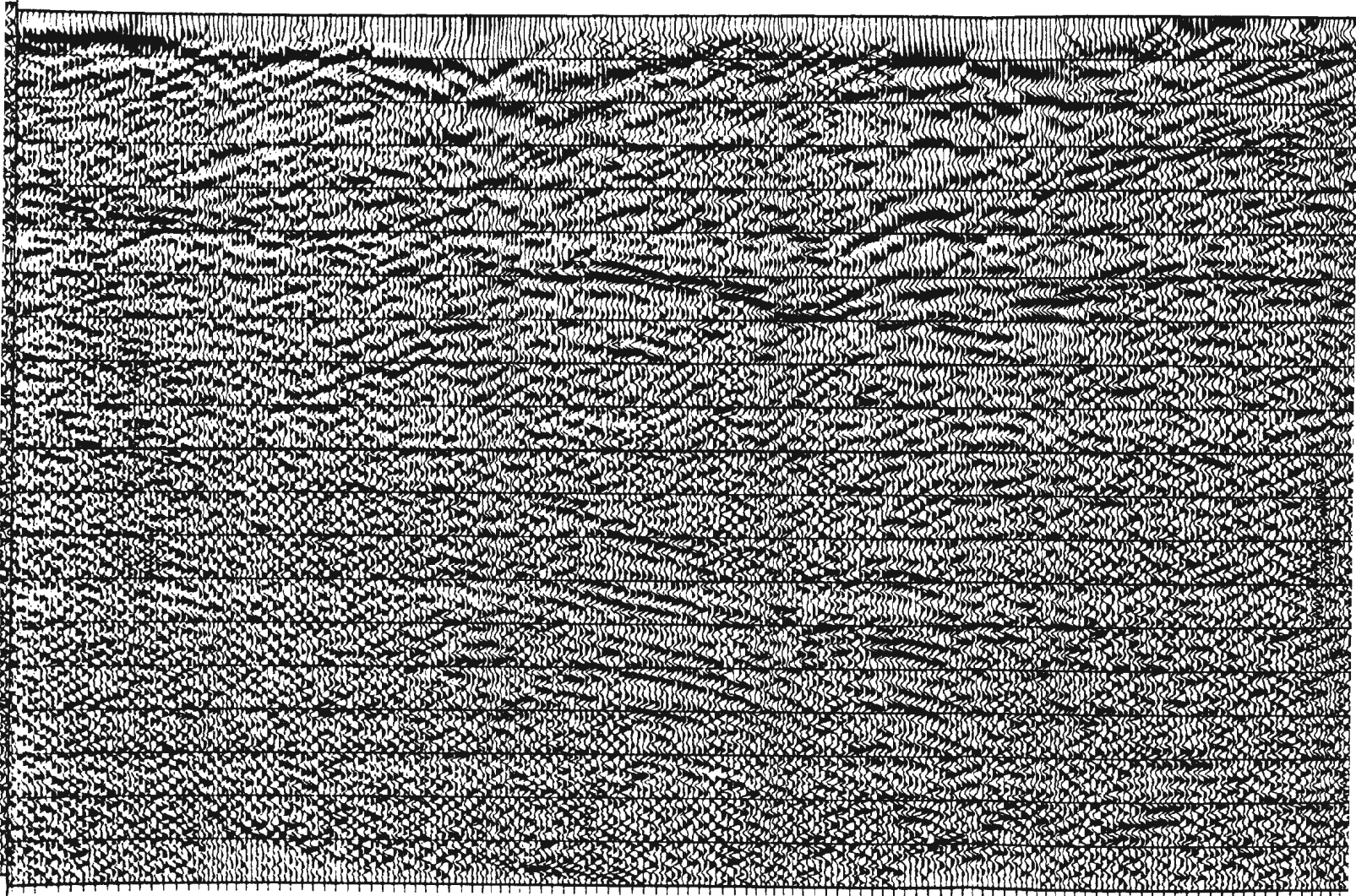


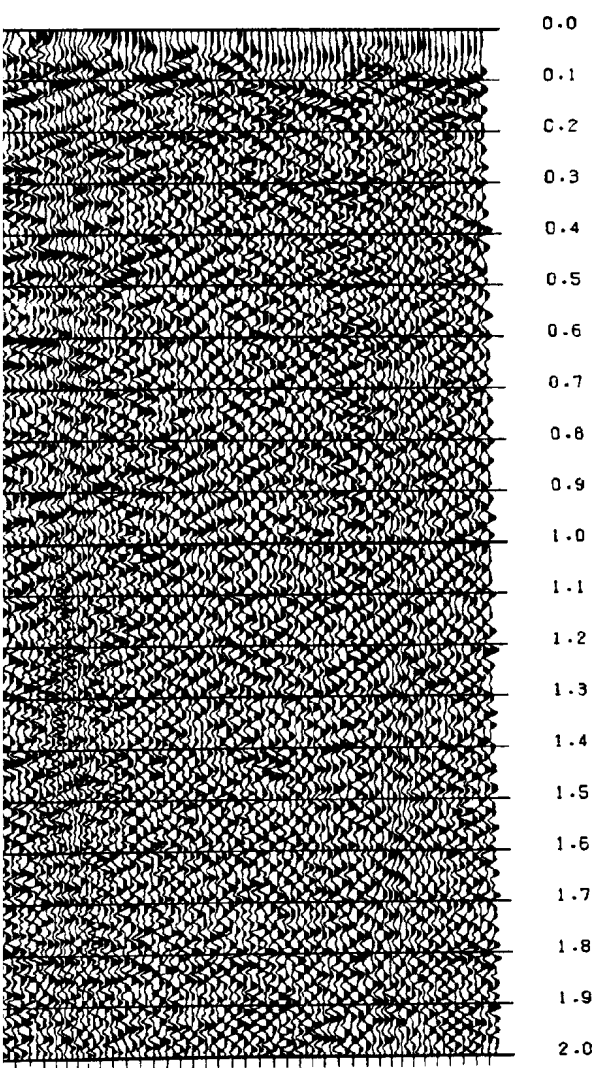
Figure 3.7 (i). Constant vel.
marks indicate velocity pick

(i). Constant velocity stack of 3300 m/s, blue
ate velocity picks.



1
1
1





CDP

ROBINSONS RIVER LINE, 1989
CONSTANT VELOCITY STACK - VEL = 3200 M/S

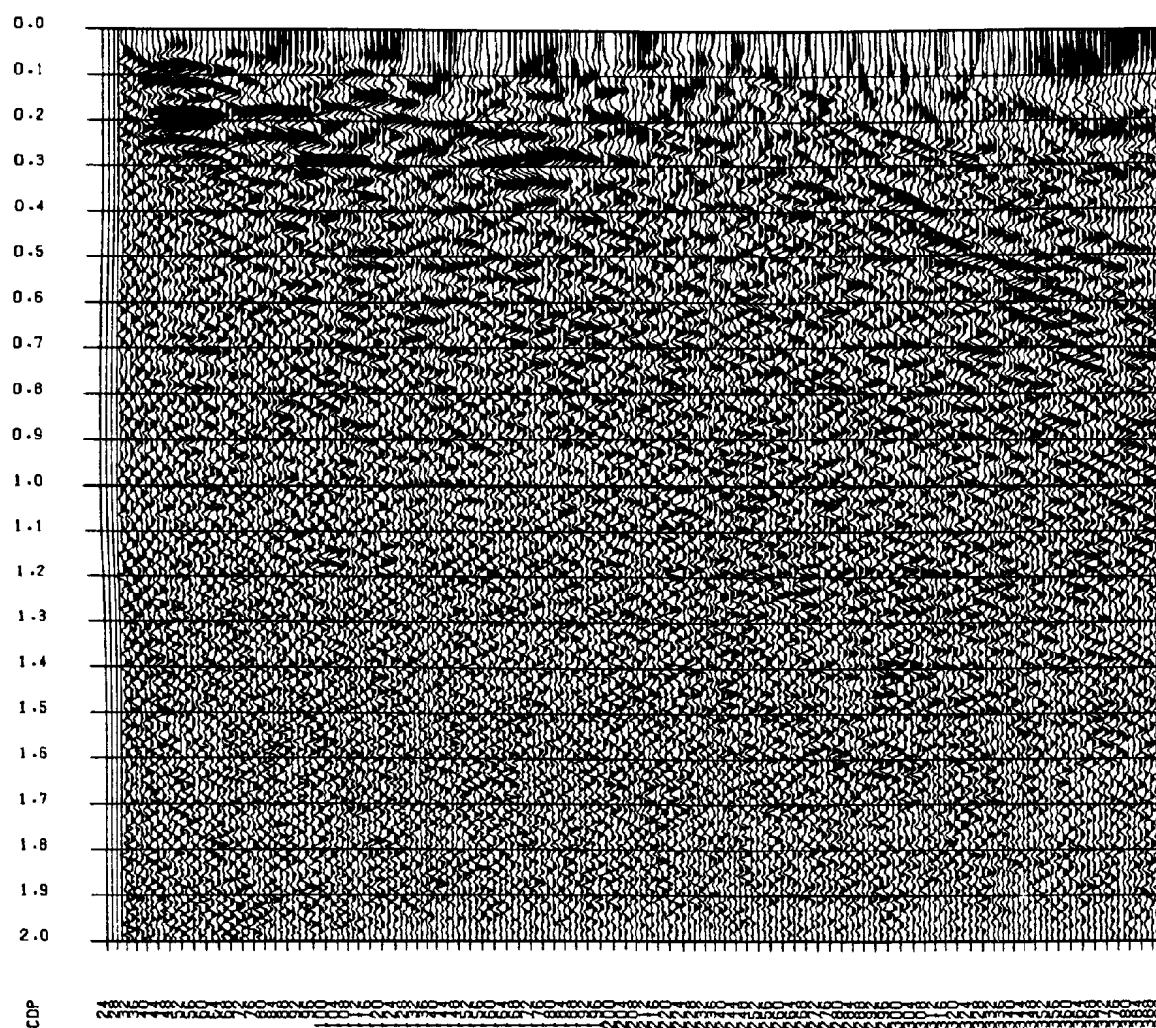
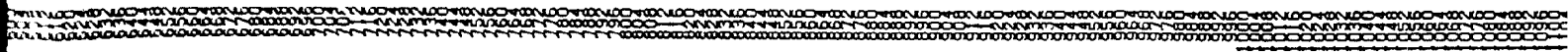
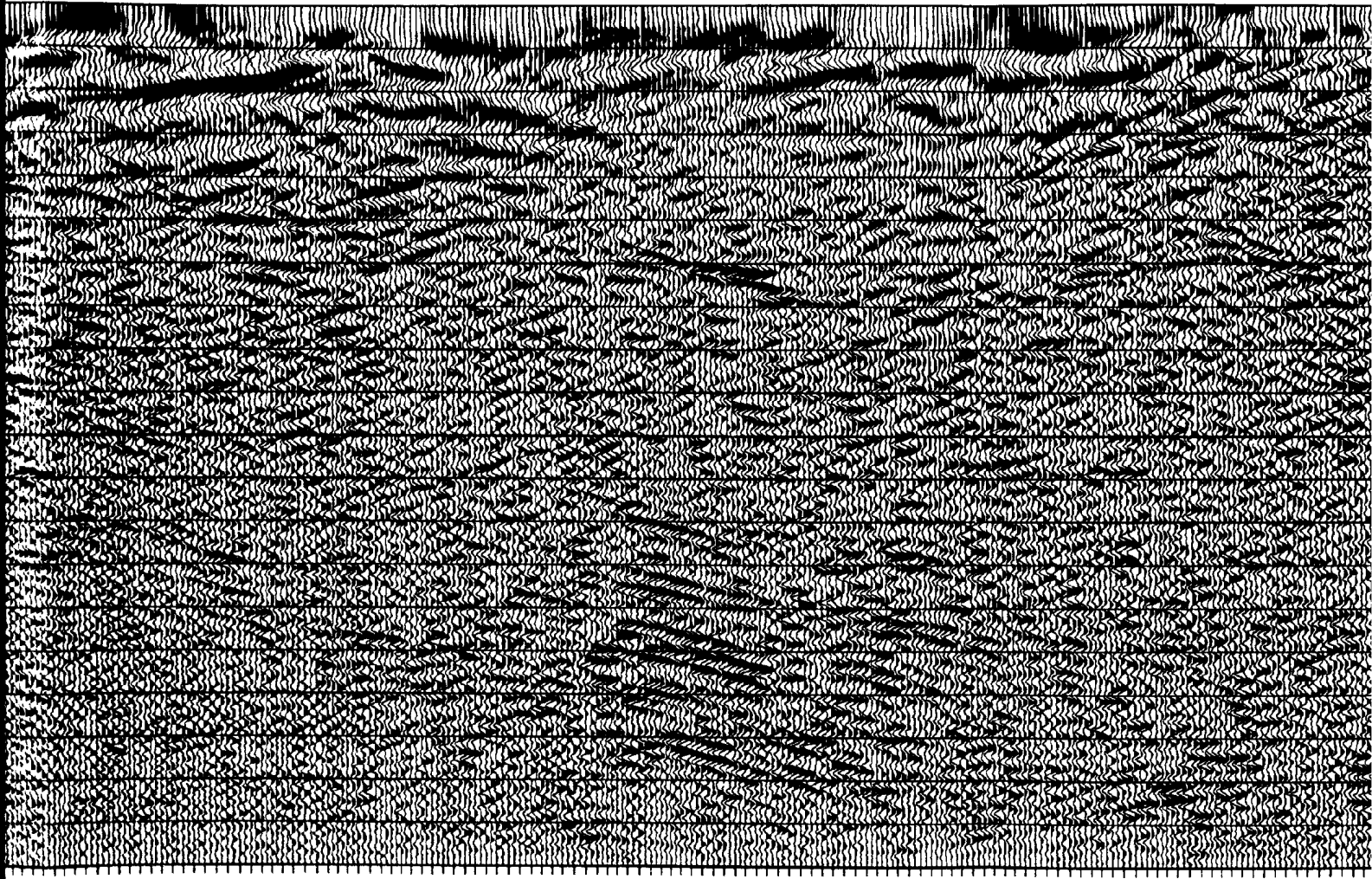


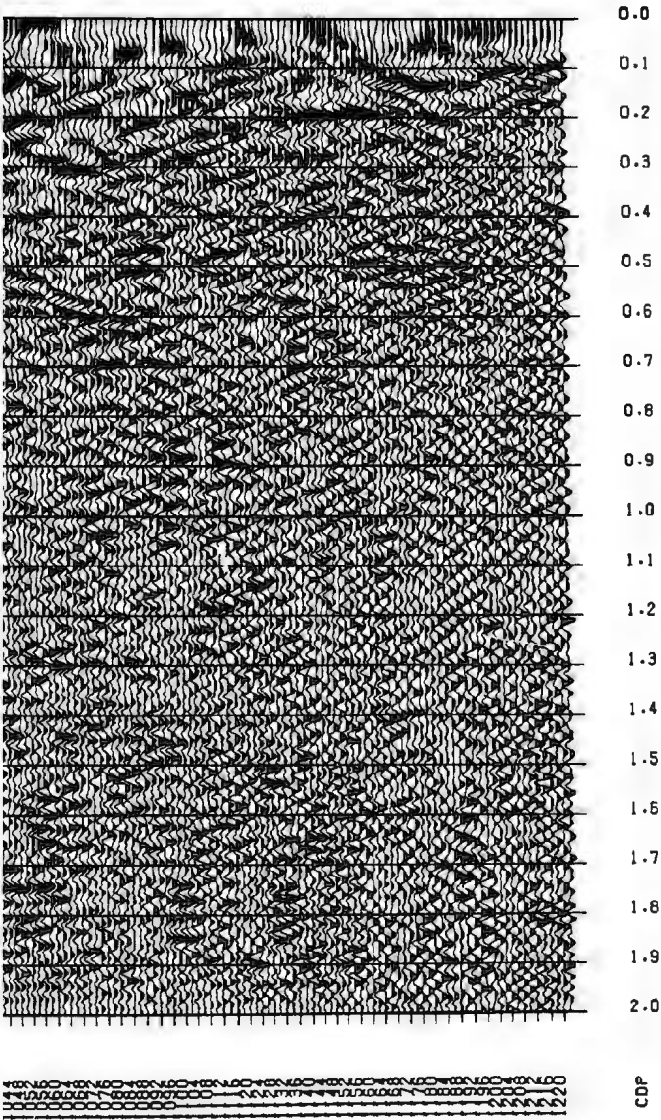
Figure 3.7 (h). Constant velocity stack of 3200 m/s marks indicate velocity picks.

A black and white image showing a dense, textured surface, possibly a book cover or endpaper. The texture is composed of a repeating pattern of small, dark, irregular shapes, creating a complex, almost abstract visual effect. The overall appearance is that of a high-contrast, grainy print.



1





7
ROBINSONS RIVER LINE, 1989
CONSTANT VELOCITY STACK - VEL = 3100 M/S

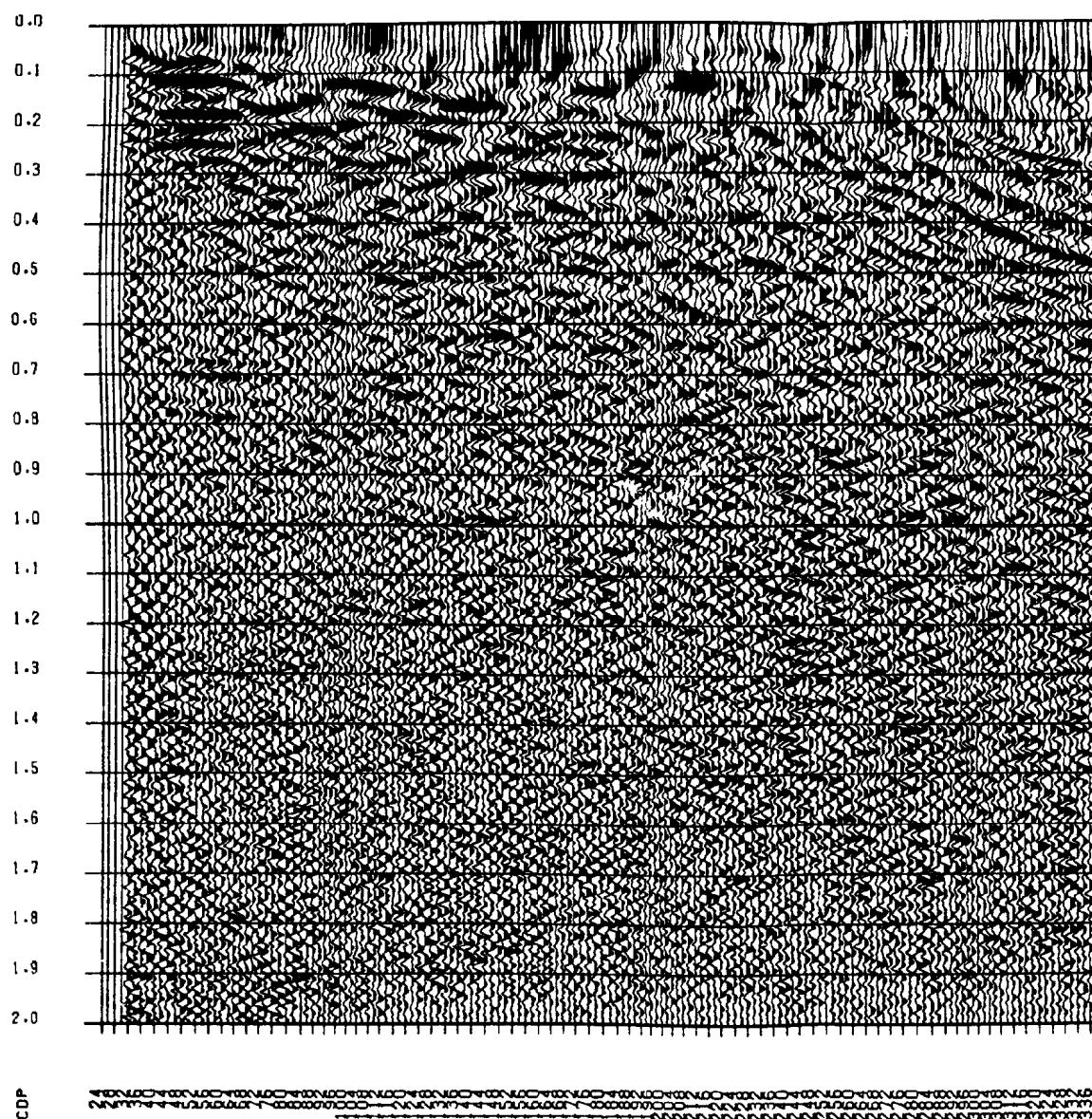
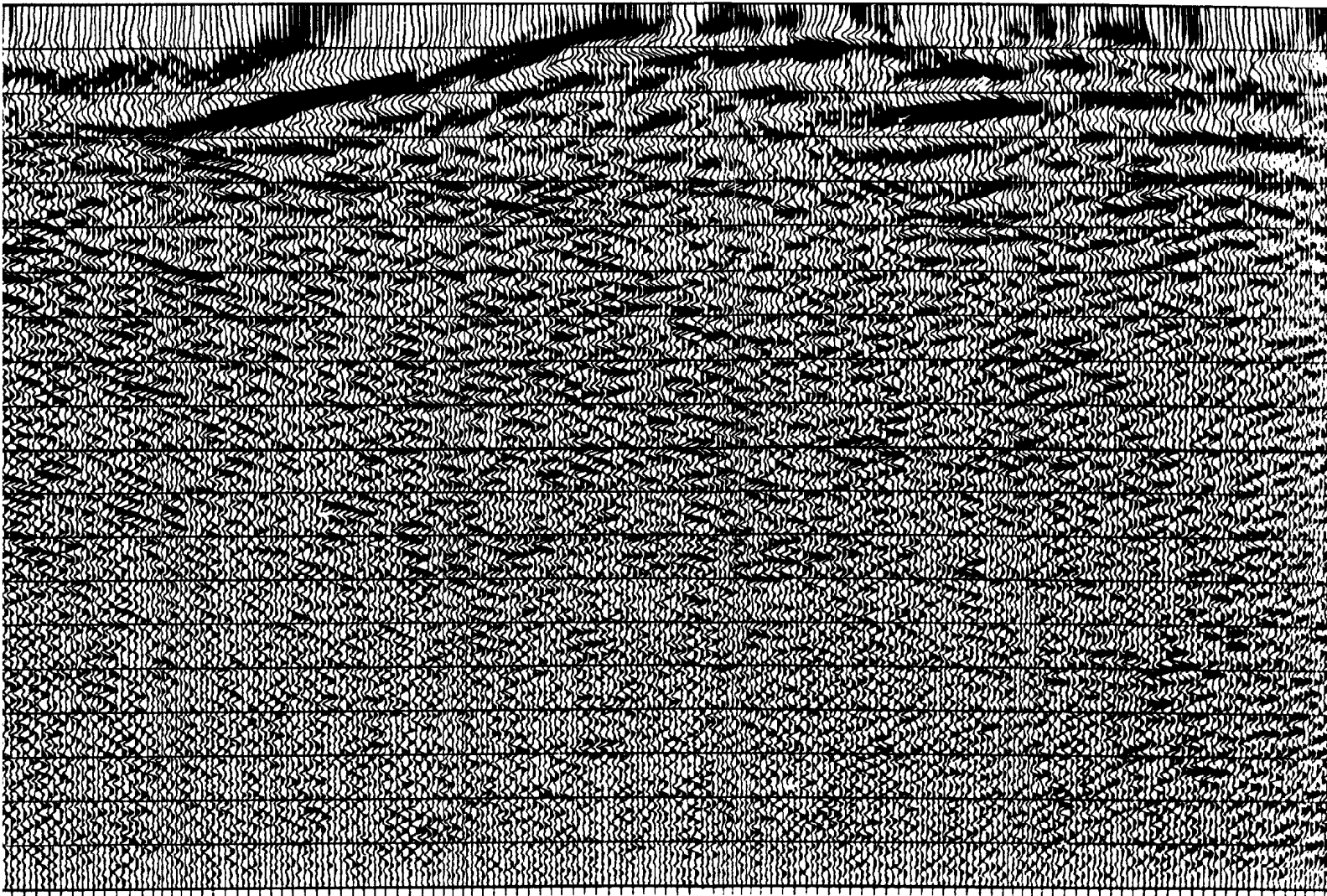


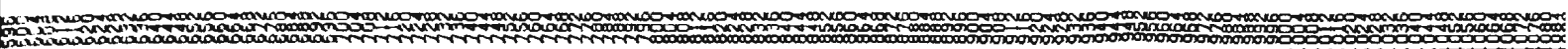
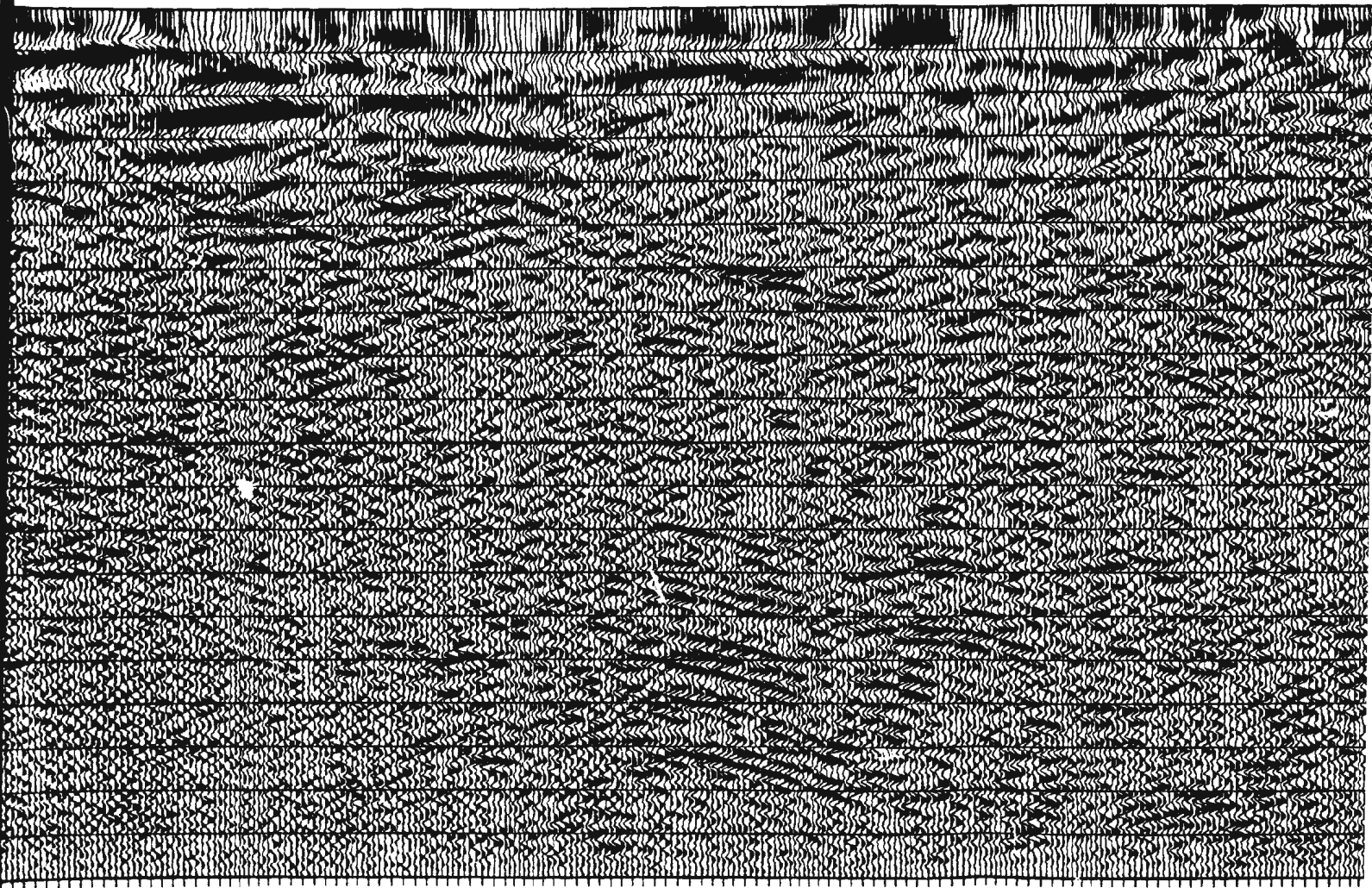
Figure 3.7 (g). Constant velocity marks indicate velocity picks.

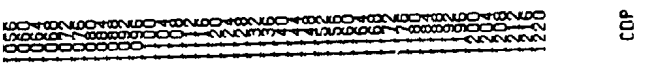
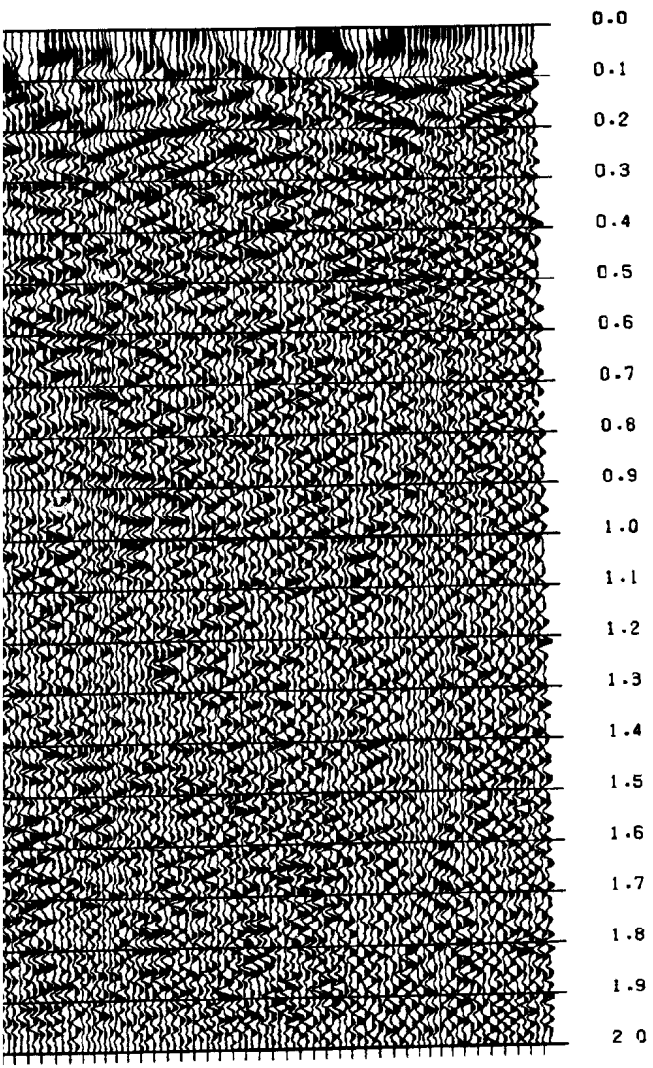
stack of 3100 m/s, blue



4000 3000 2000 1000 0 1000 2000 3000 4000 5000 6000 7000 8000 9000 10000 11000 12000 13000 14000 15000 16000 17000 18000 19000 20000 21000 22000 23000 24000 25000 26000 27000 28000 29000 30000 31000 32000 33000 34000 35000 36000 37000 38000 39000 40000 41000 42000 43000 44000 45000 46000 47000 48000 49000 50000 51000 52000 53000 54000 55000 56000 57000 58000 59000 60000 61000 62000 63000 64000 65000 66000 67000 68000 69000 70000 71000 72000 73000 74000 75000 76000 77000 78000 79000 80000 81000 82000 83000 84000 85000 86000 87000 88000 89000 90000 91000 92000 93000 94000 95000 96000 97000 98000 99000 100000

1





7
ROBINSONS RIVER LINE, 1989
CONSTANT VELOCITY STACK - VEL = 3000 M/S

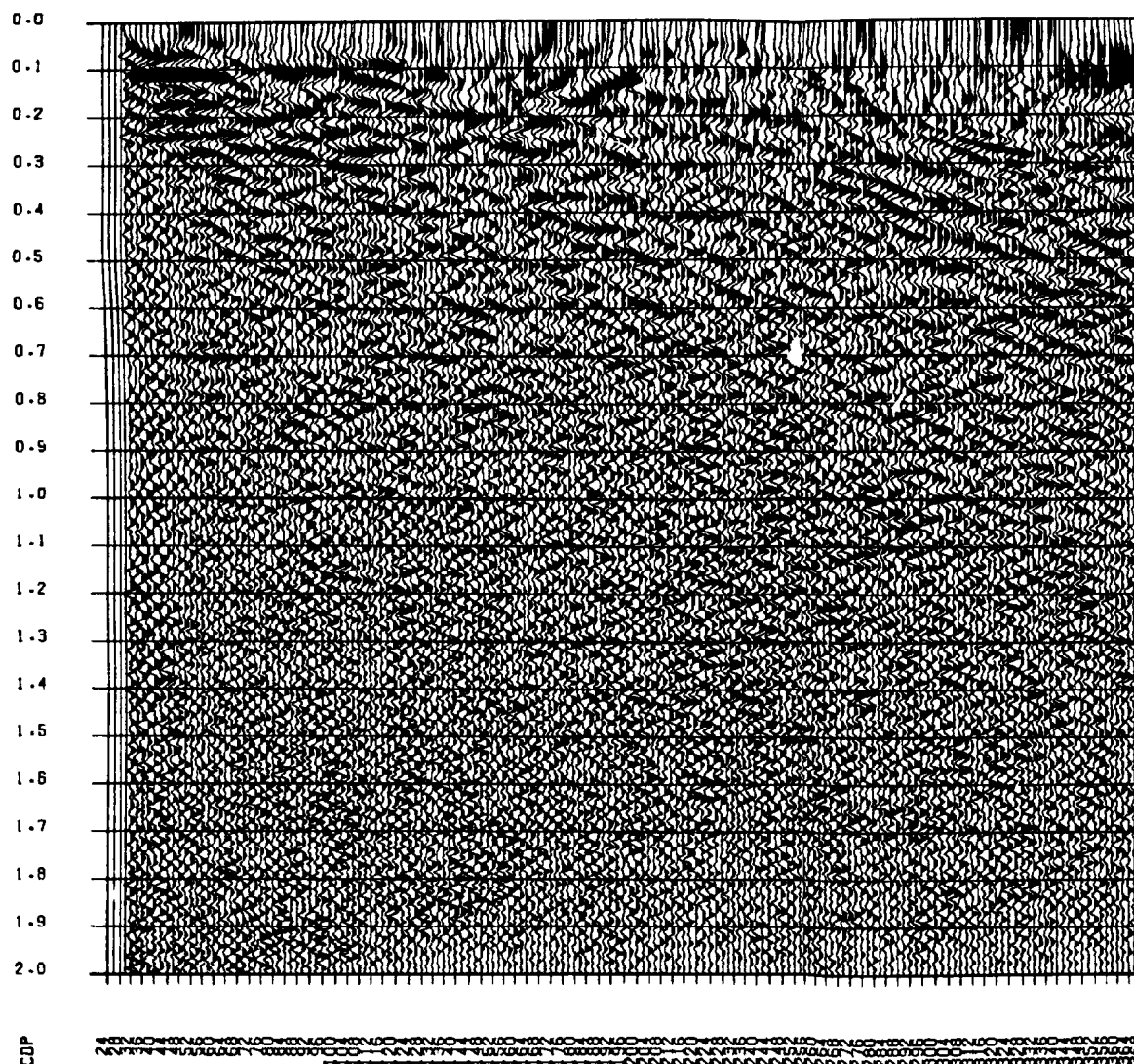
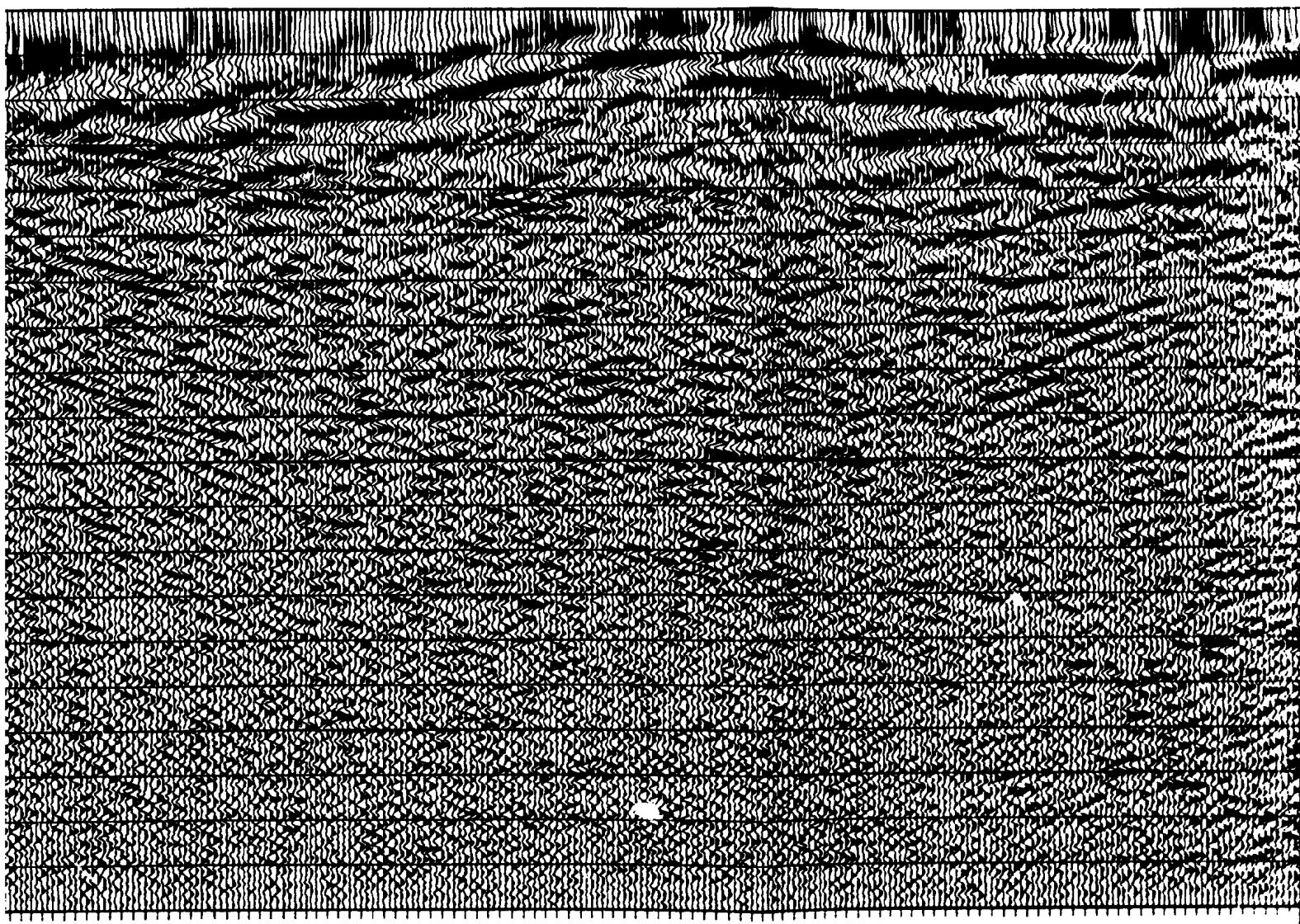


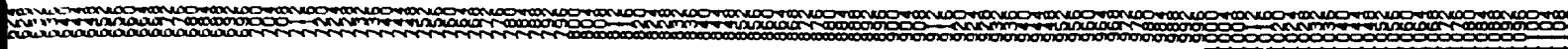
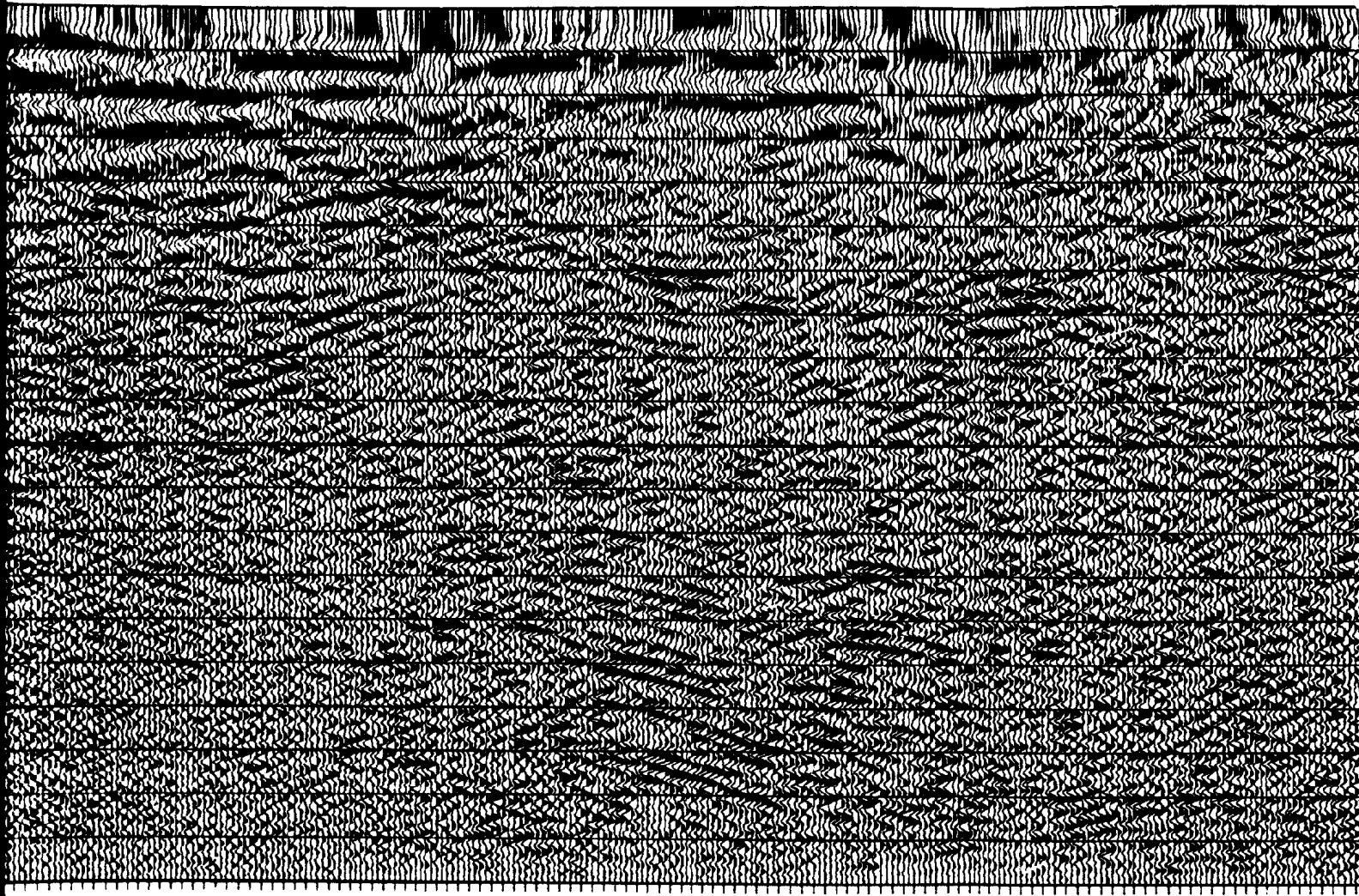
Figure 3.7 (f). Constant velocity stack. The marks indicate velocity picks.

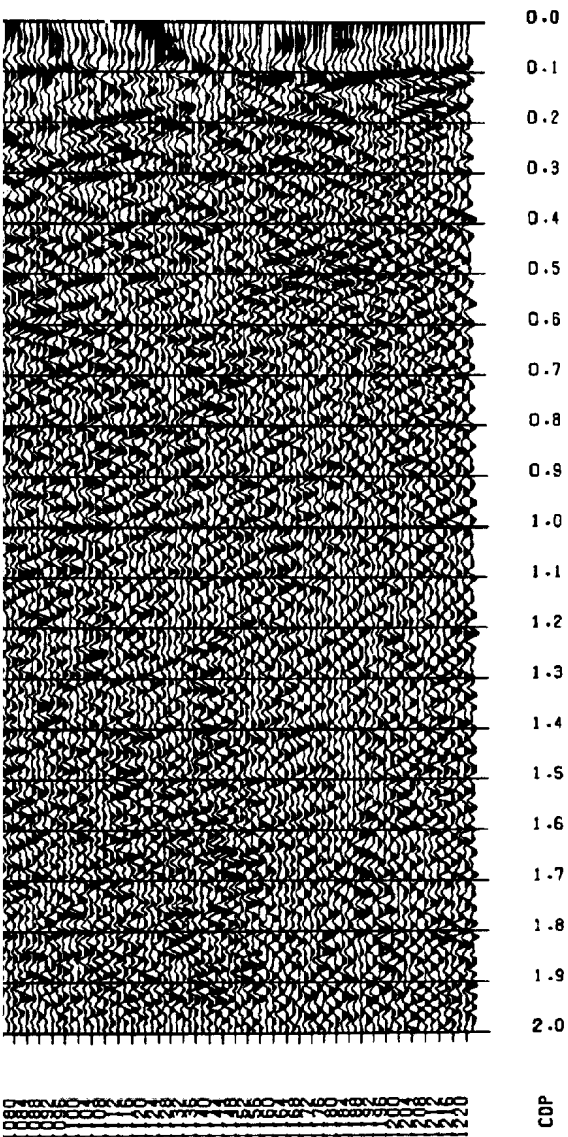
y stack of 3000 m/s, blue



1

7





ROBINSONS RIVER LINE, 1989
CONSTANT VELOCITY STACK - VEL = 2900 M/S

CDP 0.0 0.1 0.2 0.3 0.4 0.5 0.6 0.7 0.8 0.9 1.0 1.1 1.2 1.3 1.4 1.5 1.6 1.7 1.8 1.9 2.0

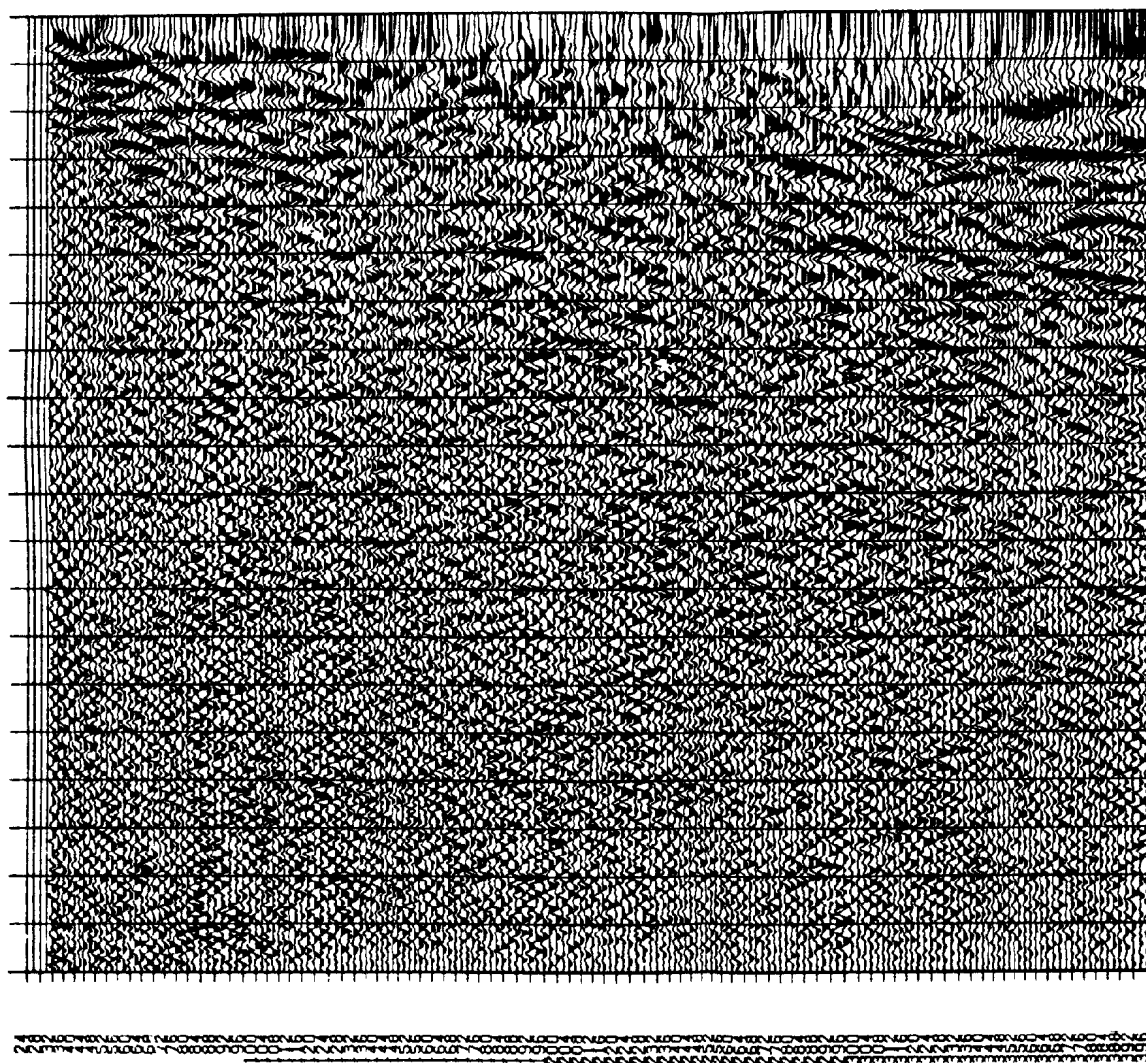
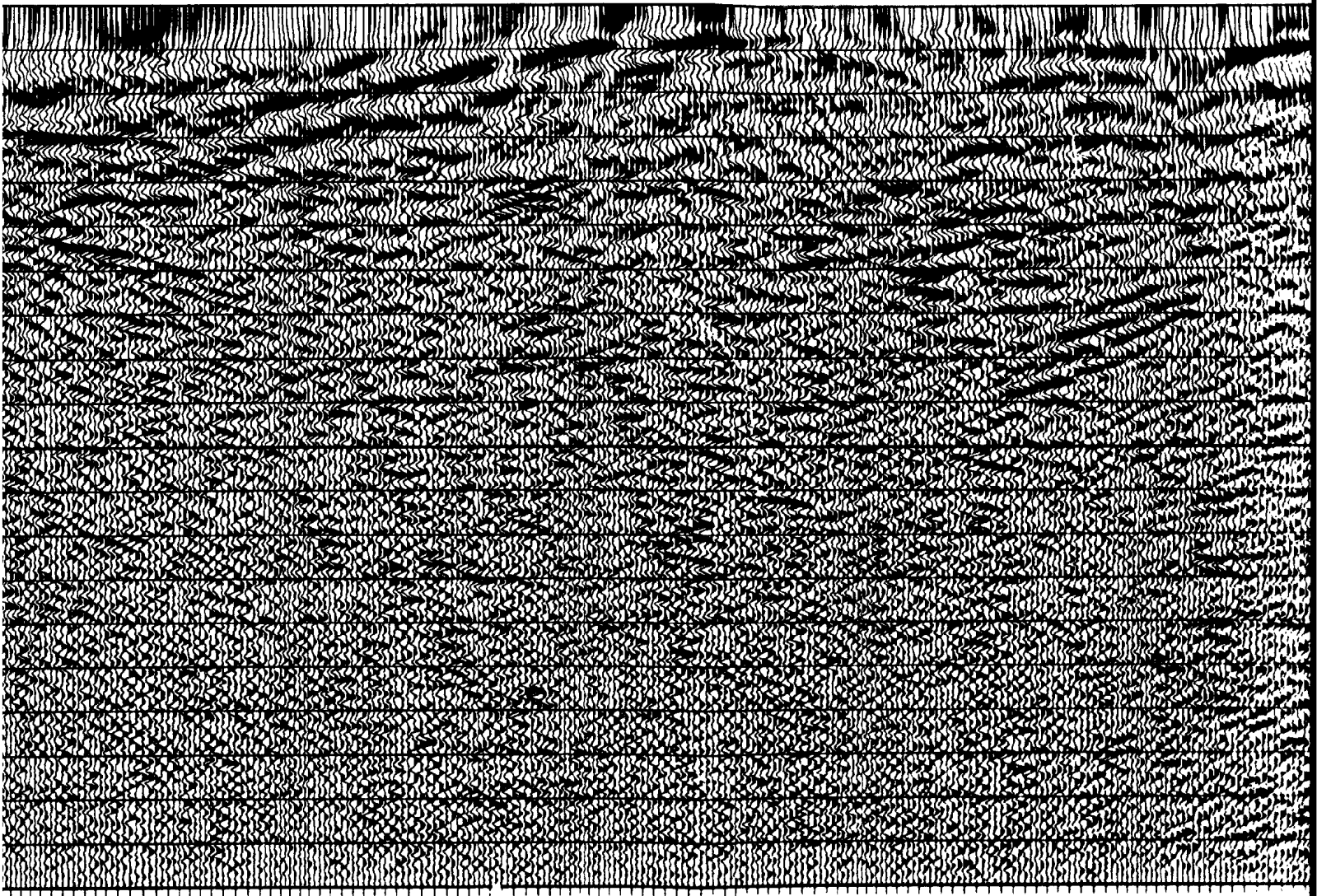


Figure 3.7 (e). Constant velocity stack marks indicate velocity picks.

ocity stack of 2900 m/s, blue
.S.

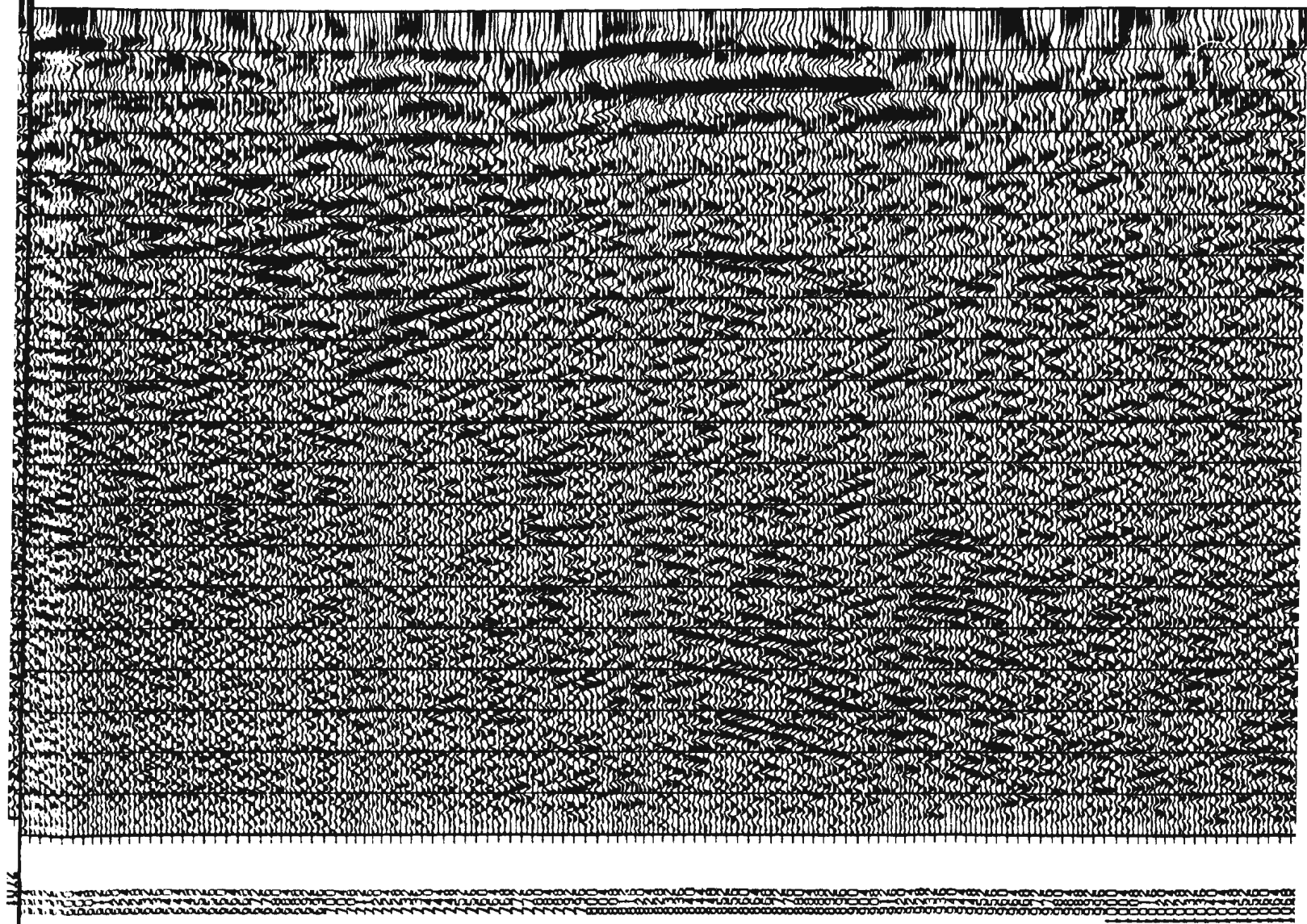


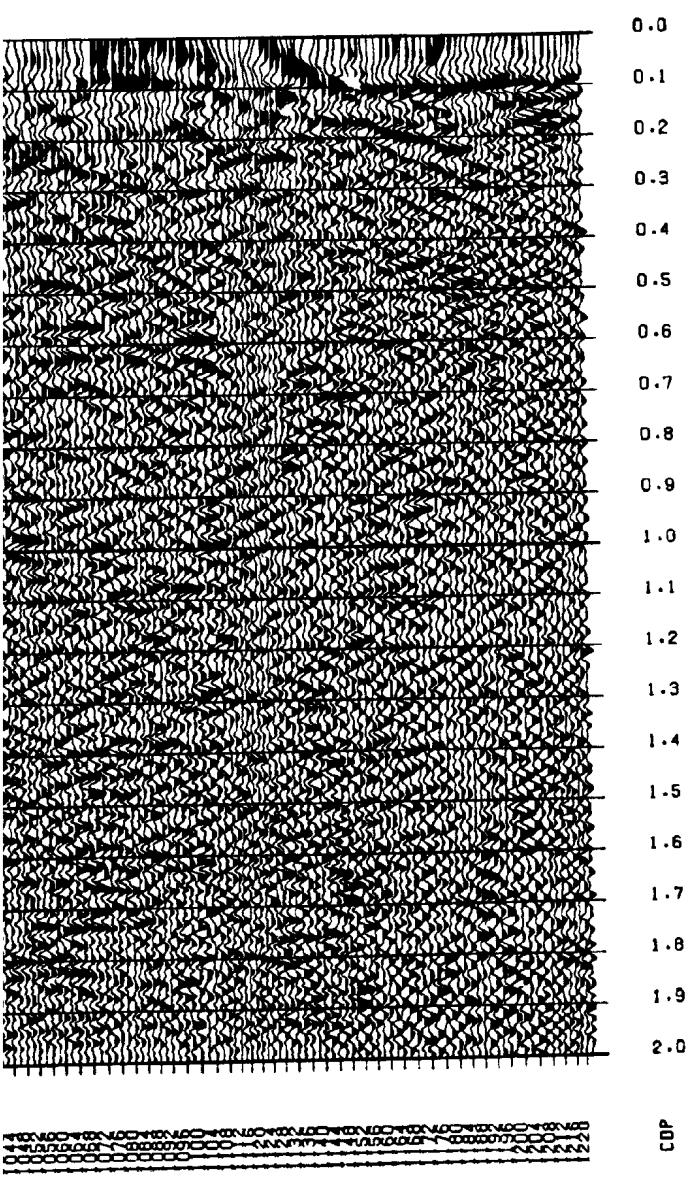
WAVELENGTHS OF 2900 M/S, BLUE
S.

1

1

9





ROBINSONS RIVER LINE, 1989
CONSTANT VELOCITY STACK - VEL = 2800 M/S

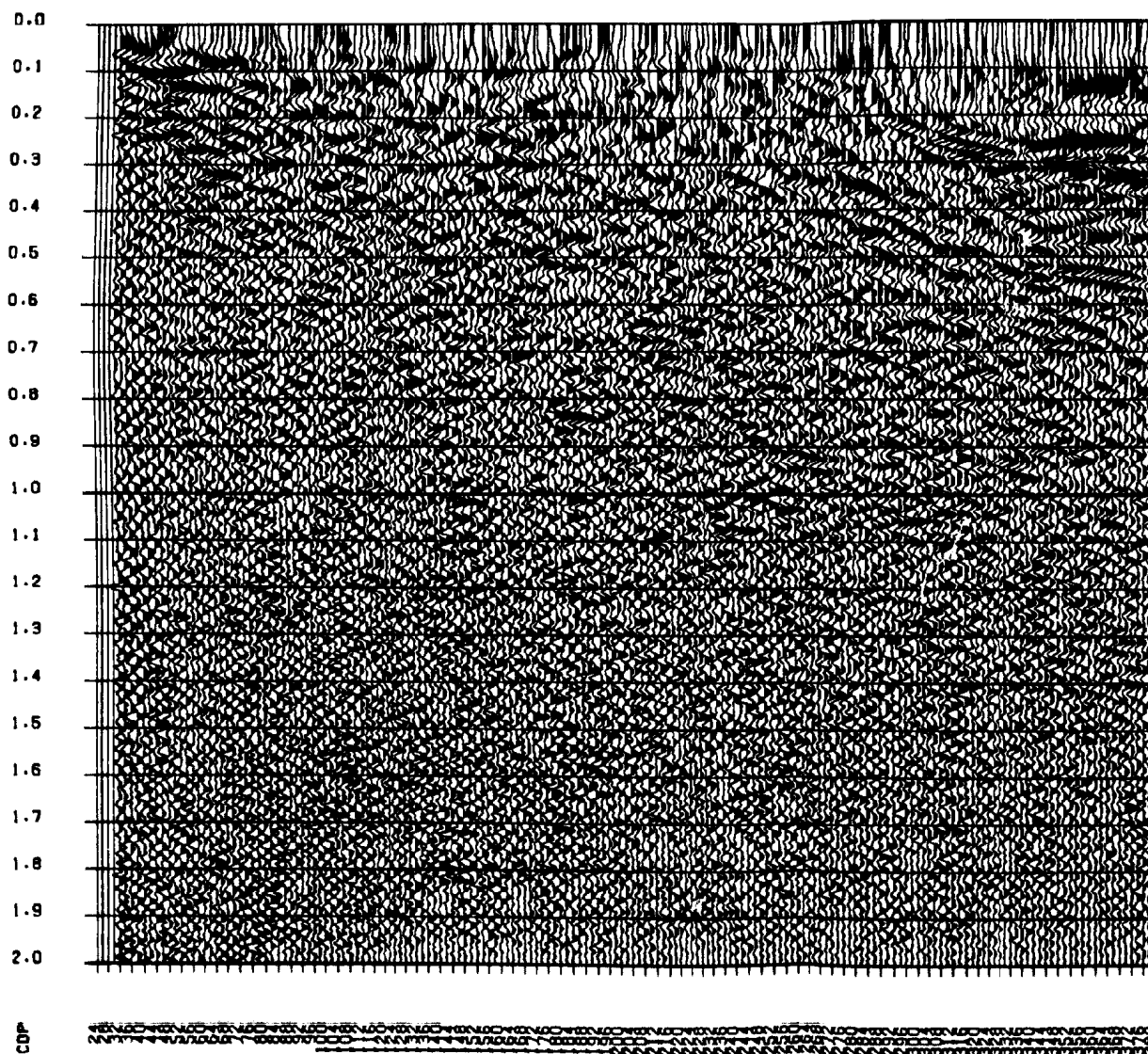
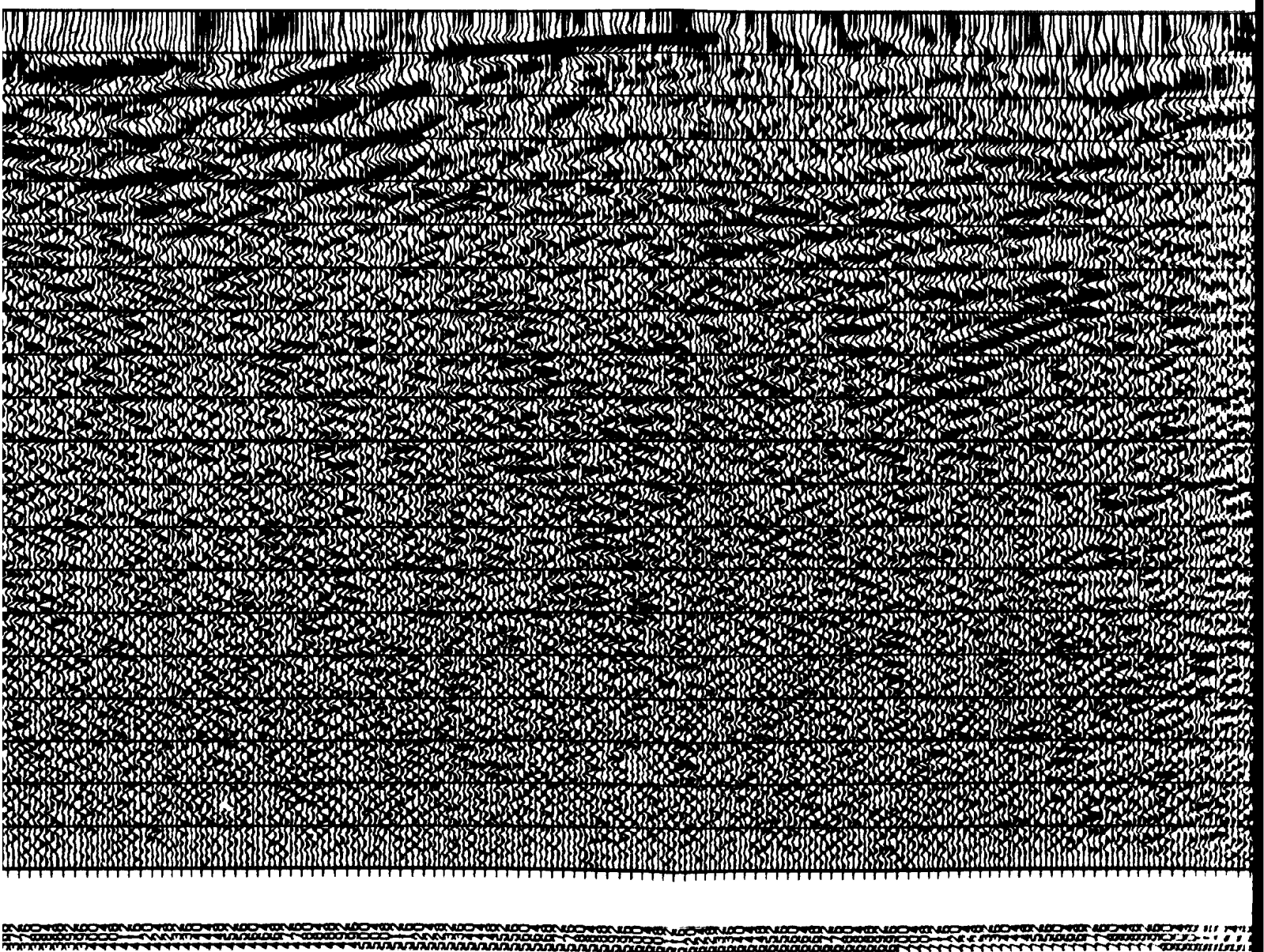
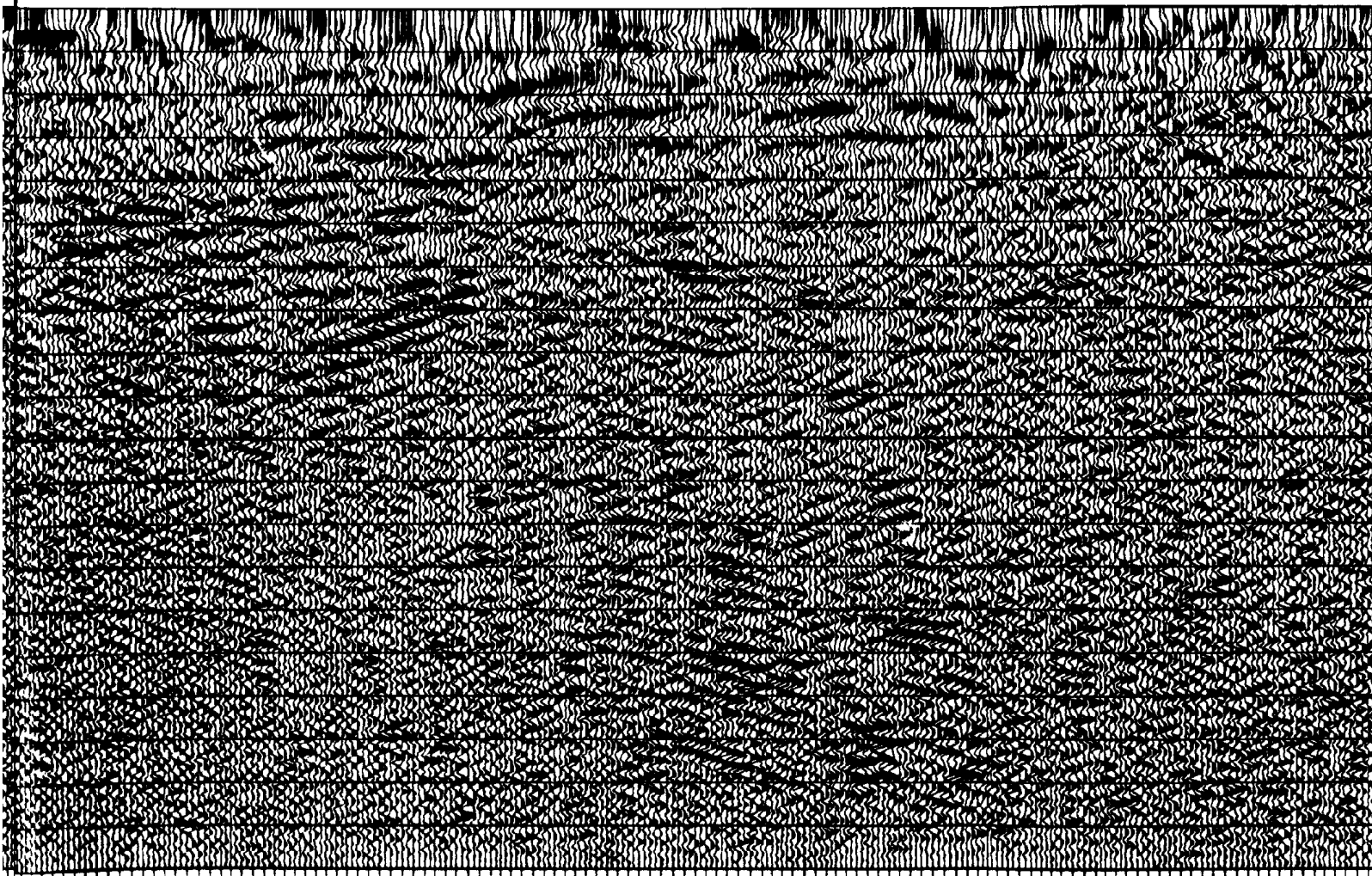
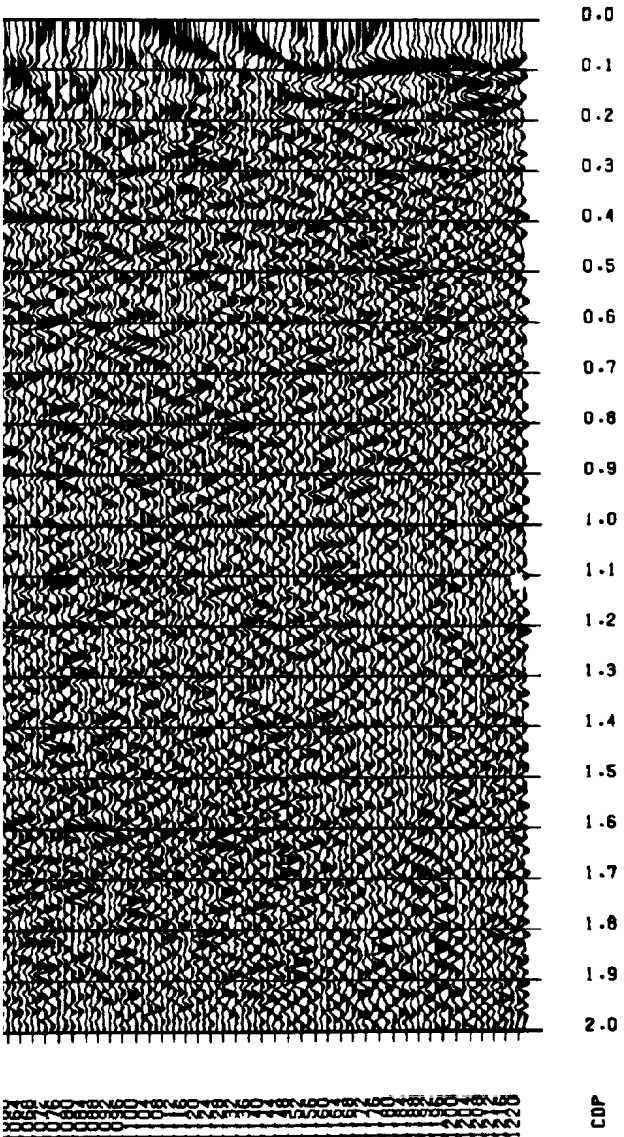


Figure 3.7 (d). Constant velocity stack marks indicate velocity picks.

ck of 2800 m/s, blue







ROBINSONS RIVER LINE, 1989
CONSTANT VELOCITY STACK - VEL = 2700 M/S

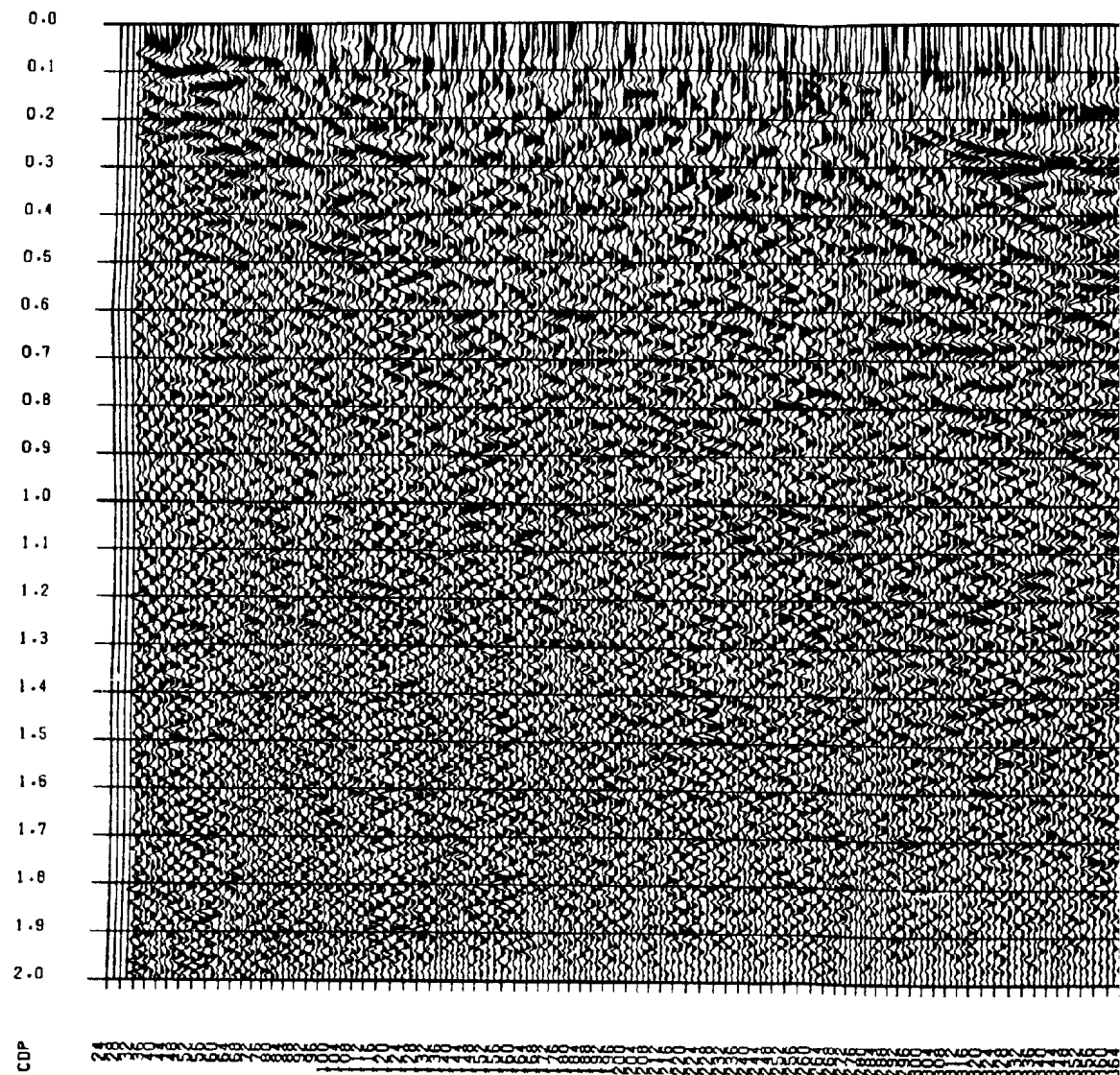
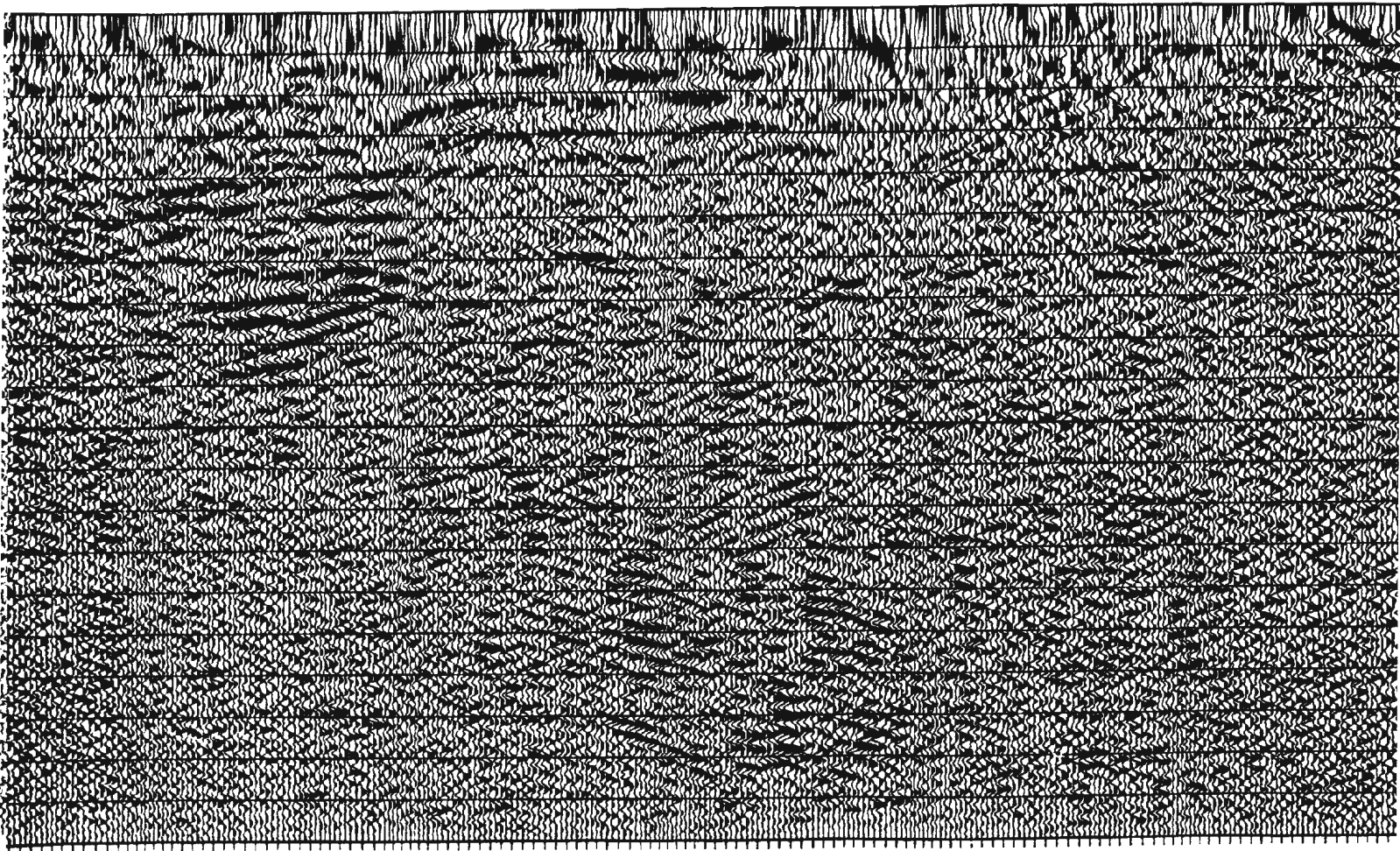
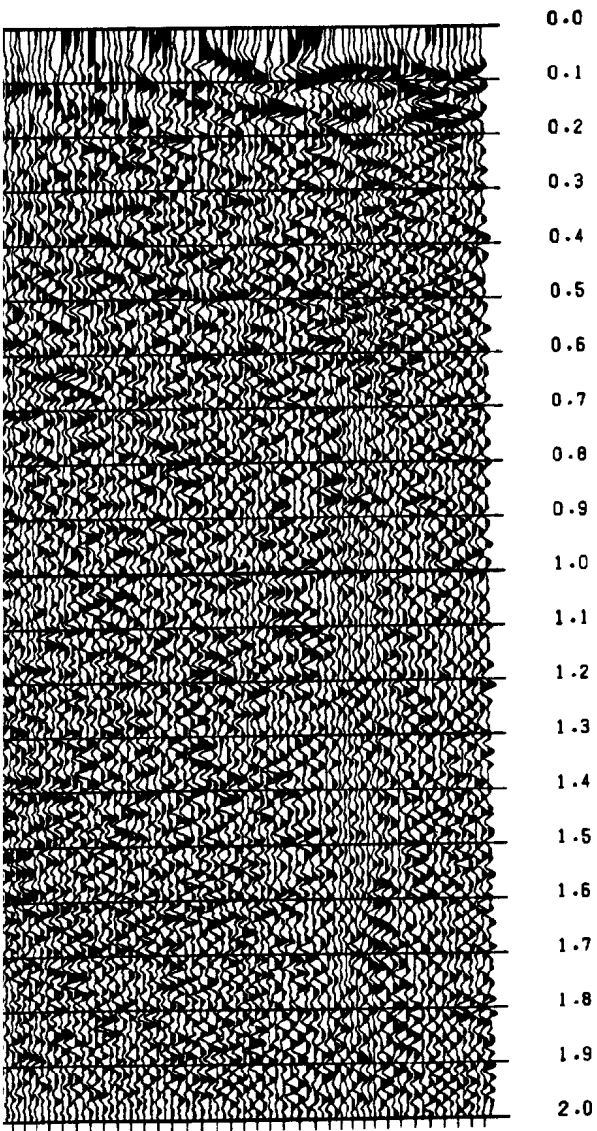


Figure 3.7 (c). Constant marks indicate velocity



1 7 1
0





001 002 003 004 005 006 007 008 009 010 011 012 013 014 015 016 017 018 019 020 021 022 023 024 025 026 027 028 029 030 031 032 033 034 035 036 037 038 039 040 041 042 043 044 045 046 047 048 049 050 051 052 053 054 055 056 057 058 059 060 061 062 063 064 065 066 067 068 069 070 071 072 073 074 075 076 077 078 079 080 081 082 083 084 085 086 087 088 089 090 091 092 093 094 095 096 097 098 099 100

CDP

ROBINSONS RIVER LINE, 1989
CONSTANT VELOCITY STACK - VEL = 2600 M/S

0.0
0.1
0.2
0.3
0.4
0.5
0.6
0.7
0.8
0.9
1.0
1.1
1.2
1.3
1.4
1.5
1.6
1.7
1.8
1.9
2.0

CDP

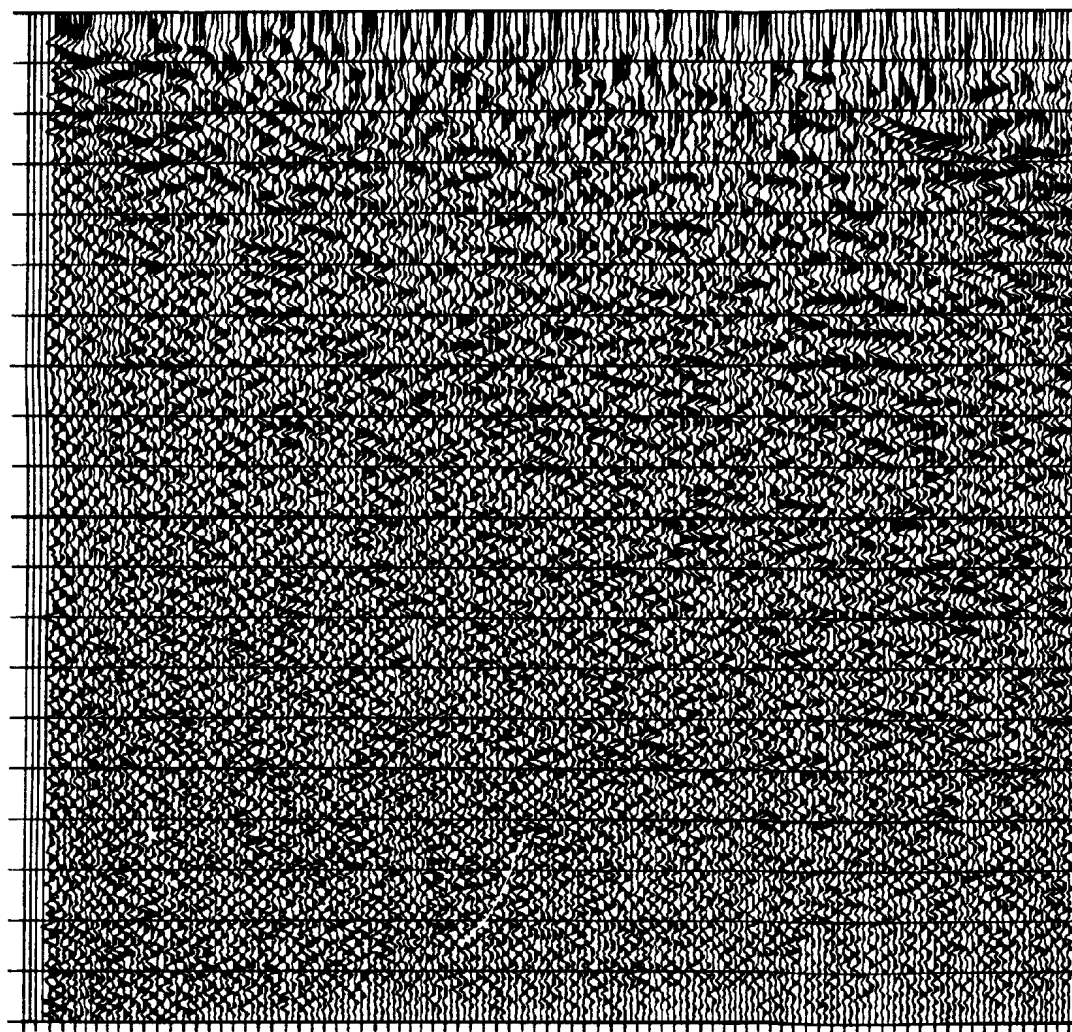
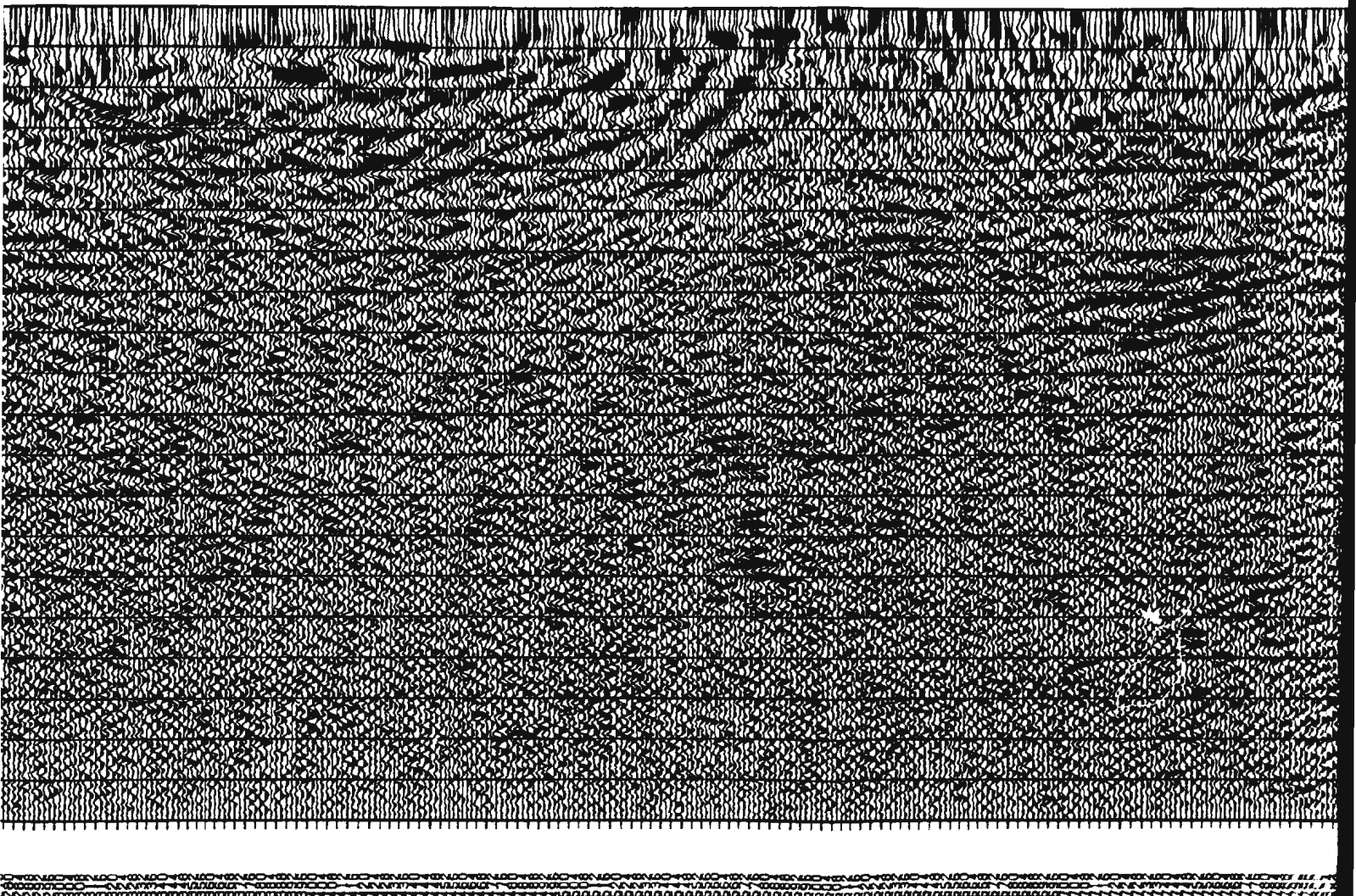


Figure 3.7 (b). Constant velocity stack. The marks indicate velocity pick

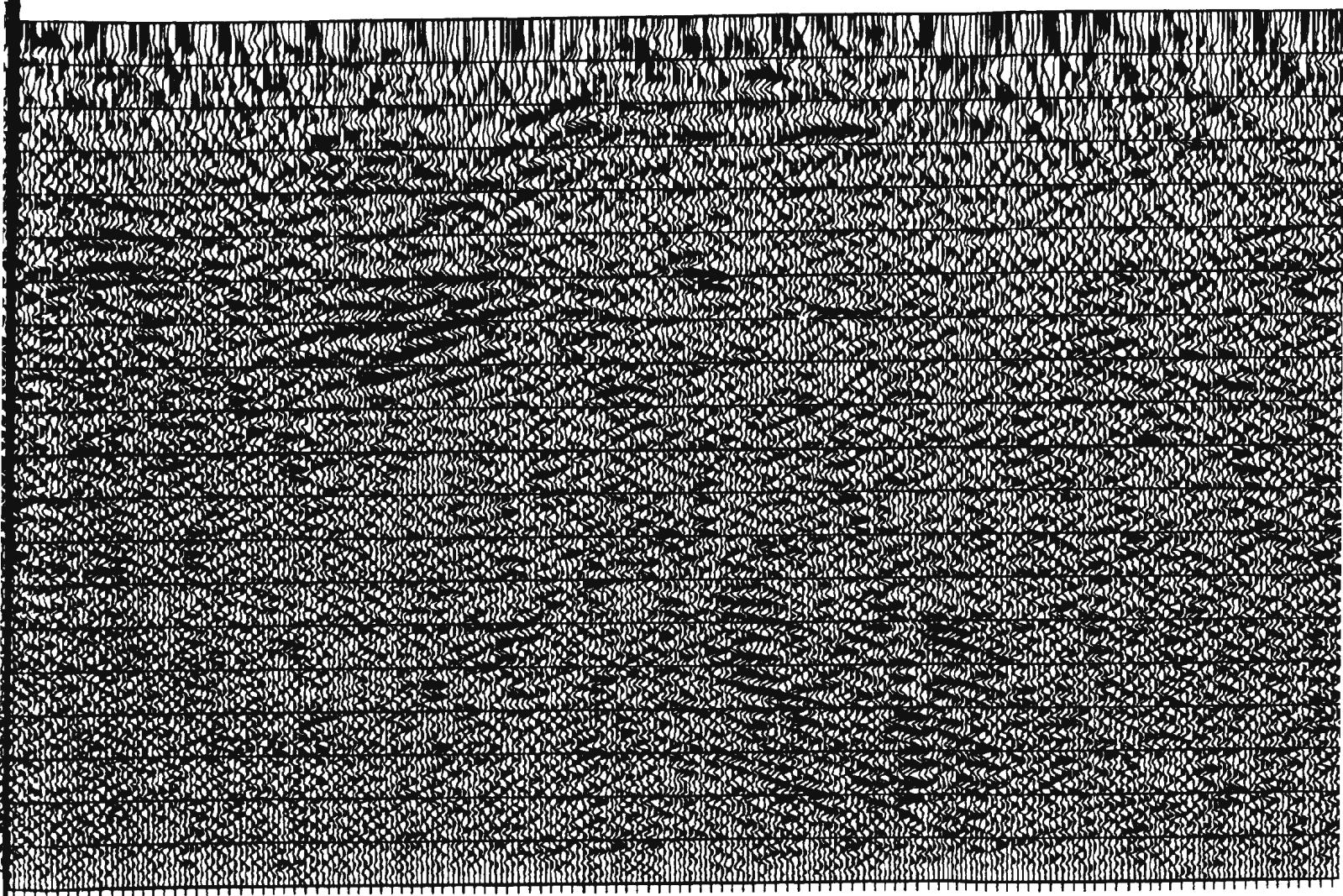
1

b). Constant velocity stack of 2600 m/s, blue
ate velocity picks.



1

1



ROBINSONS RIVER LINE, 1989
CONSTANT VELOCITY STACK - VEL = 2500 M/S

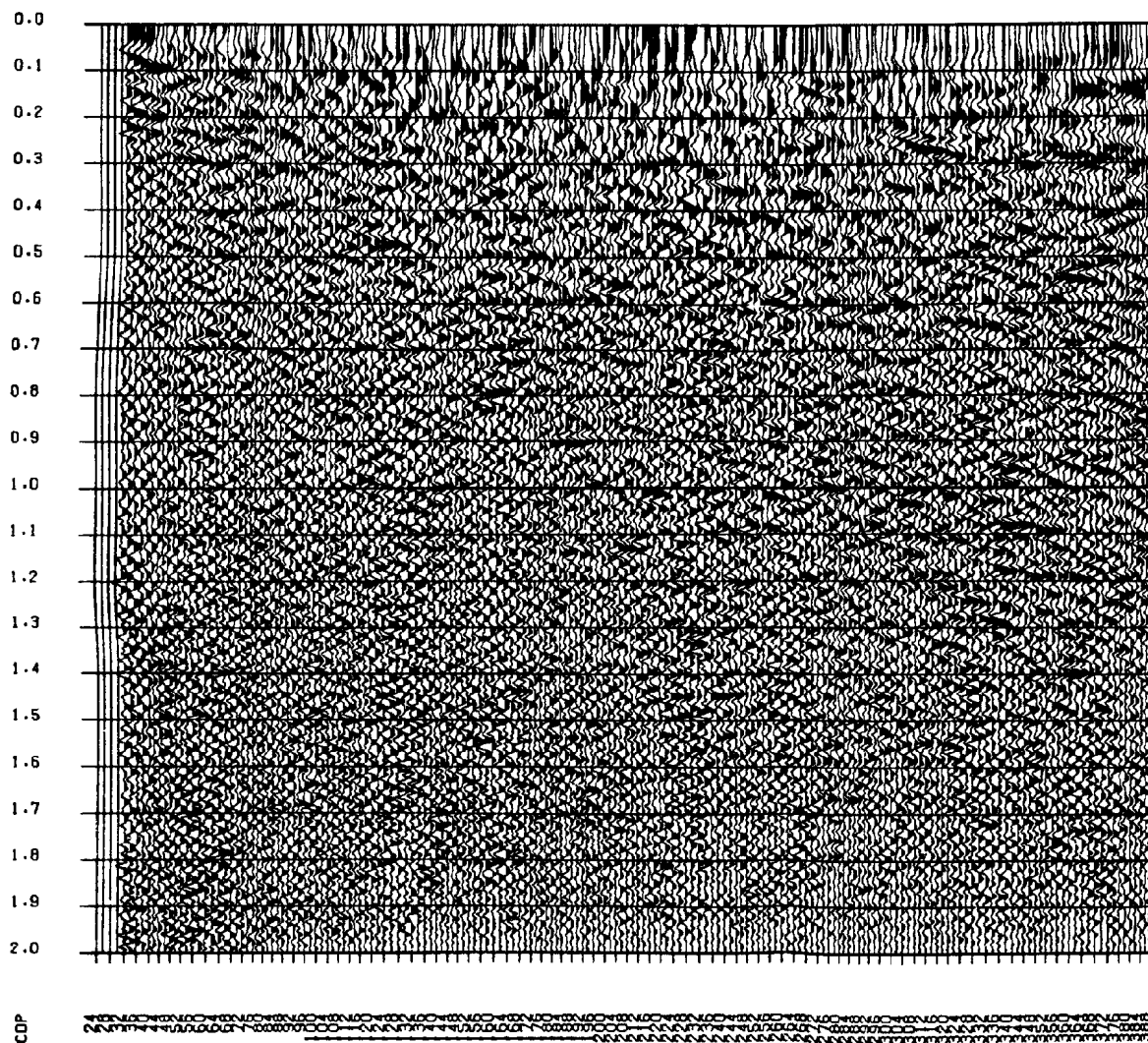
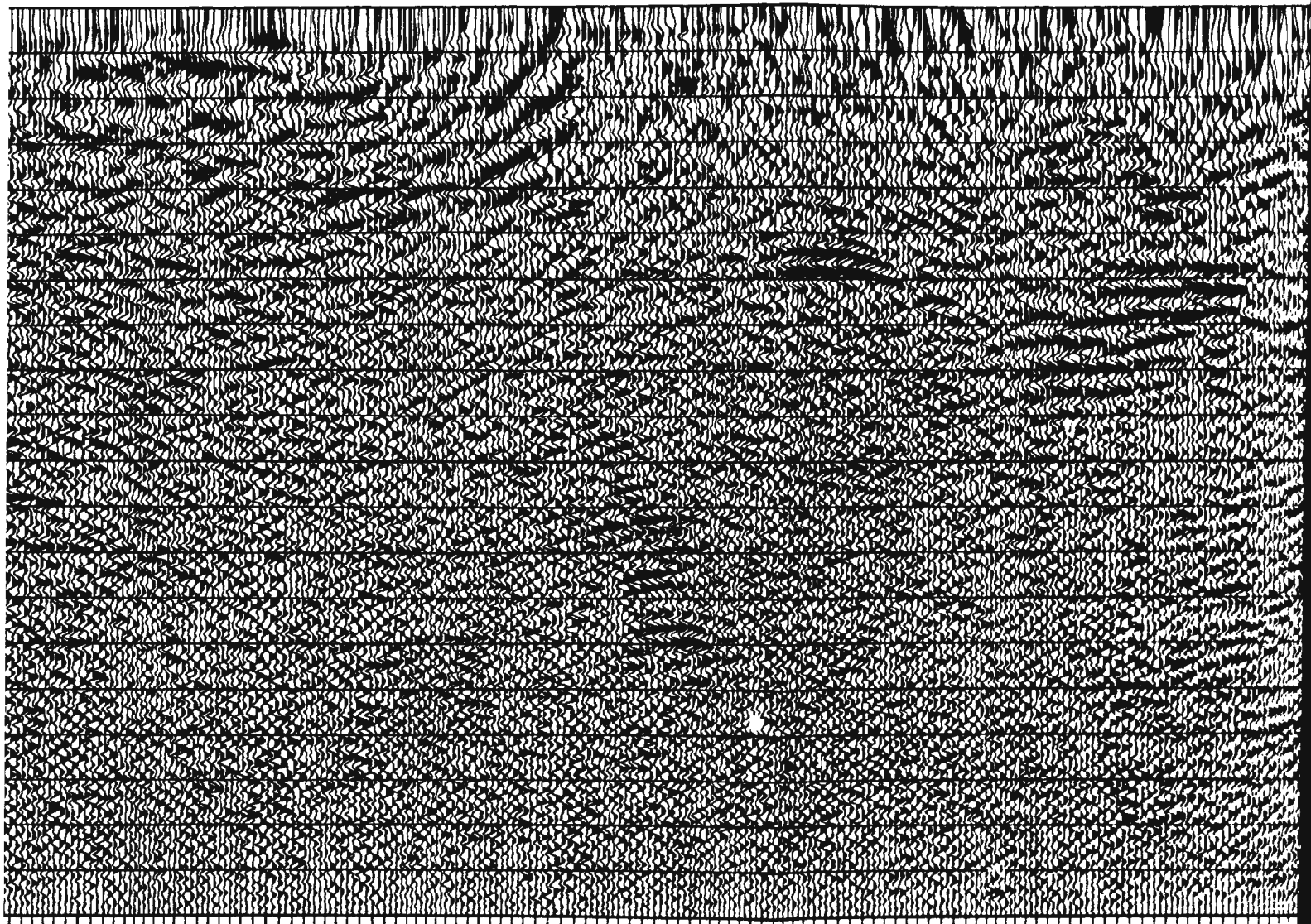
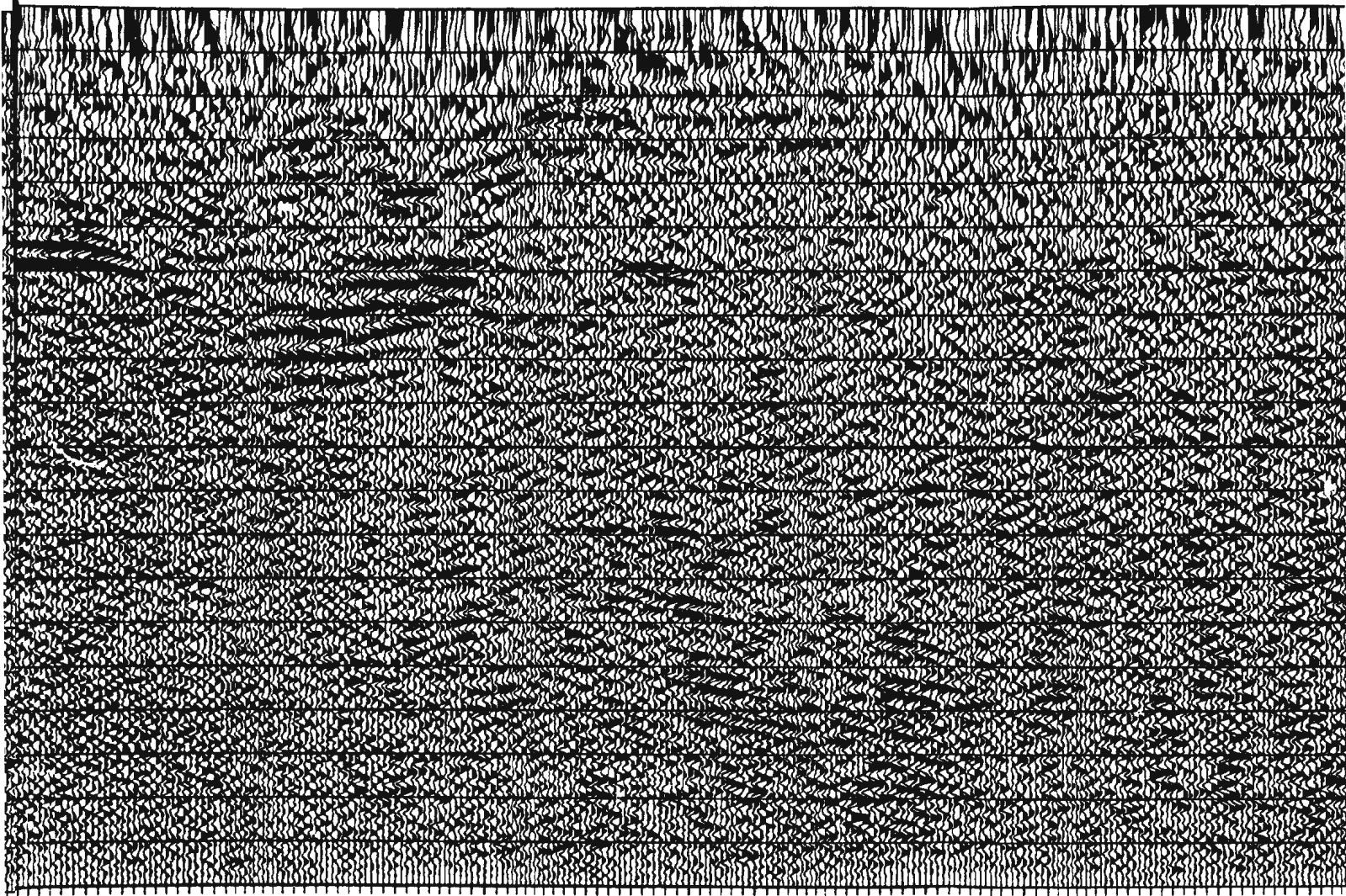


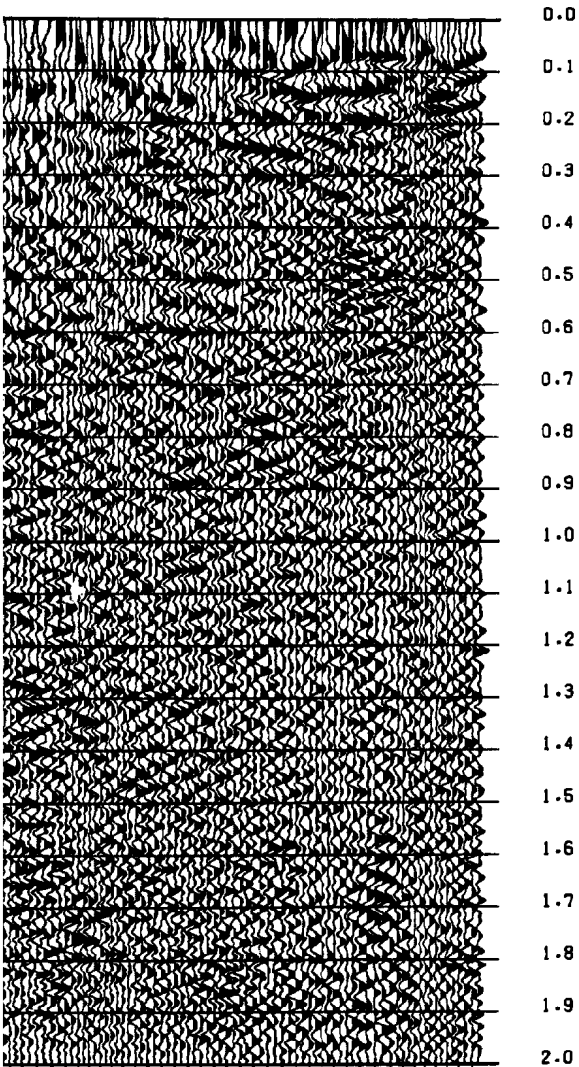
Figure 3.7 (a). Constant velocity stack
velocity picks at this velocity.

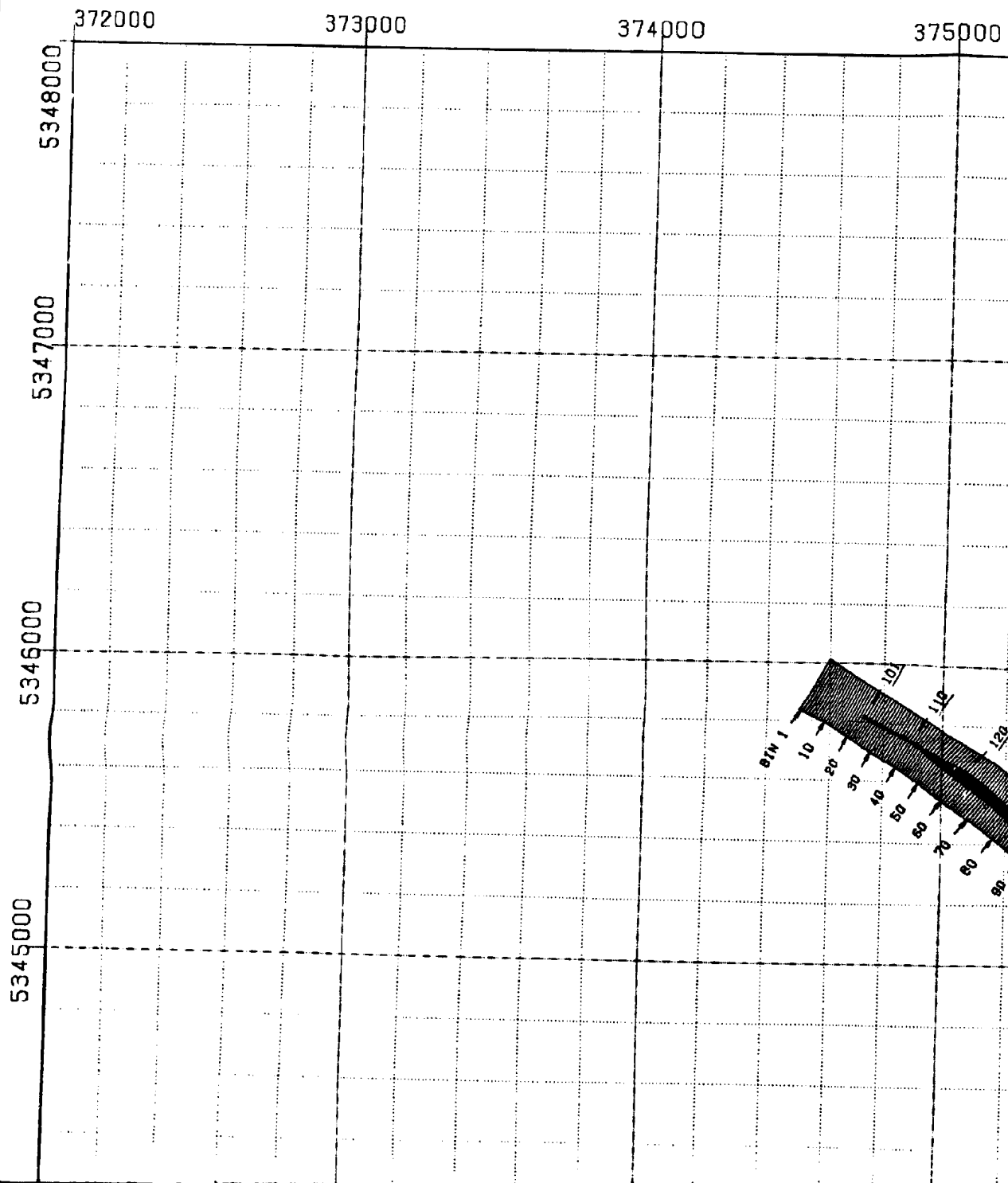
velocity stack of 2500 m/s, no
ity.



T



A barcode consisting of vertical black bars of varying widths on a white background.
COP

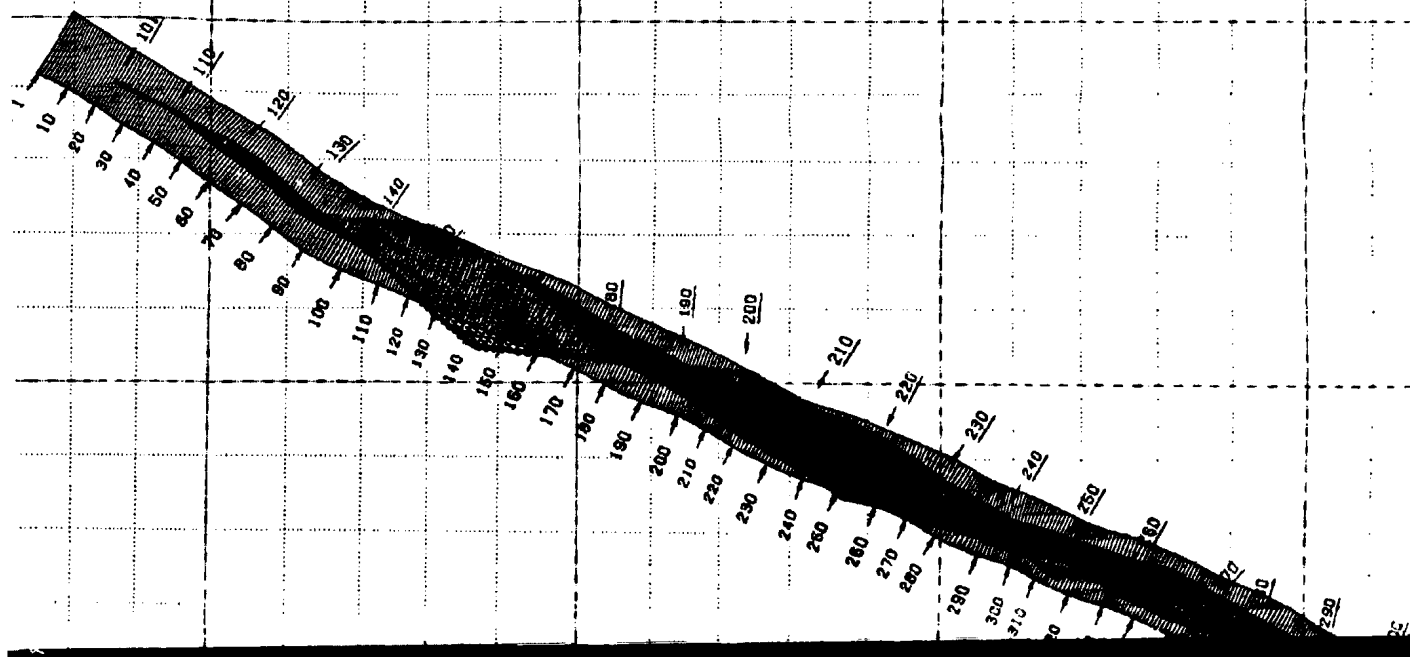


375000

376000

377000

378000



319

386000

387000

388000

5348000

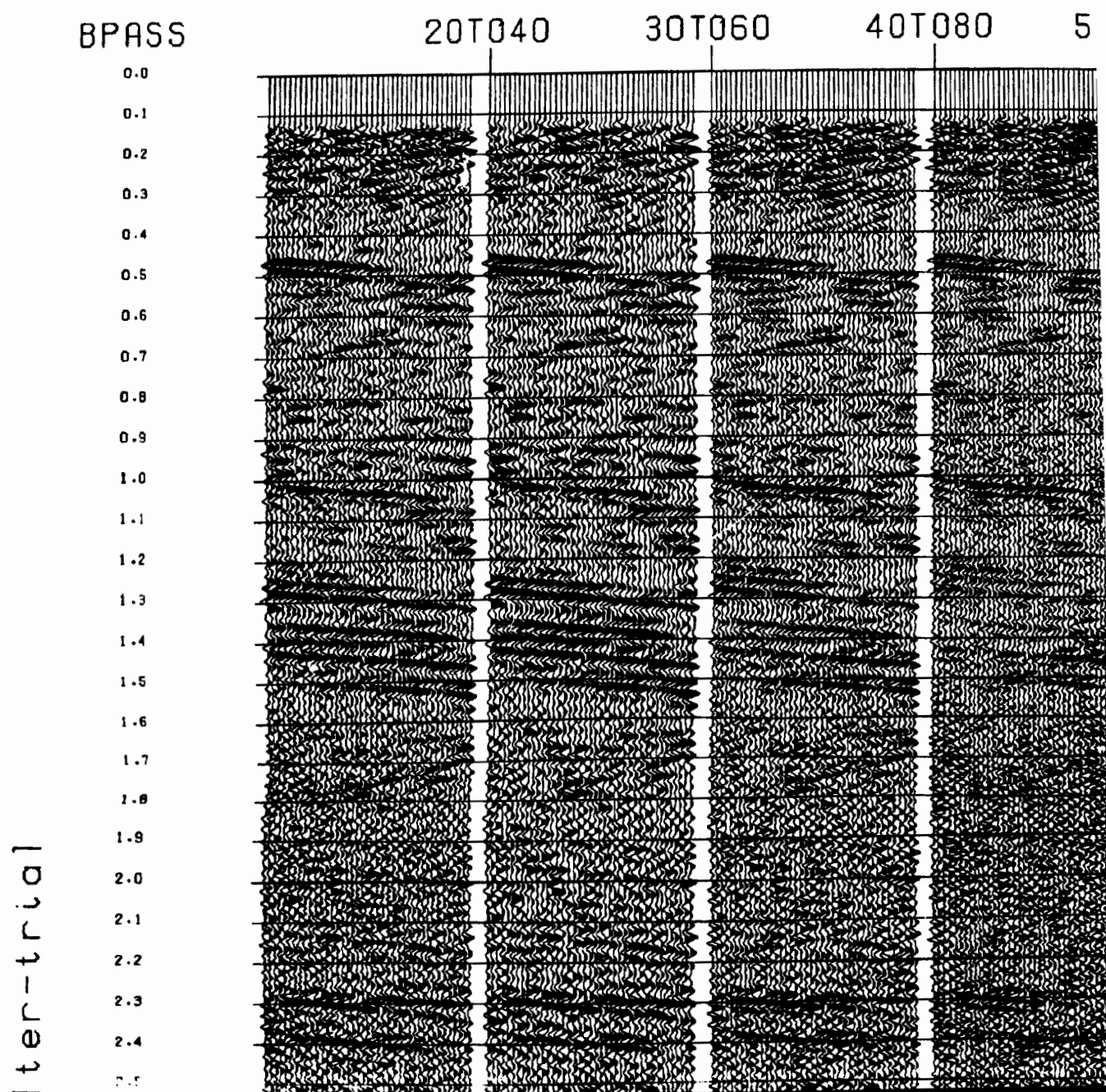
5347000

5346000

5345000

000

Figure 3.19. Bandpass filter test panels of stacked section from CMP 660 to 700. The numbers at the top of the panels indicate range of frequencies passed, for example, 20T040 means only frequencies between 20 to 40 Hz inclusive, were passed in the filter. Note how events get out of focus at high frequencies.



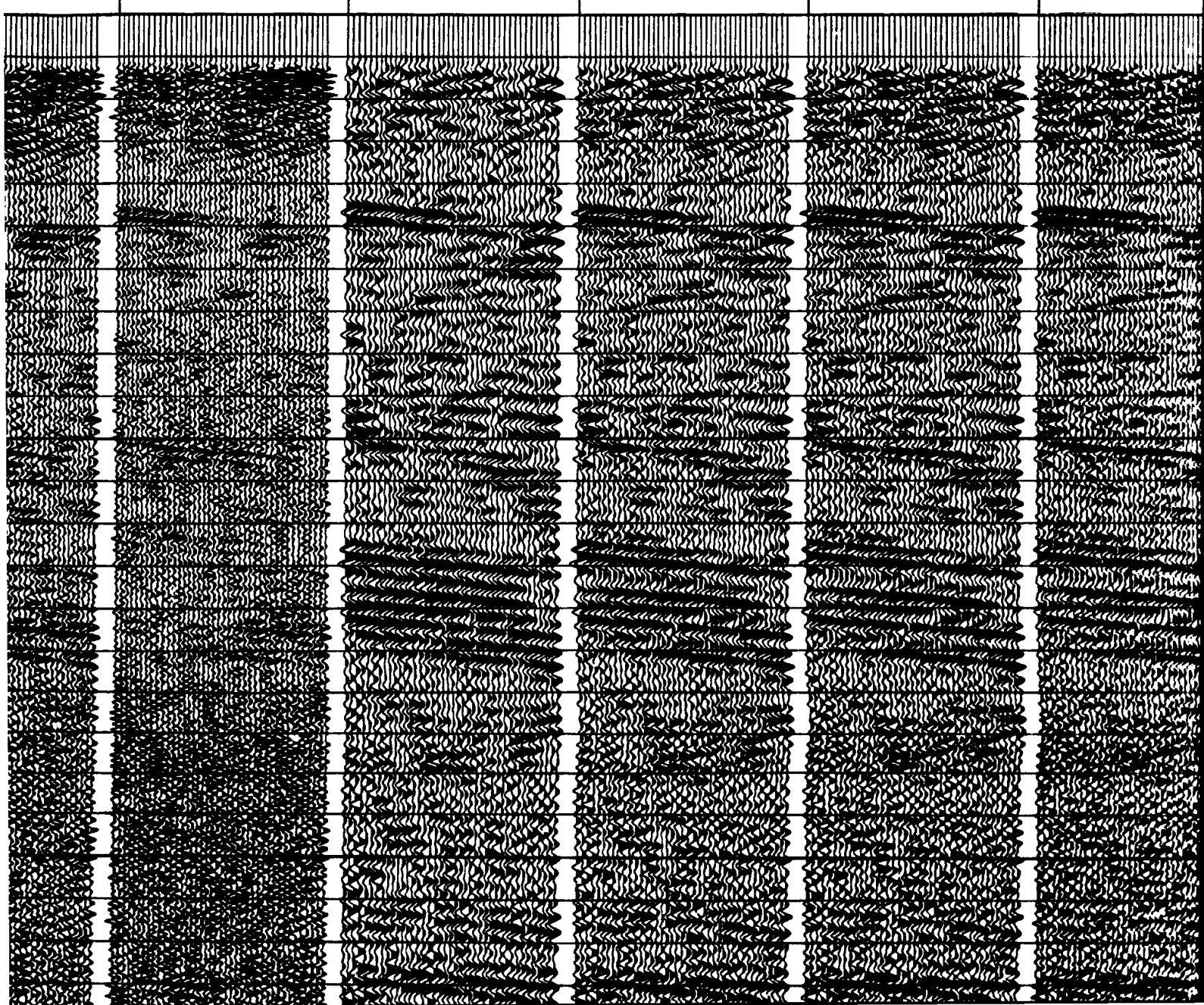
50T0100

20T030

20T040

20T050

20T090



T050

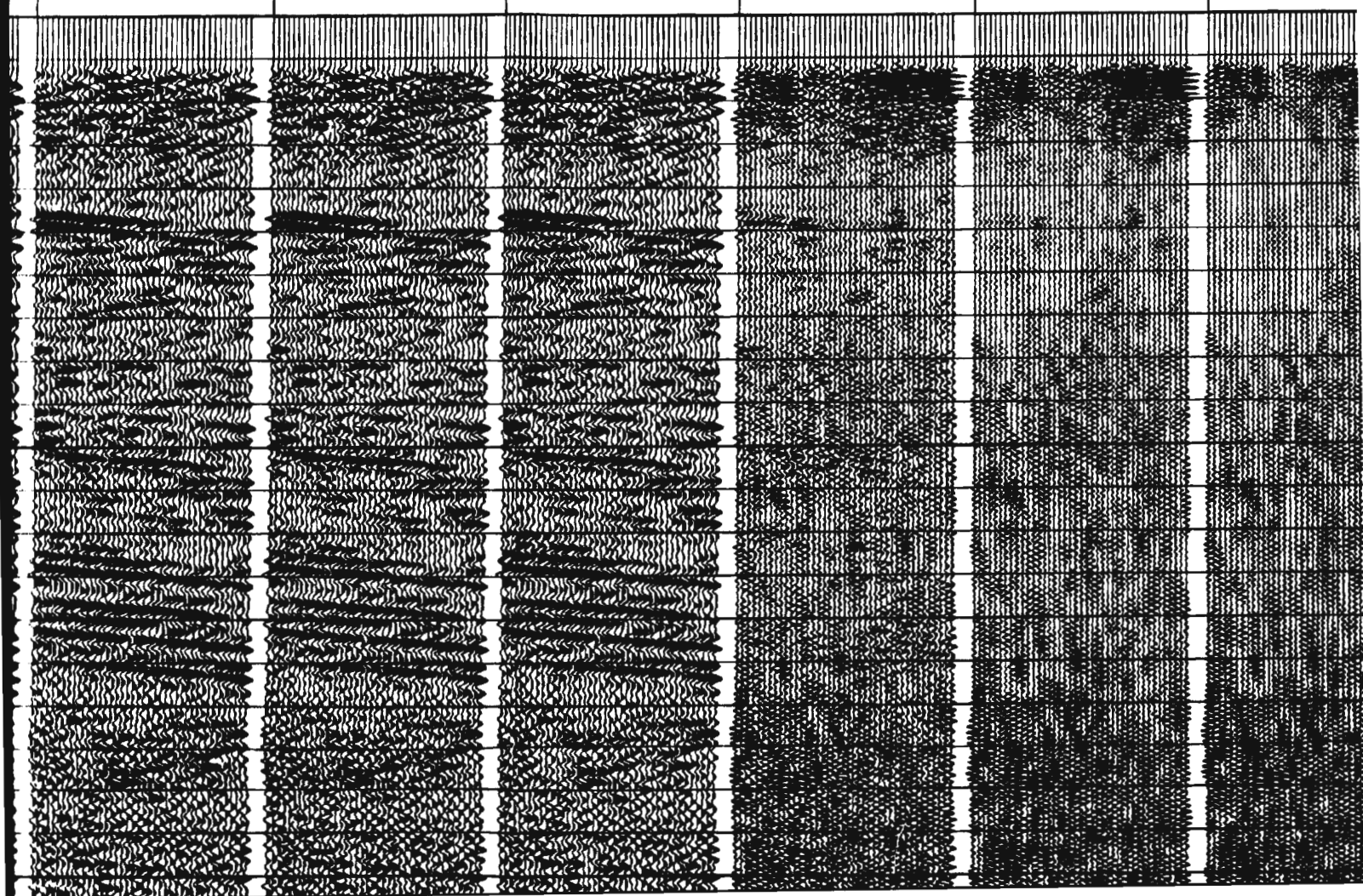
20T090

20T060

60T090

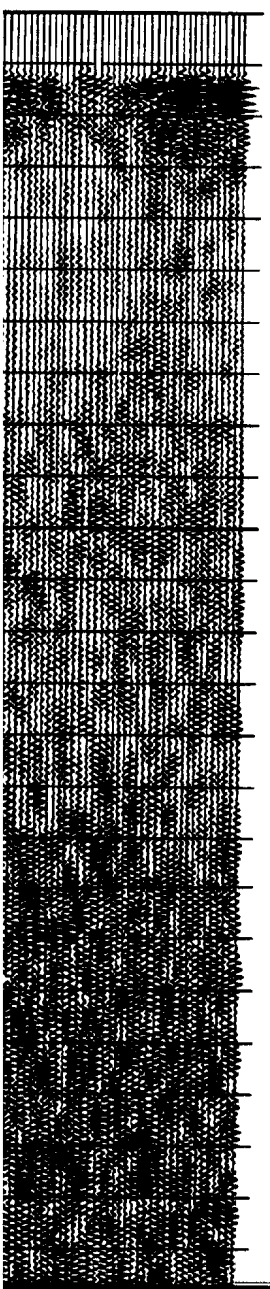
70T090

80T090



090

BPASS



- 0.0
- 0.1
- 0.2
- 0.3
- 0.4
- 0.5
- 0.6
- 0.7
- 0.8
- 0.9
- 1.0
- 1.1
- 1.2
- 1.3
- 1.4
- 1.5
- 1.6
- 1.7
- 1.8
- 1.9
- 2.0
- 2.1
- 2.2
- 2.3
- 2.4



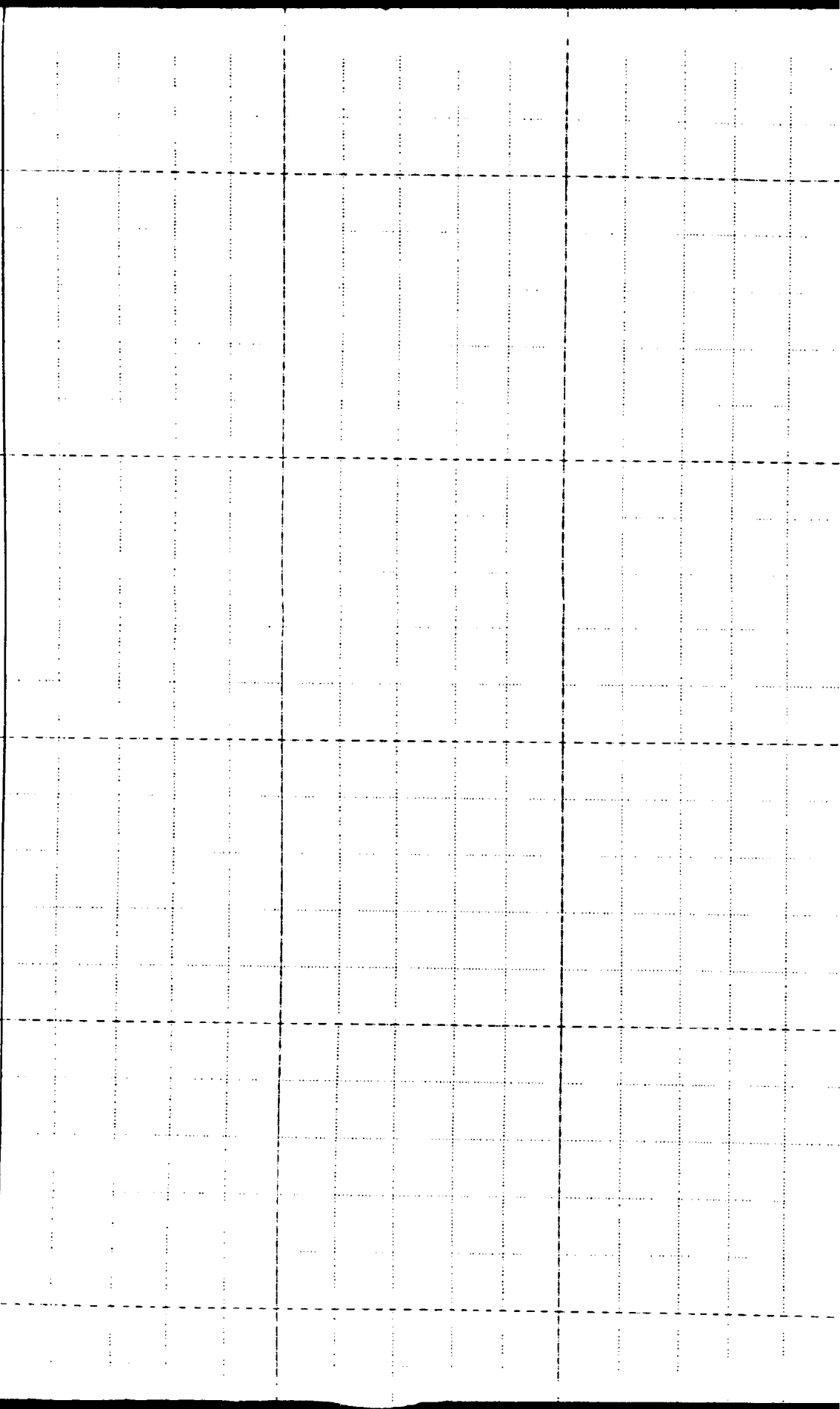
NORTHING
5343000

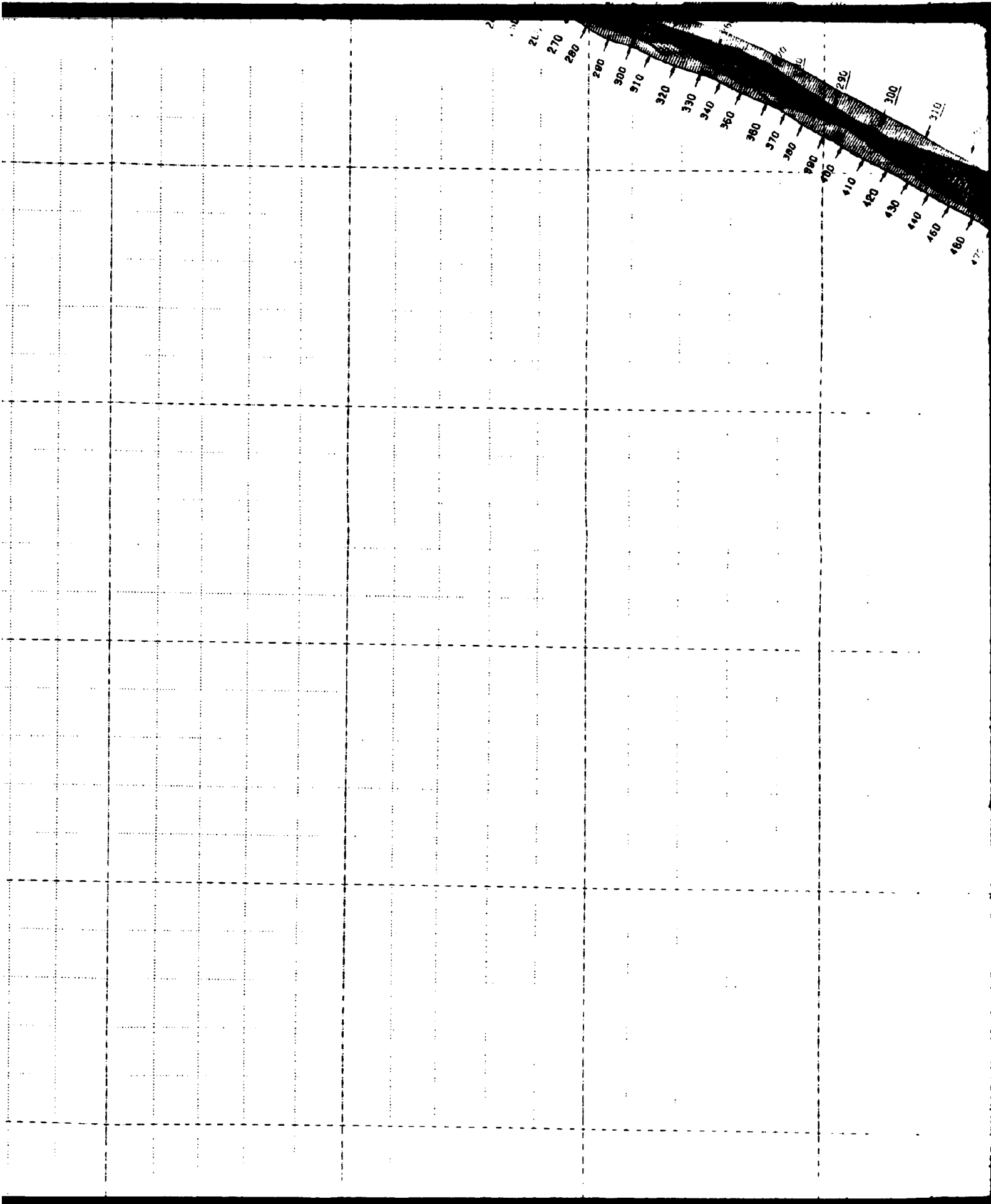
5344000

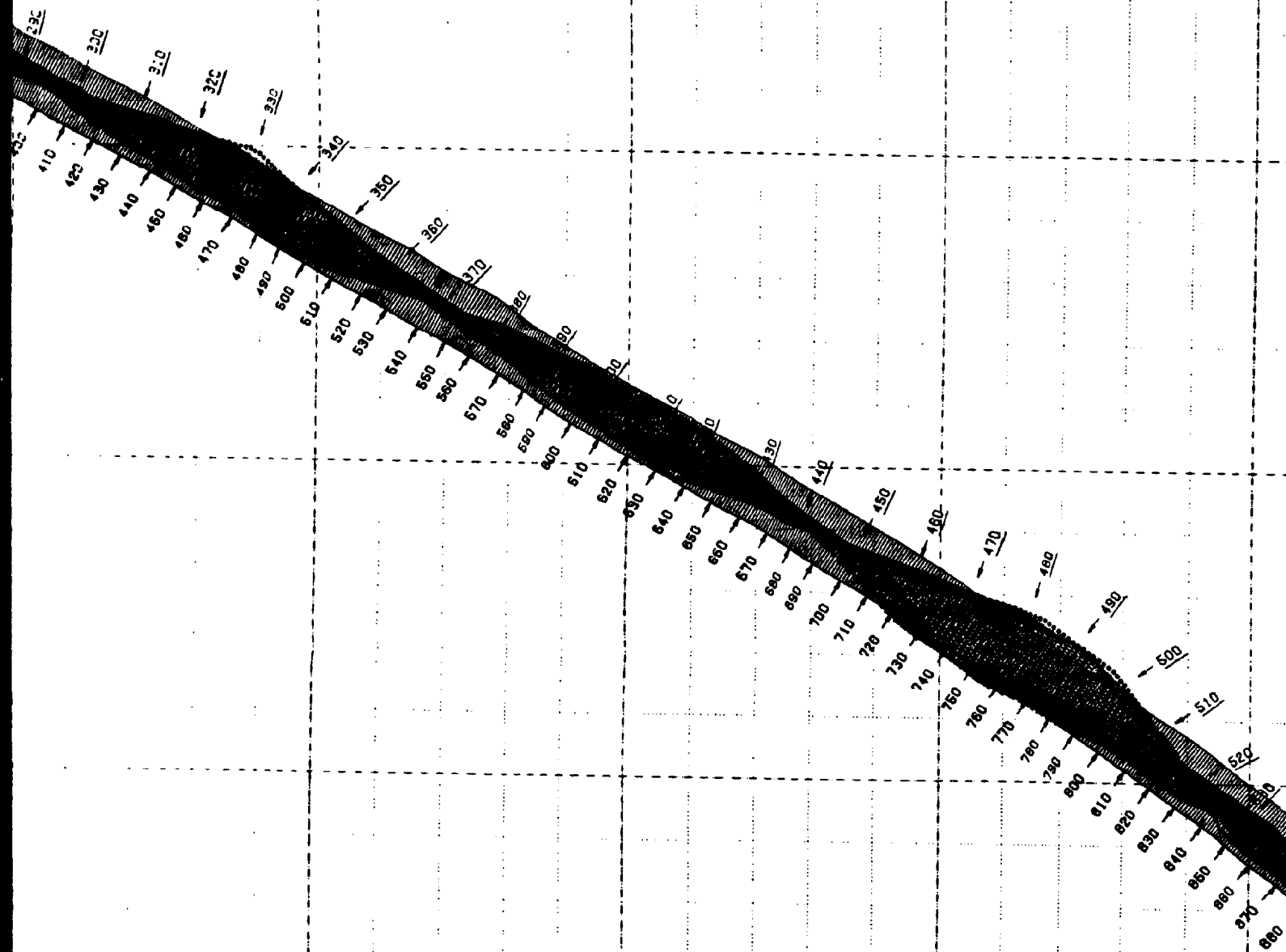
5342000

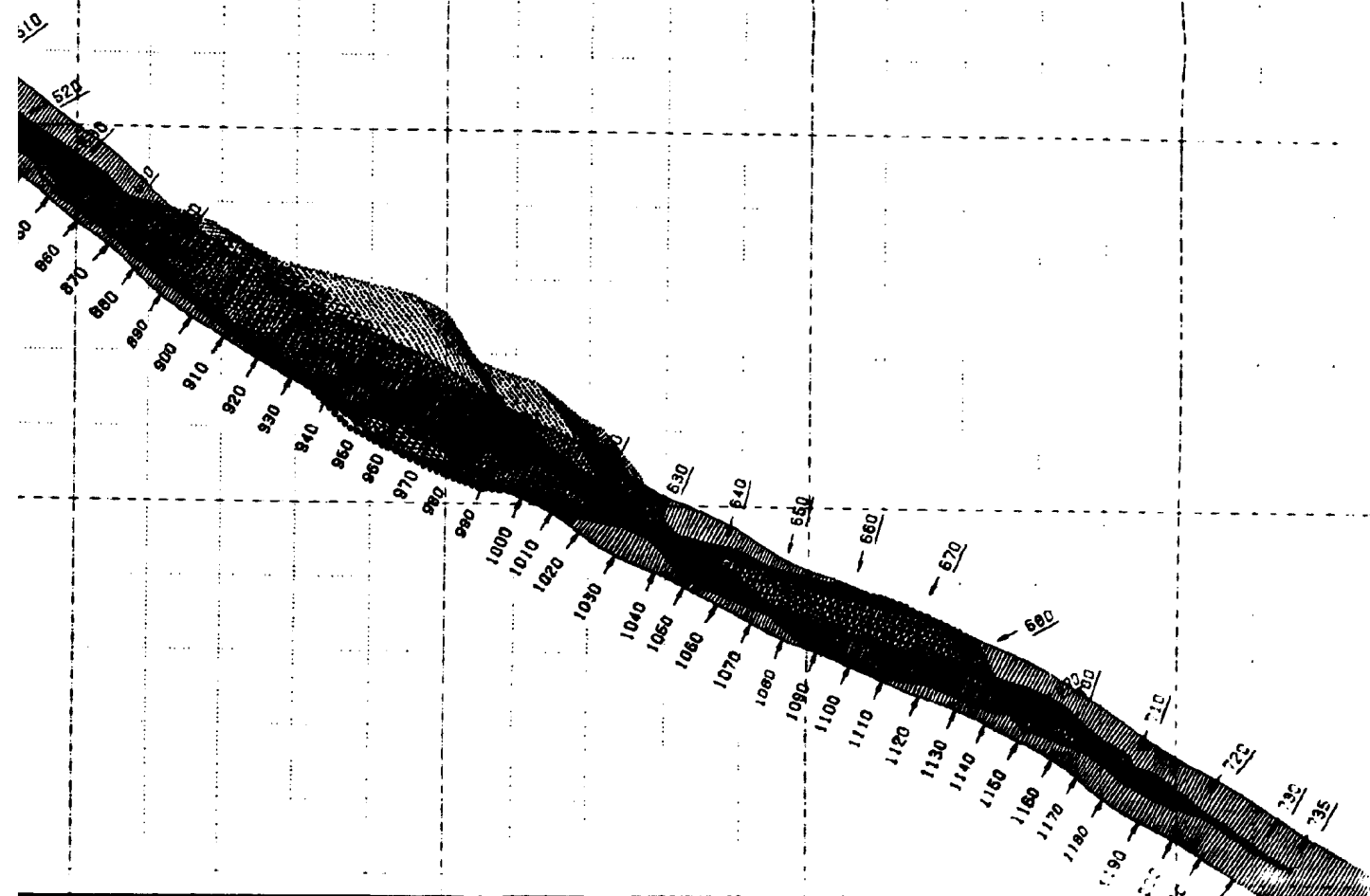
5341000

5340000









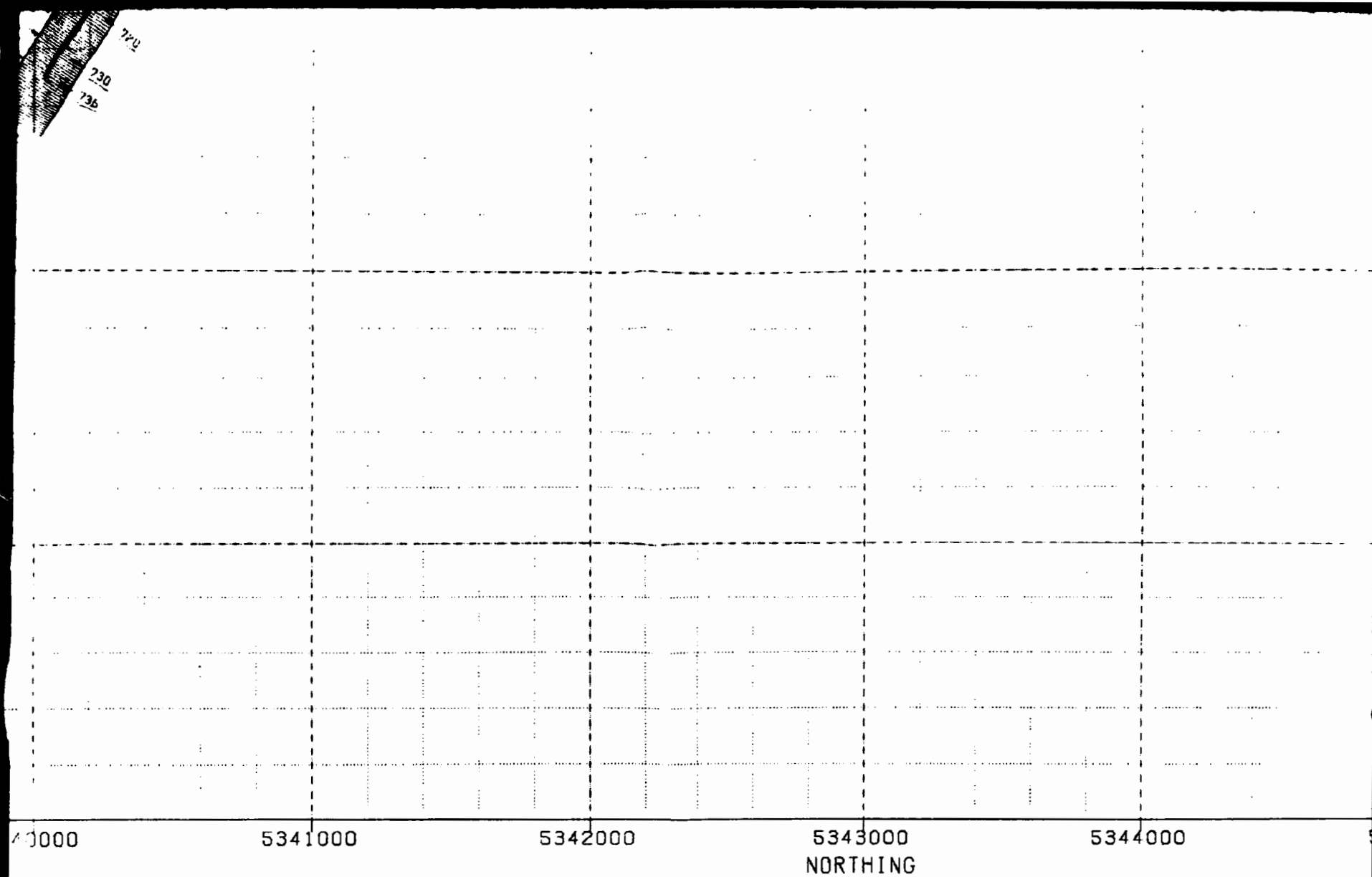


Figure 3.2. Binning strategy chart. The scale is 1:50 and the axes are in UTM zone 21 coordinates.

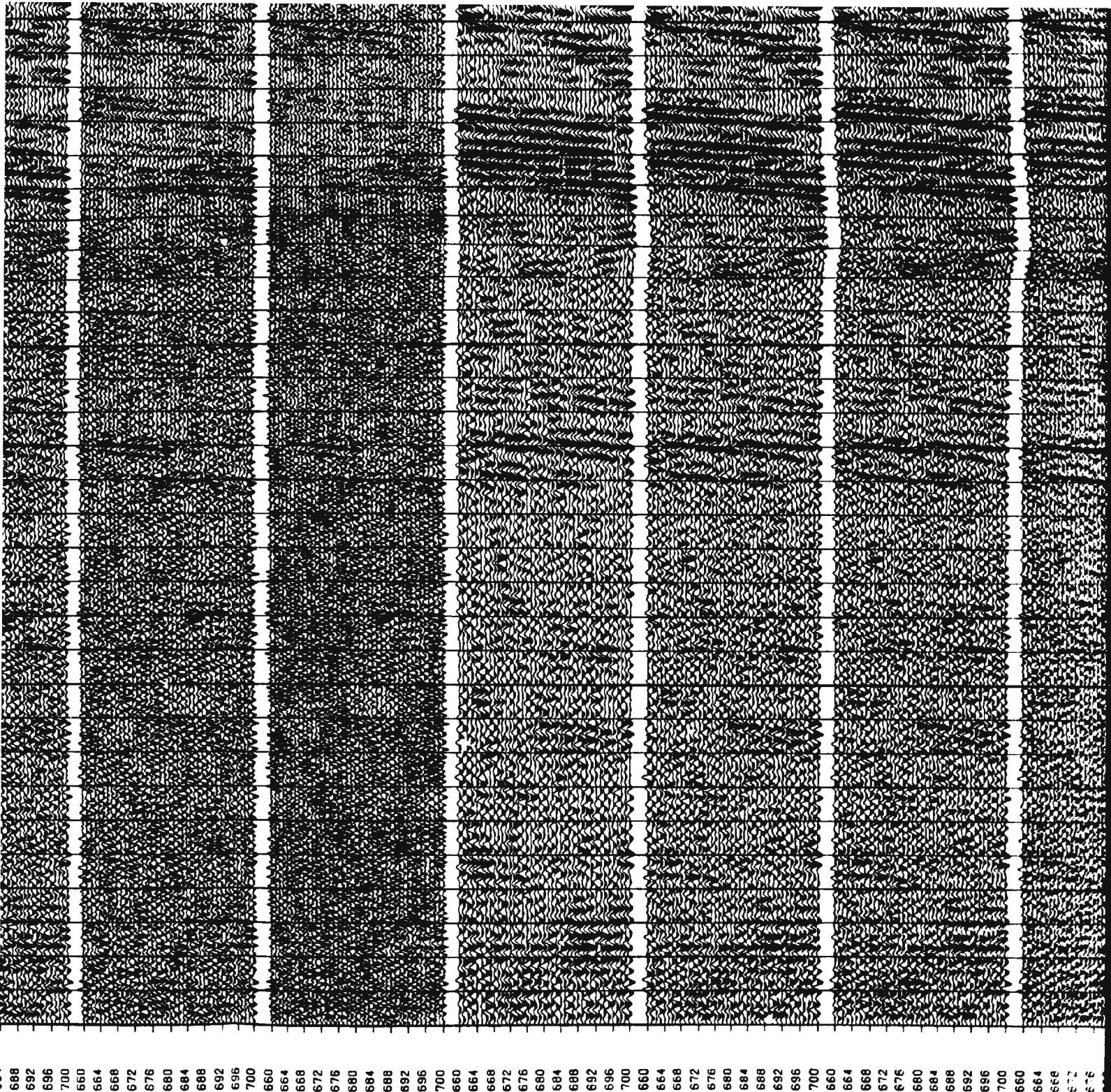
axes are in UTM zone 21 coordinates.

Post-stack bandpass filter-trial

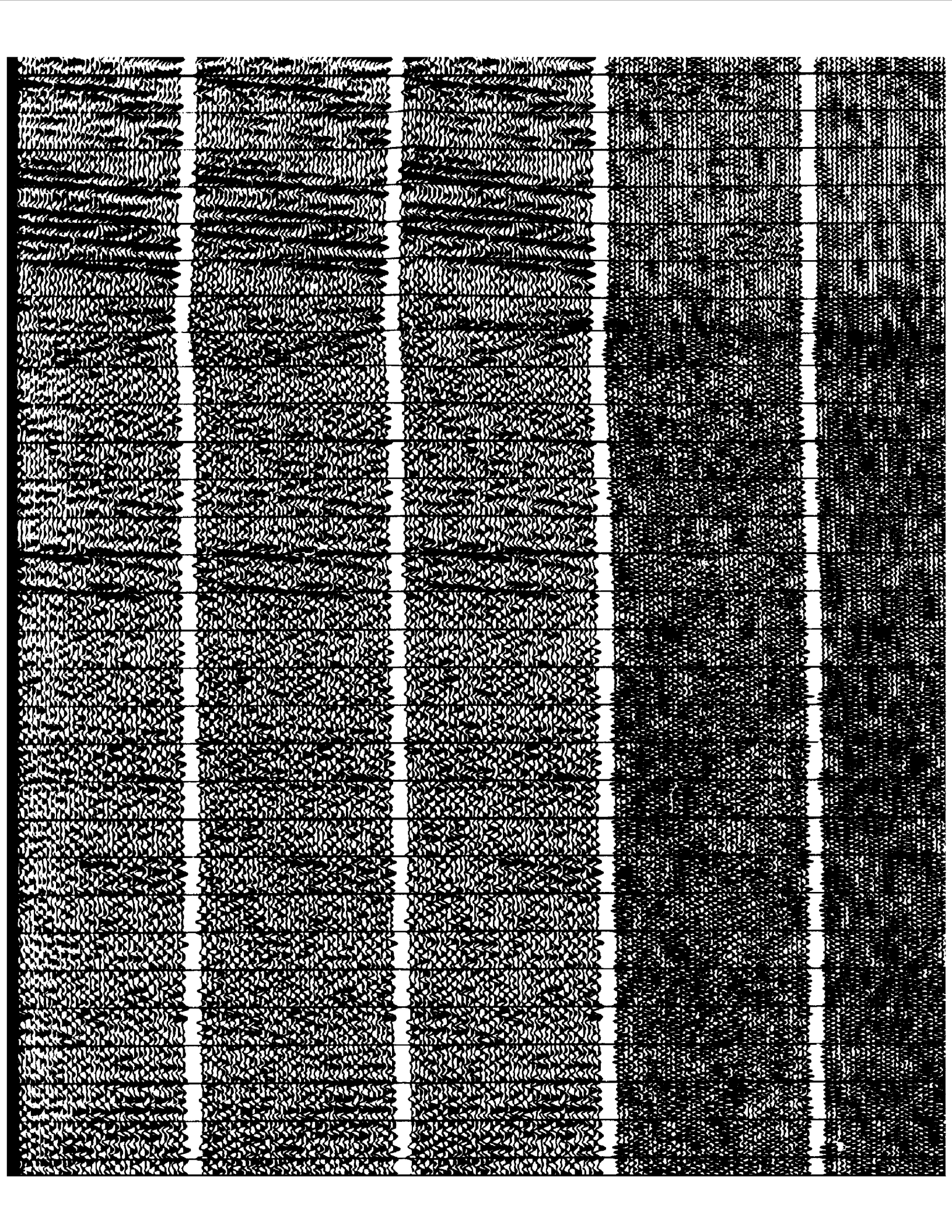
0.9
1.0
1.1
1.2
1.3
1.4
1.5
1.6
1.7
1.8
1.9
2.0
2.1
2.2
2.3
2.4
2.5
2.6
2.7
2.8
2.9
3.0
3.1
3.2
3.3
3.4
3.5
3.6
3.7
3.8
3.9
4.0

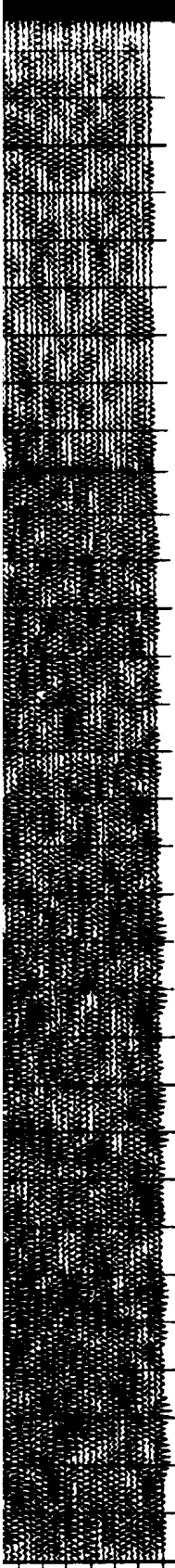
COP

660 664 668 672 676 680 684 688 692 696 700 660 664 668 672 676 680 684 688 692 696 700 660 664 668 672 676 680 684 688 692 696 700 660 664 668 672 676 680 684 688 692 696 700



688	692	696	700	660	664	668	672	676	680	684	688	692	696	700	660	664	668	672	676
-----	-----	-----	-----	-----	-----	-----	-----	-----	-----	-----	-----	-----	-----	-----	-----	-----	-----	-----	-----





0.9
1.0
1.1
1.2
1.3
1.4
1.5
1.6
1.7
1.8
1.9
2.0
2.1
2.2
2.3
2.4
2.5
2.6
2.7
2.8
2.9
3.0
3.1
3.2
3.3
3.4
3.5
3.6
3.7
3.8
3.9
4.0

1

676
680
684
688
692
696
700

CDP

5342000

5341000

5340000

5339000

5338000

372000

373000

374000

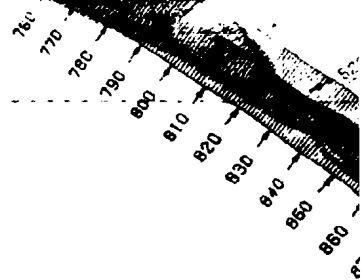
375000

375000

376000

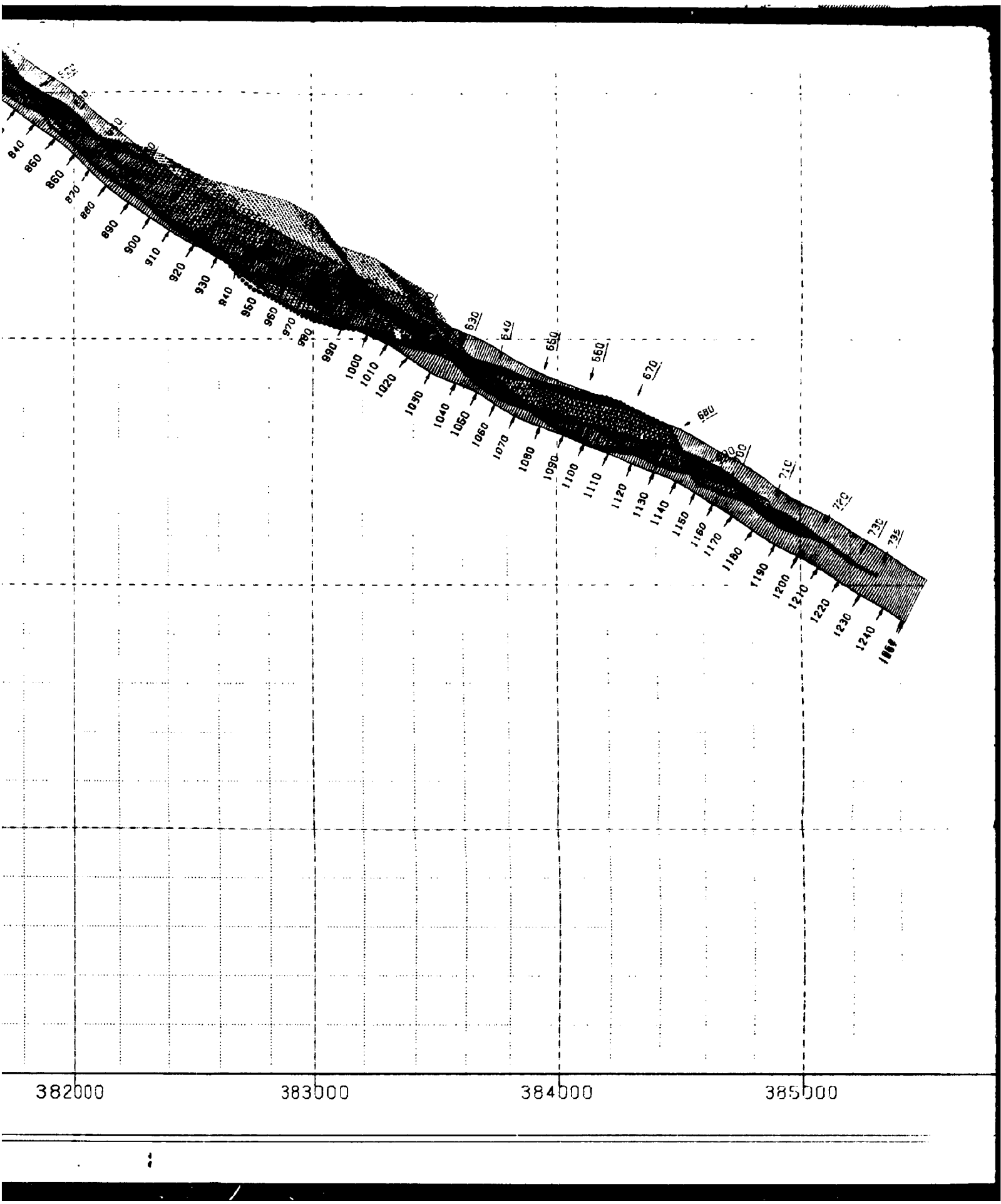
377000

378000



78000 379000 380000 381000 382000

EASTING

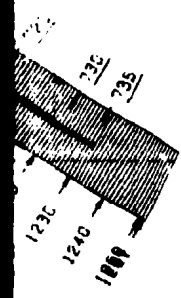


382000

383000

384000

385000



386000

387000

388000

5338000 5339000 5340000 5341000 5342000

: GPLO

- LEGEND :
- - SURVEY STATIONS
 - +
 - 991 - MID POINTS
 - 123 - BIN NUMBERS
 - STATION NUMBERS

SCALE : 1 TO 9900
UNITS: FEET




CROOKED LINE PROCESSING :

DATABASE	ROBRIVZZ
PROCESSING	
LINE STRATEGY	1
BINS STRATEGY	1

STARPAK
PROCESSING

Figure 3.2. Binning strategy chart. The scale axes are in UTM zone 21 coordinates.

axes are in UTM zone 21 coordinates.

O
13
16
3300
 METRES
NO 1
BRIVZZ
1 1



